An evaluation of LiDAR and optical satellite data for the measurement of structural attributes in British upland conifer plantation forestry

Peter Joseph Watt

An evaluation of LiDAR and optical satellite data for the measurement of structural attributes in British upland conifer plantation forestry

Peter Joseph Watt

This thesis is submitted in accordance with the regulations for the degree of Doctor of Philosophy in the University of Durham, Department of Geography, 2005.

Table of Contents

Declaration of Copyright

I confirm that no part of the material presented in this thesis has previously been submitted by me or any other person for a degree in this or any other university. In all cases, where it is relevant, material from the work of others has been acknowledged.

Signed:

Date: 15/09/2005

An evaluation of LiDAR and optical satellite data for the measurement of structural attributes in British upland conifer plantation forestry

This thesis is submitted in accordance with the regulations for the degree of Doctor of Philosophy in the University of Durham, Department of Geography
2005

Peter Joseph Watt

Abstract

This study evaluates the ability of LiDAR, IKONOS and Landsat ETM+ data to provide estimates of forest structure in British upland conifer plantations. Little use has so far been made of these technologies in the UK, whereas in some other countries remote sensing has become integral to forest management systems. The aim of this thesis is to demonstrate the application of the selected remote sensing systems to provide up-to-date and accurate information on key forest variables such as tree height, volume and density. Two upland conifer areas, located in south-west Scotland and north-east England, were used to develop and validate the regression models used to estimate these forest variables.

The ability of LiDAR to provide an accurate measurement of the ground and canopy surfaces was investigated in densely stocked plantations, typical for commercial forestry in the U.K. The results show that, despite the dense nature of the forest canopy, sufficient laser pulses penetrate through to the ground to generate an accurate Digital Terrain Model (DTM). Provided that the ground surface is accurately defined, a point density of 2 returns/m^2 will enable measurement of tree height to be made.

LiDAR-derived top heights were found to be as accurate as field-based measurements (RMSE of 0.57 m). LiDAR-derived top height is easily integrated with established Forestry Commission models to provide volume estimations. Tree density is not accurately estimated using LiDAR data (RMSE of 434 trees/ha). Results strongly suggest that predictive equations developed for top height can be transferred to other conifer forests. Furthermore, the relationship between field-measured top height and laser-derived top height appears to be stable across different conifer species.

LiDAR data can be used to identify tree species in pure and mixed stands. Two methods were developed: the first used summary measures based on the laser height distribution and the second the near infrared intensity. These measures when mapped spatially can be used to classify areas by species and to identify areas of anomalous growth and wind damage.

At a larger spatial scale, Landsat ETM+ and IKONOS data can provide height estimates up to the point of canopy closure (approximately 10 m). LiDAR-derived height can be used in place of field-based measurements to drive reflectance-based models to estimate height from optical satellite data. The methods developed are transferable to other conifer forests that are managed in a similar way.

The results from this thesis show that LiDAR, IKONOS and Landsat ETM+ data provide valuable and complementary information at a range of scales and can assist managers to make more informed resource management decisions.

Acknowledgements

Throughout this research I have been assisted by a number of people. My sincere thanks go to my supervisors Dr Danny Donoghue and Dr Nick Cox who, over the past three years, have provided valuable support and guidance. Thanks in particular to Danny, for his friendship and enthusiasm during my time at Durham and for his philosophical attitude to my many mishaps with equipment and vehicles. Thanks to Nick for his sense of humour and many patient hours spent teaching me how to use the statistical software, Stata.

Thanks are also due to the Forest Enterprise foresters, Jimmy Wilson at Galloway Forest District and David Woodhouse at Kielder Forest District for their assistance with fieldwork and constant interest in this research and in the ForestSAFE project.

On the social side many people at Durham have also made my time enjoyable. In particular; Nick Rosser, Toru and Atchan Higuchi, Huda and Aliza, Penny Widdison, Alona Armstrong, Elizabeth Mackie, Rachel Flanary, Jerry Lloyd and the Geography touch rugby team. My ForestSAFE workmates Rob Dunford and Kay McManus have made the office an enjoyable place to work. Special thanks are due to Rob for his help with fieldwork and for his constant good cheer.

On a more personal note I wish to thank my parents-in-law Don and Diane for their continual support, kindness and great food and wine! Lastly, a very special thanks to my wife Tamsin for her hours of help and encouragement and for keeping Lena amused. Now this thesis is finished I look forward to spending more time with you both!

List of Tables

List of Figures

Notation

Symbols are defined where they are introduced. The corresponding SI units are the metre (m), the nanometre (nm) the hectare (ha) the milliradian (mrad) and the second (s). Some of the more commonly used symbols are the following:

(i) Notation: Forestry variables

Variable	Name	Description
dbh	Diameter at breast height	Tree diameter at 1.3 m above ground level.
G	Basal area	The cross-sectional area of all (living) trees in a compartment measured at 1.3 m above ground height, expressed in m^2/ha.
h	Mean height	Arithmetic average height of all living trees in the stand (m).
hdom	Mean top height	The average height of the 100 trees of largest diameter per hectare (m).
K	Crown width	Crown width (m)
K_a	Crown area	Crown sectional area (m^2/ha).
K_c	Height to canopy base	Height from the ground to tree crown (m).
Kd	Canopy width to tree diameter ratio	Derived by division of *K* and *dbh*.
K_l	Crown length	Live crown height (m).
K_g	Percent green crown	Derived by division of K_l and h (%)
N	Tree density	Number of trees per hectare (trees/ha).
R^2	Multiple coefficient of variation	
S.D		Standard deviation.
Vol	Total volume	Forest stem volume >7 cm *dbh* (m^3/ha).

(ii) Notation: LiDAR terms or derived variables

Variable	Name	Description
C_v	Coefficient of variation	Relative dispersion of LiDAR-derived height distribution data. The ratio of standard deviation and mean and is expressed as a percentage.
denfp	Number first pulse returns	Number first pulse returns/m^2.
Iall	Intensity all	Mean near infrared intensity above 0.5 m.
vegp25	Vegetation intensity 25th percentile	Mean near infrared intensity above 25th height percentile.
vegp50	Vegetation intensity 50th percentile	Mean near infrared intensity above 50th height percentile.
vegp75	Vegetation intensity 75th percentile	Mean near infrared intensity above 75th height percentile.
vegp90	Vegetation intensity 90th percentile	Mean near infrared intensity above 90th height percentile.
Kurtfp	Kurtosis	Extent to which a frequency distribution of scores is concentrated around the mean or spread toward the endpoints.
LK_l	LiDAR crown length	Subtraction of the highest first pulse return from the 20th percentile height.
LK_v	LiDAR crown volume	LiDAR crown length multiplied by the percentage of canopy returns.
meanh	LiDAR mean height	LiDAR percentile that relates to field-measured mean height.
pczero	Percentage laser returns from the ground	Number of ground returns divided by total number of returns.
Skewfp	Skewness	Measure of the asymmetry of a distribution.

(iii) Forestry terminology

Definitions of common terms used in UK forestry that may not be widely used in other countries.

Compartment	Primary management unit used in forestry. Typically, compartments are homogeneous in terms of both tree species and growth.
Mean top height	Average height of the 100 trees of the largest diameter per hectare (m).
Yield class (YC)	Measure of forest productivity for single-species, even-aged plantations. It is derived from empirical models developed from extensive ground-based forest mensuration and is expressed in terms of annual volume increment (m^3/ha/year).

(iv) List of Abbreviations

ALTM	Airborne Laser Terrain Mapper (LiDAR system manufactured by Optech, Canada)
amsl	Above mean sea level
ANOVA	Analysis of Variance
BNG	British National Grid
CASI	Compact Airborne Spectrographic Imager
CW	Continuous Wave (LiDAR system)
DCHM	Digital canopy height model
DSM	Digital surface model
DTM	Digital terrain model
ESRI	Environmental Systems Research Institute
ETM+	Landsat 7 Enhanced Thematic Mapper Plus
FC	Forestry Commission
FOV	Field of view
GCP	Ground control point
GLM	Generalised linear model
GIS	Geographic information system
GPS	Global Positioning System
HRG	High Resolution Geometric (sensor onboard SPOT 5)

HRVIR	High Resolution Visible (sensor onboard SPOT 1-3)
HRVIR	High Resolution Visible Infrared (sensor onboard SPOT 4)
IMU	Inertial Measurement Unit (part of the LiDAR system)
IRS	Indian Remote Sensing Satellite
*k*NN	*k* nearest neighbour
LAI	Leaf area index
LiDAR	Light Induced Detection and Ranging
LRF	Laser range finder (part of the LiDAR system)
NFI	National Forest Inventory
NIR	Near infrared
OS	Ordnance Survey
PSP	Permanent sample plot
RADAR	Radio Detection and Ranging
RMS error	Root mean square error
RPC	Rational polynomial coefficient
ScaLARS	Scanning laser altitude and reflectance sensor (LiDAR system)
SPOT	Système Pour l'Observation de la Terre
SWIR	Shortwave infrared
Terra-ASTER	Advanced Spatial-borne Thermal Emission and Reflection Radiometer onboard the Terra satellite
TIN	Triangular irregular network
TM	Landsat 4 & 5 Thematic Mapper
TMU	Time measurement unit (part of the LiDAR system)
UTM	Universal Transverse Mercator
VIF	Variance inflation factor
VCL	Vegetation Canopy LiDAR
WGS	Woodland Grant Scheme

Appendices

The appendices are referenced according to chapter number.

Chapter 1: Introduction

This thesis investigates the potential of three optical remote sensing systems, airborne LiDAR, IKONOS and Landsat Enhanced Thematic Mapper (ETM+), for providing measures of forest structure in UK upland conifer plantations. In recent times the need to provide measurements of forest productivity, or change, at regular intervals and in a cost-effective manner has become increasingly important for commercial forest planning, especially in light of the current trend of declining softwood timber prices and the high cost of labour. This is particularly challenging where it is necessary to cover large areas that are difficult to access. Increasingly there is also a requirement to provide up-to-date information on forest resources for carbon budgeting, policy formulation, and other aspects of environmental management.

In the UK approximately 1.4 million hectares of forested land cover is fast growing non-native softwood plantation forest (Forestry Commission, 2004). Upland plantations account for approximately 60% of this total (Forestry Commission, 2004). In upland areas the collection of accurate and representative field data can be problematic due to difficult access to forest areas and variability in growth performance. In this context remote sensing offers considerable potential as a technique for providing more frequent, unbiased growth estimates of forest growing stock.

The utility of remotely sensed data as a source of forest information was recognised in the 1970s in Finland, with the systematic use of medium-resolution satellite imagery for forest inventory purposes (Katila and Tomppo 2001). This early work has been developed and adapted for use over much of the boreal forests of northern Europe and North America, using commercially available satellite imagery. The methods pioneered by Tomppo and others in Finland use data from a large number of permanent forest inventory plots, in combination with satellite spectral measurements, to derive information on wood volume by species, basal area, height and age at a forest compartment scale. This provides a key input into the National Forest Inventory (NFI). Although the use of this type of image data is well documented in boreal forests it has not been adopted for use in upland conifer plantation forests, such as those found in the UK. This is because a systematic and extensive field dataset is required and no such dataset exists in the UK.

LiDAR was first evaluated as a method for measuring tree heights in 1985 by Aldred and Bonnor and in the proceeding 20 years it was used extensively to provide estimates of forest basal area (Means et al. 1999), diameter, volume (Naesset 1997b; Holmgren, 2002) and canopy properties (Naesset & Økland 2002). The advantage of LiDAR over optical systems is its ability to provide information on both the horizontal and vertical distribution of vegetation structure.

In the UK, many forest managers believe that only aerial photography can provide the level of detail needed to assess the status of a crop, an assumption that is largely based on the ability to interpret features on the image by direct observation. Therefore, in the UK at least, there is a need to prove the scientific validity of the techniques and also demonstrate a business case for the application of remote sensing, making a clear linkage between the information needs of foresters and what remote sensing can offer. This thesis focuses on data taken from three of the most promising sensors LiDAR, IKONOS and Landsat 7 ETM+ and attempts to bridge the gap between research and operational forestry needs. More specifically, the thesis investigates the appropriateness of LiDAR for providing accurate estimates of forest variables for identifying forest species composition and for validating height estimates generated from lower-cost medium-resolution (Landsat 7 ETM+) and high-resolution (IKONOS) optical satellite data.

1.1 Aims and Objectives

Since less work has been conducted in densely stocked plantations, such as those planted in the UK, there is a requirement to test the accuracy and validity of models generated from remotely sensed data in UK forestry conditions. A series of research aims were designed to test, scientifically and practically, the potential of these data to provide reliable forest estimations for forest management purposes. Five research aims were established. The first was to evaluate the accuracy of LiDAR data and the second and third assessed the ability of LiDAR to provide estimates of tree volume, height and density and to identify tree species. Research aim four sought to test the ability of IKONOS and Landsat ETM+ to estimate forest height and the fifth examined the potential of integrating optical data and LiDAR data to provide forest height estimates. Each aim is presented in more detail below:

(i) assess the effect of canopy structure, topography and laser point density on the accuracy of measures derived from LiDAR data in dense upland conifer plantations;

(ii) assess the potential of LiDAR data to provide estimates of top height, volume and tree density. In forestry, these measures are most the commonly used to determine forest productivity and to parameterise other growth prediction models.

(iii) assess the potential of LiDAR-derived crown density variables and near infrared data derived from SPOT 5 HRG and LiDAR to identify plantation species and areas of anomalous growth;

(iv) examine the potential of Landsat ETM+ and IKONOS sensors for providing forest height estimates in upland conifer plantations;

(v) assess the potential of LiDAR for providing additional height samples and validating forest height estimates derived from Landsat ETM+ and IKONOS models.

To fulfil the aims of this thesis, a series of objectives were developed to ensure field data were collected in a robust and systematic manner and that data processing methods enabled the large volume of field and image data to be summarised effectively to provide the various forest estimates. The specific objectives are listed below.

(i) design a suitable method of digital collection of field data and positioning of tree stems under dense forest canopy;

(ii) develop a method of summarizing and deriving LiDAR variables from laser point cloud data;

(iii) develop a series of forest estimation models using LiDAR, IKONOS and Landsat ETM+ data;

(iv) design a suitable method of quantifying LIDAR near infrared intensity data.

1.2 The ForestSAFE Research Project

Much of the research presented in this thesis makes extensive use of image and field data collected as part of the EU LIFE-Environment ForestSAFE project. This is a five-year (2000-2005) European Commission (EC)-funded project that seeks to demonstrate the capability of remote sensing, combined with field data, for monitoring and updating

forest information across a range of European forest types. The project works in partnership with the UK and Swedish research institutions, namely: Durham University, Forest Research and the Swedish University of Agricultural Sciences and partners from the forest industry; the UK Forestry Commission and the National and four Regional Boards of Forestry in Sweden. The motivation for the project comes from the fact that remote sensing is still relatively under-utilised in the forestry sector across Europe. In response to this situation a number of demonstration products have been developed to highlight the potential of remote sensing for improving forest management, in terms of providing more accurate forest estimates, monitoring and mapping forest resources and providing information on sensitive woodland habitats. The project began with a conference held in Edinburgh, UK in 2002 (Forestsat 2002) that focussed on remote sensing of forests, emphasising the state of the art in scientific techniques. The project concludes by organising an international conference to be held in Borås, Sweden in June 2005 (Forestsat 2005), which will demonstrate the potential application of remote sensing to forest practitioners. This thesis has been developed from parts of the work associated with the ForestSAFE project.

For further information the reader is referred to the ForestSAFE website, http://www.svo.se/dokument/ac/kansli/ForestSafe/Web_UK/home.htm.

1.3 Structure of the thesis

This thesis is divided into ten chapters as detailed in Table 1. The thesis begins by providing an overview of plantation forestry in the UK in Chapter 2, together with a summary of how remote sensing has been used to assist forest management in other countries. Chapters 3 and 4 discuss the methods used to acquire and process the field and image data. Chapters 5 to 7 assess the accuracy and potential of airborne LiDAR to provide forest estimates and to identify and map different conifer species. Chapter 8 assesses the potential of IKONOS and Landsat ETM+ for predicting forest height; it also examines the potential of LiDAR to provide additional height measurements and to act as means of validating the satellite height estimates. Chapter 9 discusses the findings of this research in relation to other studies, taking three examples from this research and showing how these can be applied to assist foresters to make more informed resource management decisions. Lastly, Chapter 10 summarises the thesis in relation to the original aims. Future research directions are discussed in the conclusion.

Table 1.1 Structure of the thesis

Chapter title	Description	Specific detail
1: Introduction	Rationale, aims and objectives.	
2: Plantation forestry in the UK	Overview of UK plantation forestry. How remote sensing can assist in the management of this resource	Information requirements for management of forest resources Study areas
3: Field data collection and analysis	Dataset properties	Description of field data collection methods and analysis relationships between field data
4: Image Processing	LiDAR: DTM, DSM and DCHM extraction. Optical data: image rectification of Landsat ETM+, SPOT 5 HRG and IKONOS data	Description of image data and processing methods
5: Accuracy of LiDAR under dense forest canopies Research aim (i)	Accuracy of LiDAR height estimate in dense conifer plantation. Factors that affect LiDAR accuracy in UK forests.	Field survey measurements are used to compare the accuracy of the LiDAR ground surface and canopy surface
6: Forest estimates from LiDAR Research aim (ii)	Estimations of top height, volume and tree density	Use of LiDAR-derived crown density measures and distribution information from LiDAR point data to try and improve forest estimates
7: Mapping plantation species and areas of anomalous growth using LiDAR Research aim (iii)	Identify plantation species using LiDAR intensity data and LiDAR derived crown density measures.	Use of SPOT 5 NIR data to check radiometric consistency of LiDAR intensity. Development of a technique for mapping plantation species distribution
8: Using LiDAR to compare height estimates from IKONOS and Landsat ETM+ data in Sitka spruce plantation forests Research aims (iv) and (v)	Development of height models based on relationship between IKONOS and Landsat ETM+ reflectance and field data.	Use of LiDAR-derived height to provide additional sample data and to validate the accuracy of the optical height models.
9: Discussion	Comparisons with other research. Examples of potential applications	Examples of how methods and data can be applied. Comments on future sensor developments
10: Summary & conclusions	Summary Future research	Discussion of thesis aims, future research directions

Chapter 2: Plantation forestry in the UK

2.1 Introduction

Timber production from British forests is forecasted to increase from 11 million m^3/ha per year to 15 million m^3/ha per year by 2020 (Forestry Commission 2004). The Forestry Commission acknowledges that this resource must be effectively managed, taking into account a range of environmental issues, including biodiversity and water quality. Further, at a national level there is increasing awareness of the carbon sequestration potential of these plantations for which accurate information of forest area and growth are required to perform carbon accounting. Therefore, there is a growing need for more up-to-date and precise information, at a range of scales, on the status and productivity of forest resources. While it is widely acknowledged that ground survey methods to obtain such detailed inventory data are expensive and time-consuming, for remote sensing to be considered a viable alternative in the UK, its value needs to be recognised and understood at an operational level. The following sections provide a historical overview of forestry in the UK and summarise current forest management practices. Additionally, a summary of the issues that have prevented the uptake of remote sensing in UK forestry is presented. The relevance of current operational methods to UK forestry is also discussed, together with the applications of emerging techniques[1]. Lastly, the two upland conifer areas used in this research are introduced.

2.2 UK plantation forestry

The industrial revolution and the First World War depleted Britain's natural wood resources. Consequently, in 1919 the UK Forestry Commission (FC) was formed with the objective of creating a strategic reserve of timber so that Britain would no longer have to rely on imports in times of war (www.forestry.gov.uk). At this time vast areas of land deemed too poor for agriculture, were planted with fast-growing, non-native conifer species, such as Sitka spruce (*Picea sitchensis*) and lodgepole pine (*Pinus contorta*) (Figure 2.1). Sitka spruce in particular grows well in a wide range of site

[1] This chapter is not intended to provide an extensive review of remote sensing literature but more to set the context for the forthcoming chapters.

conditions, including the exposed upland areas of the UK with high annual rainfall (Hibberd 1991).

Figure 2.1 Typical upland landscape with extensive areas planted in conifers. Source: Jimmy Wilson, FE Galloway.

By 2004, 59% of the 1.4 million hectares of the plantation resource were planted with these species. Forest Enterprise (FE), the management arm of FC, manages 35% of this resource, with the remainder under private ownership. Since 1988 FC, through the Woodland Grant Scheme (WGS[2]) programme, has also assisted private woodland establishment. Statistics for 2003-2004 show that 98% of new plantations (18,000 ha) were established by the private sector, of which 61% were financed by the WGS.

2.2.1 Plantation management

Conifer plantations are typically established or restocked at over 2,500 trees/ha (Figure 2.2) with areas divided into individual compartments, according to tree species and density. At this high planting density the trees quickly out-compete any existing vegetation and dominate the site. By the time the crop reaches 10 m (about 15 to 17 years) the forest canopy has closed and the understorey vegetation replaced by a thick mat of needles (Figure 2.3).

[2] The Woodland Grant Scheme (WGS) provides monetary incentives to create and manage woodland sites in Great Britain. The Forestry Commission is responsible for administering the scheme and pays grants for establishing and tending woodlands.

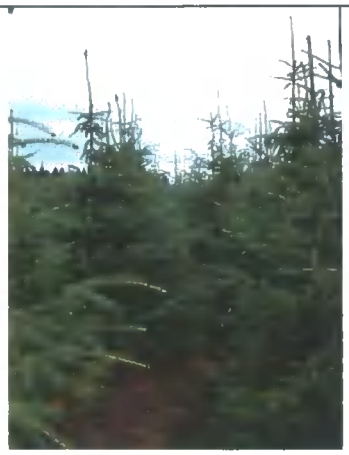

Figure 2.2 10 year old Sitka spruce crop.

Figure 2.3 17 year old closed canopy Sitka spruce crop.

Figure 2.4 Mature Sitka spruce crop.

Figure 2.5 Sitka spruce/lodgepole pine mixture.

The majority of the plantations established in upland areas are not thinned because of the perceived threat of wind damage (Figure 2.4). Consequently, tree mortality in pure species crops commonly exceeds 30%[3] by the time the crop is ready for harvesting at 45 to 60 years. In upland areas, an alternative silvicultural regime was introduced in the 1960s, when conifer species were planted as intimate mixtures. The most frequently used combination was Sitka spruce and lodgepole pine, planted either in discrete rows or alternately in the same row (Figure 2.5). The rationale was that over time the crop would self-thin to become dominated by Sitka spruce. In practice, a range of outcomes emerged, from Sitka- or pine-dominated crops to mixtures where neither species dominated. Nevertheless, the high tree density, location and extent of these plantations mean that one of the major threats during the forest rotation is wind damage (Figure 2.6).

[3] Based on sample plot measurements.

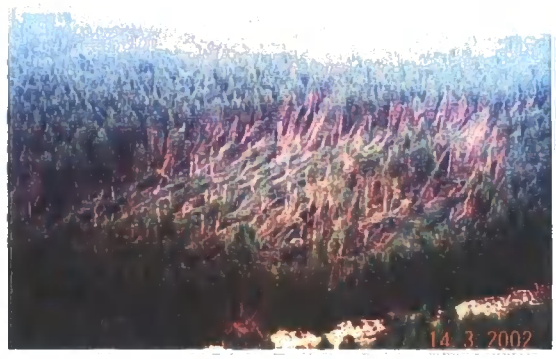

Figure 2.6 Internal wind damage Kielder forest. Source: David Woodhouse, FE Kielder.

When compared with Continental Europe and Scandinavia, UK forests are unique in terms of the prevalence of non-native species, tree density, simple silvicultural regimes (i.e. not thinned) and short forest rotations. The fast growth rates and short forest rotation mean that to manage this resource effectively up-to-date information is required.

2.3 The application of remote sensing in forestry

Historically, aerial photography has been the main source of remotely sensed data used in forestry for updating forest maps and providing estimates of height (derived from photogrammetric techniques). However, since the 1970s, more extensive use of remote sensed data has occurred. Much of this interest was fuelled by the launch of the lower resolution Landsat MSS optical satellite (80 m) and grew with the subsequent launch of the medium resolution Landsat TM (30 m) series of satellites. Since these beginnings the resolution of optical data continues to improve with launch of high-resolution satellites such as IKONOS and QuickBird ($\leq$ 1 m panchromatic; $\leq$ 4 m multispectral). Since the 1990s Airborne Laser Systems (LiDAR) have also become more readily available offering datasets that provide accurate measurements of terrain and vegetation height. In terms of estimates such as height these sources can be ranked according to accuracy, first LiDAR then aerial photography followed by optical satellite data.

2.3.1 Current methods in the UK Forestry Commission

Standard practice within FE is to inspect each forest compartment a minimum of three times during a crop rotation to assess: (i) success of establishment, (ii) expected yield, to enable production forecasting, (iii) timber quality, species composition and volume before clear-felling. This information is collected using a combination of field sample plots and 1: 10 000 aerial photography. The photography is used in conjunction with the ground survey effort to map newly planted or restocked areas, unplanted or poorly stocked areas, areas of damage and to further stratify compartments according to differences in growth or silvicultural practices. These stratified areas are termed sub-compartments. Digital compartment maps are generated manually from aerial photography and stored in the 'Forester' Geographical information System (GIS) developed specifically for the Forestry Commission by Environmental Systems Research Institute (ESRI). Additionally, 'Forester' is used to store information on the planting date, species, tree spacing, soil type and expected forest yield. All thirty forest districts use the 'Forester' software for running timber production forecasts, defining harvesting areas and managing forest inventory data. A similar management system is also used to record privately owned woodland, established under the WGS.

The use of remote sensing in the UK forest industry has not yet developed beyond the use of aerial photography. Reasons cited for this situation include: (i) the lack of users' experience with remotely sensed data (ii) cost associated with acquisition and processing of data (iii) difficulties in acquiring cloud-free optical data (iv) the lack of direct relationships between forest variables and optical data (Malthus et al. 2002; Suárez et al. 2005). Consequently, the current forest management/planning system continues to rely on information obtained from aerial photography and field survey.

For remote sensing to be adopted in an operational context in the UK, there is a pressing need to establish a strong business case. Remote sensing would need to be perceived as complementing existing management systems and to be cost-effective when compared with current methods, providing reliable and consistent results. One element of this process involves demonstrating the potential of remote sensing and highlighting its limitations, under UK plantation conditions.

Research into the potential of space-borne remote sensing for monitoring vegetation began in the 1960s principally by Colwell in the US, Ahern and Goodenough and others

in Canada and Poso and others in Finland. In particular, Colwell's research, pioneered new methods of satellite photography and reconnaissance which lead to the application of multi-band photographic imagery for monitoring forest resources. Ultimately, these advances assisted in the development of the multi-spectral scanner (MSS) onboard the first commercial satellite Landsat 1, which was launched in 1972. The MSS system was the first global monitoring system capable of producing multi-spectral data in digital format.

However, despite the availability of such data initially from MSS sensor carried on Landsat 1 (launched 1972), Landsat 2 (1975) and 3 (1978) then later from the improved TM sensor onboard Landsat 4 (1982), 5 (1984) and ETM+ sensor onboard Landsat 7 (1999), internationally there are still only a few examples of remote sensing being used to assist with forest management planning. Perhaps the best-known example is the application of the *k* nearest neighbour (*k*NN) method. The *k*NN method uses field data to assign forest variable data to unknown areas by comparing spectral similarity, weighted by distance from the nearest known plot (Holmström et al. 2001). This has been used in the Finnish multi-source National Forest Inventory (NFI) since 1990 and has since been applied to national forest inventories in Sweden and the USA.

The main constraint that restricts its application in the UK is that the *k*NN method requires a dense and regularly distributed network of sample plots that cover the range of variation expected in the forest (Katila & Tomppo 2001). Such sample information is not currently collected in a systematic manner in the UK. It is possible, however, to use an alternative method that relates the reflectance at different parts of the electro-magnetic spectrum to forest structure. This is normally done by selecting target plots from which to measure forest variables and to relate these to the reflectance data from a remotely sensed image at the same location. This latter approach is more appropriate to the UK situation as it is less reliant on a large network of sample plots. Previous research has assessed these relationships using airborne (Danson & Curran 1993;) and medium-resolution satellite data (Donoghue et al 2004; Hyyppä et al. 2000; Nilson & Peterson 1994; Puhr & Donoghue 2000; Ripple et al. 1991). Generally these studies show that some forest variables e.g. are easier to predict than others, in particular height and age. It is important to note that the strength of relationships varies between studies. For example, Hyyppä et al. 2000 recorded an R^2 of 0.26 for height in Finnish boreal

forests while Danson and Curran (1993) recorded an R^2 of 0.71. These differences in relationships can be caused by the structure of the forest canopy and by forest management practices, such as thinning. In contrast Britain's upland conifer plantations are densely planted with a simple management regime (no thinning), which causes the canopy to close at a young age. Therefore the main limitation of the method is that spectral response tends to decrease as the forest canopy closes; consequently predictions are only valid for the first part of the forest rotation. To be applied operationally in the UK, more work is needed to assess whether these relationships remain stable at different spatial resolutions (i.e. from 4 m to 30 m) and across forest regions.

More direct relationships, such as tree height, can be obtained using airborne LiDAR. The advantage of LiDAR over optical data is that the laser is able to penetrate the canopy through gaps to provide not only height information but also information on canopy structure from the distribution of laser pulses. LiDAR research has been conducted at two levels; the tree level and plot level (Naesset et al. 2004). Studies at the tree level typically use a higher density of laser returns while at the plot level lower sampling densities are used (1-4 returns/m^2). In both cases forest measurements are calculated from the laser data by relating field measurements to the vertical distribution of laser returns, or more recently, the intensity of the laser pulse return (Holmgren 2003; Donoghue and Watt, *in review*). The tree level approach generally includes more processing steps than the stand level method as it requires that each tree is located before any estimations are conducted. Stand level estimates are made by matching laser data to field plot measurements and using the plot-level relationship to generate estimates at the stand level. In Norway, the laser data and forest records are used to stratify the forest based on site quality (height and age) prior to estimation (Naesset & Økland 2002). Previous studies have shown at either level that, although LiDAR data are more costly than optical data, their accuracy is indisputable. In particular, LiDAR data have been used to provide estimates of forest basal area (Means et al. 1999), diameter, volume (Naesset 1997b; Holmgren 2002) and canopy properties (Naesset & Økland 2002). In establishing tree height and volume the accuracy of LiDAR-derived estimates is reported to be similar to or better than manual field measurement methods (Holmgren 2003; Naesset 2002). Consequently LiDAR data are now used operationally in Norway (marketed on the premise that better data results in better decisions) to provide forest estimates at the compartment level (Eid et al. 2004; Naesset 2005).

This research evaluates LiDAR as a method of estimating forest parameters at the plot level. Compared with other countries less work has been conducted in the UK, and there is some uncertainty as to whether LiDAR flown over densely planted conifer plantations (planted at densities exceeding 2,500 trees/ha) will yield similar results. The ForestSAFE project has provided the first opportunity to evaluate a range of remotely sensed data over British upland conifer forests, from high-resolution IKONOS and LiDAR to medium-resolution SPOT and Landsat ETM+ data. These data were complemented by extensive ground-based survey. However, there remains a need to investigate a wide range of issues relating to the use of remotely sensed data in the UK, including the accuracy of estimations, repeatability of results, compatibility with existing forest management systems, cost effectiveness and geographical transferability.

2.4 Study areas

The two upland areas used for this study are located in Galloway Forest District, in south-west Scotland, and Kielder Forest District, in north-east England (Figure 2.7). These Forest Districts cover the range of forest conditions found in the UK.

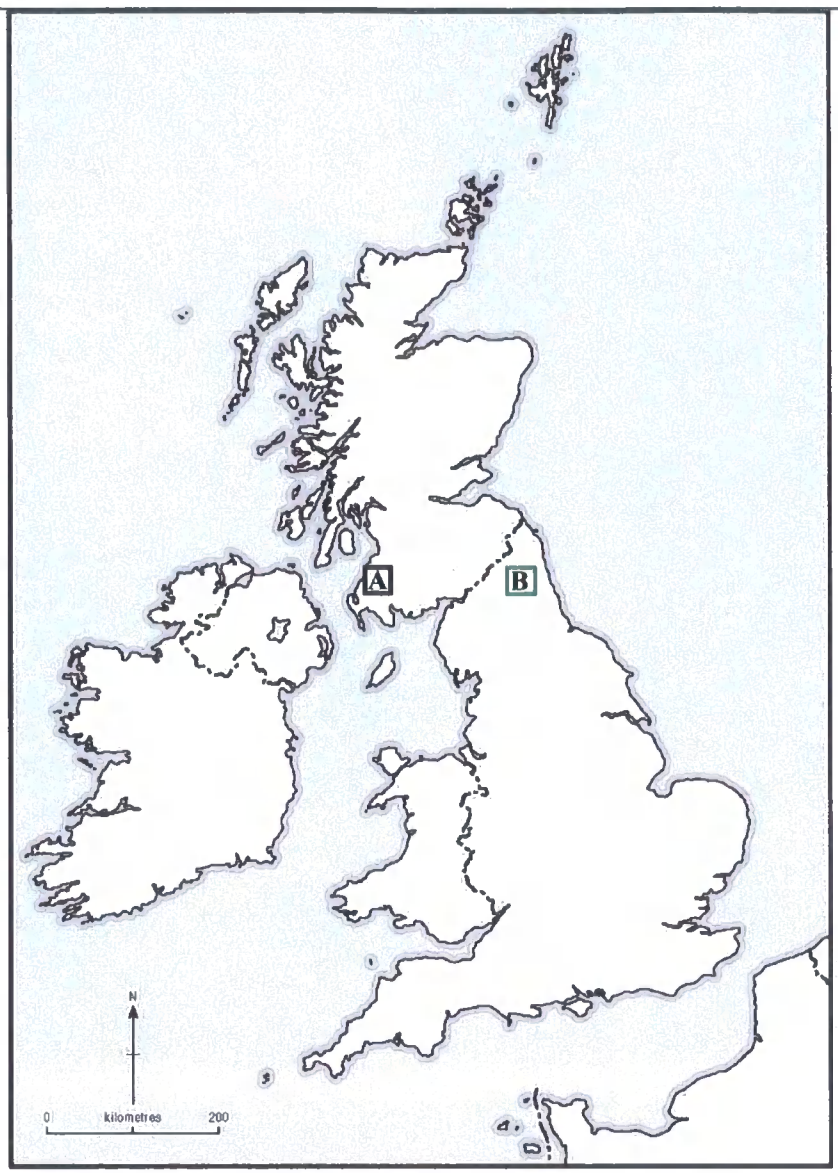

Figure 2.7 Location of (A) Galloway and (B) Kielder forest study areas.

In Galloway Forest District the elevation ranges from sea level to 515 m above mean sea level (amsl). The majority of plantations are established below 350 m amsl. Kielder Forest District covers a similar elevation range from 200 to 600 m amsl, with plantations established up to 400 m amsl. The combined planted areas of these districts are some 110,000 hectares, evenly divided between the two forest districts (Figures 2.8 and 2.9). Each has an annual harvest of 500,000 m^3/ha per year. Combined they yield 10% of the UK's annual timber production (Forestry Commission 2004). These districts are the largest in terms of planted area[4] and timber production in their respective countries. The predominant plantation species is Sitka spruce, although

approximately 22% of each district is afforested using a combination of species, with Sitka spruce and lodgepole pine the most common combination (source FE GIS).

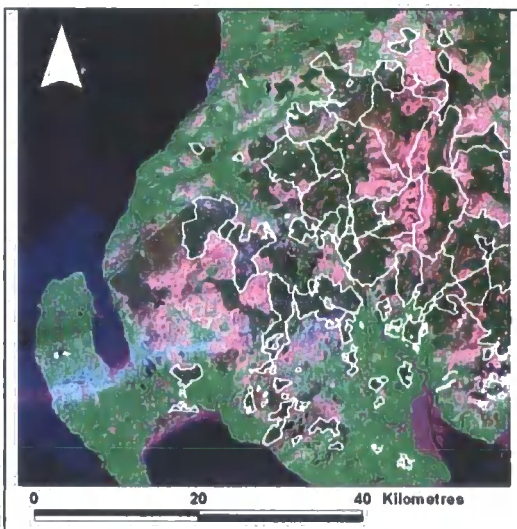

Figure 2.8 Plantation distribution Galloway forest district. Image showing part of a Landsat 7 ETM+ scene (display bands 1,4,3)

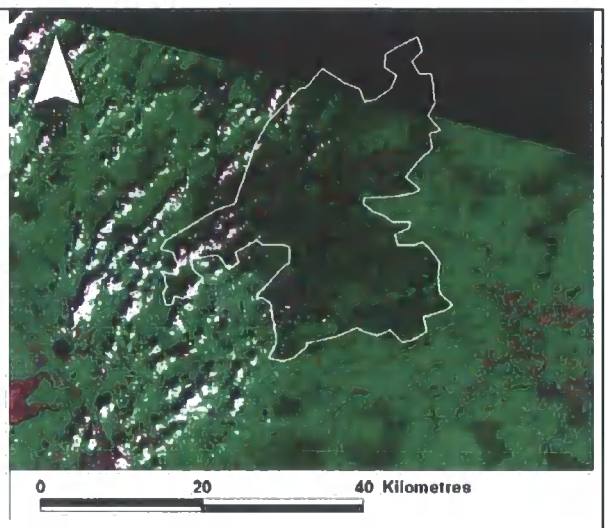

Figure 2.9 Plantation distribution Kielder forest district. Image showing part of a Landsat TM scene (display bands 1,4,3)

The management of these areas is hindered by their isolation and difficult field conditions. The large size of forest compartments (>50 ha) also makes it difficult to identify and map areas of growth variability and internal wind damage. Usually aerial photography, flown at five-yearly intervals, is used to assist in mapping these areas. However, in recent years coverage has been insufficient to provide current information on the state of the resource (pers comm. Jimmy Wilson Galloway Forest District; David Woodhouse, Kielder Forest District). Remote sensing data provide the opportunity over both areas to better manage this resource at a range of scales from the sub-compartment to the compartment level.

[4] Kielder forest is one of the largest man-made forests in Europe (www.kielder.org).

Chapter 3: Field data collection and analysis

3.1 Introduction

The main objective of this chapter is to describe the methods used for collection of the forest mensuration data in the field. Field data were collected from two upland conifer forests, Kielder forest in north-east England and Galloway forest in south-west Scotland. More detailed forest measurements were made in the Kielder study area, so these data have been used as the basis for generating the relationships between the forest variables, height, volume and tree density, and the image datasets (the focus of Chapters 6 and 8). The measurements included biophysical measures, which are commonly recorded during a conventional forest inventory (tree diameter and height), and more detailed measurements such as tree crown measurements (crown width, length, ratio and area). These data were matched to the precise spatial location of each tree within the sample plot, to enable a direct comparison between field and LiDAR height measurements. An analysis was also conducted to determine the relationship between field-measured height and various crown measurements, which potentially provide indicators of forest productivity and a way of separating different forest crops (e.g. pure Sitka spruce (*picea sitchensis*) from Sitka spruce/ lodgepole pine (*pinus contorta*) mixtures). The same measurements, summarised at plot level, also enable the study of factors that may affect the accuracy of LiDAR height estimates (the focus of Chapter 5). The Galloway study area contains a wider selection of plantation species and growth outcomes and so plots established in this area were used to assess the ability of LiDAR to discriminate plantation species and map areas of anomalous growth (the focus of Chapter 7).

3.2 GIS datasets

A summary of the GIS datasets used in this research is presented in Table 3.1. Forest Enterprise Kielder & Galloway kindly supplied their forest compartment boundary information, including an associated database containing information on stand age, species composition and yield class[5]. It was from this information that the study area and the ground sample points were selected. By using a combination of Ordnance

[5] Yield class is derived from empirical models developed from extensive ground-based forest mensuration. These models are used to provide a measure of forest productivity for single-species, even-aged plantations.

Survey and Forestry Commission datasets for geo-correction of the image data, a greater selection of ground control points (GCPs) was extracted.

Table 3.1 Summary of the GIS datasets

Coverage	Data Source
Compartment boundaries, roads, waterways	Forest Enterprise
1:50 000 Meridian data 1:50 000 OS raster data 1:2 500 Land line data	Ordnance Survey
Forest Compartments selected for survey Sample plot location points	University of Durham & Forest Enterprise

3.3 Field data collection

Field sample plots in forestry can provide an unbiased sample of the population of trees that is representative of the forest structure. The objective of the inventory dictates what measurements are recorded. This might range from measurement of tree numbers to see if a forest area has been established as a commercial crop to more intensive survey that includes the measurement of tree height and diameter. In many cases forest areas are stratified prior to measurement, to attempt to reduce the number of sample plots required. In the UK, a combination of aerial photography, field plots and a GIS are used to stratify areas according to age, species and growth rate. The number and size of the field survey plots required is usually a compromise between establishing sufficient sample plots to account for the degree of variation in the forest measurements and the cost. The Forestry Commission forest inventory guidelines suggest that sample plot size should be no smaller than 0.01 ha.

In this study sample plot measurements are the basis for generating relationships between the image datasets and a range of measured forest variables including forest height (top height and mean height), volume and tree density. In accordance with Forestry Commission principles forest plots were no smaller than 0.01 ha and were spread over a number of forest compartments, representative of the forest structure.

In the Kielder test area, sixty sample plots were measured in 2003. These plots were used to establish relationships between the image data and measured forest variables and are hereafter referred to as the reference dataset. A further 30 sample plots were also measured in 2004 for the purpose of validating the height predictions obtained from

the 2003 dataset (hereafter referred to as the validation dataset). Both datasets were distributed over a range of age classes, tree species combinations and site types. More sample plots were established in pure Sitka spruce compartments because this reflects the distribution of species compositions found within the study area.

In Galloway, twenty sample plots were established in two age classes, 33 and 48, as the focus of the survey was to provide measurements in closed canopy crops, covering a range of plantation species and yields. Table 3.2 provides a summary of the field data, while the distribution of plots by age and species for the Kielder study area is shown in Figure 3.1.

Table 3.2 Summary of Kielder and Galloway field sample plot data

Dataset	Survey Date	Sample Size	No. Plots		Age Range	GPS information
Kielder		(ha)	Pure	Mixture	(years)	
Reference	2003	0.02	24	4	9 to 60	All tree *xy* positions recorded
Reference	2003	0.16	1	1		
Validation	2004	0.02	30		3 to 53	Plot centres only
Galloway						
Reference only	2003	0.02	17	3	33 and 48	Plot centres only

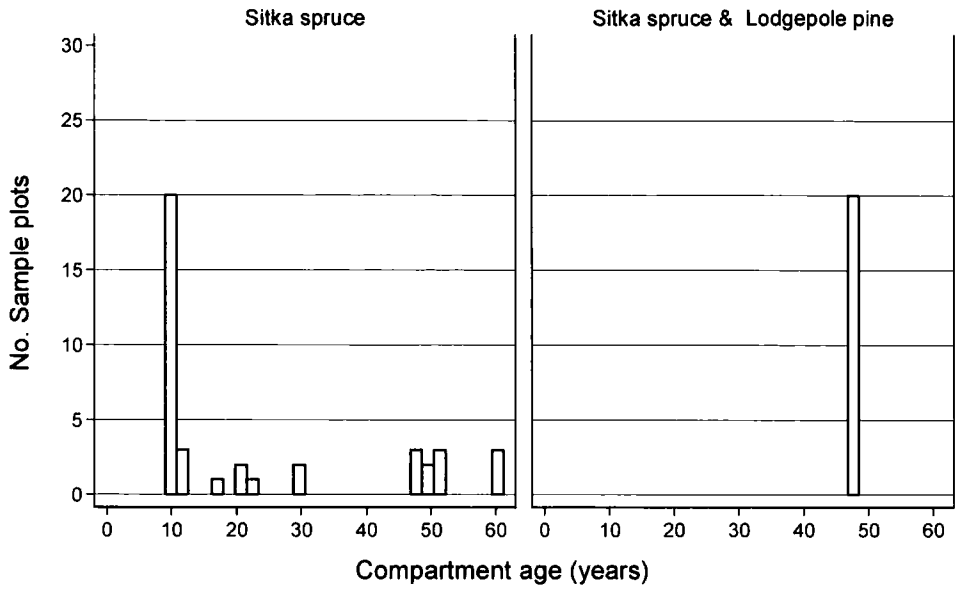

Figure 3.1 Age class range and species composition for Kielder forest reference dataset.

To locate the plot in relation to the image data requires accurate positioning of sample plots. Plots must also be laid out more than 50 m from the edge of forest compartments and wind-damaged areas. This is particularly important when extracting reflectance values above sample plots from 30 x 30 m Landsat ETM+ pixels, to reduce the potential for mixing reflectance values from different land cover types (Puhr & Donoghue 2000). Compartment edges were excluded by buffering to 50 m from the compartment boundary in a GIS. The location of the first sample plot within each compartment was randomly selected using a seeding function in a GIS and subsequent plots were established at 100 m intervals. In the field, navigation to each sample point to within ± 5 m was possible using a handheld GPS. Once the plot had been located, more precise coordinates were recorded using a Leica series 300 differential Global Positioning System (dGPS); this process is described in further detail in section 3.1.2. The location and spatial distribution of the Kielder and Galloway sample plots are presented in Figures 3.2 and 3.3.

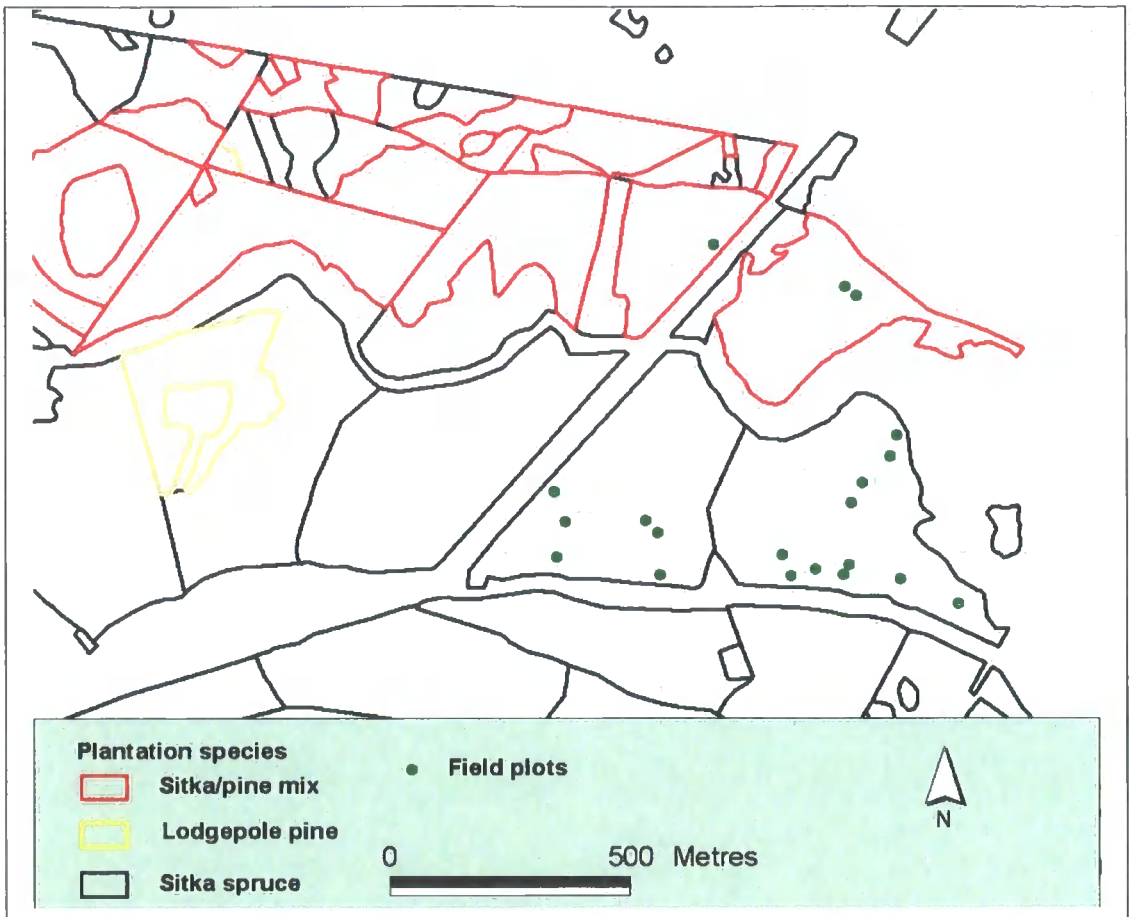

Figure 3.2 Location of Galloway forest field sample plots (lat. 55° 07′ N long. 4° 32′ W)

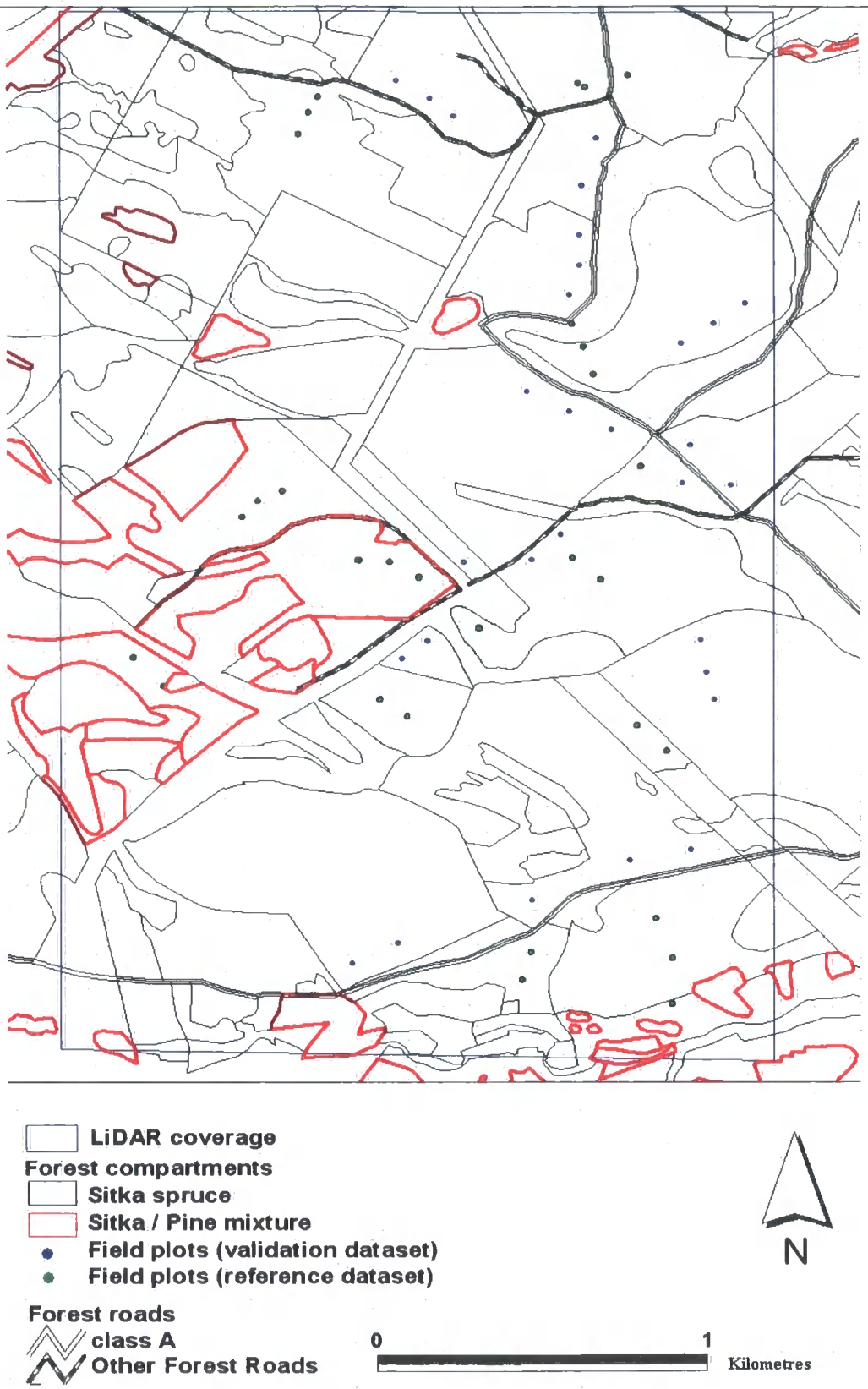

Figure 3.3 Location of Kielder forest field sample plots (lat. 55° 13′ N long. 2° 49′ W).

3.3.1 Sample plot design

Forest measurement data were recorded using two sample sizes, square plots of 0.16 ha (40 x 40 m) and conventional circular forest inventory plots of 0.02 ha (Figures 3.4 and 3.5). The purpose of the larger square plots of 0.16 ha was to capture forest data at a scale that was equal to, or greater than, the spatial resolution of the sensors being evaluated. This approach has been adopted by researchers investigating LiDAR (Suárez et al. 2005) and optical sensors (Donoghue & Watt, *in review*).

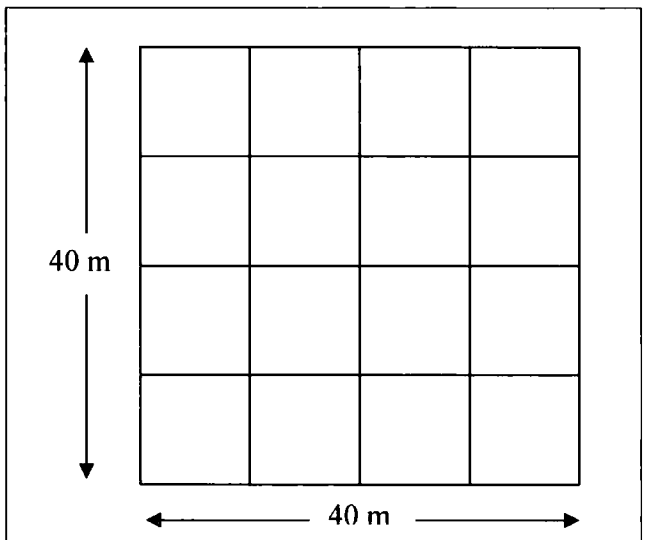

Figure 3.4 0.16 ha sample plot layout.

To improve manageability, each 0.16 ha plot was further subdivided into a matrix of 16 sequentially numbered 0.01 ha plots (10 x 10 m), as illustrated in Figure 3.4. The four corner points of each 0.01 ha plot were marked with a wooden stake and carefully surveyed, using a digital distance-measuring device (Vertex hypsometer). The dimensions of each plot were checked, by measuring the distance between two diagonal stakes. If the dimensions of the sample plot were correct then this distance should have been equal to 14.14 m. Every tree in a plot was labelled, using a plastic marker with an identification ID that included the plot and tree number. This allowed each tree to be clearly identified, which is important when the biophysical and tree position measurements are made separately.

In addition to this dataset, sixty, 0.02 ha circular sample plots were established for reference (30 plots) and validation purposes (30 plots) in the Kielder study area and a further twenty in the Galloway study area. The boundary of these plots was 7.98 m from the centre and this was also determined using a digital distance-measuring device (Figure 3.5). The tree marking method used on the 0.16 ha plots was also followed for the 0.02 ha plots

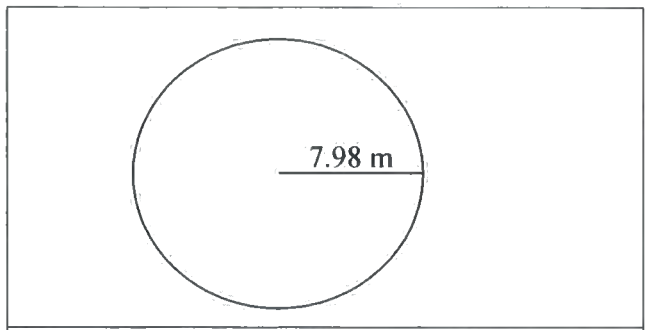

Figure 3.5 0.02 ha circular sample plot layout

3.3.2 Position of ground sample plots

Plot centres were re-surveyed using a Leica series 300 dGPS (Figure 3.6). This system is a differential GPS with the ability to provide positional data to an accuracy of ± 0.05 m when the antenna's view of the sky is unobstructed.

Figure 3.6 Differential GPS measurement of sample plot centre.

The differential GPS comprises two units, one set up as a reference receiver and the other as a rover unit, as illustrated in Figure 3.7. The reference station records the range measurements broadcast by the GPS constellation and compares this with the actual site coordinates. The range corrections are then calculated using the phase difference of the two carrier waves, L1 and L2 (19.05 and 24.45 cm respectively), between the reference station and the satellite. Once the phase difference has been resolved, it is possible to provide these range corrections to the rover GPS unit. One constraint is that the rover GPS receiver must be operated in close proximity to the GPS station, to ensure that any satellite orbit and atmospheric delay (ionosphere and troposphere) errors are common to both (Dye and Baylin 1997).

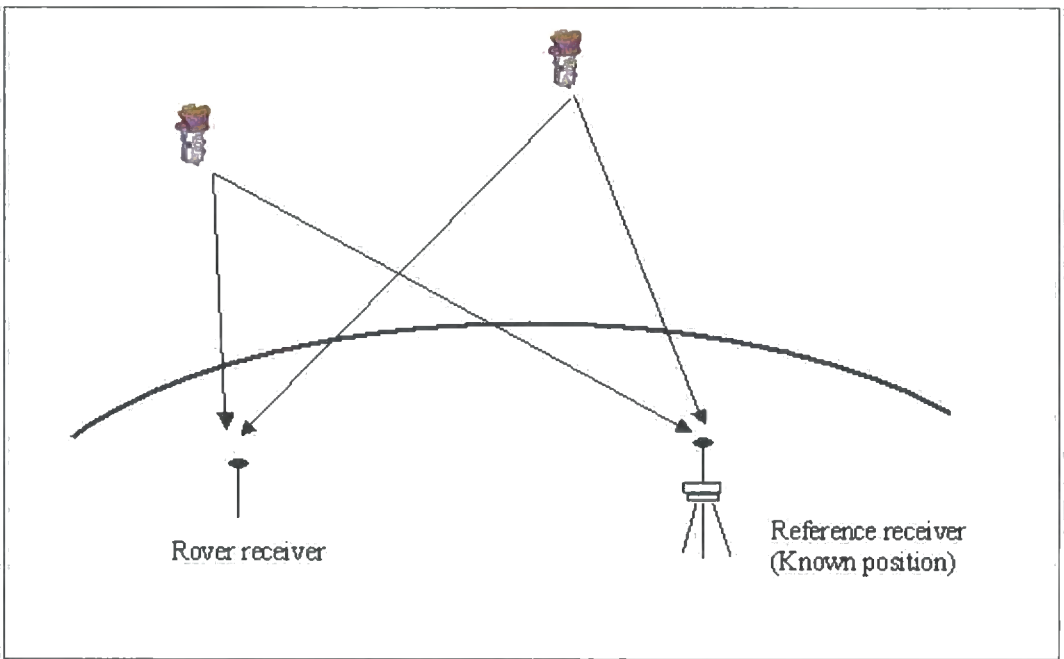

Figure 3.7 Differential GPS arrangement used to acquire sample positions.

A temporary benchmark was established in the study area, because the distance to the Ordnance Survey (OS) permanent GPS reference stations was greater than the recommended 50 km. The precise position of the temporary benchmark was obtained by recording 5 hours of data, in the same location, over a two-week period and post-processing these data with corresponding measurements collected by the OS GPS reference stations. Recording data over a two-week period eliminates errors in position coordinates caused by atmospheric delay. After correction, the horizontal and vertical accuracy of the benchmark was thought to be ± 0.05 m, which is more than adequate for this application.

Sample plot positions were measured using two different GPS surveying techniques, static and kinematic. The static method was used in closed canopy forest, because of the difficulty in maintaining a constant, uninterrupted signal. The procedure adopted involved elevating the GPS antenna into the canopy, using an 8-metre telescopic aluminium pole. The pole was positioned over the middle of wooden stakes marking the plot centre or plot boundary. Observations were recorded at 1-second intervals and continued until the L1 and L2 phase difference had been resolved. The time taken to resolve the phase difference depended on the number and elevation of the available satellites. Typically, 15 to 40 minutes was required to calculate an accurate position (± 0.40 m) for each point. Calculation of the positional accuracy was based on the average error of four repeat surveys.

The kinematic technique was used in younger plantations (i.e. less than 10 m in height) where it was possible to maintain the GPS signal as the antenna's view of the sky was not obstructed. The kinematic process involves initialising the GPS on the benchmark; once this position has been determined subsequent points can be surveyed relatively quickly, provided that the GPS signal is uninterrupted.

3.3.3 Position of individual trees

The position of every tree within the sample plot was determined directly, using GPS or through the application of trigonometric principles. The method adopted depended on the height of the trees and the density of the forest canopy. For sample plots located in closed canopy forest, where it was difficult to receive a constant GPS signal, tree positions were determined using the distance and angle measurement of the tree relative to the plot corner, marked by a wooden stake (Figure 3.8). The calculation involves two parts, firstly resolving the angle between each tree and the corner post using the law of cosines (Equation 3.1) and secondly, using Pythagoras' theorem to determine the x and y offset (in metres) of each tree from the selected post, by calculating h and i as illustrated in Figure 3.8.

$\cos B = \frac{(a^2 + c^2 - b^2)}{2ac}$	Equation 3.1 The law of Cosines

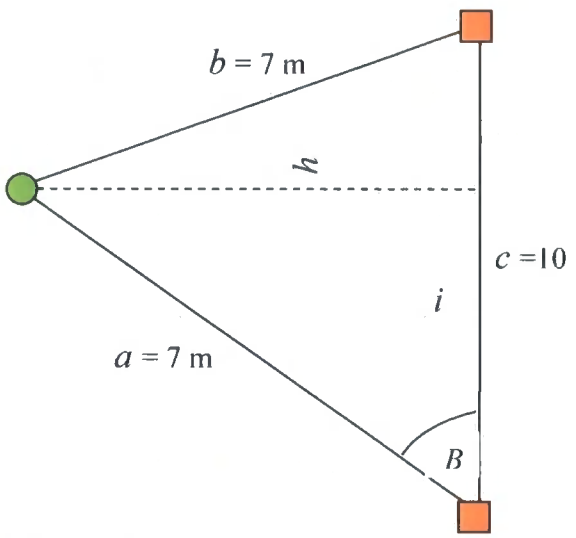

Where:

Corner post (known position)

Tree stem (unknown position)

From equation 3.1

Angle $B = 44.4°$

Calculate h and i to give tree position in x and y

$h = \sin(B) \times a$

$i = \cos(B) \times a$

Figure 3.8 Positioning of trees in closed canopy plots.

In the example shown in Figure 3.8 the tree position is offset by 4.8 m in x and 5 m in y.

In the smaller 0.02 ha circular plots tree positions were determined by their distance and bearing from the plot centre or edge, which was a known differential GPS reference point (Figure 3.9). Tree distance was measured using a digital distance-measuring device and bearing was measured using a prismatic compass, with an expected standard error of up to 0.30 m.

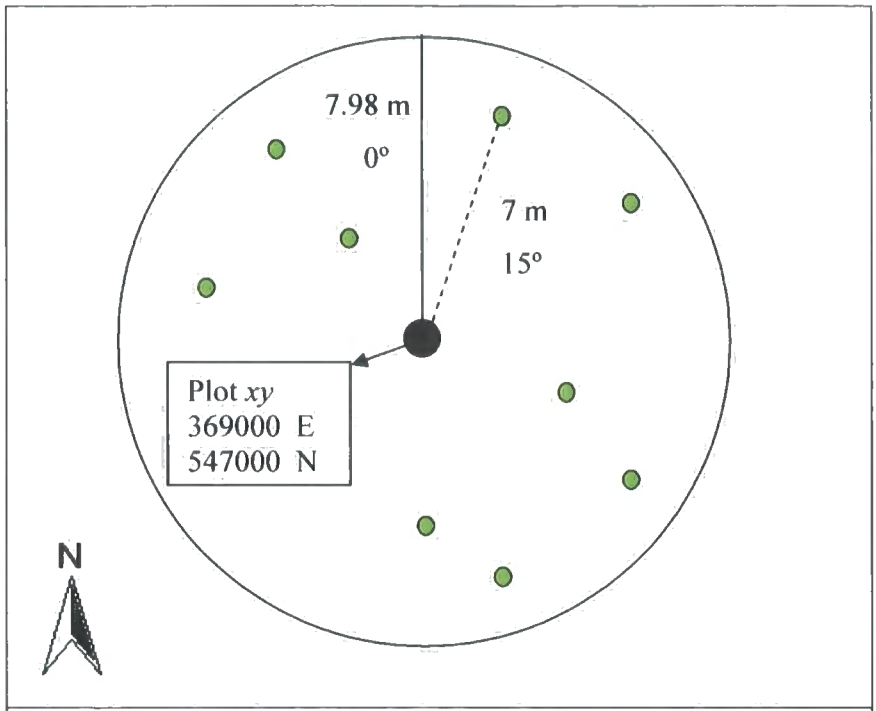

Figure 3.9 Individual tree positions in 0.02 ha plot.

Taking into account the positional accuracy of the differential GPS unit for determining the location of the plot centre, the maximum error of a tree's position is expected to be 0.70 m.

3.4 Measurements of forest structure

Forest measurements included those usually made as part of a standard forestry inventory, such as tree diameter and height. In the Kielder study area more detailed measurements were also made, that characterised the size and structure of the tree crown, as discussed in section 3.4.2. In the Galloway study area only standard inventory plot measurements were made (tree diameter and height), as the principal use of this dataset was to provide information on species composition and dominance. These plot data are used for species identification in Chapter 7.

The Forestry Commission's forest compartment database was used to provide information on species and planting date. Tree measurements were recorded digitally, using a handheld computer that synchronised and downloaded data to a relational database. Table 3.3 provides summary information from the Kielder and Galloway plots measured in 2003; a description of each measurement and the equation used to derive it follows.

Table 3.3 Summary of standard forest inventory measurements by study area

Study area	Description	Units	Mean	S.D	Min.	Max.
Kielder						
Age	Crop age	years	24.0	18.6	9.0	60.0
dbh	Diameter	cm	19.8	2.8	14.0	25.2
G	Basal area	m^2/ha	56.2	10.9	26.2	80.0
h	Mean height	m	11.4	6.8	1.5	22.0
h_{dom}	Top height	m	14.5	8.0	3.4	25.5
N	Tree density	trees/ha	3,055	2,188	1,150	12,300
V	Volume	m^3/ha	561	102	309	742
Galloway						
Age	Crop age	years	35	5.5	33	48
dbh	Diameter	cm	17.8	3.3	11.71	24.23
G	Basal area	m^2/ha	56.6	12.1	33.3	74.5
h	Mean height	m	-	-	-	-
h_{dom}	Top height	m	19.2	3.0	13.5	23.9
N	Tree density	trees/ha	2,154	401	1,428	2,809
V	Volume	m^3/ha	480	156	189	697

3.4.1 Standard inventory measurements

(i) Diameter and basal area

Diameter at breast height (*dbh*) is defined as the girth at 1.3 m above ground level. On sloping ground the accepted convention is to measure ground level from the upper side of the tree; for leaning trees the measurement should be from the ground level on the under side of the tree (Hamilton 1975). In every plot, all trees greater than 7 cm were measured to the nearest one cm using a diameter tape. The basal area of the stem at breast height was calculated using Equation 3.2 and from this basal area per hectare was derived.

Where: g = basal area of tree i, m^2/ha dbh = diameter at breast height, m	$g = \frac{\pi}{40000} dbh^2$	Equation 3.2 Basal area

(ii) Tree height

In the Kielder dataset total height of all trees was measured regardless of diameter. This is a departure from a standard inventory where only a sample of tree heights would be measured in each plot. However, it enabled the spatial location and height of every tree in the sample to be plotted and compared to the LiDAR height values. Height was measured using a Vertex hypsometer, with care taken in densely stocked plots to identify the top of each tree.

In the Galloway dataset only the top height (h_{dom}) trees in each plot were measured. Top height is defined as the average height of the 100 largest diameter trees in each hectare. This is commonly used as an indicator of site quality, since it is relatively unaffected by tree thinning operations (Philip 1998). Using the same ratio, top height was calculated by taking the average height of the two trees with the largest diameter in each 0.02 ha plot.

(iii) Tree dominance (recorded in the Kielder dataset only)

Each tree was classified using a classification method (Bechtold 2003) based on tree crown size and proximity to neighbouring trees. Five crown classes are typically used in forestry: dominant, co-dominant, sub-dominant, suppressed and dead. These are described in detail below and illustrated in Figure 3.10.

Dominant - Trees with crowns that extend above the average of the tree crowns and receive light from directly above and some from the sides.

Co-Dominant - Trees with crowns that form the general level of the crown cover and receive full light from the top, but very little from the sides.

Sub-Dominants - Trees that are shorter than dominants and co-dominants, but their crowns extend into the canopy of dominant and co-dominant trees. They receive little

direct light from above and none from the sides. As a result, intermediates usually have small crowns and are very crowded from the sides.

Suppressed - Trees with crown entirely below the general crown level and receiving no direct light from either above or below.

Dead - No live tree crown.

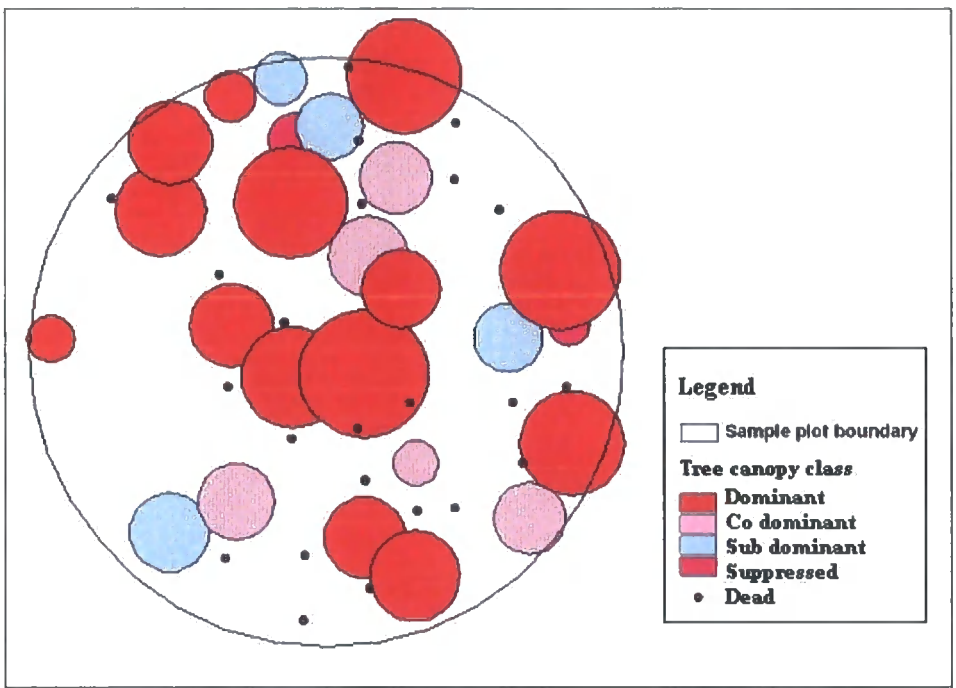

Figure 3.10 Plan view of 0.02 ha sample plot trees classified by dominance in Kielder forest.

(iv) Tree density and volume

The variable tree density (*N*) is based on all trees in the sample plot regardless of whether they are dead or alive. Stocking levels were typically greater than 2,000 trees/ ha, but reached 12,300 trees/ha in areas with high levels of natural regeneration. At a tree density of 2,000 trees/ha the rate of mortality increases as the crop height increases, with mortality higher in species mixtures (up to 48%) compared with pure species (<30%). Tree volume was calculated using the Forestry Commission method from their Forest Mensuration Handbook (Hamilton 1975). In this method, volume estimates are derived from the product of basal area (*G*) and tree form height. Form height is in turn the product of mean height of the plot (*h*) and the crop form factor[6]. Thus, the product of tree basal area, tree height and form factor gives an estimate of tree volume. Tree

[6] A form factor is a summary of the overall stem shape and is expressed as the ratio of a tree's volume to the volume of a specified geometric solid of similar basal diameter and height. Most commonly, the form factor of a tree is based on a cylinder.

volumes were only calculated for sample plots where the tree diameter was greater than 7 cm and therefore had been recorded. In Kielder, volume ranged from 309 to 742 m^3/ha and the average volume was 506 m^3/ha. While a narrow range in crop age was measured in the Galloway dataset, the plots show a larger variation in volume (189 to 697 m^3/ha); a range that is typical of mixed species plantations and better performing pure Sitka spruce crops.

3.5 Correlation between tree height and standard forest inventory measurements

Many of the measured structural variables and their derivatives are strongly correlated with height and are inter-dependent (Table 3.4). These facts are well documented in forestry and such relationships are routinely used to provide estimates of woodland growth and volume (Philip 1998). Estimates are typically made using growth models developed from allometric relationships between variables, such as tree diameter at breast height (*dbh*), tree top height and density. Often the data used to derive these models are based on measurement of permanent research plots, established over a range of tree species and site conditions.

Table 3.4 Correlation between height and standard forest inventory measurements: Kielder forest reference dataset.

Variable ($n = 60$)	Description	h	Age	dbh	G	h_{dom}	N	V
h	Mean height	1.00						
Age	Crop age	0.90	1.00					
dbh	Diameter	0.80	0.88	1.00				
G	Basal area	0.68	0.28	0.63	1.00			
h_{dom}	Top height	0.90	0.95	0.67	0.67	1.00		
N	Tree density	–0.56	–0.50	–0.79	–0.16	–0.54	1.00	
V	Volume	0.54	-	0.30	0.95	0.78	0.16	1.00

The strongest correlations are between mean height (h) and other measures of height such as top height (h_{dom}) with a correlation of 0.90. This is expected, as the measures of height are related. h and *dbh* are also strongly correlated, as shown in Figure 3.11, with *dbh* increasing proportionately with increases in tree height.

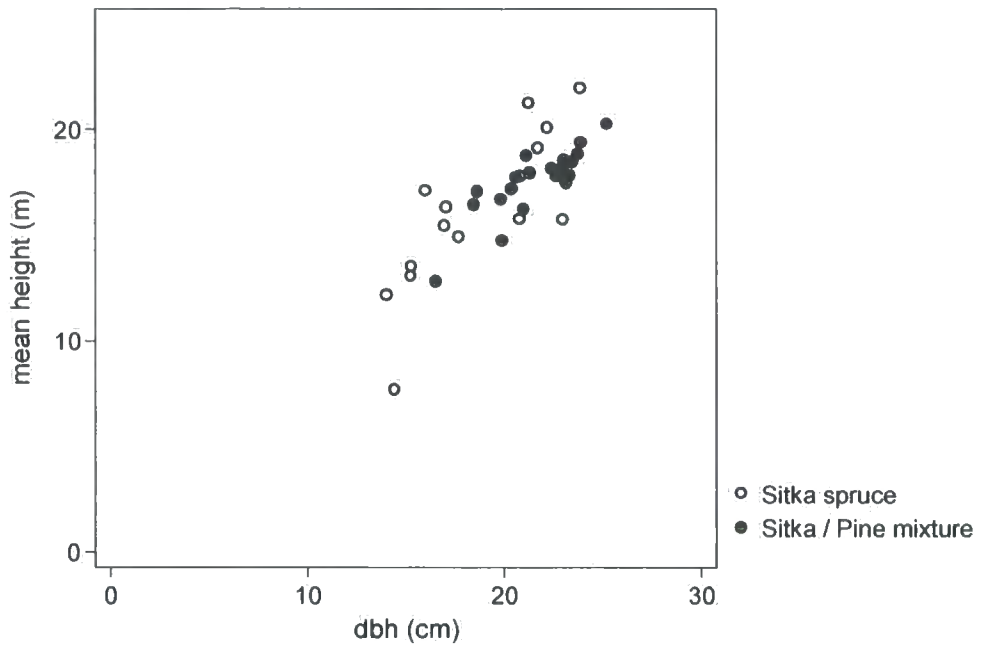

Figure 3.11 The relationship between mean height and *dbh:* Kielder forest reference dataset.

A similar trend is also observed between h and basal area (G) and crop age. Weaker correlations are noted between tree density (N) and volume (V), indicated by coefficients of –0.56 and 0.54 respectively. Removal of the two sample plots with high levels of natural regeneration (>12,000 trees/ha) changes the correlation between h and tree density from –0.56 to –0.81. The correlation between *dbh* and N is also strong (r = –0.75) as shown in Figure 3.12 with *dbh* increasing as N decreases. Strong correlations are also observed between G and V and h and V.

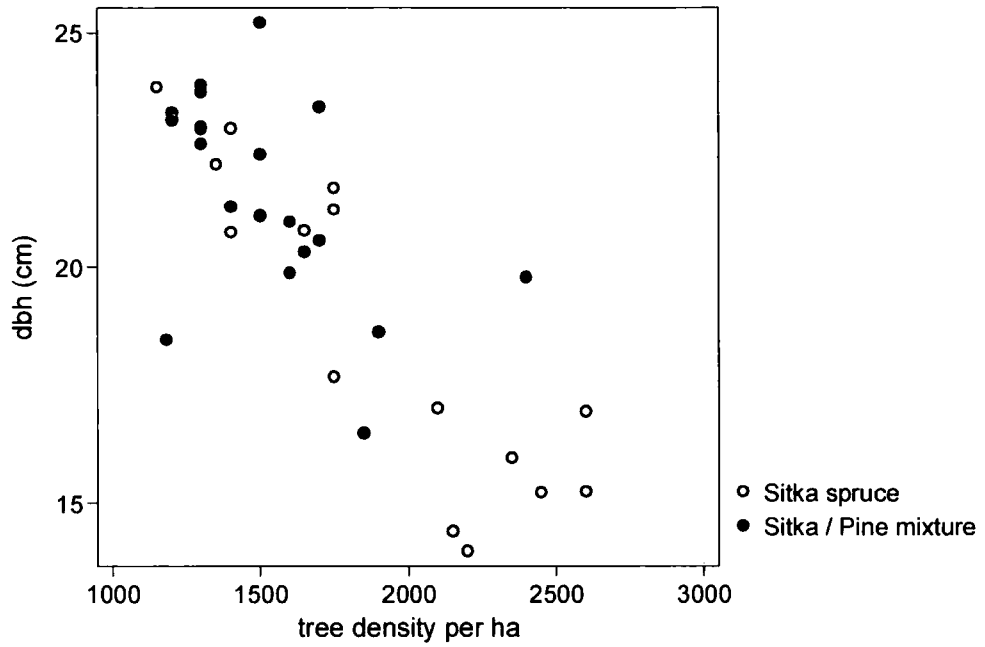

Figure 3.12 The relationship between *dbh* (cm) and tree density (trees/ha): Kielder forest reference dataset.

3.5.1 Measurements of forest canopy structure

Measurement of forest canopy structure is not routinely carried out as part of a forest inventory. However, measurements of tree crowns have been used extensively in research, as indicators of the health and vigour of forest trees (Zarnoch et al. 2004). The purpose of collecting canopy measurements was to (i) investigate how the canopy structure affects the penetration of LiDAR pulses through dense forest stands, and in turn the accuracy of LiDAR-derived height estimations and (ii) compare the canopy structure of pure species crops and species mixtures (iii) find a field-based measure of canopy structure that adequately describes the forest structure and that can be measured using LiDAR (focus of Chapters 6 and 7).

In the field, three direct measurements of tree canopy structure were recorded, crown width (K), length (K_l) and height (K_c), as illustrated in Figure 3.13. All tree crown measurements were made in accordance with the methods published by Philip (1998).

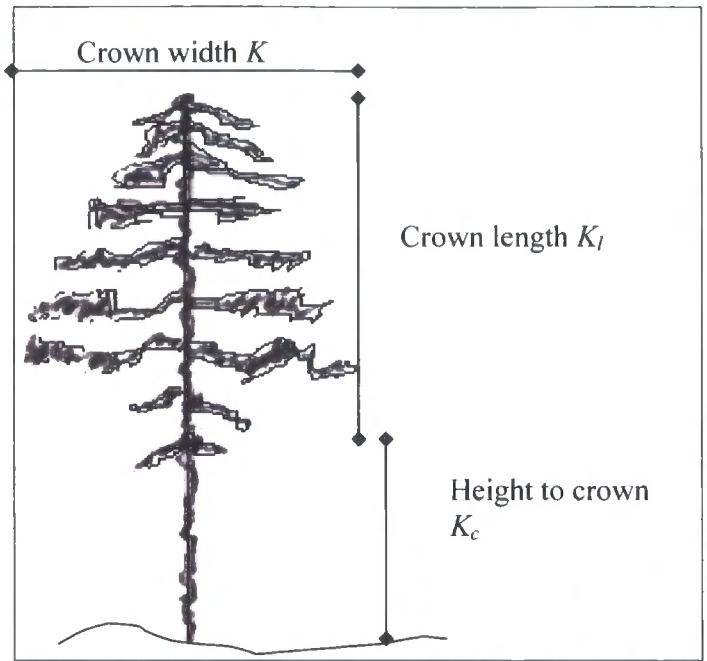

Figure 3.13 Canopy measurement illustration

From these measurements an additional three ratio variables, live crown ratio (K_g), crown to tree diameter ratio (Kd) and crown cover (K_a), were derived, using the direct measures of canopy structure. In the case of the ratio variables, tree height and diameter data were also used. Table 3.5 provides a summary of the canopy measurements. A detailed description of the methods adopted is provided in the following sections.

Table 3.5 Summary of forest canopy measurements: Kielder forest reference dataset.

Variable (n = 58)	Description	Units	Mean	S.D	Min.	Max.
K	Crown width	m	2.5	0.8	0.9	4.6
K_l	Crown length	m	4.8	1.9	1.5	9.6
K_c	Height to canopy base	m	6.2	5.8	0	16.8
K_g	Live crown ratio	%	60.3	33.4	18.0	100
Kd	Crown/ tree diameter ratio	-	26.6	14.8	9.0	49.0
K_a	Crown cover	%	74.0	12.5	43	105

(i) Crown width and length

The crown width (K) of all living trees in the plot was measured. Crown width was determined as the average of two perpendicular crown diameters, across and along the planting row. The dimensions between opposing edges of the crown were taken using a distance measuring device (Equation 3.3).

$K = \frac{(K_1 + K_2)}{2}$	Equation 3.3 Crown width

Crown length is the distance along the main axis from the tree tip to the base of the crown. It is obtained by subtracting the total tree height from the height to the lowest green whorl of branches (K_c) (Equation 3.4).

Where: K_l = live crown height, m h = total tree height, m K_c = height to crown, m	$K_l = h - K_c$	Equation 3.4 Crown length

Live crown ratio (K_g) is calculated by dividing total tree height by live crown height (m) (Equation 3.5). It is defined as the percentage of the canopy supporting live green foliage and is a measure of site capture.

Where: K_g = live crown ratio, % h = total tree height, m K_l = live crown height, m	$K_g = \frac{h - K_l}{h} \times 100$	Equation 3.5 Live crown ratio

The crown width (K) to *dbh* ratio (Kd) is calculated by dividing the canopy width by the tree *dbh*. It provides a measure of the productive capacity of the site in terms of basal area growth and has been found to vary between species (Philip 1998).

Where: Kd = Crown to diameter ratio K = Crown width, m *dbh* = Diameter breast height, m	$Kd = \frac{K}{dbh}$	Equation 3.6 Crown to diameter ratio

(ii) Crown cover

Crown cover (K_a) is used as a measure of canopy density and competition. It is determined by measuring the area of ground covered by tree canopies (K), excluding overlap and gaps within individual canopies. This was plotted in a GIS using K to set a circular buffer distance from the stem position. It should be noted that this can only be considered an approximation of the crown shape since it is rare to observe circular tree crowns in even-aged conifer plantations. More often the crowns grow along or across rows in the direction of forest gaps. An indication of variation in canopy shape can be provided through calculating the overall variation between the two crown width measurements used to calculate K. For young crops (<10 m) where the amount of sunlight is not restricted there is little canopy width variation at this growth stage, but as the canopy closes light availability decreases, which can lead to irregular shaped crowns. Overall canopy width differences in closed canopy crops at the plot level range from 0.9 to 4.6 m with an average of 2.5. Figure 3.14 shows an example of a closed canopy plot located in a mature Sitka spruce/ pine species mixture, planted using a 3x3 species matrix (i.e. 3 rows of pine, then 3 rows of spruce). Sitka spruce is the dominant species, with the majority of the pine in an advanced stage of decay. Green circles denote the extent of Sitka spruce crowns; red circles denote lodgepole pine crowns; black points denote the location of dead trees.

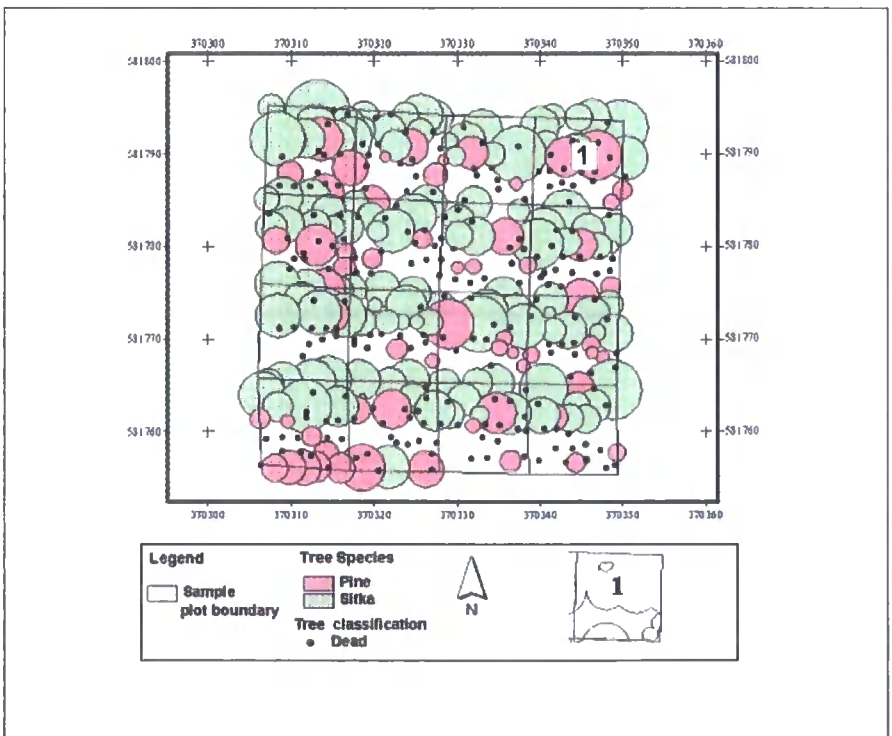

Figure 3.14 Distribution and size of tree crowns in a plantation mixture: Kielder forest reference dataset.

To estimate plot area occupied by the canopy, individual crowns were merged to eliminate the overlap between adjacent crowns and clipped to the plot extent. An example for one plot is presented in the legend of Figure 3.14 (plot marked 1). However, owing to the difficulties in estimating canopy cover as described above and it's poor correlation with other forest variables this measure was not used for further analysis (See Table 3.6)

(iii) Canopy closure

Estimates of canopy closure can be made using a range of techniques and specialist instruments. These range from digitising hemispherical photography, taken using a fish-eye lens, to more sophisticated instruments designed to measure below-canopy light conditions. Both methods are typically used to provide estimates of leaf area index (LAI) or canopy gap fraction. However, a simpler estimate of canopy closure can be calculated by recording the type and proportion of understorey vegetation present in each sample plot. This research used this simpler approach to obtain an estimate of the percentage of vegetation cover in each sample plot a 1-metre square quadrat split into 4 equal quadrants were laid out. Plots consisting of less than 50% dead vegetation on the forest floor were classified as closed canopy and those with more than 50% understorey vegetation as open canopy (Puhr & Donoghue 2000).

3.5.2 Correlation between height and canopy structure

Since canopy height is easily estimated from LiDAR, it is useful to determine how the different measures of canopy structure are related to field-measured height; and how the measures of canopy structure differ between forest species. Table 3.6 provides a summary of correlations between mean height and the various measures of canopy structure. The strongest correlations observed ($r \geq 0.70$) are between variables that are derived directly or indirectly from mean height, i.e. crown length (K_l) and live crown ratio (K_g). The weakest relationship is between height and crown cover ($r \leq 0.21$); for these two variables the relationship is non-linear.

Table 3.6 Correlation between mean height and measures of canopy structure: Kielder forest reference dataset.

Variable (n =35)	Description	h	K	K_c	K_l	K_g	Kd	K_a
h	Mean tree height	1.00						
K	Crown width	0.70	1.00					
K_c	Height to canopy base	0.97	0.61	1.00				
K_l	Crown length	0.74	0.76	0.57	1.00			
K_g	Live crown ratio	0.94	–0.61	–0.97	–0.54	1.00		
Kd	Crown/ tree diameter ratio	–0.95	–0.59	–0.93	–0.68	0.95	1.00	
K_a	Crown cover	–0.21	0.29	–0.29	0.08	0.19	0.23	1.00

The relationships between mean height and the measures of canopy structure, K and K_l, are very similar. Figure 3.15 shows the relationship between mean height and K. In pure Sitka spruce, crown width increases with height up to 3 m and then begins to decrease once a mean height of 15 m has been reached. The point where maximum crown width is reached coincides with canopy closure, as measured by the absence (–) or presence (+) of ground vegetation. Beyond canopy closure tree competition limits further crown development and consequently crown width becomes smaller. Crown width is more variable in the species mixtures, where Sitka spruce starts to dominate the site and the presence of the pine diminishes. In these mixed stands the Sitka crowns are larger than in pure Sitka spruce stands of the same height.

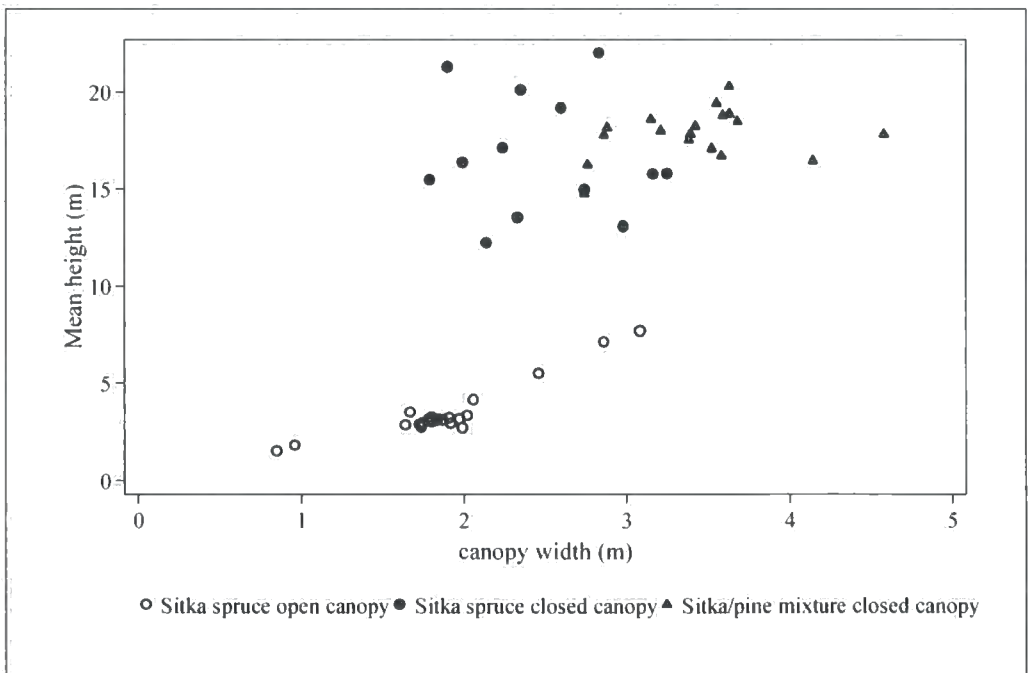

Figure 3.15 Relationship between mean height and crown width: Kielder forest reference dataset.

The two ratios of K_g and *Kd* are negatively correlated with mean height, as indicated by Figures 3.16 and 3.17.

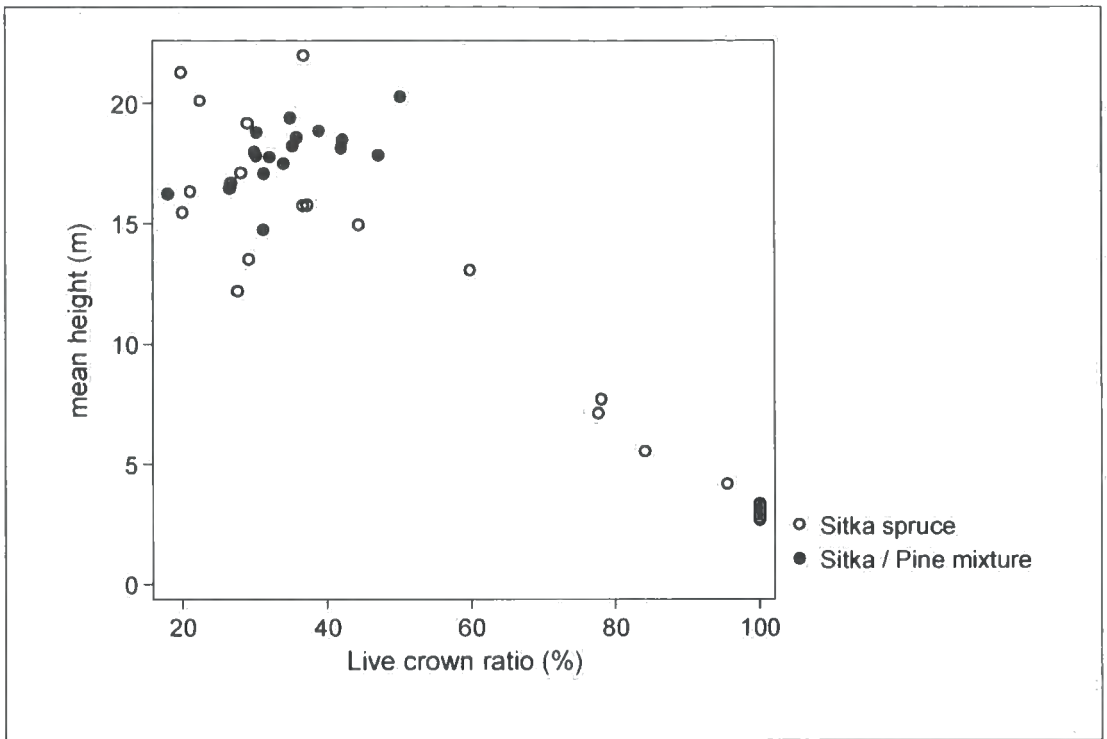

Figure 3.16 Relationship between live crown ratio and mean height: Kielder forest reference dataset.

In the case of K_g, larger live crown ratios are generally associated with healthier, faster-growing trees. The decline in crown ratio is therefore related to tree competition in dense stands, causing the overall crown length to decrease as trees increase in height. More variation in K_g is observed in species mixtures than in pure Sitka stands, where higher tree mortality opens the canopy and the remaining tree crowns expand to fill the gaps. The result, as shown in Figure 3.17, is a clumpy canopy structure, with gaps emerging where the pine has died.

Kd follows the same trend as K_g with the ratio decreasing in a linear fashion as tree height increases. Higher ratios are observed in newly established trees, which have larger canopies in relation to their tree diameter. As tree height increases, the size of the tree canopy decreases, but tree diameter continues to increase (Figure 3.18). The main outliers in the graph are located within the plantation mixtures. Trees in these plots have larger canopies, resulting in higher ratio values for any given height.

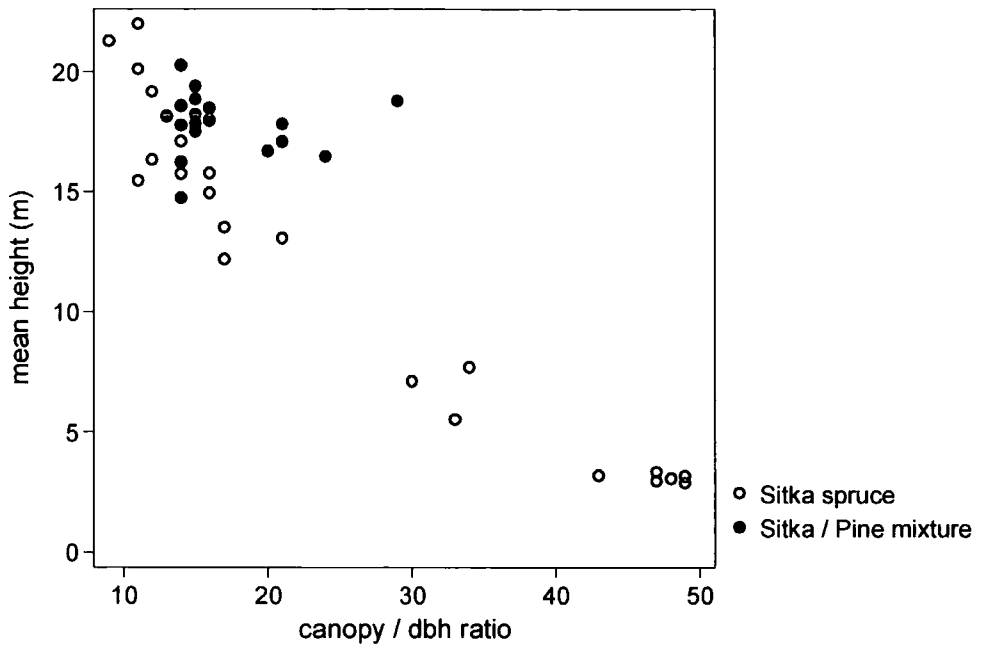

Figure 3.17 Relationship between crown to diameter ratio and tree height: Kielder forest reference dataset.

The relationship between h and canopy area (K_a) is non-linear. K_a increases quickly as the trees establish, peaking at canopy closure (approximately 10 m canopy height) and then declining as mortality increases due to tree competition (Figure 3.18). Whilst some variation in canopy area between pure Sitka spruce of similar ages is observed, the species mixtures are more variable, ranging from 57 to 92%. As with K_g, tree competition is the main factor affecting K_a with the presence of pine diminishing as the Sitka begins to dominate the stand.

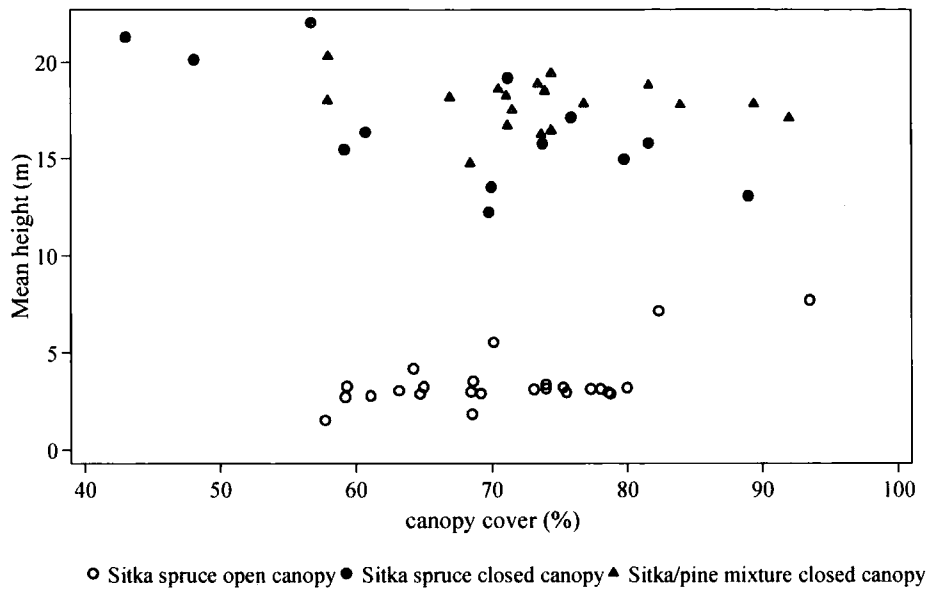

Figure 3.18 Relationship between mean height and canopy cover: Kielder forest reference dataset.

3.6 Summary

The sampling strategy focused on selecting plantations representative of a range of crop ages and species. The position of field plots and trees was accurately identified, to enable the formation of relationships between field plots and remote sensed data. Verification by repeat survey measurements in open forest canopies indicated that plot centres and individual trees were accurate to ± 0.05 m. In closed canopy plots, the positions of plot centres and individual trees was accurate to ± 0.40 m and ± 0.30 m respectively, summing to a total positional error of ± 0.70 m. In closed canopy crops this level of accuracy should enable the location of individual trees.

Analyses of standard inventory measurements reveal some differences in growth between species mixtures and pure species crops. Species mixtures generally have wider and larger tree canopies than pure crops, punctuated by structured gaps where the pine portion of the mixture is in decline. The most promising measures of canopy structure are the simplest; canopy length, canopy to *dbh* ratio and live crown ratio all provide useful measures for describing canopy density. Conversely, crown area is weakly related to other structural variables and for this reason it is not used here in further analysis. The accuracy of LiDAR height estimations derived from selected canopy measures is investigated in Chapter 5. In Chapter 6, LiDAR-derived canopy

density measures are developed based on empirical measurements and in Chapter 7 these measures are used to differentiate species mixtures.

Chapter 4: LiDAR, optical image data & processing

4.1 Introduction

The main objective of this chapter is to describe the LiDAR and optical image datasets and processing methods used in this research. The datasets comprise medium-resolution Landsat 7 ETM+ (30 m) and SPOT 5 HRG (10 m), high-resolution IKONOS (4 m) satellite imagery and airborne Light Detection and Ranging (LiDAR) data. These provide a representative cross-section of image data currently available on the commercial market, in terms of cost, as well as spatial, radiometric and spectral resolution.

The focus of the research is to evaluate the potential of different image data for providing estimates of forest height and structure. Specifically it assesses the application of LIDAR data to providing estimates of forest height, volume and tree density, and the application of SPOT 5 HRG data to identifying forest plantation mixtures. Landsat 7 ETM+ and IKONOS data are used to provide estimates of forest height. The first stage in this process is to prepare images for use in quantitative analysis. Different processing methods are applied to LIDAR and optical satellite images, which reflect the different modes in which the data are acquired. Regardless of image data type, the objective at the end of the image processing chain is to extract laser points or image pixels over the field sample plot. Using these data, estimates are derived from empirical relationships between field observations and image data.

This chapter is divided into two sections: firstly, a description of the image data; and secondly, an explanation of the processing steps for each of LIDAR, Landsat 7 ETM+, SPOT 5 HRG and IKONOS data.

4.2 LiDAR and optical image data

The data used in this research offer a range of spatial, radiometric and spectral resolutions to forest remote sensing, as summarised in Table 4.1. The area covered, sensor revisit period and cost also vary between the sensors with a tendency for the coverage to decrease (or be customised) and for cost to increase as the resolution increases. Forest mapping or estimates of forest variables at the forest compartment level are usually made using cheaper large-scale medium-resolution imagery (10 to 30

m) such as Landsat 7 ETM+ and SPOT 5 HRG, while finer resolution image data such as
IKONOS (1 m panchromatic band and 4 m multi-spectral capability) and LiDAR can provide more detailed assessments of forest structure. One characteristic of LiDAR that differentiates it from Landsat, IKONOS or any other passive optical sensor is its ability to provide both horizontal and vertical information on vegetation structure.

All of the optical satellite sensors considered in this research have almost identical spectral band passes in the blue-green, green, red, near infrared and panchromatic bands. Landsat 7 ETM+ also records data in the short-wave infrared and thermal wavelengths (Table 4.1). The Airborne LiDAR used also records the near infrared intensity of the laser pulse, but strictly speaking these data are not radiometrically calibrated to a standard (discussed further in Chapter 7). As the wavelengths measured by the sensors overlap (see Table 4.1), sensors with different spatial and radiometric resolutions can be compared. However, in this research, only multi-spectral bands located in the visible, near infrared and short-wave infrared and the Galloway LiDAR near infrared data are used.

Table 4.1 Characteristics of LiDAR, IKONOS, SPOT 5 HRG and Landsat 7 ETM+ data.

Spectral band(s) (nm)	Pixel size.	FOV	Re-visit Period	Operational Coverage
LiDAR Optech 2033 and 3033				
1064	0.20 m, at 1,000 m	User defined	User defined	First 2033 system delivered in 2001
IKONOS Panchromatic				
530-930	1 m	11 x 11 km at nadir	3-5 days off-nadir 140 days nadir	September 1999 to present
IKONOS Multi-spectral				
Band 1 Blue/Green: 450-520	4 m			
Band 2 Green: 520-600				
Band 3 Red: 630-690				
Band 4 Near IR: 760-900				
SPOT 5 HRG Panchromatic				
480-710	5 m	60 x 60 km	5 days off-nadir 26 days nadir	May 2002 to present
SPOT 5 HRG Multi-spectral				
Band 1 Green: 500-590	10 m			
Band 2 Red: 610-680				
Band 3 Near IR: 780-890				
Band 4 SWIR: 1580-1750				
Landsat 7 ETM+ Panchromatic				
520-900	15 m	185 x 175 km	16 days	April 1999 to present. Line scanner correction defect on all data after May 31st 2003
Landsat 7 ETM+ Multi-spectral				
Band 1 Blue/ Green: 450-520	30 m			
Band 2 Green: 520-600				
Band 3 Red: 630-690				
Band 4 Near IR: 760-900				
Band 5 SWIR: 1550-1750				
Band 6 Thermal: 2080-2350	60 m			
Band 7 SWIR: 1040-1250	30 m			

4.2.1 Airborne Light Detection and Ranging

LiDAR is an active remote sensing technique that measures distance to a target. As the speed of light is constant, LiDAR records the time taken for a laser pulse to reflect back from the target to the sensor. This time measurement is then converted to an accurate distance or slant range (e.g. 1 ns time = 15 cm). LiDAR systems can be divided into two general modes of operation: continuous wave (CW) and pulsed (Baltsavias 1999a). They are distinguished in part by the size of the laser footprint (the area illuminated by the laser on the ground), which is typically smaller for pulsed systems (0.10 - 1 m) than

for CW systems (10 – 100 m) (Hudak et al. 2002). Continuous wave laser systems emit a continuous wave of light, which is converted into travel time by measuring the phase change in the transmitted signal (Wehr and Lohr 1999). In contrast, pulsed laser systems measure discrete returns (up to five) or digitise the full-waveform. According to Lim et al. (2003), in 2003 only one commercial CW laser system existed. This system, the Scanning Laser Altitude and Reflectance Sensor (ScaLARS), was developed and is operated by the Institute of Navigation, University of Stuttgart. However, by 2004 continuous wave capability was also added to the Swedish TopEye (MK II) and Optech (ALTM 3100) small footprint laser systems.

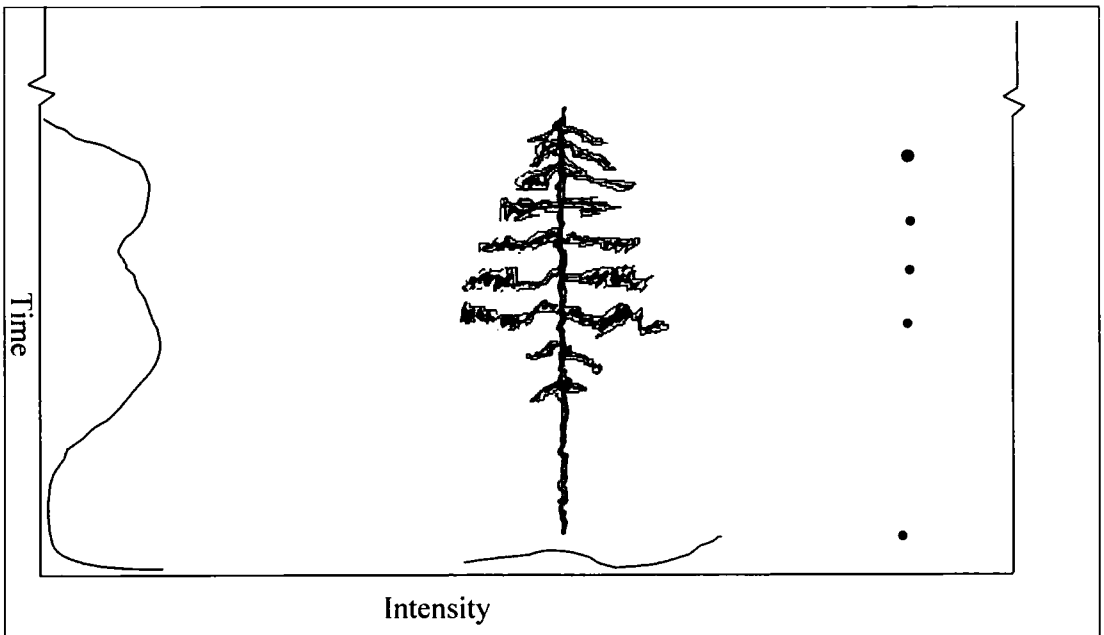

Figure 4.1 Comparison of continuous wave and discrete LiDAR systems. After Lim et al. (2003).

The major components of an airborne laser system include a laser range finder (LRF), scanner, control and processing unit. A Global Positioning System (GPS) and an Inertial Measurement Unit (IMU) are also integrated. The GPS provides the precise location of the aircraft, while the IMU records the roll, pitch and yaw of the sensor (Figure 4.2).

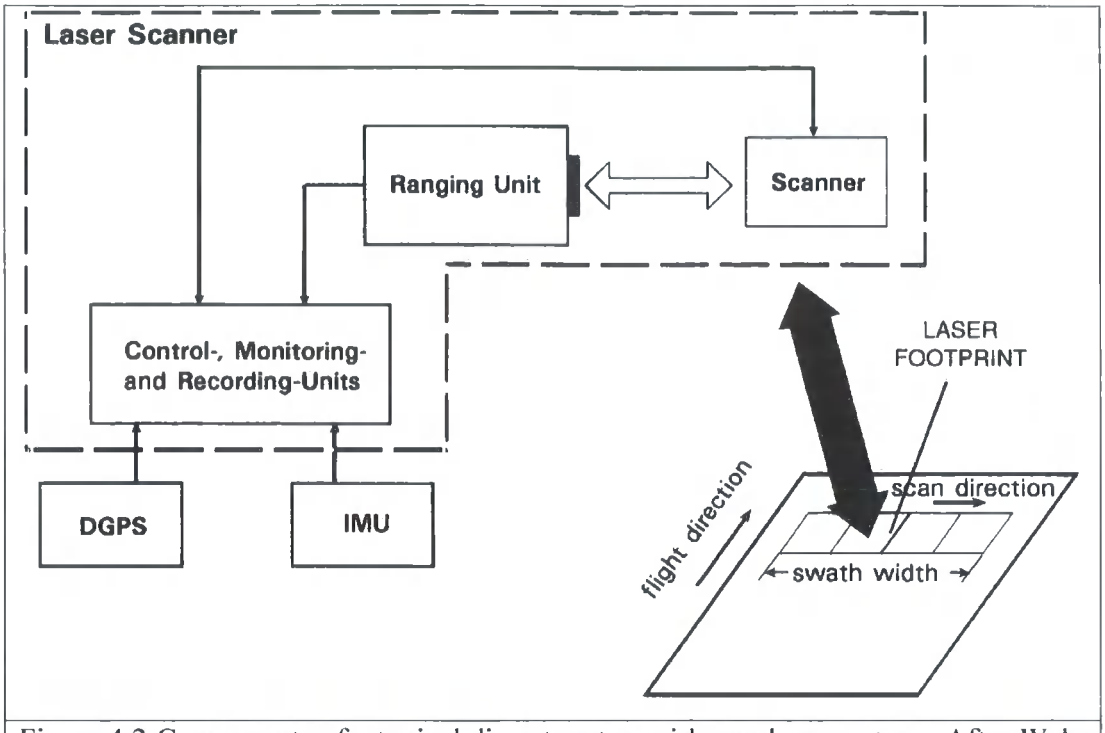

Figure 4.2 Components of a typical discrete return airborne laser system. After Wehr and Lohr (1999).

The first component, the LRF, comprises the emitting laser and receiver. Both share the same optical path ensuring that the field of view (FOV) is the same for both the transmitter and receiver. The laser is able to generate over a short distance a highly directional and powerful pulse of light (pulse laser systems) or a continuous wave of light (continuous wave systems). The optical wavelength of the laser depends on the system design, and may range from 532 nm for bathymetric lasers to 1535 nm for terrestrial lasers. The most sensitive laser detectors are available in the near infrared between 800 and 1100 nm, so most LiDARs used for terrestrial applications operate within this range. The swath width and laser footprint (the area illuminated by the laser on the ground) of the scan for any given height or distance to the target is a function of beam divergence and the instrument's scan angle or FOV (Equation 4.1).

Where: sw = swath width, m h = flying height, m θ = scan angle, °	$sw = 2\,h \tan\left(\frac{\theta}{2}\right)$	Equation 4.1

For example, at a flying height h of 800 m and scan angle θ of 10° the swath width is 140 m. The laser point density depends on the forward speed of the aircraft, sensor altitude and pulse repetition rate.

4.2.2 LiDAR and optical image data

A summary of the image data used over each study area is presented in Table 4.2. The size of each study area is defined by the extent of the area flown by the LiDAR. Consequently, only a small part of the satellite data is used.

Table 4.2 Summary of LiDAR and optical image datasets over the two study areas.

Location	Sensor	Date	Image extent (km)	Study area (km)	Sun elevation / azimuth (°)	Dynamic range (bit)	Sensor scan / off nadir angle (°)
Kielder	IKONOS	03/03/2002	11 x 11	2 x 3	31/163	11	30 Sensor pointing West
Kielder	Landsat 7 ETM+	02/09/2002	185 x 175	2 x 3	41/155	8	0
Kielder	LiDAR	28/03/2003	2 x 3	2 x 3		Not radiometrically calibrated to a standard but most returns 8-bit	10 scan direction E/W
Galloway	SPOT 5 HRG	17/04/2003	60 x 60	1 x 2	44/172	8	16 Sensor pointing West
Galloway	LiDAR	15/06/2003	1 x 2	1 x 2		Not radiometrically calibrated to a standard but most returns 8-bit	9 scan direction E/W

4.2.3 Satellite data

(i) Kielder study area

Over the Kielder study area (6 km^2), the Landsat 7 ETM+ data (path 204 / row 22) was acquired on 2 September 2002 (Figure 4.3) and the IKONOS data on 3 March 2002 (Figure 4.4). IKONOS and Landsat 7 ETM+ follow sun-synchronous and near polar orbits crossing the equator between 10:00 and 10:30 am daily. At the time of

acquisition of the Landsat 7 ETM+ data the sun elevation and azimuth were 41° and 155° respectively. The IKONOS scene was acquired at an off-nadir angle of 30° with the sensor pointing west. If compared to a scene acquired at nadir the ground sample distance decreases from 3.2 m for all multi-spectral bands to 4 m and from 0.82 m in the panchromatic band to 1 m. Also, since the scene was acquired in March (late winter) the sun elevation was 31° with a corresponding sun azimuth of 163°. Consequently, the amount of topographic shadow is more pronounced in the IKONOS image than in the Landsat 7 ETM+ image. This is countered to some extent by the increase in the radiometric resolution of IKONOS which is 11-bits (2,048 shades of grey) compared to the 8-bit of Landsat data (256 shades of grey). The increased dynamic range of IKONOS enables better discrimination between objects in shadow (www.spaceimaging.com, accessed 12/09/04).

The IKONOS data were supplied as a Geo Ortho Kit product, which means that a Rational Polynomial Coefficient (RPC) camera model is also provided in place of the physical sensor model[7], which is kept confidential for commercial reasons. The camera model mathematically describes the mapping from latitude, longitude, and height to line and sample in the image, thereby enabling photogrammetric processing to remove the effects of undulating terrain. The Landsat 7 ETM+ was supplied in level 1G format, meaning that it had been geometrically processed to remove system distortions (but not geometrically corrected to a map projection), radiometrically calibrated to radiance units and finally quantized to digital numbers.

The level of detail between the Landsat ETM + and IKONOS image over the same area is different, as shown in Figures 4.3 and 4.4. On the Landsat scene it is possible to differentiate between large areas of harvesting, young plantations and mature plantations.

[7] Physical sensor models represent the physical imaging process based on orbital information such as the Earth's curvature, atmospheric refraction, and lens distortion. These parameters are used to describe the position and orientation of the sensor relative to the object's position.

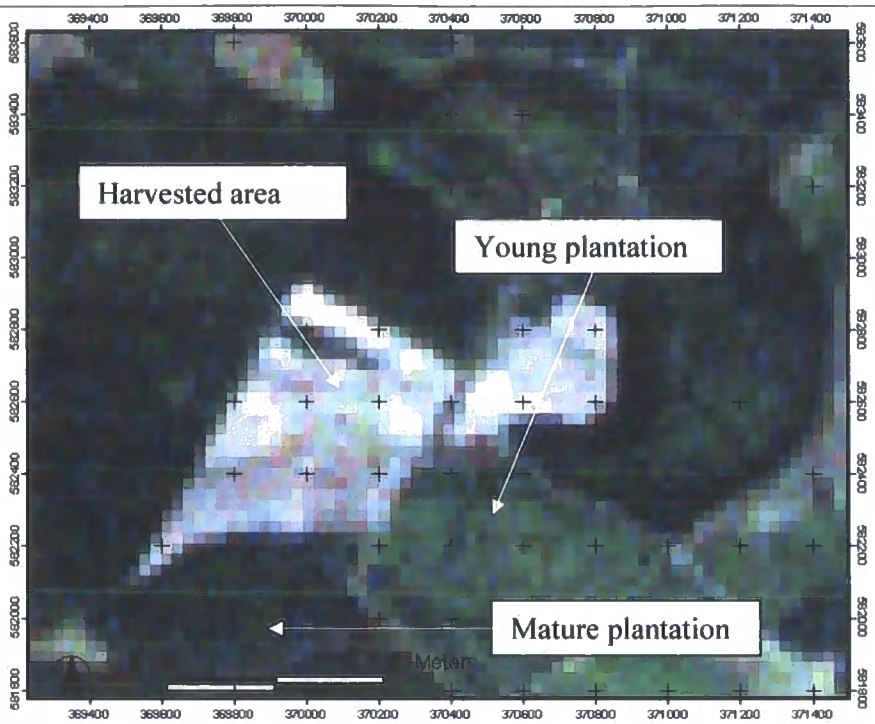

Figure 4.3 Sample of Landsat 7 ETM+ image displayed as a true colour composite using blue/green, green and red spectral bands (display bands 1, 2 and 3).

The improved spatial and radiometric resolution of the IKONOS scene means that the same areas are more clearly identified (Figure 4.4). Replacing the green band in the image composite with the near infrared band further enhances harvested areas. In this example the strong near infrared response is caused by the presence of logging waste. Also, areas of shadow are visible along the north facing edges of plantations due to the sensor's look angle (30°) and azimuth (41°) at the time of collection.

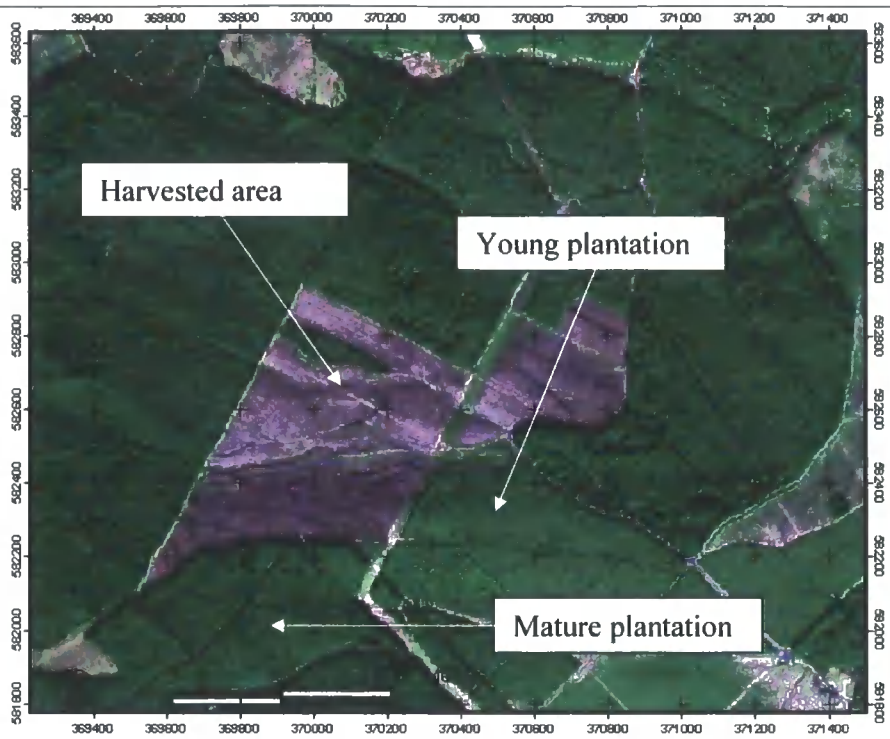

Figure 4.4 Sample of IKONOS image displayed as false colour composite using blue/green, near infrared and red spectral bands (display bands 1, 4 and 3).

(ii) Galloway study area

Over the Galloway study area the SPOT 5 HRG[8] 10 m multi-spectral scene (column 21 / row 238) was acquired on 17 April 2003. The orbit characteristics of SPOT 5 HRG are similar to both Landsat 7 ETM+ and IKONOS with the equatorial crossing time also 10:30 am. At the time of acquisition the sun elevation and azimuth were 44° and 172° respectively. Like IKONOS, the SPOT 5 HRG High Resolution Geometric (HRG) sensor can be pointed off-nadir (up to 30°). Over the study area the data was collected at 16° and therefore there was no change in the spatial resolution of the image. Also, since the topography is predominantly flat (maximum slope is 14°) the off-nadir angle is less important. Like the Landsat 7 ETM+ and IKONOS images, forest and non-forested areas are readily apparent on the SPOT 5 HRG scene. However, the increased spatial resolution enables discrimination of conifer species, areas of variable growth and wind damage, which are not as obvious from visual interpretation of the coarser Landsat 7 ETM+ image (Figure 4.5).

[8] The SPOT 5 HRG was supplied with a similar level of processing (processed to level 1B) as the Landsat 7 ETM+ data.

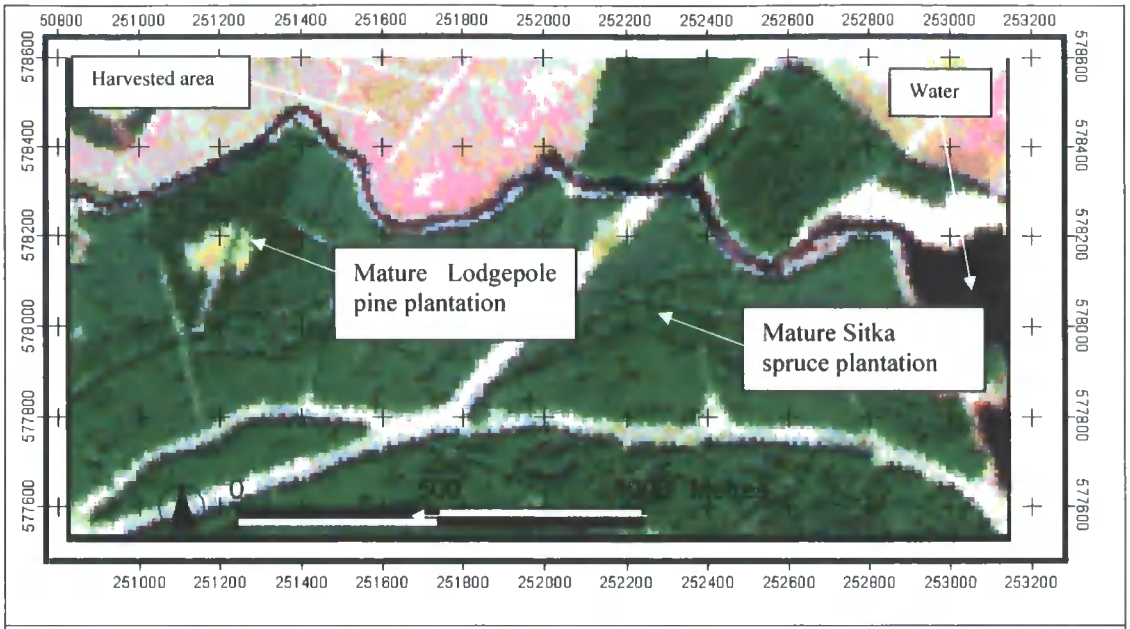

Figure 4.5 SPOT 5 HRG image displayed as false colour composite using green, near infrared and red spectral bands (display bands 1, 4 and 2).

4.2.4 LiDAR data

(i) Kielder forest

The LiDAR data were acquired on the evening of 26 March 2003 (Figure 4.6) by the UK Environment Agency using an Optech ALTM 2033 laser scanning system. The ALTM 2033 is a 33 kHz discrete return system that operates at 1064 nm (near infrared), capturing two returns (first and last) for each laser pulse. The system collects data by scanning perpendicular to the direction of flight, resulting in a zig-zag pattern of irregularly spaced data points (Figure 4.7). The 6 km^2 study area was covered by twelve flight lines, 305 m wide with an approximate overlap of 70% between adjacent swaths, orientated in the north-south direction. The scan angle of the sensor was set to 10° with a total field of view of 20° giving a forward point spacing of 1.8 m between scan lines and lateral point spacing of 0.3 m within scan lines.

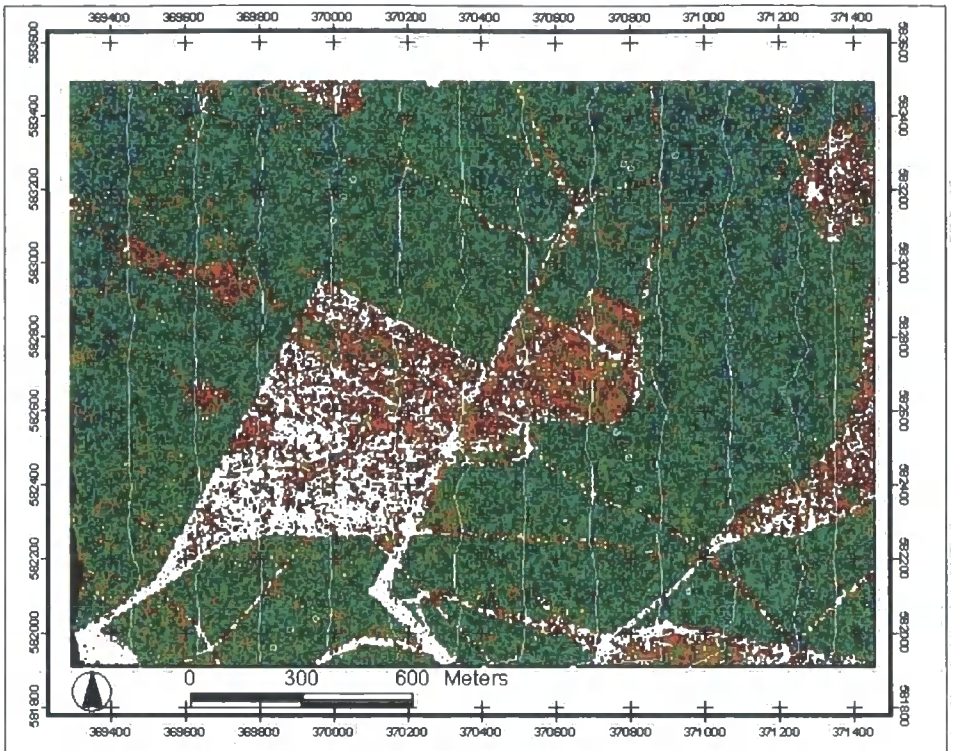

Figure 4.6 LiDAR point data displayed using LiDAR intensity values. White lines are flight lines.

On average, laser measurements were made at a density of 2 to 3 returns per metre (calculated using first pulse data), but point density is lower where the scan lines did not overlap, as illustrated in Figure 4.7. The altitude of flight was 950 m above mean sea level at an aircraft speed of 70 m s^{-1}. At this altitude, the footprint diameter of the laser on the ground is approximately 0.20 m at nadir. The *xyz* position (easting, northing and elevation) and intensity of each pulse were supplied geo-referenced to British National Grid. The height of the *z* position was supplied as elevation above the Ordnance Survey of Great Britain 1936 Newlyn Datum. The accuracy report that accompanied the LiDAR data indicates the accuracy in *x* and *y* position is 0.60 m and in *z* position is 0.15 m.

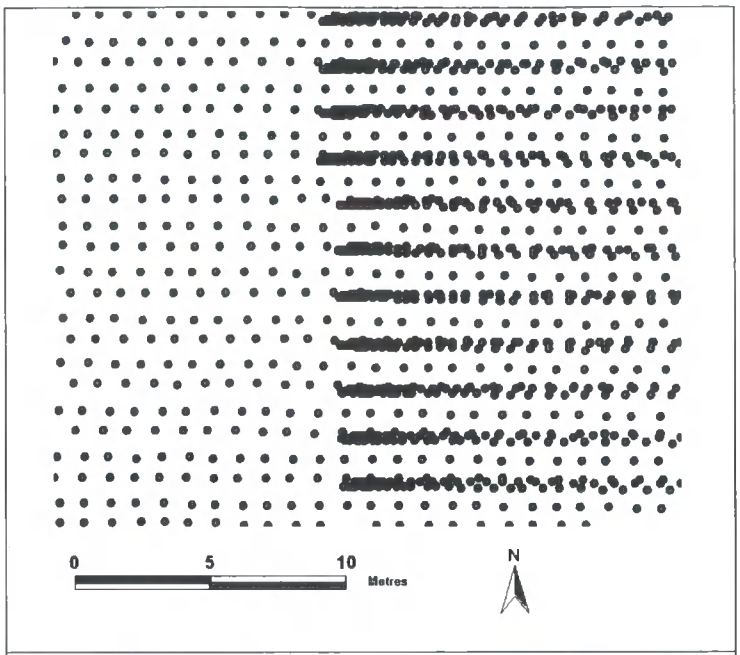

Figure 4.7 LiDAR scanning pattern on the ground between adjacent scan lines. Left side of the image shows area of no overlap between adjacent scan lines.

(ii) Galloway forest

LiDAR data was acquired on 15 June 2003 at 17:45 using an Optech ALTM 3033 instrument operating at a flight altitude of 1,250 m amsl. At this altitude the size of the laser footprint on the ground is 0.25 m at nadir. The study area (2.5 km^2) was covered by 10 overlapping flight lines orientated in an east-west direction. The laser data was acquired at scan angle of <9° and at point density of 4 returns/m^2. Overall, the specifications of this system are very similar to the ALTM 2033 in terms of laser scan rate, horizontal and vertical accuracy, laser wavelength and number of pulses recorded. The main difference is that the 3033 has a more powerful laser, so potentially the system can be operated from higher altitudes.

4.3 Image processing

There are a number of processing steps that are required before the datasets can be used for further analysis. Different processing methods are applied to the LiDAR and optical satellite images, reflecting the different modes in which the data are acquired. Overall, more steps are required in the processing of the LiDAR data, mostly because of the lack of image processing packages that have inbuilt LiDAR analysis tools. Terrascan software is used to process the LiDAR data to generate laser height values above the

ground. However, further processing to extract the various forest metrics requires user-defined routines in the statistical analysis program Stata. In comparison, optical satellite data are relatively easily processed, as well-defined image processing routines exist. The image processing package ENVI was used in this research.

The objective at the end of the image processing chain, regardless of the imagery type, is to extract laser points or image pixels over the field sample plot. Using these data, estimates are derived from the empirical relationships between field observations and image data. Section 4.3.1 describes the basic image processing steps used to extract this information from LiDAR data, for the Kielder and Galloway study areas. However, advanced processing steps (highlighted on the relevant method diagrams) are not included in this chapter, but instead described in subsequent chapters. Section 4.5 describes the process of preparing the optical satellite image for further analysis. Only the process of geo-correction is described in detail.

4.3.1 LiDAR processing

The LiDAR data were delivered as ASCII point files containing four columns, each comprising x, y, z, i (easting, northing, elevation and intensity) data separated into first and last pulse return data. To improve the manageability of these data, the flight lines for each area were merged into separate files and tiled. For the Kielder study area this process resulted in the creation of two datasets of approximately 7,000,000 points[9]. At this stage the data in the ASCII files represented a series of points containing information on the position and elevation of the surfaces from which they were reflected. To calculate canopy height from these data the laser pulses were separated into pulses that reached the ground surface and those that did not. This process is often referred to as *filtering* and the large number of points requires that it is semi-automated. Once separated, two surfaces are generated: a digital terrain model (DTM) from the ground points and a digital surface model (DSM) from the canopy points. The difference between the two models provides a measure of forest canopy height, often referred to as a digital canopy height model (DCHM). The following section details the processes involved in generating the DTM, DSM and DCHM, while the process is summarised in Figure 4.8.

[9] This number of points implies a file size of 130 megabytes.

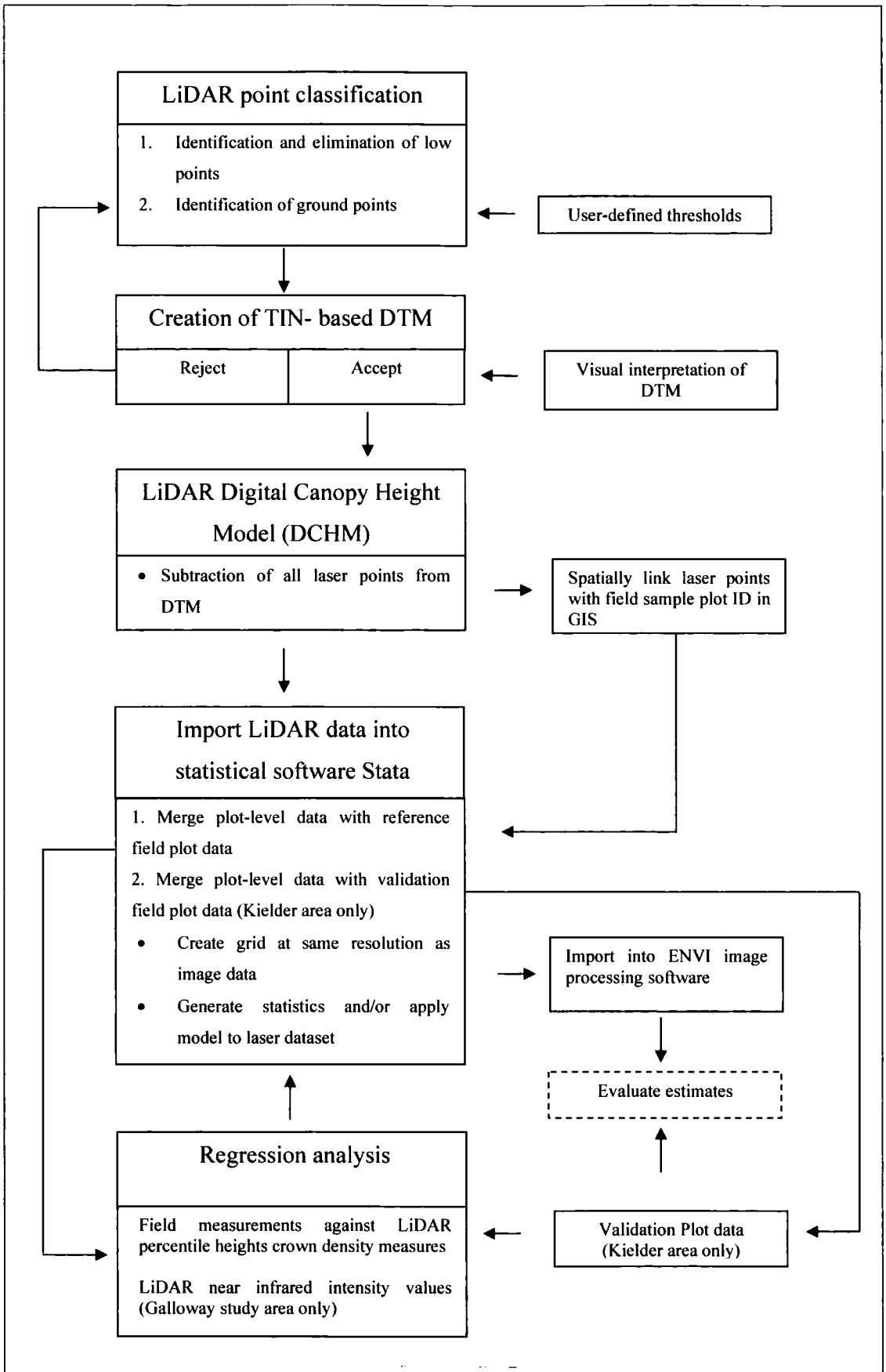

Figure 4.8 Summary of LiDAR image processing steps.

4.3.2 Classification of LiDAR points

In discrete return LiDAR data, the first pulse returns represent the first significant echo in the LiDAR waveform. In forested areas this is associated with the forest canopy. The last pulse return represents the last significant echo in the LiDAR waveform which can be associated with the ground surface. Not all last pulses penetrate to the ground surface and in dense forests a high proportion are returned from the upper canopy. This pattern is seen in Figures 4.9 and 4.10, which show the distribution of first and last pulse returns over a closed canopy sample plot. From this example it is clear that the first pulse data (coloured in black) has failed to penetrate through the forest canopy to the terrain surface, whereas approximately 23% of last pulses (coloured in red) were returned directly from, or close to, the terrain surface.

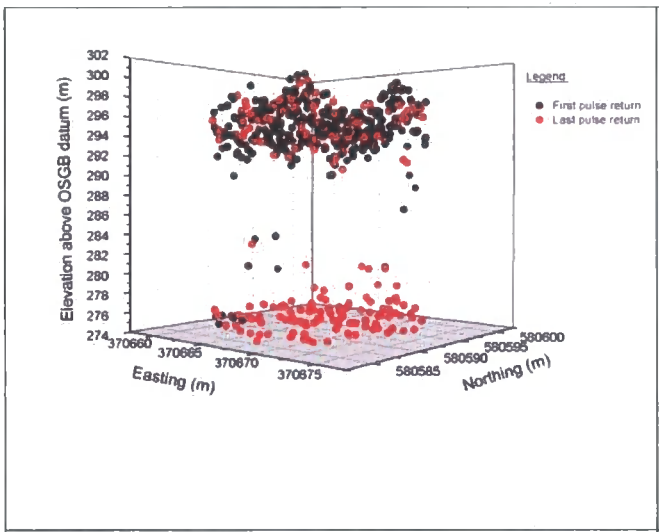

Figure 4.9 3D plot showing the distribution of LiDAR returns in a sample plot established in a mature Sitka spruce plantation.

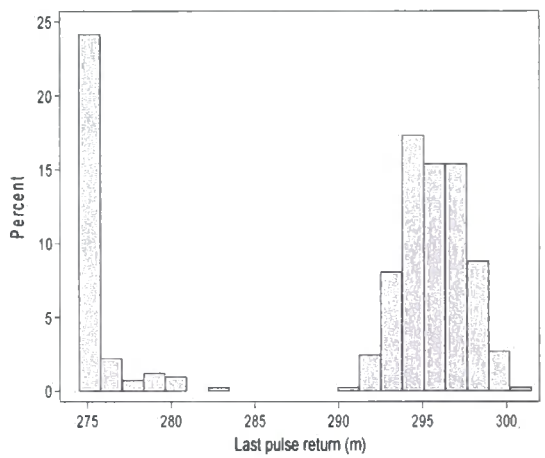

Figure 4.10 Histogram showing distribution of last pulse LiDAR returns in the same sample plot.

(i) Ground DTM from laser data

Filtering vegetation returns from point cloud data is the first step in derivation of the terrain surface or DTM. Several filtering algorithms have been developed to obtain a DTM from laser data. An explicit assumption made in filters is that the lowest returns in point cloud data are ground returns. All filters operate at a local neighbourhood level using either raw point cloud data or data resampled into an image grid. Within this local neighbourhood, points are filtered based on discontinuity measures, such as differences in height and slope between points or distance to Triangular Irregular

Network[10] (TIN) facets or parameterised surfaces (Sithole & Vosselman 2004). Points are added to or removed from the *ground surface,* based on a set discontinuity threshold, which is often user-defined.

In this research the filtering algorithm, embedded in the Terrascan software developed by Axelsson (2000), was used. This routine is an iterative algorithm that combines filtering and thresholding methods and is designed to model surfaces with discontinuities, such as those found in urban areas (Sithole & Vosselman 2003). Although originally designed for use in urban areas, the algorithm has been widely used for the identification of ground surface points and generation of DTMs under forests (Holmgren et al. 2004; Hyyppä et al. 2004; Maltamo et al. 2004; Xiaowei et al. 2004).

The next steps involved in generating the DTM in Terrascan are shown in Figures 4.11 b to d. For reference, a 1: 10 000 aerial photograph (Figure 4.11a) shows the general location, with the extent of the laser data marked by the orange box. Note that this is included for ground orientation purposes and does not overlay exactly with the other image extracts.

[10] A TIN is constructed using a network of non-overlapping triangular elements, with the vertices at the sample points.

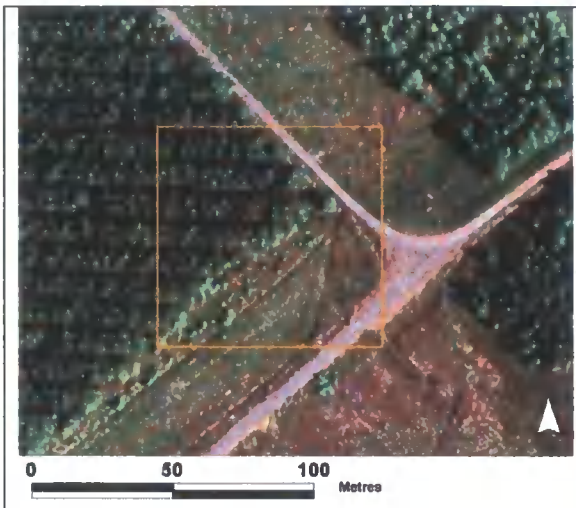

Figure 4.11a 1:10 000 aerial photograph of reference area.

Figure 4.11b Last pulse laser data coloured using return intensity.

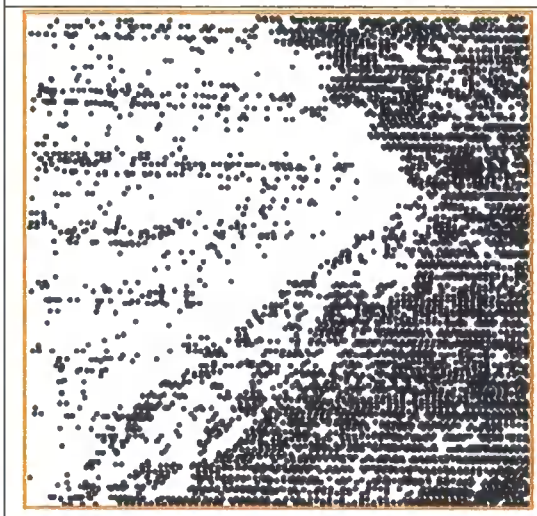

Figure 4.11c Ground points identified after filtering process.

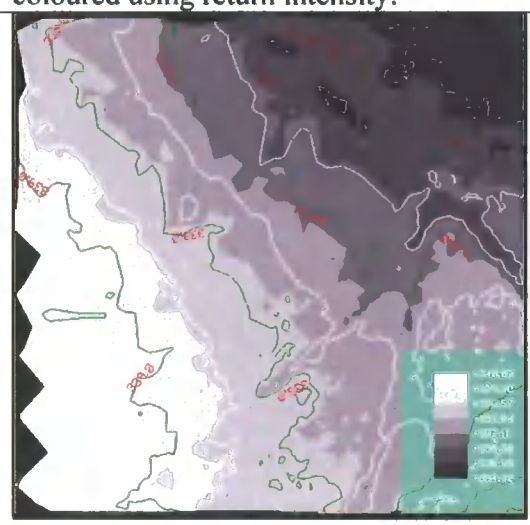

Figure 4.11d DTM interpolated from ground points.

Firstly, the last pulse laser points are loaded (Figure 4.11b) and low points in the data identified and removed. Low points occur when the distance from aircraft to ground has been incorrectly recorded. These may be caused by recording errors in the Time Measurement Unit (TMU) or by multipathing[11] of the LiDAR return by vegetation. Next, the ground classification algorithm is initiated (result shown in Figure 4.11c). Initially, this algorithm generates a sparse TIN by selecting from neighbourhood minima, within a user-defined search window size (i.e. 60 x 60 m^2 area). The assumption is that within this area there will be at least one hit on the ground and that the lowest point is a ground hit. Selection is progressively densified with new points

[11] Multipathing is caused by reflection of the laser pulse by a number of surfaces before it is returned to the sensor. This time delay means that the distance to the target is incorrectly calculated.

added to the TIN if they are below user-specified iteration angle and distance thresholds (Figure 4.12).

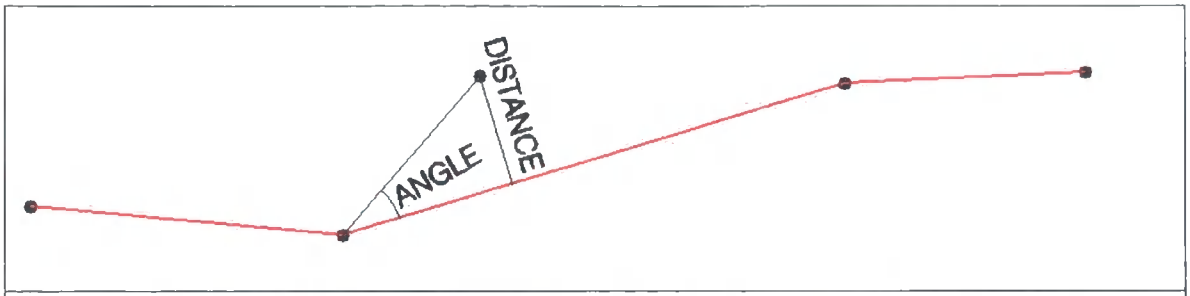

Figure 4.12 Iteration angle and distance used in the Terrascan DTM algorithm. After Soininen (2002).

The iteration angle sets the maximum allowable angle between each point and the TIN facet, while the distance parameter sets the minimum allowable distance to each triangle node. The higher the iteration angle and distance, the more likely it is that points with higher elevations are added to the model. At the end of each iteration a new threshold is computed, based on median values. These are estimated from histograms, which are calculated using the angle and distance of each point, relative to the TIN facet. The iterative process ends when there are no points remaining below the user-defined thresholds. The result of this process is shown in Figure 4.11c. Lastly, these points are interpolated from the TIN to produce the DTM surface as shown in Figure 4.11d.

Results from the Terrascan software are almost instantaneous, which means they can be visualised and parameters altered and refined. For the first run, the default search window size was 60 x 60 m, the iteration angle was 8° and distance values were 1.4 m.

In open areas satisfactory results were obtained. However, in areas with a low percentage of ground returns, errors were observed in the DTM, in the form of undulations in elevation (Figure 4.13a). Based on this result the search window was increased to 100 x 100 m, so that the number of potential points from which the algorithm could seed was increased. Additionally, the distance parameter was decreased from 1.4 m to 0.5 m, to reduce the number of vegetation points being added to the TIN. Using these settings vegetation points were removed and the ground surface was better defined (Figure 4.13b).

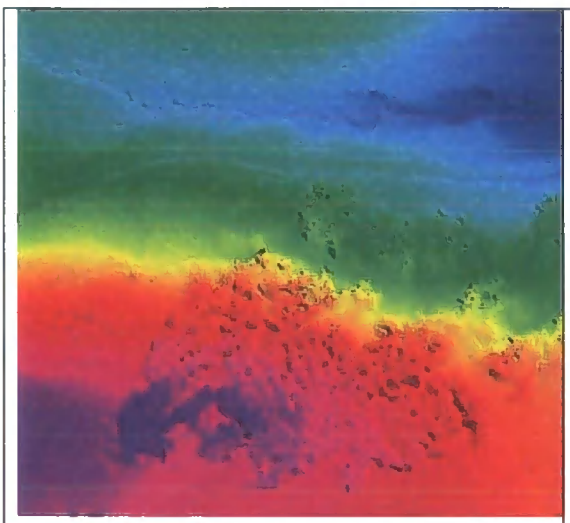

Figure 4.13a DTM created using default settings.

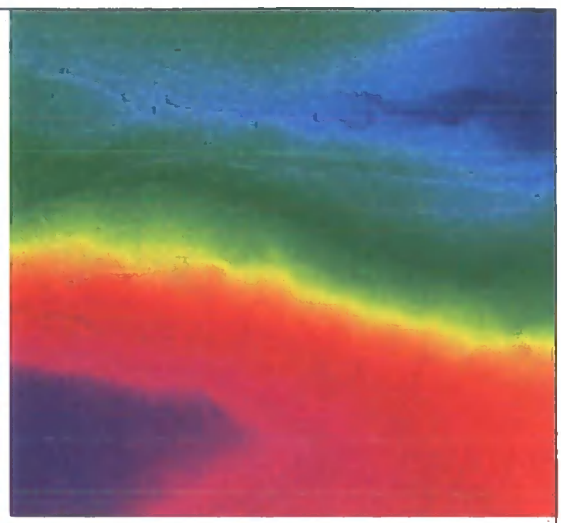

Figure 4.13b DTM created using refined settings.

4.4 Laser Digital Canopy Height Model

Using the DTM as a reference, all remaining returns (first and last) above the DTM were classified as vegetation returns. At this stage, point values were still elevation values above the OSGB 1936 Newlyn Datum. The relative height of each point was calculated by subtracting the height of the first return points from the DTM. In forested areas this relative height was considered to be the canopy height and in open areas, ground or close to ground height. Over the study area the LiDAR canopy heights ranged from 0 to 35 m, which is higher than the range in the tree height data (Figure 4.14).

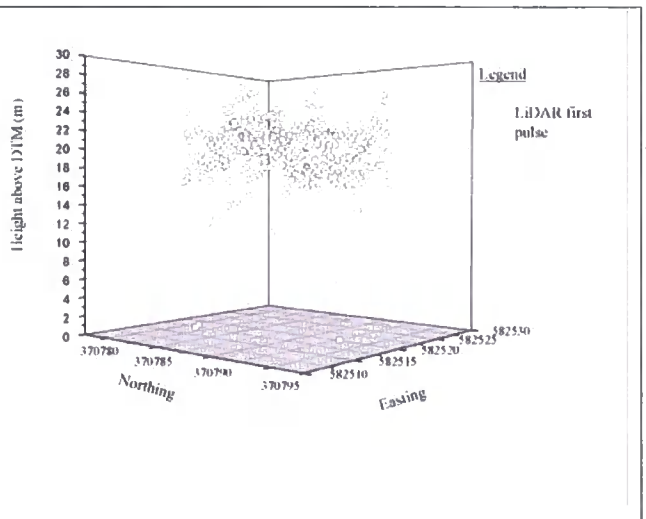

Figure 4.14 The distribution of first pulse returns over a closed canopy crop.

The LiDAR dataset was then divided into two datasets:

(i) LiDAR data over the reference plots in the Kielder and Galloway study areas

(ii) LiDAR data over the entire coverage areas.

In both cases data were exported from Terrascan in a class, x, y, z, i (the class field used to denote first or last pulse) ASCII format and imported into the statistical software program Stata.

Terrascan is able to produce surfaces in the form of TINs or grids based on the lowest, median and highest point values. If a DCHM is all that is required, common practice is to generate the DCHM from the highest returns in first pulse data, using a defined neighbourhood or grid cell size (Gaveau & Hill 2003; Hyyppä et al. 2004). The disadvantage is that this provides only a single canopy height measure and essentially discards any additional information that may be determined from the point cloud distribution. However, using routines developed in Stata, a DCHM and other statistical measures can be produced, while retaining the original point structure of the data.

4.4.1 Merging field and laser datasets

A link was made between the LiDAR data and the field dataset, in order to analyse the relationship between the two. This process comprised two stages: firstly, the LiDAR data for each reference and/or validation plot were exported to a GIS, to register the point data spatially with the sample plot ID and to clip the LiDAR data to the extent of the ground sample plot; secondly, data were imported into Stata. See Appendix 4.0 for details of these stages.

In Stata, the LiDAR point data were coded with the plot ID and merged with the field measurements, using the corresponding plot ID as a common link. Some data redundancy results from this process, as the number of first and last pulse observations exceeds the number of field observations. Consequently, the plot-level summary statistic in each column was duplicated to match the number of first and last pulse records (57,000 in the case of the Kielder reference dataset). The issue of data redundancy was overcome by tagging the first observation with a binary variable, so that only one value was used in any calculations.

4.4.2 Computations at plot-level

The plot-level dataset was used to identify relationships between field measurements and first and last pulse height distributions. A series of statistics were derived from these distributions, including height percentiles, measures of canopy density and the shape of the height frequency distribution. Previous research has shown that for a given plot size and canopy structure, a certain percentile in the height distribution exists that corresponds to the canopy height of interest (Magnussen & Boudewyn 1998; Naesset & Økland 2002; Naesset & Bjerknes 2001). Consequently, percentiles corresponding to the 0 to 99th percentiles of the laser canopy heights were derived for each plot. In addition, other variables were created to provide information on canopy density, such as the number of ground returns and the skewness and kurtosis of LiDAR frequency distribution. Additional details relating to these statistics are provided in Chapters 6 & 7.

4.4.3 Processing laser data at the dataset level

The three ASCII files containing the LiDAR data were imported into Stata and processed separately[12]. The subsequent processing steps were to: (i) determine the spatial resolution of the output grid, which can be either user-defined or matched to resolution of the optical data; (ii) output grid statistics or apply estimation equations developed using the plot-level dataset; (iii) export the estimation grid in ASCII format and import into the image processing package ENVI.

(i) Determining the spatial resolution of the grid

The level of rounding applied to the x and y coordinates defines the spatial resolution of each grid cell (Stata routine documented in Appendix 4.1). The resolution selected can be either user-defined or based on the resolution of the optical data. It is important to note that the grid size selected should not exceed the spatial resolution of the laser data. In this context, selecting a grid resolution of less than 1 m would provide biased results, as the number of laser returns (1 to 2 returns per m^2) would be insufficient to provide an accurate representation of the data. In this study a grid with a spatial resolution of 4 m^2 was used. At this resolution this provided 6 canopy returns per grid with a range of 4 to 12 returns per grid. Figures 4.15 and 4.16 provide an example of the rounding process. Figure 4.15 shows the point data, prior to rounding, with a numbered 2 x 2 m grid

[12] This is because of computer processing limitations.

superimposed over the data. The rounding process groups the points, based on their x and y coordinates, as shown in Figure 4.16. At the end of this process all of the original points are assigned to the centroid point of each 2 x 2 m grid cell.

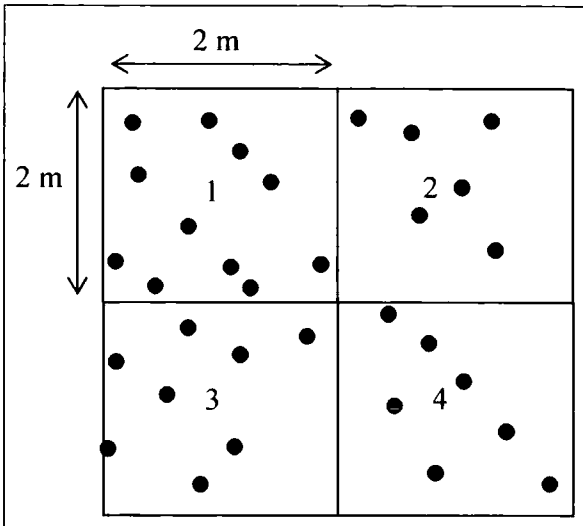

Figure 4.15 Point distribution before rounding.

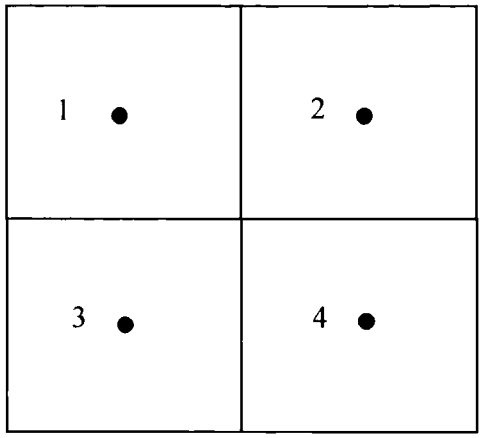

Figure 4.16 Point distribution after rounding.

(ii) Calculating grid statistics & exporting to ENVI

In the rounding process, the structure of the point data is nevertheless retained making it possible to use all the return data to provide summary statistics (i.e. LiDAR height percentiles, percentage ground returns or shape measures such as skewness or kurtosis) at the defined grid size. The results of statistical calculations can be added to a new column in the data file. From this point, any combination of statistics can be exported in an ASCII format to an image processing software package and added as a series of image bands. For example, the DCHM can be generated, by identifying the highest return in each grid cell, and exported as a single image band in an ASCII file. For reference, Figure 4.17a shows the 1: 10 000 aerial photograph with the general location of the area of interest. Over the same area, Figure 4.17b shows the DCHM displayed, using 2 m height increments and gridded at a 2 m spatial resolution. Other statistical measures that summarise the point return data in each grid cell can also be added. By mapping these variables at the scale of the dataset, different combinations can be used, to assist in the identification of forest types and/or provide additional quantitative information that can be used to describe the forest structure. Figure 4.17c shows the same area, using maximum and median height and the 10^{th} percentile of LiDAR height

in a three band composite image, with the statistics displayed using the red, green and blue colour channels. Additionally, the graph to the left shows canopy height values at the location of the red cross for each band (or statistic).

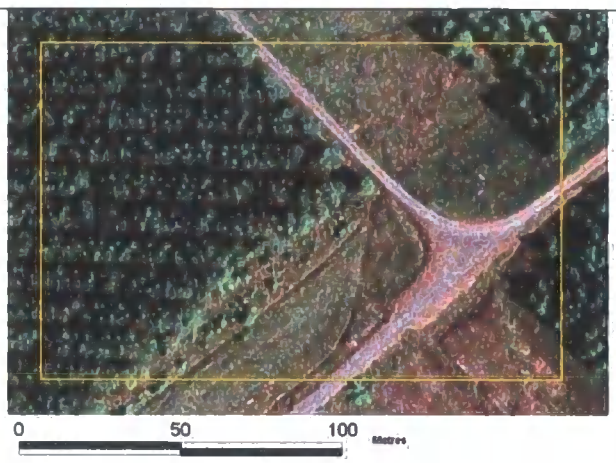

Figure 4.17a 1:10 000 aerial photograph of reference area

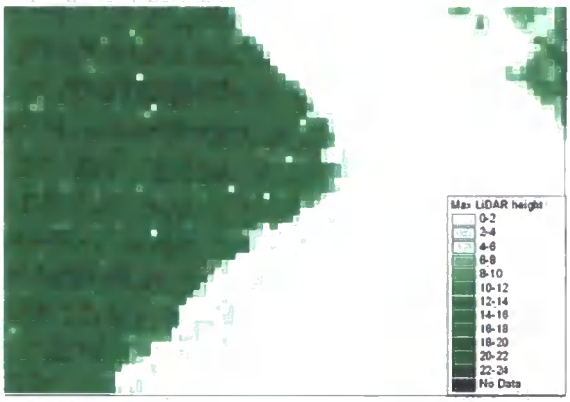

Figure 4.17b Maximum height grid at 2 m spatial resolution

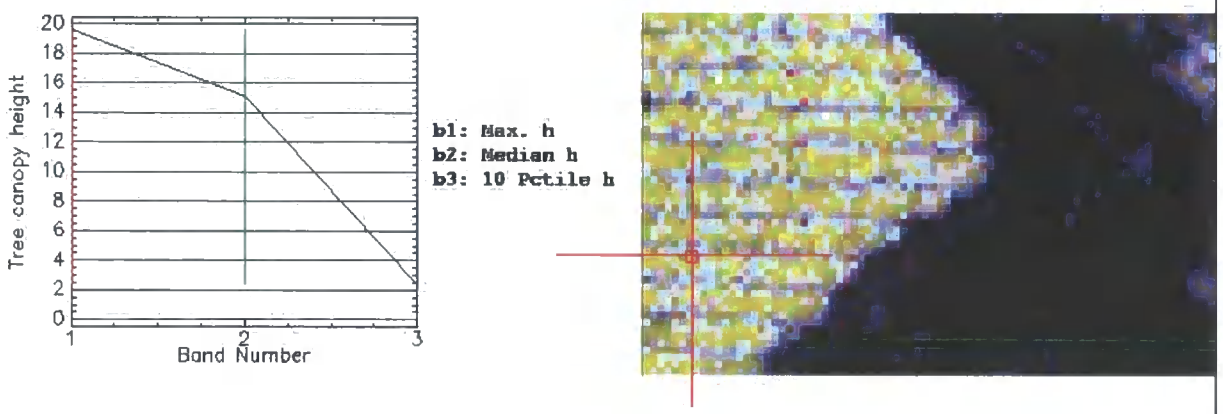

Figure 4.17c Composite image based on maximum height, median and 10th height percentile.

4.5 Optical imagery

The processing methodology, used to prepare the satellite data, is presented in Figure 4.18. This process enables the extraction of pixel values corresponding to the location of field sample plots. These are exported to Stata, so that relationships between reflectance values and forest height can be analysed. As this method is identical to that described for the LiDAR processing, it is not repeated in this section. Processing steps highlighted in Figure 4.18 are not presented in this section, but are described in more detail in the relevant chapters.

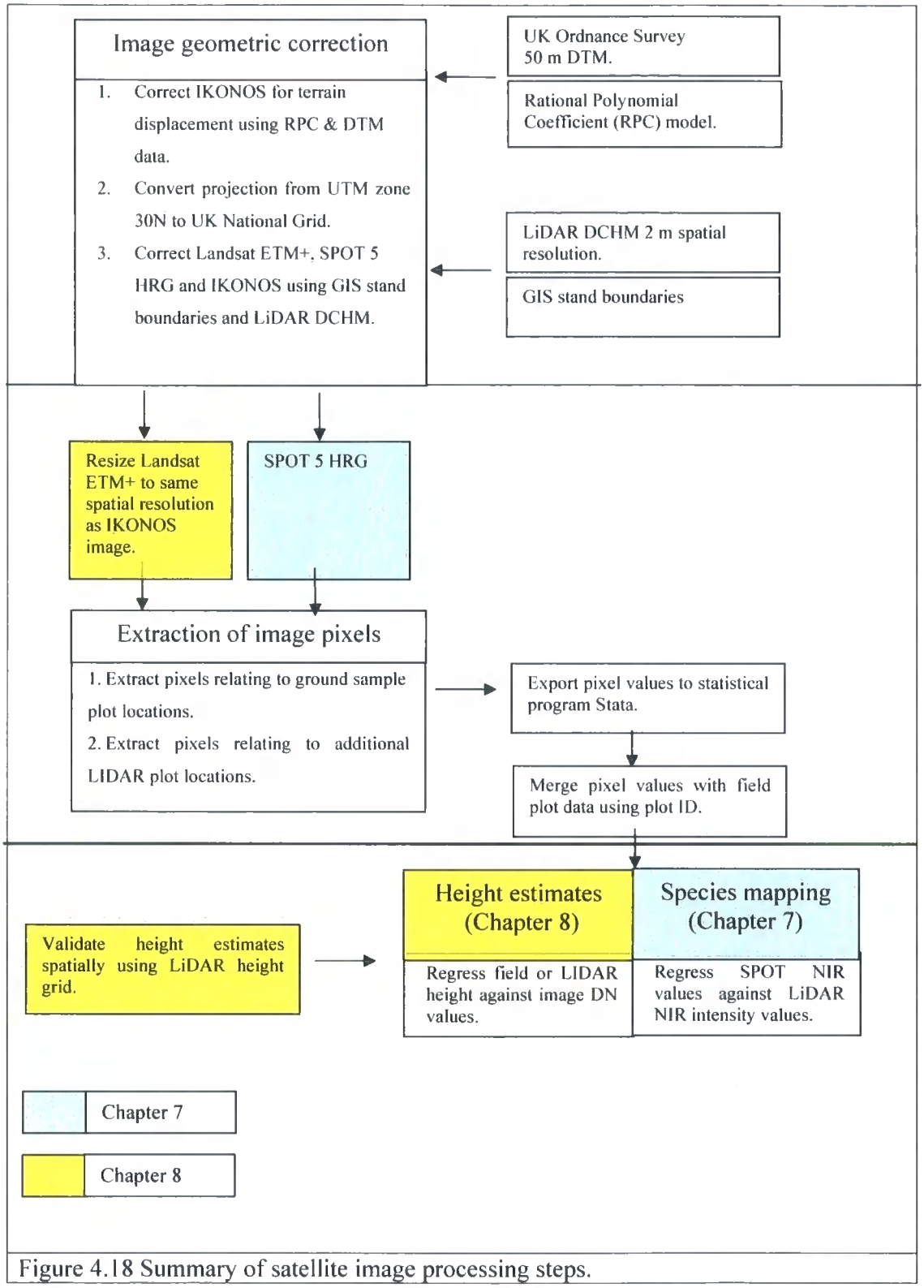

Figure 4.18 Summary of satellite image processing steps.

4.5.1 Geometric correction

Prior to geometric correction, the expected positional accuracy of a Landsat 7 ETM+ scene is 50 m and for the IKONOS Geo Ortho Kit product 15 m (Space Imaging, 2004). Therefore geometric rectification is essential to ensure that land surface features are accurately positioned in geographic space and can be precisely integrated or compared with other geographically registered data. The geometric rectification of the Landsat 7 ETM+ and Ortho-correction of IKONOS datasets was performed using ENVI image processing software using 40 GCPs. The correction process can be divided into three stages, which are described below.

(i) IKONOS Ortho-correction

IKONOS data includes a description of the camera geometry at the time of acquisition, supplied in the form of the Rational Polynomial Coefficient (RPC) model. The RPC model uses ratios of cubic polynomials to express the transformation from ground surface coordinates (*latitude*, *longitude*, *elevation*) to image coordinates (*line*, *column*) (Lutes, 2004). By using the RPC model and a DTM it is possible to remove distortions in the imagery caused by terrain, so that image features have correct planimetric coordinates. Since the RPC model is calculated over the entire IKONOS scene, it is not possible to use the LiDAR DTM, as the area of coverage is smaller than that of the IKONOS. However, in the UK a geo-referenced DTM, at a 30 m posting, is widely available through the Ordnance Survey[13]. Although the DTM resolution is coarse, it is suitable for this purpose as the ground topography over the study area is gently undulating (mean slope <10°).

The IKONOS data was matched with the 30 m DTM and the RPC coefficients applied (process described in Appendix 4.2). However, after the application of RPC coefficients, the IKONOS image did not exactly overlay the LiDAR data. There are two possible causes for positional error: (i) the DTM resolution was not high enough to adequately represent the ground surface, (ii) and/or there were positional inaccuracies in the supplier's RPC coefficients. Di et al. (2003) reported that geo-positioning could be improved through the inclusion of extra Ground Control Points (GCPs). Figure 4.19a shows the IKONOS image prior to ortho-correction and Figure 4.19b shows the 30 m

[13] The DTM resolution has recently been updated to a 10 m posting, but this was not available at the time of processing these data.

DTM used to provide the elevation values. The final ortho-corrected image is shown in Figure 4.20b after the addition of extra GCPs.

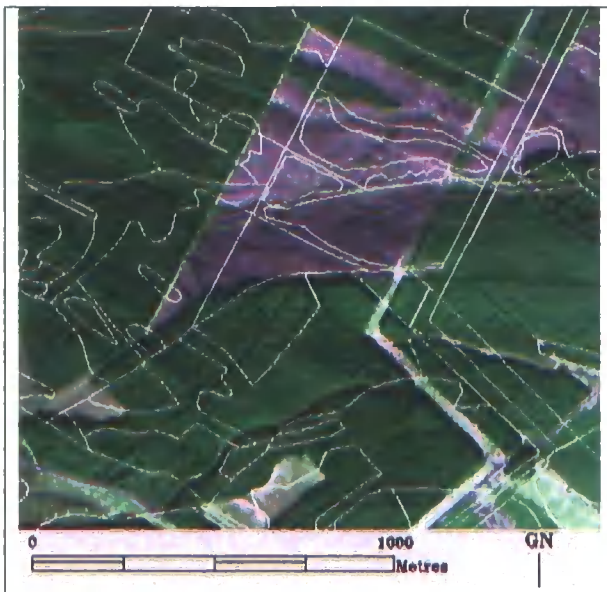

Figure 4.19a IKONOS data prior to ortho-correction overlaid with forest boundary data.

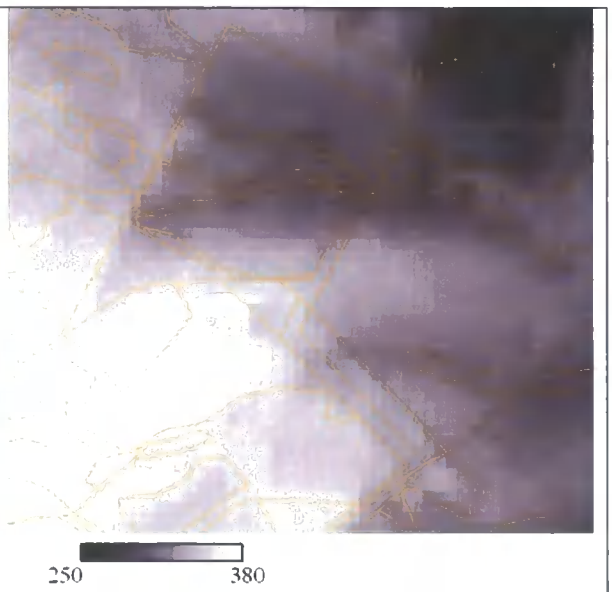

Figure 4.19b OS thirty metre DTM overlaid with forest boundary data.

4.5.2 Projection of satellite data to UK National Grid

The Landsat 7 ETM+, SPOT 5 HRG and IKONOS data were delivered projected to zone 30N of the Universal Transverse Mercator (UTM) using the World Global System 1984 (WGS84) Datum. UTM is a grid-based projection that divides the world into 60 north-south zones, each covering a strip 6° wide in longitude. These zones are numbered consecutively, beginning with zone 1 between 180° and 174° west longitude, progressing eastward to zone 60 between 174° and 180° east longitude (Iliffe, 2003). All field and stand boundary GIS data are projected using the UK National Grid projection. This projection is also based on the Transverse Mercator projection, with a modified scale factor and transformed local origin[14]. Therefore, to be able to overlay the different datasets, it was necessary to re-project the Landsat 7 ETM+ and IKONOS data. This was achieved in ENVI, using triangulation transformation and nearest neighbour re-sampling, which ensures that the radiometric integrity of the original image data is retained.

[14] Scale factor on central meridian UK National Grid (0.9996012717); UTM zone 30 (0.9996). True origin UK National Grid lat 49° N long 2° W (Map coordinates East 400,000, North 100,000 in metres) UTM zone 30 lat 0° long 3° W (Map coordinates East 500,000, North 0 in metres).

4.5.3 Geo-correction of Landsat 7 ETM+, SPOT 5 HRG and IKONOS data

Despite having re-projected images to the UK National Grid, additional control points were necessary, to match the image data with GIS boundaries and field plot positions. For the Kielder and Galloway study areas, about 40 matched pairs of GCPs were collected from the LiDAR data[15] (over the study area only) and the FC forest compartment database. In the Kielder study area, the Landsat 7 ETM+ and ortho-corrected IKONOS data were rectified, using the same GCPs, thereby minimising errors in the rectification procedure. The root mean square (RMS) error for each image was less than a pixel (4 m for the IKONOS, 5 m for the SPOT 5 HRG and 30 m for the Landsat 7 ETM+). Images were rectified using both a triangulation transformation, where the warp is exact at the GCP and error increases away from the point, and nearest neighbour re-sampling, which ensures that the radiometric integrity of the original image data is retained. This process generated co-registered images, where the coordinates of a particular feature on one image exactly match the coordinates of the same feature on another image. Figures 4.20a and 4.20b provide examples of corrected images over the Kielder study area.

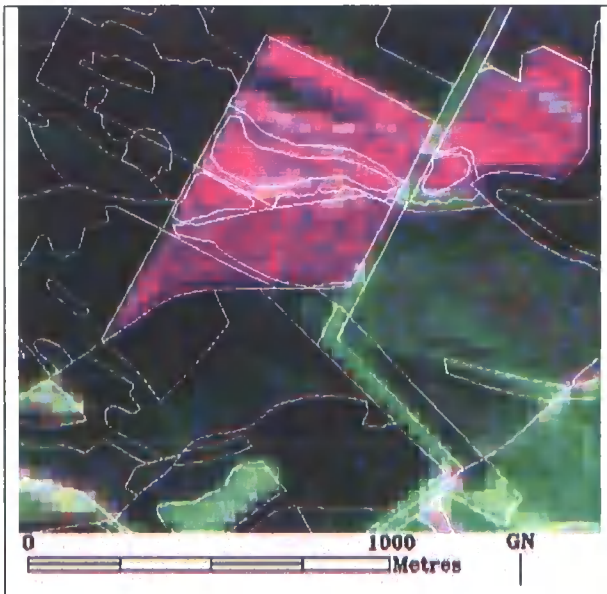

Figure 4.20a Geo-corrected Landsat 7 ETM+ image displayed as a false colour composite using blue/green, near infrared and red spectral bands (display bands 1, 4 and 3).

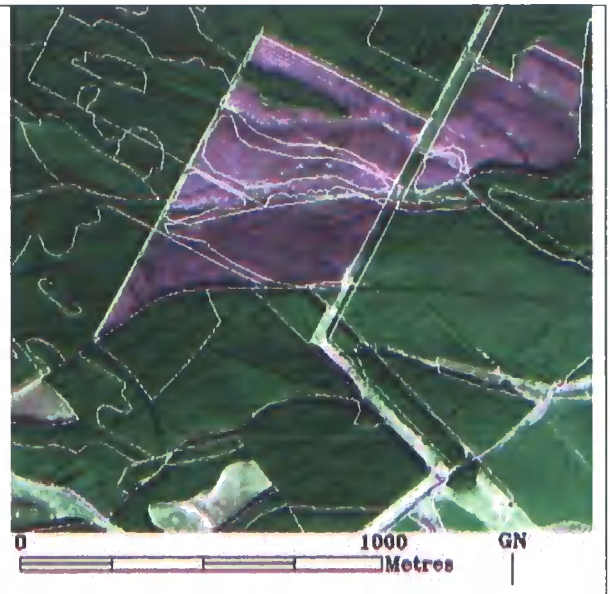

Figure 4.20b Ortho-corrected IKONOS image displayed as a false colour composite using blue/green, near infrared and red spectral bands (display bands 1, 4 and 3).

[15] According to the accuracy report provided by the LiDAR data supplier the expected planimetric accuracy of the LiDAR is expected to be ± 0.60 m.

4.6 Summary

The objective of this chapter was to describe the processing methods used to prepare the LiDAR and Landsat 7 ETM+, SPOT 5 HRG and IKONOS satellite data for further analysis. These data represent a cross-section of commercially available, remotely sensed data that can be used to assist with management of forest resources. They also represent a range of spatial, radiometric and spectral resolutions, which enable direct comparisons to be made of their ability to provide quantitative forest estimates in upland conifer plantations. The main findings include:

1. The band passes of different sensors are very similar, but spatial and radiometric resolutions are quite different.
2. Although the image data are collected within the same growing season, the off-nadir angle of IKONOS data and sun angle differences between IKONOS and Landsat may cause differences in reflectance values recorded over the forest.
3. User-defined routines, developed in the statistical analysis program Stata, enable calculation of various laser metrics at any spatial resolution.
4. LiDAR provides an accurate source of data, which can be used to geo-correct satellite data to accuracies of less than an image pixel. This allows the positions of field plot data to be accurately matched to image data.

The processed image data from this chapter are analysed in the four subsequent chapters as follows:

1. **Chapter 5 - Assessment of the accuracy of LiDAR**: the accuracy of the laser-derived DTM and DCHM are compared with the field-measured data.
2. **Chapter 6 - Estimation of forest parameters using LiDAR**: LiDAR-derived percentile heights and crown density measures are used to provide estimates of top height, volume and tree density.
3. **Chapter 7 - Mapping species mixtures**: LiDAR-derived crown measurements and near infrared intensity values are compared with spectral information from the SPOT 5 HRG data, to identify and map conifer plantation species and species mixtures (lodgepole pine and Sitka spruce).
4. **Chapter 8 – Estimating forest height using IKONOS and Landsat 7 ETM+**: IKONOS and Landsat 7 ETM+ data are used to estimate forest height. LiDAR is also used to provide additional samples of height and to validate height estimates derived from satellite data.

Chapter 5: Accuracy of LiDAR under dense forest canopies

5.1 Introduction

In forestry, tree height is one of the key variables used to make estimates of timber volume and to derive forest growth models. This is primarily because tree height is relatively easily measured and is strongly related to stem volume and diameter. This thesis seeks to test the hypothesis that LiDAR is able to provide measurements of forest height that are at least as accurate as field-based measurements and therefore could be used in their place. The objective of this chapter is to assess the accuracy of LiDAR measured height[16] in densely stocked UK conifer plantations. The assessment is made by comparing a Digital Terrain Model (DTM) with field-measured ground elevation data and a Digital Canopy Height Model (DCHM) with individual tree height data (tree level dataset[17]). The analysis is expanded to plot level so that the influence of factors relating to crown density, laser pulse density and terrain can also be assessed.

5.1.1 Previous research

A number of studies suggest that the accuracy of tree height measurements derived from LiDAR data in coniferous forests is comparable to field-based measurements (Holmgren 2003; Hyyppä et al. 2000; Naesset 1997; Persson et al. 2002). However, it is also widely acknowledged that LiDAR can underestimate tree height in conifer-dominated forests, due to the low probability of a small-footprint laser pulse intercepting the tree apex (Nilsson 1996; Naesset 1997; Popescu et al. 2002). Another potential source of error is inaccurate representation of the underlying terrain elevation, as the tree height or DCHM is determined by subtracting the Digital Surface Model (DSM) from the Digital Terrain Model (DTM). Therefore, the accuracy of the height measurement is affected by the ability of the LiDAR pulse to penetrate to the forest floor. Penetration rates of Continental European conifer-dominated stands are reported to be between 17 and 33% of the canopy, depending on the density of the understorey (Kraus and Pfeifer 1998; Naesset 2002). Compared with these forests, UK plantations

[16] The analysis is conducted using the raw LiDAR height measurements with the LiDAR data compared with field-measured height.

[17] The tree level dataset refers to measurements recorded for individual trees in each sample plot that were positioned using the dGPS. Plot level dataset refers to the average of all trees in each sample plot.

are extremely dense, with stands commonly exceeding 2,500 trees/ha (Donoghue et al. 2004; Watt 2002). At this density the number of laser returns from the terrain surface decreases quickly, to less than 10% in stands of 10 m height (Figure 5.1).

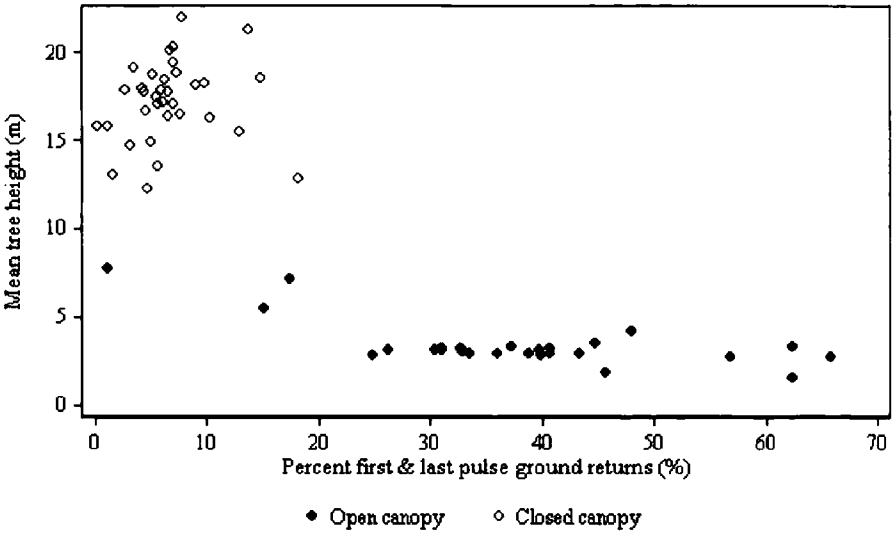

Figure 5.1 Mean tree height against the percentage of LiDAR ground returns.

Few LiDAR-based studies have been conducted in UK conifer forests because datasets are unavailable. One notable exception is a study by Suárez et al. (2005), which evaluated the potential of combining LiDAR and aerial photography for tree height estimation. However, at the time of writing, no research has been published that specifically investigates the accuracy of LiDAR-derived height and the factors that might affect the accuracy in densely stocked UK upland conifer plantations. If LiDAR data are to be used to provide estimates of forest height or height-related canopy structural measurements, such as canopy length, it is important to determine the accuracy of the estimate and to identify possible sources of error.

5.2 Methodology

The accuracy of the two LiDAR surfaces, the DTM and DCHM, was tested through comparison with field measurements of ground elevation and tree height respectively. To test the DTM accuracy, eight transects and a series of spot heights distributed along forest roads were measured. Measurements of a flat hard surface, like a road, provide a check on the accuracy of the LiDAR instrument.

To test the accuracy of the DCHM, the heights of 99 trees were measured using a digital hypsometer. Figure 5.2 shows the location of the surveyed points, overlaid on a 1:10 000 aerial photograph. Height measurements, recorded at plot level, were used to assess the influence of a range of factors on the precision of the LiDAR estimate, such as canopy structure, terrain slope and the number and percentage of LiDAR returns.

Figure 5.2. Location of ground transects and spot elevation measurements.

5.2.1 Description of measured sites

Transects and measured sample plots can be classified into four site types: forest road, grassland, open canopy and closed canopy. Spot heights, recorded on the road surface, provide a benchmark, as this is a hard non-penetrable surface and so can be used to test the accuracy of the LiDAR system. Photographs of the different site types are provided in Figure 5.3, and are described below:

(i) Forest road

Four-metre wide compacted gravel forest road. The surface gradually slopes away from a centre ridgeline. Reference points were collected in the centre of the road, avoiding potholes and areas of excessive slope.

(ii) Grassland

A mixture of rushes and sedges. The ground surface is covered by a dense mat of vegetation and is not visible from the air.

(iii) Open canopy

Open canopy is defined by the presence of >50% grass species in the understorey vegetation. The understorey surface is a diffuse mix of clumps of grass, bare soil and tree stumps. Trees are generally less than 10 m in height.

(iv) Closed canopy

Closed canopy is defined by the absence of understorey vegetation, specifically where <50% of the understorey vegetation is grasses. Trees are generally greater than 10 m in height and their crowns are classified as dominant, co-dominant, sub-dominant and suppressed. The understorey surface is devoid of vegetation but has a thick mat of tree needles.

Forest road

Grassland

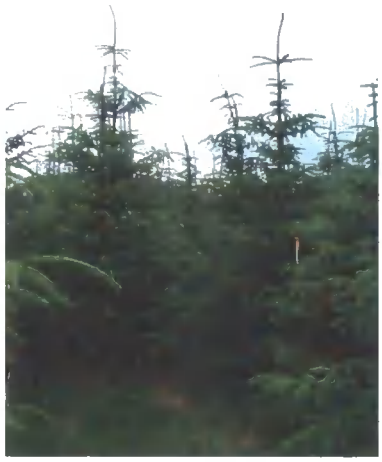

Open canopy

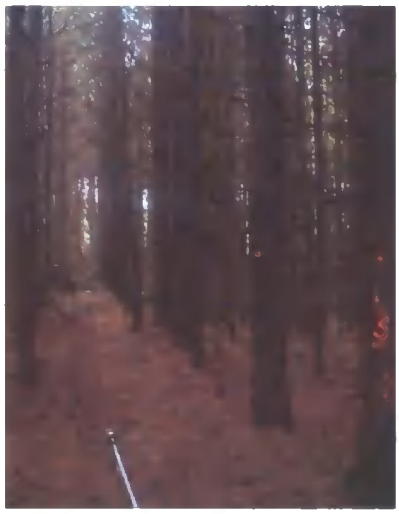

Closed canopy

Figure 5.3 Example photographs of the four site types measured during the ground survey

5.2.2 Forest transects

Seven of the eight transects were measured in forested areas. These were distributed over a range of a canopy development stages and terrain slope angles. Each transect traversed sample plots that had already been established as part of the field inventory, to ensure that tree position, canopy dominance, canopy structural measurements and height information were known (measurement methods detailed in Chapter 3). The following methodology describes measurement of the ground surface and tree height data.

(i) Ground surface measurements

Each transect was initiated either on the temporary benchmark (red triangle on Figure 5.2) or on points established on the road, using the differential GPS (marked yellow). Additional points were established when the line of sight was obstructed and it was

necessary to change the direction of the survey. Ground elevation measurements were made every 1 m, using a laser ranging theodolite (Leica Total Station 1100). From these measurements the horizontal (x and y) and vertical distance (z) of the ground elevation, relative to the benchmark position or GPS point, were calculated[18] and converted to British National Grid (BNG) Eastings and Northings. All height values (z) were calculated in metres above the Ordnance Survey 1936 datum. Using the Terrascan software, the corresponding elevation value for each point was extracted from the 2 m resolution LiDAR DTM.

(ii) Tree height measurement

In each sample plot only trees classed as dominant were included in the analysis. Dominant trees are the tallest, with the widest canopies, and are therefore easily separated from surrounding LiDAR returns. In sample plots with closed canopy forest, all tree crown classes other than dominant (i.e. co-dominant, sub-dominant and suppressed) were excluded. In sample plots with open canopy forest, all trees were included, as there is no tree competition at this growth stage and therefore the tree crown classes have not developed. Figure 5.4 illustrates the position of each dominant tree in the canopy, relative to the DTM and first pulse laser data, for 0.02 ha sample plots measured in the two canopy types.

In both cases dominant tree canopies receive a number of LiDAR hits, as shown in Figure 5.4. As a consequence of overlapping LiDAR scan lines, the density of LiDAR returns is twice as high in the closed canopy plot (2 returns/m^2) than in the open canopy plot.

[18] Prior to conversion the magnetic declination (4.35° W) was subtracted from each bearing measurement.

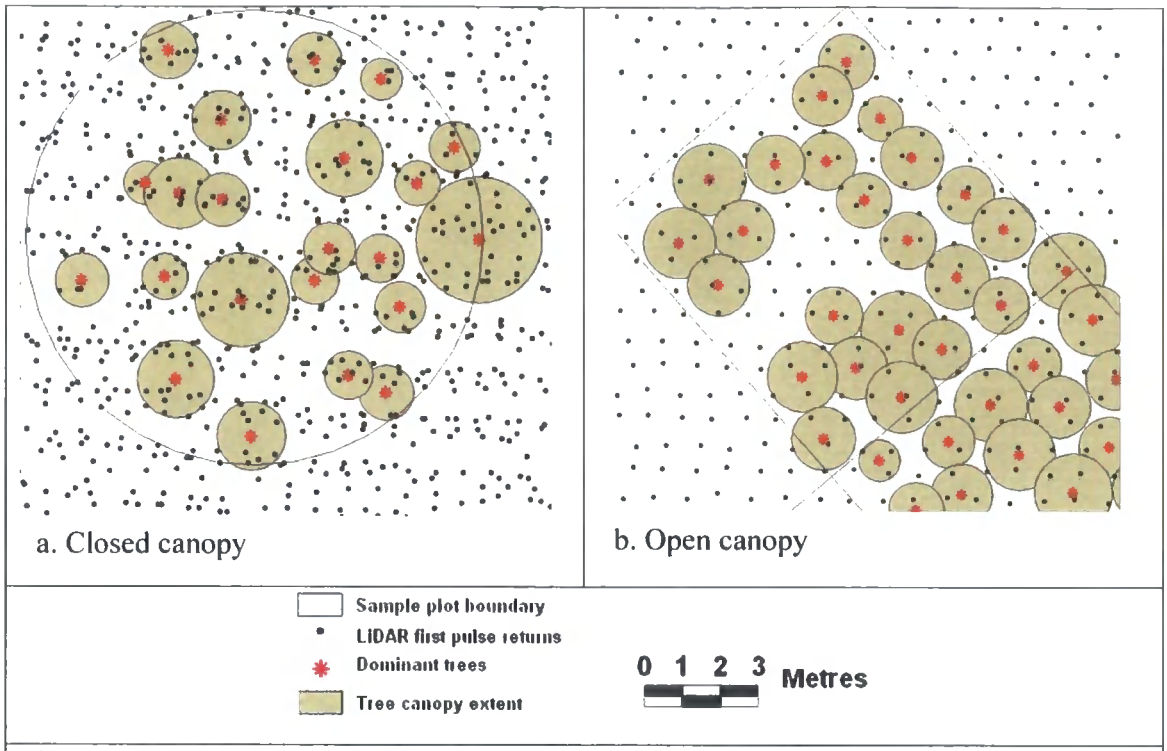

Figure 5.4 Positioning of dominant trees relative to the first pulse laser data.

Using only the highest point returns from the LiDAR first pulse data, a DCHM with a resolution of 2 m was created (same resolution as the DTM). At this scale, the resolution of the DCHM is large enough to cover each canopy, but also small enough not to capture multiple tree canopies. This resolution accounts for the horizontal positioning accuracy of the LiDAR data (± 0.60 m) and tree position data (± 0.40 m). Using Terrascan software, tree point positions were overlaid with the 2 m resolution LiDAR DCHM and corresponding elevation values extracted.

5.3 Accuracy of the DTM

A summary of the differences between the ground-measured DTM and the LiDAR DTM for the five site types is presented in Table 5.1. Previous work by Baltsavias (1999b) and Gaveau and Hill (2003) states that the vertical precision of Optech's airborne laser scanners (ALTM 1020, 1210 and 2033), operated over open areas with flat hard surfaces, is ± 0.15 m. Table 5.1 shows that the range of height values recorded on the forest road is between –0.18 m and 0.15 m (i.e. ± 0.18 m), which is close to this threshold. The slight discrepancy between measurements (0.03 m) is probably due to the uneven nature of the forest road surface.

Table 5.1 Summary statistics for the elevation residuals by site class

Site Reference	Mean (m)	SD (m)	Min. (m)	Max. (m)	No. survey points
Forest road	–0.026	0.12	–0.18	0.15	5
Grassland	0.47	0.09	0.23	0.68	24
Open canopy	0.24	0.13	–0.23	0.59	41
Closed canopy	0.17	0.46	–1.16	1.16	222

In all other cover types the average elevation residual in LiDAR varies according to surface type, from forest road surface (–0.026 m) through grassland (0.47 m) to open and closed canopy (0.24 m and 0.17 m respectively). While the mean residual of the grassland site is higher than that of open forest canopy, greater variation is observed in the surface under open forest canopy, as shown in Figure 5.5. This indicates that the grassland surface is more homogeneous than the surface under open forest canopy.

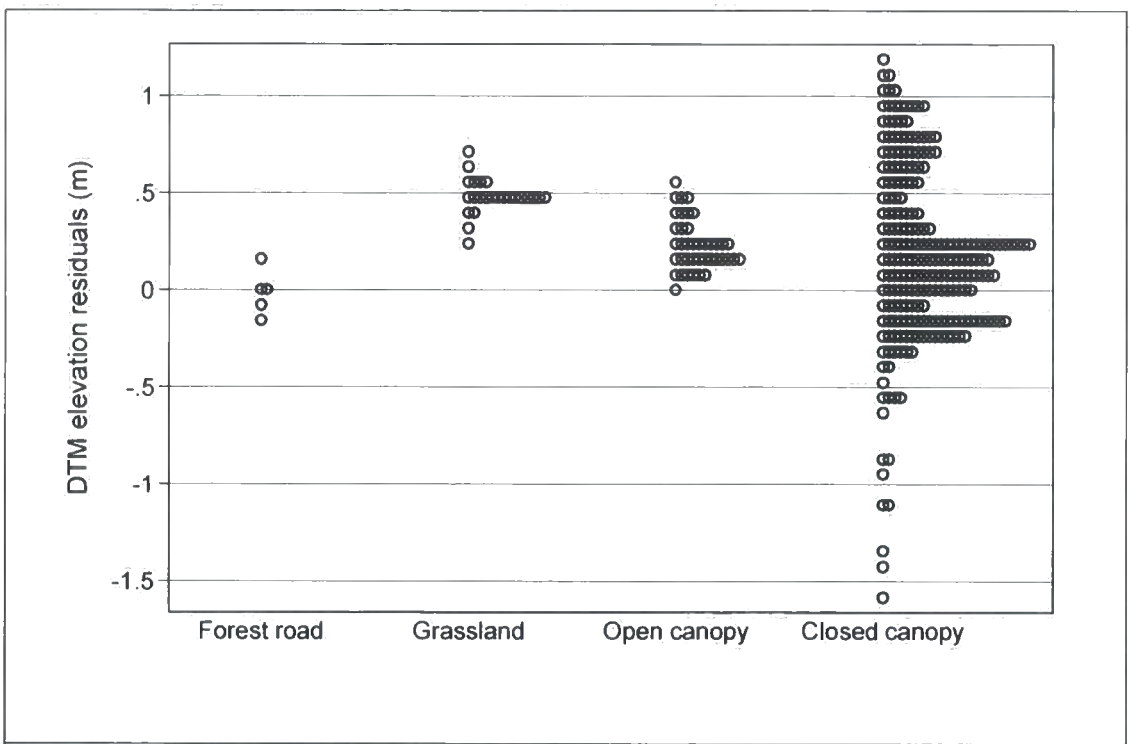

Figure 5.5 Distribution of elevation residuals for the DTM by site type.

(i) Grassland

Over-estimation of the grassland surface height is probably due to the inability of the laser to penetrate the thick grassland vegetation layer, although it is possible that this could have also been caused "smoothing" during the generation of the TIN. The mean error (0.47 cm) is thought to be close to the actual grass height at that time of year[19]. This is supported by the apparent planimetric accuracy of the LiDAR surface, where undulations in the ground-measured surface and the LiDAR-measured surface mirror each other (as indicated by the dashed orange line in Figure 5.6). Although some discrepancies are observed, it is suggested that these reflect variations in the surface of the grassland vegetation layer.

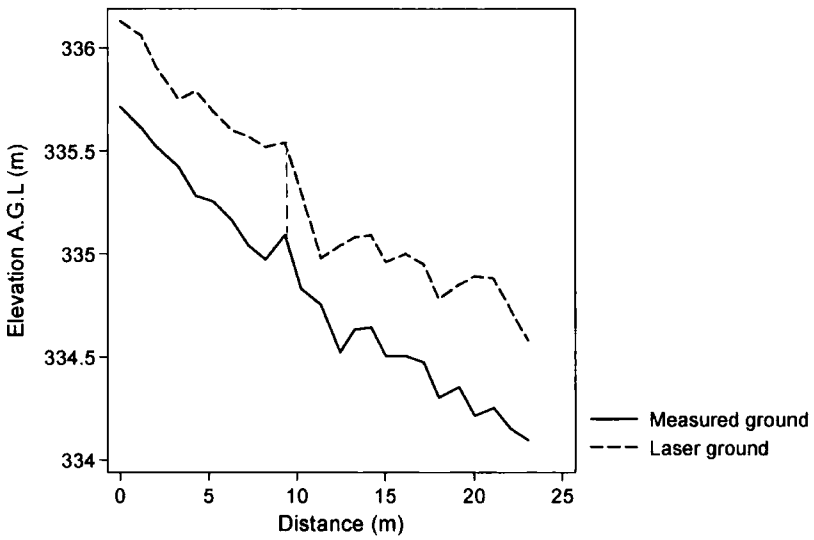

Figure 5.6 Survey transect through a grassland site, retrieved from ground survey and DTM

(ii) Open forest canopy

Analysis of the dot plot (Figure 5.5) indicates that residuals in open canopy areas are generally positive. The positive bias means that the ground surface is overestimated, although the overestimation is no greater than 0.59 m with a mean of 0.24 m. From the distribution of errors, shown in Figure 5.5, it is observed that 95% of LiDAR returns do not penetrate to the ground surface. However, the absence of large negative residuals suggests that the density of ground returns is high enough to record subtle undulations in the terrain.

[19] LiDAR survey completed 26th March 2003 with ground transects measured August 2004.

(iii) Closed forest canopy

The largest variation in the residuals is observed in the closed forest canopy, which comprises 6 transects (n =222). The range in residuals (–1.16 to 1.16 m) means that ground surface can be underestimated or overestimated by the same amount. The distribution of error, presented in the dot plot, suggests that 90% of the residuals lie between –0.3 and 1 m. The negative error values suggest that in some areas the number of returns from the ground surface is insufficient to characterise the underlying topography, as shown in Figure 5.7. In this example, it can be seen that the low point density, coupled with the distribution of points, results in both under- and over-estimation of the ground surface, compared with the measured surface.

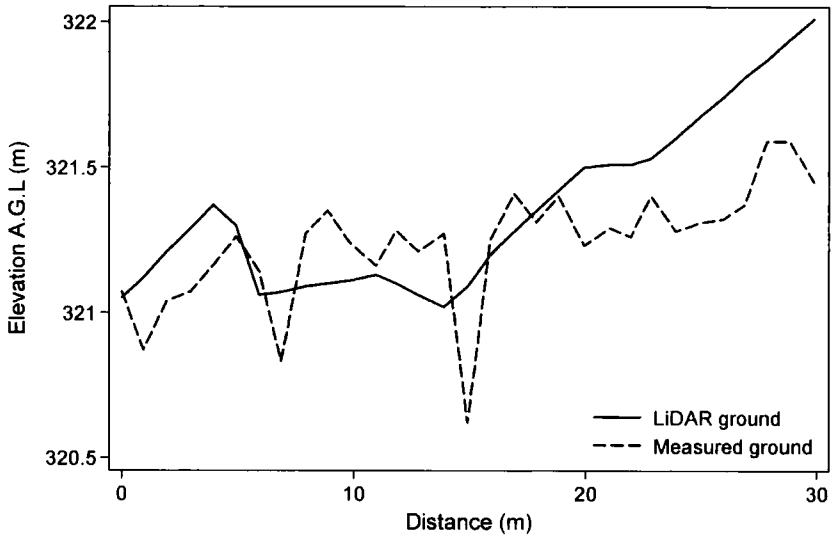

Figure 5.7 Survey transect through a closed canopy site, retrieved from ground survey and DTM.

5.4 DCHM accuracy

The process of generating the DCHM involves subtracting the DTM from the DSM, thus any errors inherent in the DTM are propagated to the DCHM. In mitigation, the DCHM was normalised by subtracting the mean DTM error (using the values in Table 5.1) for each forest site class from the height of each tree (derived from the DCHM). For example, in open canopy plots the DTM is overestimated by 0.24 m, so this amount was subtracted from DCHM. Table 5.2 provides a summary of the differences between

field-measured tree heights and those derived from the LiDAR DCHM for the two forest canopy classes.

Table 5.2 Summary statistics for the DCHM elevation residuals, by canopy class ($n = 99$)

Site Reference	Mean (m)	SD (m)	Min. (m)	Max. (m)	No. trees
Closed canopy	–1.71	1.33	–4.12	1.77	80
Open canopy	–1.73	0.68	–2.57	–0.39	19

The difference between means of the two canopy classes is small; in both cases tree heights are underestimated by approximately 1.7 m. The higher standard deviation observed in the closed canopy class indicates that there is greater variation here than in the open canopy class (1.33 and 0.68 m respectively). The range of values in the closed canopy data (–4.12 to 1.77 m) shows that tree height can be either under- or over-estimated. In contrast, in an open canopy situation, heights of trees are consistently underestimated. The overall relationship between the DCHM and measured height is shown in Figure 5.8. The line of best fit used to predict dominant height from the DCHM, derived using least-squares, has an intercept of 1.07 m, with an RMS error of 1.66 m and $R^2 = 0.99$. Comparison with the $y = x$ line shows that tree heights below 20 m are underestimated, while those above 20 m can be either overestimated or underestimated.

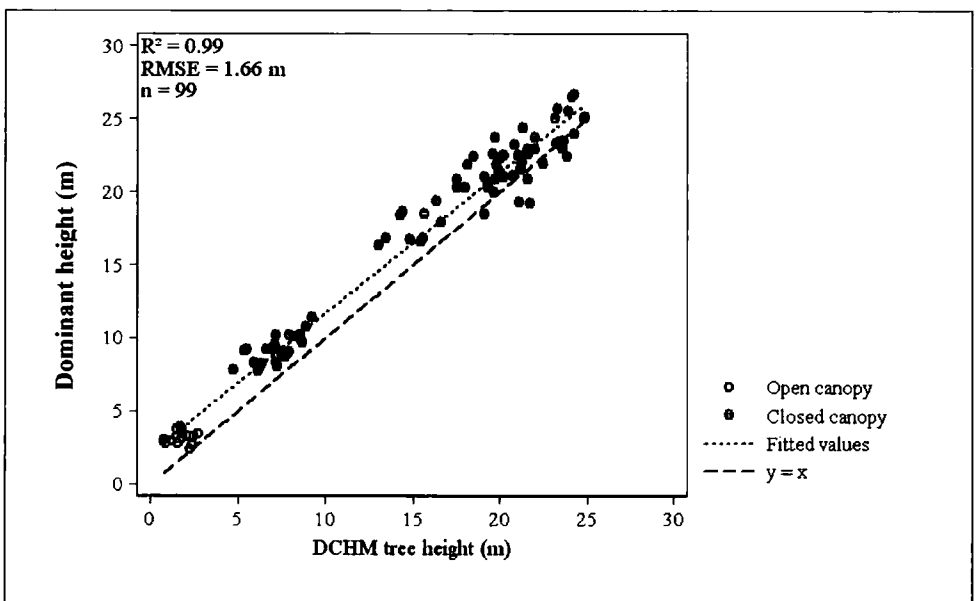

Figure 5.8 Estimated tree height in the DCHM (dominant trees only) against field-measured tree height.

The frequency distribution (Figure 5.9) shows the spread of the height residuals in both canopy classes. In open forest canopy a systematic underestimation of height is observed, with approximately 75% of the residuals falling between –1.29 and –2.57 m. In contrast, in closed forest canopy the height residuals show more variability. Approximately 85 % of the residuals are negative which indicates that tree height is more often underestimated. Approximately 15% of the residuals are positive which suggests that tree height can also be overestimated.

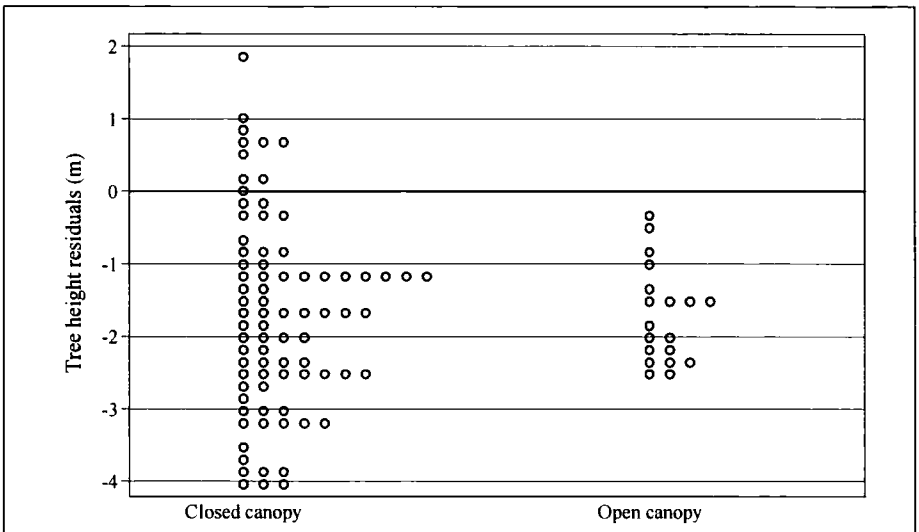

Figure 5.9 Distribution of height residuals in the DCHM, by site type.

The pair plot (Figure 5.10) illustrates the difference between the means of two height measures, DCHM and field-measured height (h_{dom}), against dominant tree height aggregated to the plot level. Closer scrutiny of the positive height residuals reveals that these values can be attributed to two closed canopy sample plots with tree heights greater than 20 m. Pyysalo and Hyyppä (2002) and Naesset and Økland (2002) noted that the accuracy of hypsometer-measured tree height in Scandinavian forests was less than 0.5 m. For trees greater than 25 m, however, the error can be up to 1.5 m. According to the hypsometer manufacturer Haglöff, a calibrated instrument has an absolute accuracy of ±0.01 m (www.haglofsweden.com) and therefore most of the observed error must be due to the operator. The largest error observed in this research is 1.3 m, slightly less than that observed in the two Scandinavian studies.

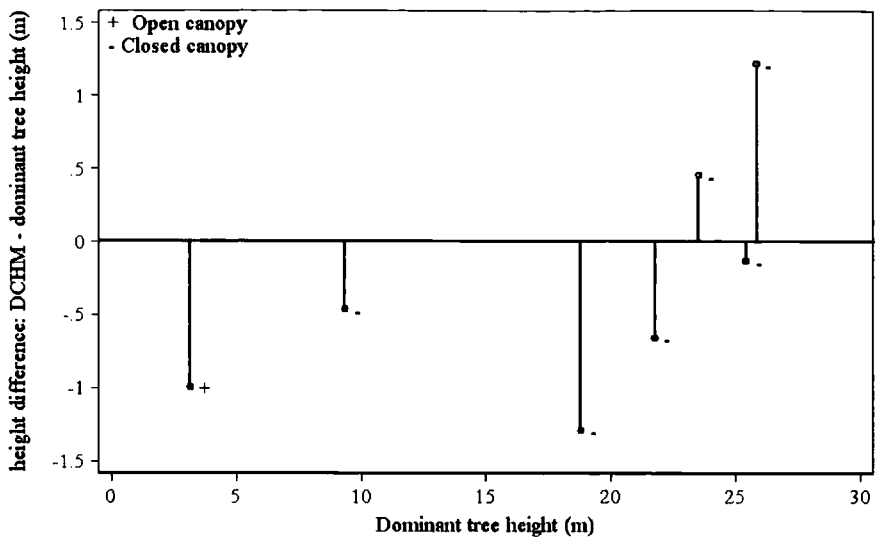

Figure 5.10 Difference between dominant tree height in the DCHM and mean field plot dominant height.

5.5 LiDAR height estimates at the plot level

To assess the influence of variables such as canopy structure, terrain slope and LiDAR sampling density, the analysis was expanded to include all 60 sample plots. This analysis was conducted at plot level, rather than tree level. Initially the height difference for each plot was calculated by subtracting the maximum LiDAR height from field-measured dominant tree height. The difference is the sum of errors from the DTM, tree height measurement and LiDAR system. Figure 5.11 shows the plot level relationship between dominant height and the DCHM, and for comparison, Figure 5.8 (introduced earlier) shows the relationship between dominant height and the DCHM at tree level.

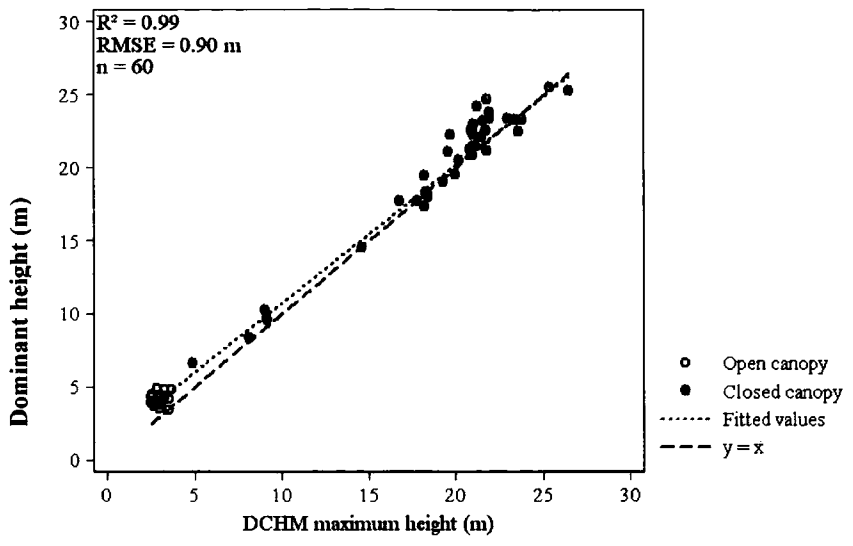

Figure 5.11 Estimated canopy height in the DCHM against field-measured dominant tree height, at plot level.

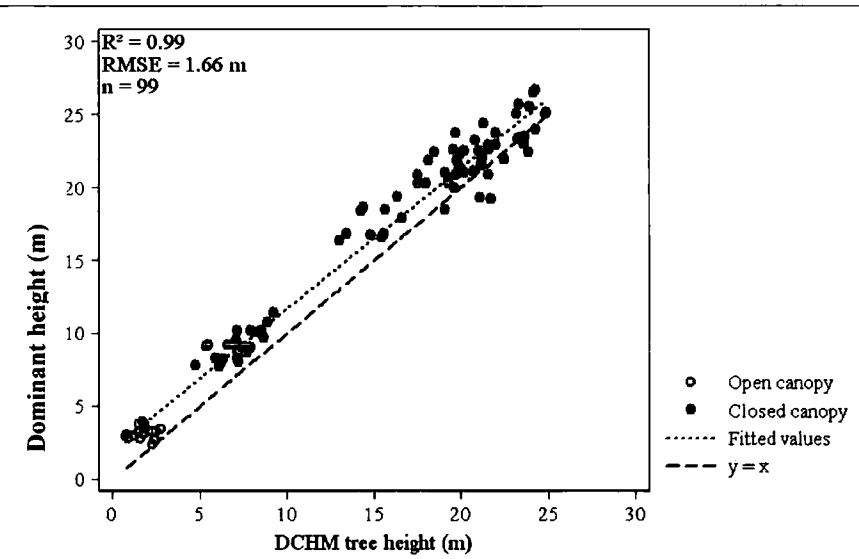

Figure 5.8 (**repeated for reference**) Estimated tree height in the DCHM against field-measured dominant trees.

Both tree and plot level relationships are similar, as indicated by the R^2 (0.99), however the RMS error is higher for the tree level dataset (1.66 m cf. 0.90 m). This is to be expected since the comparison for the plot level dataset is based on the mean plot value, rather than individual tree heights. This has the effect of reducing the height variation, which leads to the lower RMS error.

5.5.1 Effect of forest structure and LiDAR related variables on LiDAR height estimates

The difference (or residual) between the measured and predicted height at plot level was analysed by evaluating the correlations in Table 5.4 and graphically using scatterplots (Figures 5.11 to 5.13). Table 5.3 summarises the selected variables used in the analysis. These variables can be divided into three groups: (i) general forest structure, namely timber volume, dominant height and tree density; (ii) measures of canopy structure, namely canopy width and length, live canopy ratio, canopy to tree diameter ratio and canopy area (iii) terrain and LiDAR scanner-related variables, namely ground slope, LiDAR point density and percentage of ground returns.

Table 5.3 Summary statistics of forest structure, terrain, LiDAR return density and percent ground returns: Kielder forest dataset.

Variable	Description	Units	Mean	S.D.	Min.	Max.
$n = 60$						
V	Total volume	m^3 /ha	289.41	280.36	0.00	792.58
hdom	Dominant height	m	14.05	8.52	3.40	25.50
N	Tree density	trees /ha	3175	1723	1450	12300
K	Crown width	m	2.49	0.82	0.85	4.58
K_l	Crown length	m	4.75	1.96	1.51	9.59
K_g	Live crown ratio	%	63.17	33.42	17.98	100
Kd	Crown/tree *dbh* ratio	-	26.98	14.96	9.00	49
K_a	Crown cover	%	71.18	9.99	43.00	94
denfp	No. First pulse returns	returns/m^2	2.87	2.20	1.00	9.00
pczero	Ground returns	%	5.83	5.19	0.17	18.63
slope	Ground slope	°	4.33	2.44	1.00	16.00

Table 5.4 shows correlations between the various plot level variables and the residual height values. All variables evaluated are weakly correlated (≤ 0.42) with residual height (*Hres*). However, the correlation between selected field-measured variables is strong, as noted previously in Chapter 4. Scatterplots are used to further evaluate the effect of forest structure and LiDAR related variables on height measurements made using LiDAR.

Table 5.4 Correlations between residuals and each of the variables: Kielder forest dataset.

Variable	Description	*Hres*	*V*	h_{dom}	*N*	*K*	K_l	*Kd*	K_g	K_a	*denfp*	*pczero*	*slope*
Hres	hdom max − LiDAR hgt	1.00											
V	Total timber volume	0.06	1.00										
h_{dom}	Top height	0.10	0.96	1.00									
N	Tree density	−0.24	−0.10	−0.20	1.00								
K	Crown width	−0.09	0.67	0.72	−0.44	1.00							
K_l	Crown length	−0.02	0.73	0.73	−0.40	0.77	1.00						
Kd	Crown/tree *dbh*	−0.21	−0.91	−0.96	0.25	−0.61	−0.70	1.00					
K_g	Live crown ratio	−0.23	−0.89	−0.95	0.20	−0.63	−0.56	0.95	1.00				
K_a	Crown cover	−0.14	−0.24	−0.18	−0.31	0.30	0.09	0.22	0.18	1.00			
denfp	% first pulse returns/m^2	0.18	0.02	0.04	0.07	0.11	−0.16	−0.02	−0.11	0.12	1.00		
pczero	% Ground returns	−0.17	−0.76	−0.82	0.36	−0.71	−0.69	0.83	0.82	−0.11	-0.18	1.00	
slope	Ground slope	0.42	0.06	0.08	−0.19	−0.07	0.12	−0.16	−0.10	−0.17	0.04	-0.10	1.00

5.5.2 Analysis of height residuals using scatterplots

In scatterplots the symbols – and + are used to indicate closed canopy (absence of understorey vegetation) and open canopy (presence of understorey vegetation), respectively. A horizontal line at zero is added to each scatterplot to divide the residuals into positive (over-estimation of height) and negative values (under-estimation). An estimate of error in field height measurements is added, by using the largest positive difference between the LiDAR and field height measurement (1.22 m[20], as identified on Figure 5.12a). It is assumed that this error is not just additive but is also present as an under-estimate of the same magnitude. The two dashed lines drawn on each scatterplot indicate the minimum and maximum error in the field-measured height, for closed canopy plots only.

(i) General forest structure

The same patterns noted earlier in tree level data are also observed at plot level, with tree height consistently underestimated if errors associated with tree height measurements are ignored. Figures 5.12a and b show scatter in the residual height against total volume and dominant height. A similar pattern in the residual error is observed in both variables, with errors initially high (0 to −2.2 m) then decreasing at canopy closure (10 m tree height) and then steadily increasing as tree volume and height increase. Interestingly, almost all of the residuals outside the 1.22 m threshold occur in the closed canopy plots located in plantation mixtures. There is no obvious relationship between the size of the residual error and tree density, as is shown in Figure 5.12c. However, it is noted that less error is observed in closed canopy plots when tree density is less than 2,000 trees/ha. Above this density there is no apparent structure in the error.

[20] Note field height residual value is less than the 1.3 m observed in section 5.1.4, as the calculation is at plot level.

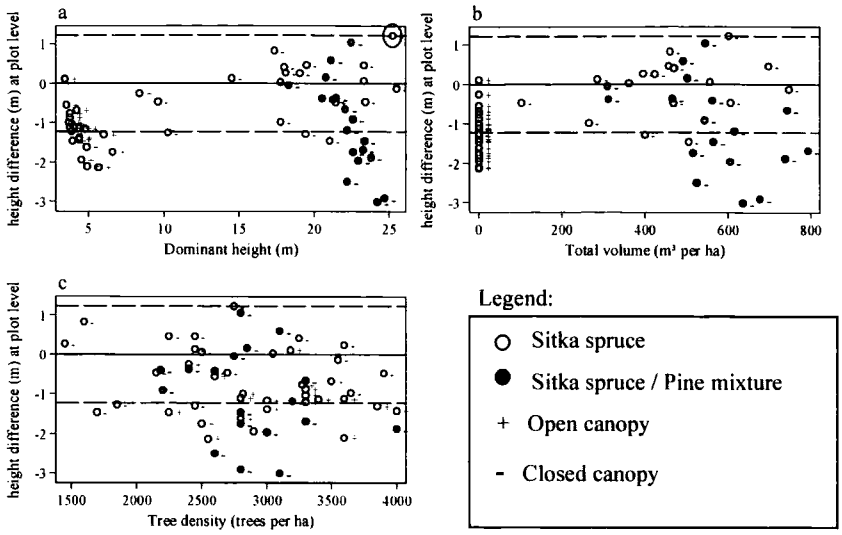

Figure 5.12 Height difference between DCHM and field-measured dominant height against measures of general forest structure.

(ii) Measures of canopy structure

Four measures of canopy structure are presented in Figures 5.13 a to d, to assess their effect on LiDAR response. No linear trend is apparent in the scatter of the residuals for crown width or length (Figure 5.13a and b), but it is clear that size of the height underestimation is similar in both closed and open canopies. This pattern is also observed in the canopy to tree *dbh* ratio (*Kd*), with error increasing at high and low ratios (Figure 5.13c). *Kd* provides a measure of crown width, relative to tree diameter, and is highly correlated with total volume (−0.91) and dominant tree height (−0.96). Lower ratio values are associated with taller trees and greater tree volumes (Figure 5.13d).

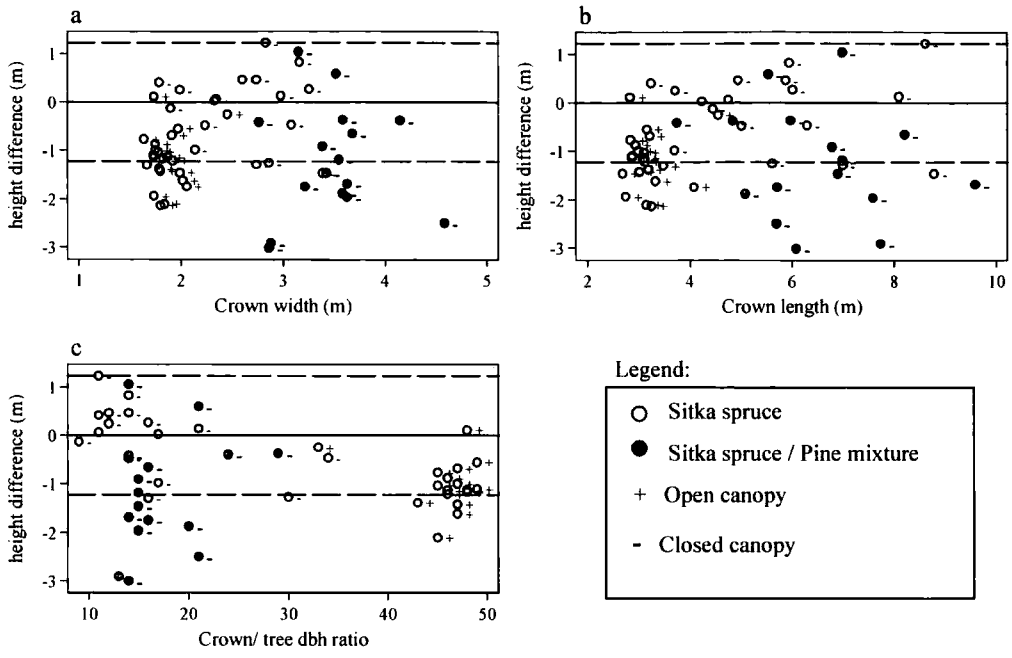

Figure 5.13 Height difference between DCHM and field-measured top height against measures of forest canopy structure.

(iii) Terrain and LiDAR scanner related variables

A pattern in residual error begins to emerge when the density of first pulse returns (Figure 5.14a) and the percentage of returns from the ground surface (Figure 5.14b) are considered. In open canopy plots height underestimation decreases as the number of first pulse LiDAR returns increases above 2 returns/m^2. In closed canopy plots the same pattern is not obvious, since most of the residual error lies within the 1.22 m threshold, even at 1 return/m^2. Plots located in plantation mixtures consistently lie outside this threshold. In this study increasing the number of returns from 2 to 8 returns/m^2 did not appear to result in a substantial reduction in error.

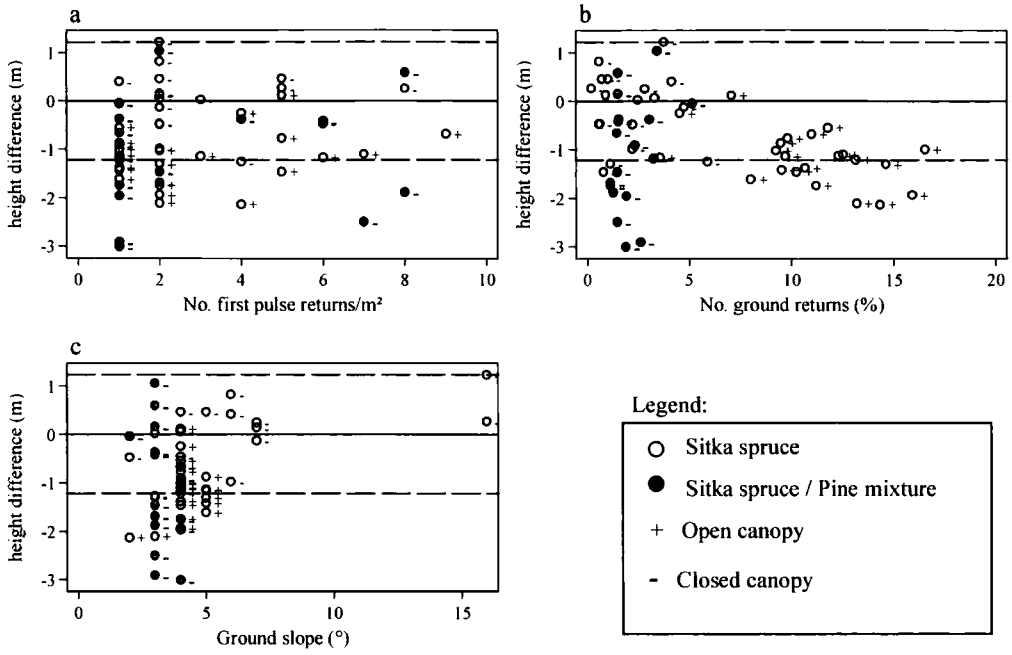

Figure 5.14 Height difference between DCHM and field-measured dominant height against measures of terrain and LiDAR scanner-related variables.

Less than 5% of LiDAR pulses are returned from the ground in closed canopy and up to 17% in open canopy plots (Figure 5.14b). In open canopy plots, the error increases as the percentage of ground returns increases, indicating that the error is not associated with the ground DTM, but more with the DCHM. In closed canopy plots the situation is more complex and substantial variation is observed between sample plots. Plots containing a mixture of species show the greatest variation. Analysis of Figure 5.14c suggests that there is no relationship between slope and the differences in height. The presence of two plots above 15° slope inflates the correlation (r = 0.44), but this is probably related to errors in field measurement of tree height rather than ground slope.

5.6 Discussion

The objective of this chapter was to assess, in dense conifer plantations, the accuracy of the two LiDAR surfaces, the DTM and the DCHM, and the influence at plot level of canopy structure, terrain slope and LiDAR sampling density. This section evaluates: (i) the accuracy of the LiDAR instrument; (ii) the accuracy of LiDAR in open canopy crops; (iii) the accuracy of LiDAR in closed canopy crops; (iv) the accuracy of LiDAR height estimates compared with field height estimates.

(i) The accuracy of the LiDAR instrument

The discrepancies between the raw LiDAR point data and the reference points measured on forest roads (± 0.18 m) are close to the vertical tolerances expected from the Optech 2033 instrument (± 0.15 m). Also, the planimetric accuracy in x and y of the LiDAR survey is thought to be less than the published value of ± 0.60 m for this instrument. This concurs with the error levels noted by Baltsavias (1999) and Gaveau and Hill (2003), who also evaluated Optech's airborne laser scanners (ALTM 1020 and 1210). Therefore, LiDAR system error appears negligible and does not contribute substantial error to the canopy height estimations.

(ii) The accuracy of LiDAR in open canopy plantations

Results presented in section 5.2 show that in open canopied forests the number of ground returns is high enough (≤17%) to create a DTM that characterises the ground surface. The mean overestimation of the ground surface is 0.24 m, which is comparable to the height of the understorey vegetation. In contrast, the DCHM does not accurately record the tree apex, which leads to an average tree height underestimation of 1.71 m. At this growth stage the tree shape is conical and is characterised by a thin elongated leader, positioned above the tree crown, as shown in Figures 5.15a and 5.15b.

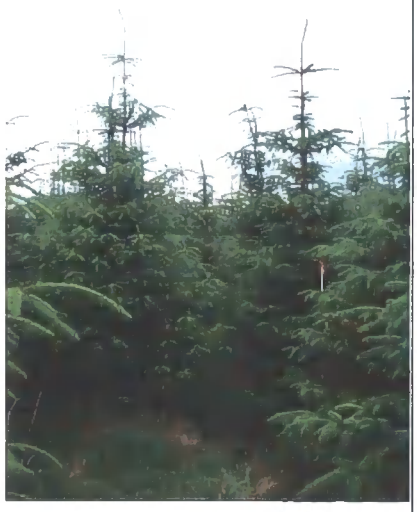

Figure 5.15a Photograph of a Sitka spruce open canopy crop.

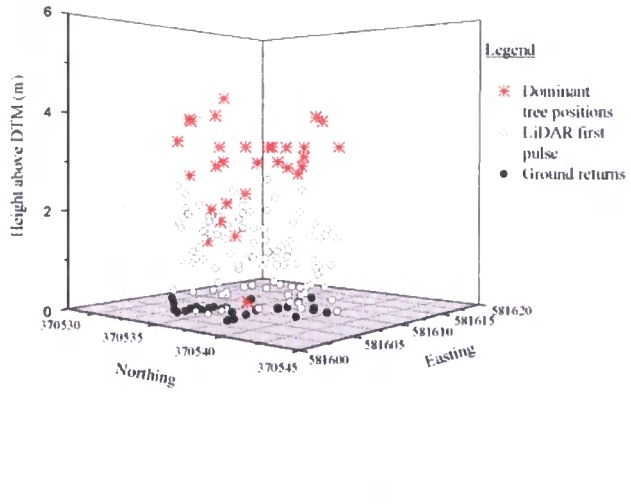

Figure 5.15b 3D plot showing tree locations and LiDAR first return and classified ground returns in a Sitka spruce crop.

When the data are analysed at plot level (Figure 5.14a) the size of the height underestimation decreases to around 1 m, as the number of LiDAR returns/m^2 increases above 6 returns/m^2.

(iii) The accuracy of LiDAR in closed canopy plantations

In closed canopy stands the DTM generally overestimates ground surface height by 0.17 cm, with an associated SD of ± 0.46 m. However, plot level data suggest that larger errors are observed in plantation mixtures than in pure Sitka spruce stands. Density and structure of the canopy are the most important factors influencing the accuracy of the DTM. This applies, even at higher LiDAR sampling rate, as dense canopy structure presents little opportunity for the laser to penetrate to the ground surface, except along rides or through forest gaps. Consequently, the number of ground returns is low (≤5%) and, depending on the canopy structure, unevenly distributed. The low number, and uneven distribution, of ground returns presents a problem in situations where the ground is undulating and the forest canopy is very dense. LiDAR point coverage becomes too clustered and irregular to create a DTM (at any resolution) characterising the ground surface. This effect is illustrated in Figure 5.16a, which shows an example of a structured plantation mixture of Sitka spruce and lodgepole pine with trees planted on the top of ridges. Figure 5.16b shows the first return and classified ground return distribution and the location of field-measured dominant trees for the same sample plot. For comparison, Figure 5.17a and b show a pure Sitka plantation of the same age, planted at the same tree density with trees also planted on ridges.

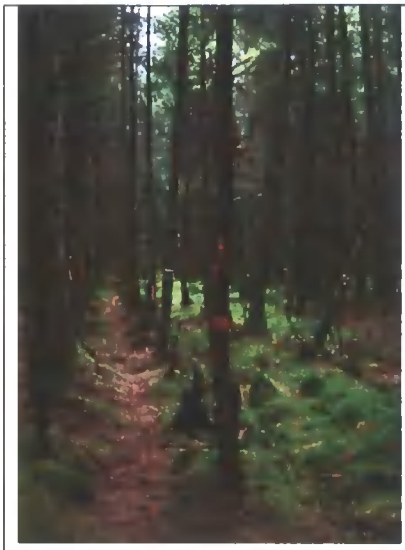

Figure 5.16a Photograph of a structured Sitka spruce/lodgepole pine mixture.

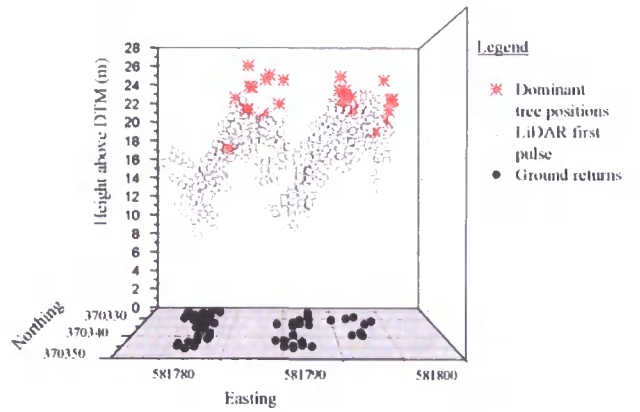

Figure 5.16b 3D plot showing tree locations, LiDAR first return and classified ground returns for a 20 x 20 m square sample plot located in a structured Sitka spruce/lodgepole pine mixture.

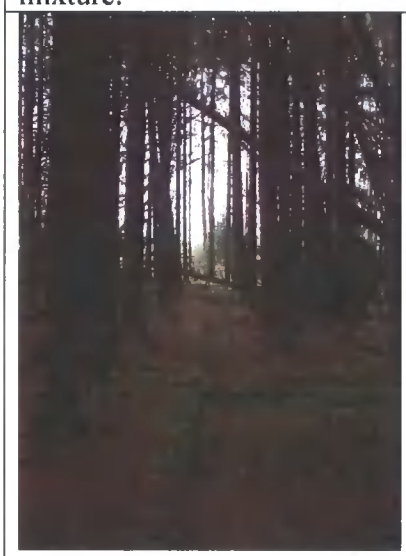

Figure 5.17a Photograph of a pure Sitka spruce crop.

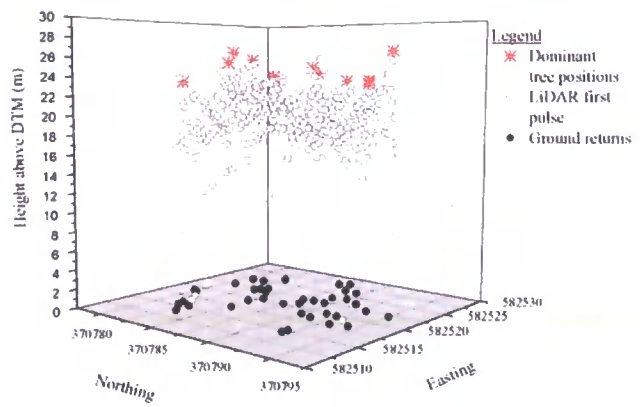

Figure 5.17b 3D plot showing tree locations, LiDAR first return and classified ground returns for an 8 m circular sample plot located in a pure Sitka crop.

In both stands, the percentage of ground returns is the same (~5%), but the spatial distribution is very different, with a linear clustering of LiDAR ground returns observed in the species mixture. This effect can be explained by Figure 5.13c, which presents height residuals versus *Kd*, physical differences are observable in the canopy structure between pure Sitka spruce and Sitka spruce/lodgepole pine crops. In the species mixture the canopy is much wider, longer and denser where Sitka spruce dominates, but quite sparse where the pine has died. This results in almost all of the ground returns

being confined to canopy openings that develop along plantation rows where the pine trees are dead or decaying. In contrast, in a pure Sitka spruce crop, tree competition creates localised gaps in the tree canopy. This fragmented canopy structure allows a more equal distribution of LiDAR returns.

Overall, tree height underestimation in the DCHM is 1.71 m with a SD of 1.33 m. However, if error in field height measurements (± 1.22 m) is taken into consideration, then error is overstated and more likely to be about 0.5 m. LiDAR sampling density is an important factor in determining how accurately the upper canopy surface is defined. The canopy surface becomes more homogeneous as tree height increases and the canopy closes (Figure 5.12a), indicating that a LiDAR density of 2 returns/m^2 is sufficient to characterise the canopy surface in closed canopy crops. Species mixtures are the exception; in these stands the canopy surface is discontinuous, characterised by tall Sitka spruce flanked by rows of dead pine (Figure 5.16b). This causes large variations in canopy height, which are not accurately defined at lower LiDAR return densities.

(iv) The accuracy of LiDAR height estimates

If the relationships between height residuals are assessed at plot level, it appears that LiDAR measured height is less accurate than field height measurements in young open canopy stands and closed canopy plantation mixtures. In young plantations (i.e. canopy <15 m) field height measurements made using traditional measurement methods are expected to be within ± 0.5 m, and ± 1.2 m for closed canopy plantations (i.e. canopy >15 m). In comparison LiDAR operates to within ± 2 m. However, it is likely that this level of error would be reduced if a regression equation were applied to the LiDAR data, particularly in young, open canopied plantations, where height is systematically underestimated. Furthermore, the inclusion of LiDAR-derived measures of crown density and shape could improve the accuracy of the height estimation, in both open and closed canopies. This is the focus of analysis in Chapter 6. It is, however, difficult to improve the estimation wherever the DTM is not accurately defined, as DTM and DCHM errors are inseparable. In this context, species mixtures are particularly problematic, as potentially large errors are observed in the DTM. Any improvement in height estimate is, therefore, restricted to improvement in the accuracy of the DCHM.

These estimates need to be treated with caution, as the level of accuracy is hard to determine without additional field checks.

5.7 Conclusions

When all potential sources of error are included, LiDAR is capable of measuring canopy height to within ± 2 m. The largest single source of error is observed in the DCHM. However, as forest canopy develops, small increases in the DTM error are also noted. Other specific observations include:

1. DTM error increases as tree height and canopy cover increase, but is most pronounced in plantation mixtures.
2. Dense canopy structure of plantation mixtures influences LiDAR penetration through the canopy. Therefore, increasing the density of LiDAR returns over 2 points/m^2 will not necessarily improve the accuracy of the DTM.
3. In open canopy crops the main error is found in the DCHM as LiDAR pulses are reflected from the lower canopy rather than the tree apex.
4. Error in the DCHM decreases as canopy closes, but this is not the case in plantation mixtures where the fragmented canopy structure causes larger variation in the DCHM, compared with pure Sitka spruce crops.
5. Errors in field height measurement are a substantial source of error.
6. As tree density and ground slope change, there is no substantial difference in accuracy between LiDAR and field-measured height.
7. Overall, the largest errors are in the DCHM, not the DTM.
8. The height difference between LiDAR and field measurements for young crops is large, but this error is systematic and could, in theory, be corrected. This is examined in Chapter 6.
9. Inclusion of LiDAR-derived measures of canopy density and shape might improve the accuracy of the height estimation in both open and closed canopies. However, larger errors may still be observed in plantation mixtures. This is also evaluated in Chapter 6.

Chapter 6: Forest estimates from LiDAR

6.1 Introduction

This chapter assesses the accuracy of forest parameter estimations, such as tree height, volume and density, derived from laser scanning data. A three-stage process is used: First, bivariate regression methods are used to generate relationships at the plot level between field measurements (of height, volume and tree density) and the various laser height percentiles. Second, additional LiDAR-derived crown density measures are calculated and included as predictors in multiple regression models. Third, results from selected regression models for top height, volume and tree density are compared with an independent dataset.

6.2 Forest estimates from LiDAR

Previous research has shown that LiDAR can be used to provide accurate estimates of forest variables that at present are measured using manual field collection and aerial photo interpretation methods (Holmgren 2003; Hyyppä et al. 2000; Naesset 1997; Persson et al. 2002). Forest estimates (of height, volume and biomass), using laser data, are often based on statistical measures derived from the distribution of laser point data. Magnussen and Boudewyn (1998) showed that for a given plot size and canopy structure, a certain percentile in the LiDAR height distribution exists that corresponds to the canopy height of interest (i.e. mean height). Other researchers have also noted that the inclusion of measures of canopy characteristics derived from the laser height distribution, in combination with selected laser height percentiles, have proven useful for estimating tree density (Naesset 2002) and timber volume (Nelson et al. 1984; Means et al. 1999; Naesset & Økland 2002). Sections 6.2.1 and 6.2.2 describe the methods used in this research to calculate the laser percentiles and canopy density measures.

6.2.1 Calculation of Laser height percentiles

For each sample plot, the first and last return pulses above 0.5 m were divided into quantiles corresponding to the 5, 10, 20,...,90, 95, 99 and 100 percentiles of the laser canopy heights. The 0.5 m threshold accounts for undulations in terrain caused by mechanical site preparation (as noted in section 5.15). Other researchers have used higher height thresholds (up to 3 m) to eliminate laser returns from the

understorey vegetation layer (Naesset 2002; Riaño et al. 2004). Lower thresholds are appropriate in UK conifer forests, because high numbers of trees are planted per hectare (>2,000 trees/ha) which leads to early forest canopy closure and ensures that an understorey is unable to develop.

Often both last and first pulse height distribution data are used when estimating forest variables. For example, in the literature it is common to see different statistics derived from these distributions (i.e. percentile height or distribution measures), which are then used as predictors to derive forest estimates (Naesset 2002; Riaño et al. 2004). Although not explicitly stated, the assumption is that distributions of laser returns are different for first and last pulses and therefore each provides additional information about the canopy structure.

However, this assumption does not appear to be valid for this dataset (60 sample plots) if all first and last pulse height returns above the 0.5 m threshold are compared (Figure 6.1). In this region both the frequency and laser pulse distributions are very similar. The degree of similarity can be tested statistically using a two-tailed *t* test. Where the *t* test is used to compare the mean heights of the last and first pulse returns for each sample plot, the results show that first and last pulse data are not different at the 5% significance level (see Appendix 6.1). The only exception is below the 0.5 m threshold where the frequency of last pulse ground returns is greater than the first pulse (identified on Figure 6.1 by the yellow line).

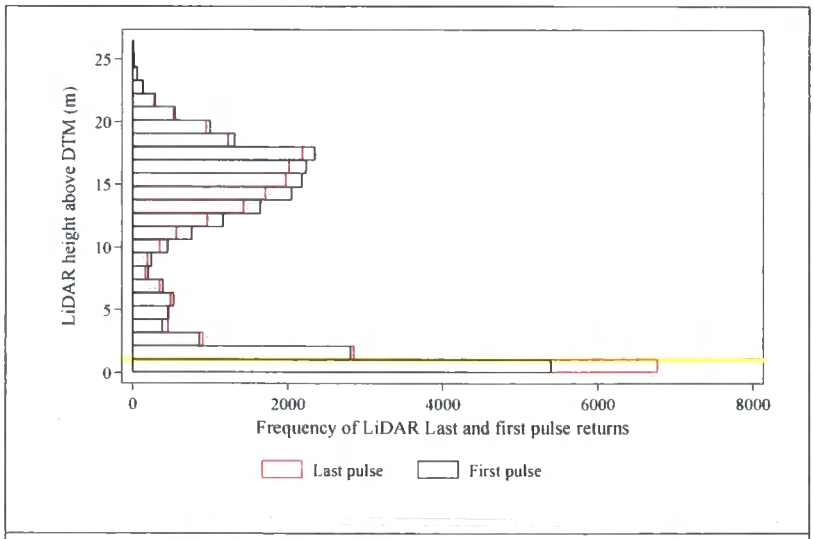

Figure 6.1 LiDAR height frequency distribution data for first and last pulses based on returns from field sample plots.

As there is no difference in distributions, the inclusion of last pulse data does not provide additional information on canopy structure. Consequently, height percentiles generated from last pulse data were not considered in this analysis.

6.2.2 Crown density measures

In addition to height, a number of variables that describe canopy structure can also be calculated from LiDAR distribution. As previously stated, these have been used to improve estimates of volume and tree density. Four field measures of crown density/ structure, that are sensitive to change in forest height and tree species composition, have been identified in Chapter 3. These are crown width (K) and length (K_l) and ratios, live crown (K_g) and crown width to tree diameter (Kd). For reference, the definitions and equations used to calculate each measure in Chapter 3 are shown in Figure 6.2.

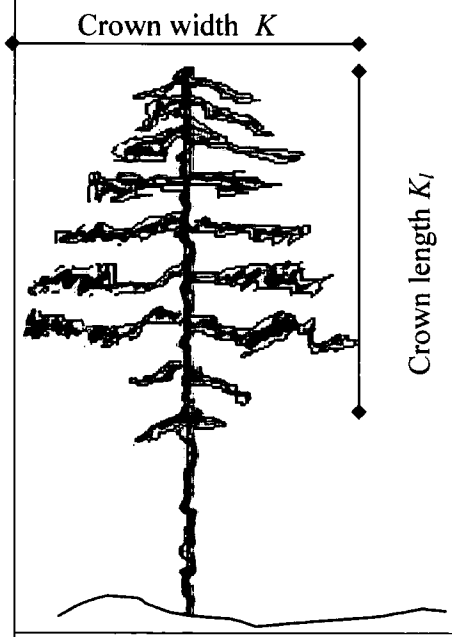

Live crown ratio (K_g)

$$K_g = \frac{h - K_l}{h} \times 100$$

Where:
K_g = live crown ratio, %
h = total tree height, m
K_l = live crown height, m

Crown to tree diameter ratio (K_d)

$$Kd = \frac{K}{dbh}$$

Where:
Kd = Crown to tree diameter ratio
K = Crown width, m
d_{bh} = Diameter breast height, m

Figure 6.2 Field-based forest canopy measurements.

Two further variables describing canopy structure are also calculated: skewness and kurtosis (see Equations 6.2 and 6.3). Table 6.1 presents summary statistics of all the plot level, LiDAR-derived canopy density measures, together with a description of each measurement and the method/equation used to derive it. To compare suitability of each measure, each is plotted against Kd, as this is highly correlated with field-measured height, volume and tree density.

Table 6.1 Summary statistics of LiDAR-derived canopy and canopy density measurements.

Variable	Description	Units	Mean	S.D.	Min.	Max.
pczero	Percent ground returns	%	6.70	4.49	0.34	18.20
Lk_l	Crown length	m	5.02	2.83	0.36	16.93
C_v	Coefficient of variation	-	0.26	0.13	0.09	0.51
Lk_v[21]	Crown volume (Riaño et al. 2004)	-	396.00	235.22	52.46	832.64
Skewfp	Skewness	-	–0.10	–0.72	1.95	1.54
Kurtfp	Kurtosis	-	3.63	1.75	2.03	11.96

(i) Percentage of ground returns

The percentage of ground returns (*pczero*) provides a simple measure of canopy density and is calculated by dividing the sum of all first and last pulse observations with height values below 0.5 m, by the total number of returns. All returns above this threshold are considered to be canopy hits. Intuitively, *pczero* decreases as canopy height increases and the forest canopy closes (scatterplot presented in Chapter 5, Figure 5.1). Analysis confirms that the percentage of ground returns is highly correlated (see Table 6.2) with top height and tree density ($r \leq 0.82$), but less so with volume (−0.37). Further, it is also highly correlated with all field-measured canopy density measures; canopy width, length, live crown ratio and crown/tree *dbh* ratio ($r \leq 0.73$).

(ii) Crown length and volume

Crown length and volume are more complex measures of canopy density, as the calculation requires some field knowledge of canopy structure - crown length in this case. LiDAR-derived crown length (LK_l) was calculated by subtracting the highest first pulse return from each of laser percentile heights (i.e. 5, 10, 20,...,90, 95, 99, and 100). Each crown length was compared with field-measured crown length (K_l) using regression analysis. From all possible permutations crown length, based on the 20th percentile height, yielded the highest R^2 and lowest RMS error of 0.65 and 1.17 m,

[21] Despite its name LiDAR-derived crown volume is dimensionless. It is calculated using a method suggested by Riaño et al. (2004) where crown length is multiplied by the percent of first pulse LiDAR vegetation returns.

respectively (see Appendix 6.2). Crown volume (Lk_v) was estimated using the method suggested by Riaño et al. (2004) where Lk_l is multiplied by the percentage of canopy returns, which is the complement of *pczero*. Inclusion of the percentage of canopy returns provides a representation of the proportion of total area covered by the canopy. It is worth noting that the relationship between field-measured crown volume (K_v) or crown cover (K_a) and Lk_v is weak ($r = 0.43$ and $r = -0.16$). These values are not shown in Table 6.2. This is attributed to two factors. Firstly, field-measured K_v is derived, using a model of a cone and, therefore, is a more complex approximation of crown volume. Secondly, in the case of field-measured crown area (K_a), the measurement does not account for the presence of dead trees, which have no measurable crown, while the LiDAR-derived measure does.

Lk_v is highly correlated (see Table 6.2) with the three forest variables of interest: top height, volume and tree density ($r \leq 0.69$), and the four field-measured canopy density measures, crown width and length and ratios Kd and K_g ($r \leq 0.71$). Lk_v values increase as tree height increases and the forest canopy closes. This is caused by an increase in the percentage of returns from the canopy. Figure 6.3 shows the relationship between Lk_v and crown width / tree diameter ratio (Kd).

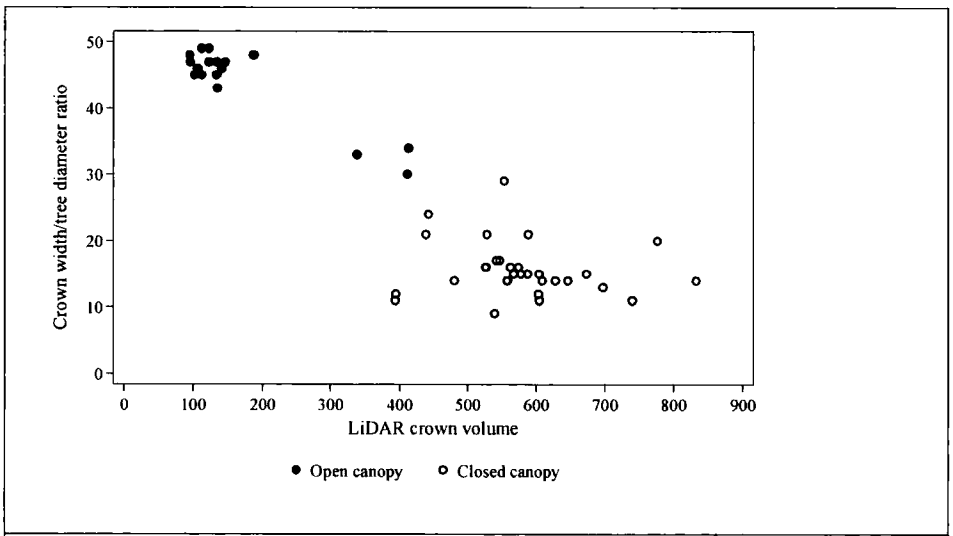

Figure 6.3 LiDAR crown volume against (based on 20th laser percentile) crown width / tree diameter ratio (Kd).

Table 6.2 Summary of correlations between field-measured and LiDAR-derived variables.

	Variable	Description	K	K_l	K_g	Kd	$Hdom$	V	N	$Pczero$	Lk_l	C_v	LK_v	$Skewfp$	$Kurtfp$
Field-based measurements	K	Crown width	1.00												
	K_l	Crown length	0.77	1.00											
	K_g	Live crown ratio	–0.63	–0.56	1.00										
	Kd	Crown/tree dbh ratio	–0.61	–0.70	0.95	1.00									
	$hdom$	Top height	0.72	0.73	–0.95	–0.96	1.00								
	V	Total volume	0.28	0.41	–0.67	–0.77	0.91	1.00							
	N	Tree density	–0.80	–0.78	0.81	0.84	–0.88	–0.52	1.00						
LiDAR-derived measurements	$Pczero$	% Ground returns	–0.74	–0.73	0.88	0.89	–0.87	–0.37	0.82	1.00					
	Lk_l	Lidar crown length	0.68	0.77	–0.86	–0.90	0.93	0.67	–0.83	–0.83	1.00				
	C_v	Coefficient of variation	–0.61	–0.64	0.95	0.95	–0.92	–0.66	0.80	0.88	–0.81	1.00			
	Lk_v	Lidar crown volume	0.71	0.79	–0.88	–0.92	0.94	0.69	–0.85	–0.88	0.99	–0.85	1.00		
	$Skewfp$	Skewness laser first pulse	–0.64	–0.55	0.72	0.70	–0.73	–0.20	0.73	0.69	–0.64	0.71	–0.65	1.00	
	$kurtfp$	Kurtosis laser first pulse	0.16	0.22	–0.40	–0.37	0.42	0.24	–0.36	–0.25	0.36	–0.35	0.34	–0.63	1.00

(iii) Coefficient of variation

The coefficient of variation (C_v) summarises the relative variation, or dispersion, of the LiDAR height distribution within each sample plot. It is the ratio of standard deviation and mean and is expressed as a percentage (Equation 6.1).

Coefficient of variation	$C_v = \frac{S.D.}{mean} \times 100$

Equation 6.1

As a measure of crown density, higher C_v values indicate sparse, open canopies and low C_v values dense, closed canopies (e.g. <20%). The inclusion of C_v has proven useful to other researchers for estimating basal area, volume and biomass (Naesset 1997; Naesset & Økland 2002; Nelson et al. 1997).

C_v is highly correlated (see Table 6.2) with the three forest variables of interest, top height, volume and tree density ($r \leq 0.80$), and the four field-measured canopy density measures; canopy width and length and the ratios Kd and K_g ($r \leq 0.61$). Figure 6.4 shows the relationship between C_v and crown width/ tree diameter ratio (Kd).

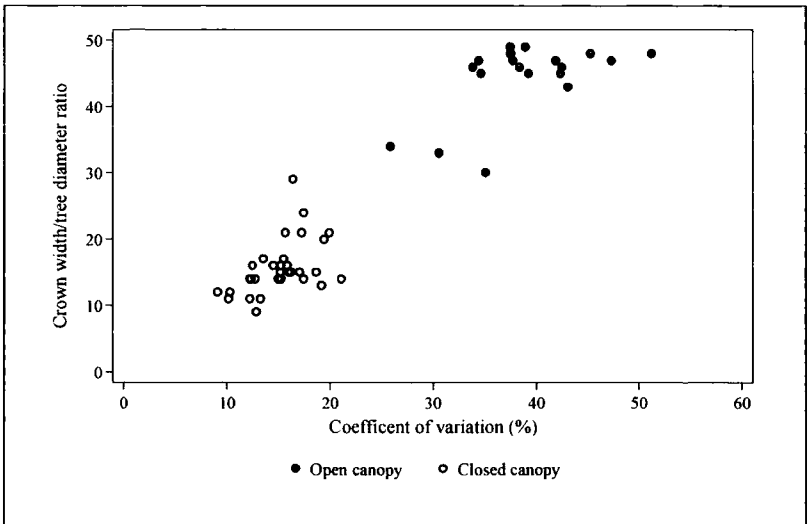

Figure 6.4 Coefficient of variation against crown width / tree diameter ratio (Kd).

(iv) Skewness and Kurtosis

Skewness (*skewfp*) and kurtosis (*kurtfp*) of LiDAR height distribution also provide measures of canopy structure and density. Here, the classical measures of skewness and kurtosis are used, where $\bar{y}$ is the mean of a variable y, s is the standard deviation, and n is the number of first pulse returns.

Skewness	$\frac{\sum_{i=1}^{n}\left(Y_i - \bar{Y}\right)^3}{n s^3}$

Equation 6.2

Kurtosis	$\frac{\sum_{i=1}^{n}\left(Y_i - \bar{Y}\right)^4}{n s^4}$

Equation 6.3

If returns from the forest canopy are solely considered, then as trees increase in height and the canopy develops, skewness and kurtosis of the laser height distribution change. This concept is demonstrated in Figure 6.5, which shows the histograms of the laser height distribution for four forest plots with different height and species compositions.

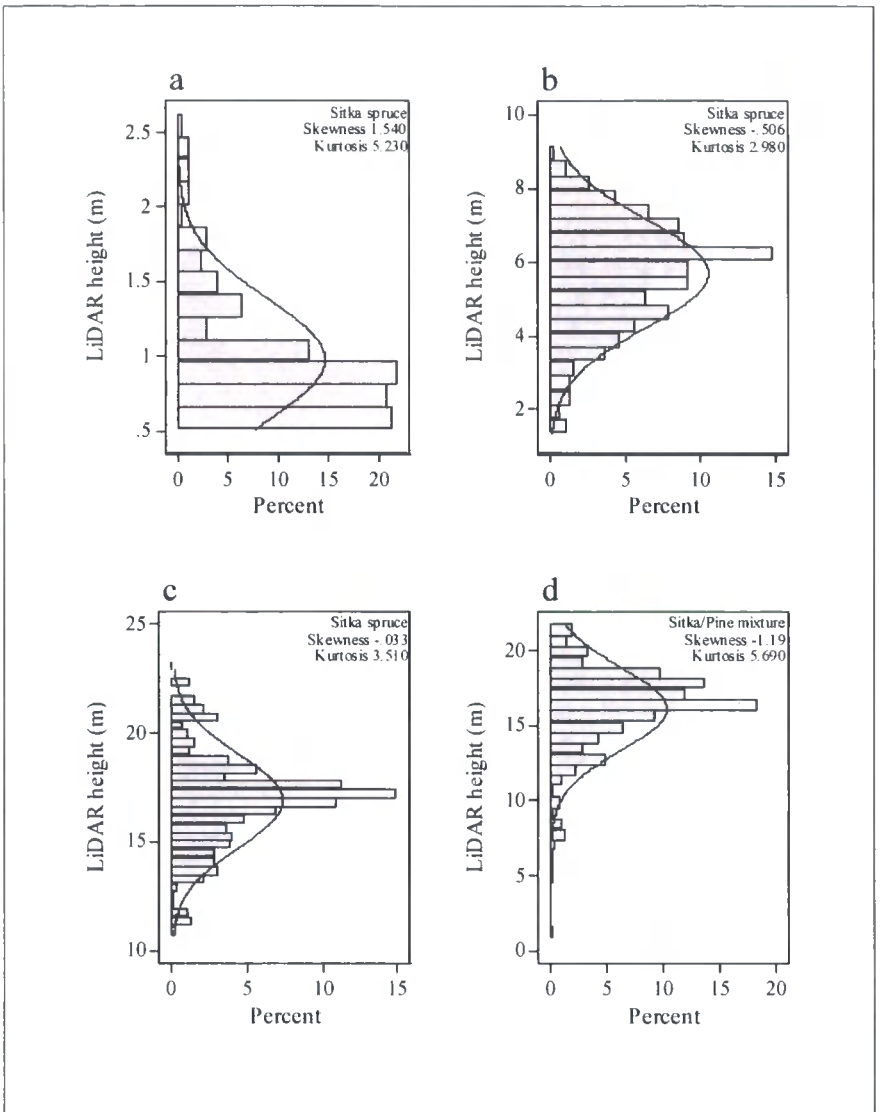

Figure 6.5 Laser height distribution for four forest plots at different growth stages; also included is a plot containing a mixture of Sitka spruce and lodgepole pine.

Compared with a normal distribution (curve plotted on each graph), the symmetry observed in each plot is different. Young plantations with open canopies show positive skewness[22] (1.54), indicating that the majority of the laser returns are reflected from the lower canopy. Canopies in transition approximate a symmetric distribution (Figure 6.5b) and closed canopies show negative skewness (Figures 6.5c and d). In closed canopies, the higher the negative skewness, the more homogeneous the forest canopy. In this context, sample plots that have denser and wider canopies show higher skewness values, which is one characteristic that separates species mixtures from pure Sitka

[22] The skewness direction is indicated by the position of the mean and median relative to the mode. If distributions are positively skewed, the mean and median are typically to the right of the mode and if negatively skewed, the mean and median are typically to the left of the mode.

spruce crops (Figures 6.5c and d). In comparison, kurtosis, which is a measure of the "peakedness" of the height distribution, is less sensitive to variations in canopy structure. Unlike skewness, kurtosis is not directional (i.e. negative or positive), so open canopies may have similar kurtosis to closed canopies.

This is demonstrated in Figure 6.6, which plots skewness and kurtosis against canopy width. Compared with skewness, kurtosis is more erratically scattered and shows no relationship with crown width: high kurtosis values are recorded at both low and high crown widths. Consequently, kurtosis is weakly correlated with field and LiDAR measurements ($r \leq 0.16$). In contrast, skewness shows moderate to strong correlations with LiDAR canopy measurements ($r = 0.55$ to 0.72) and higher correlations with top height and tree density ($r = 0.73$). Volume is poorly correlated ($r = -0.20$). For this reason, skewness is considered the more promising of the two measures for describing canopy structure.

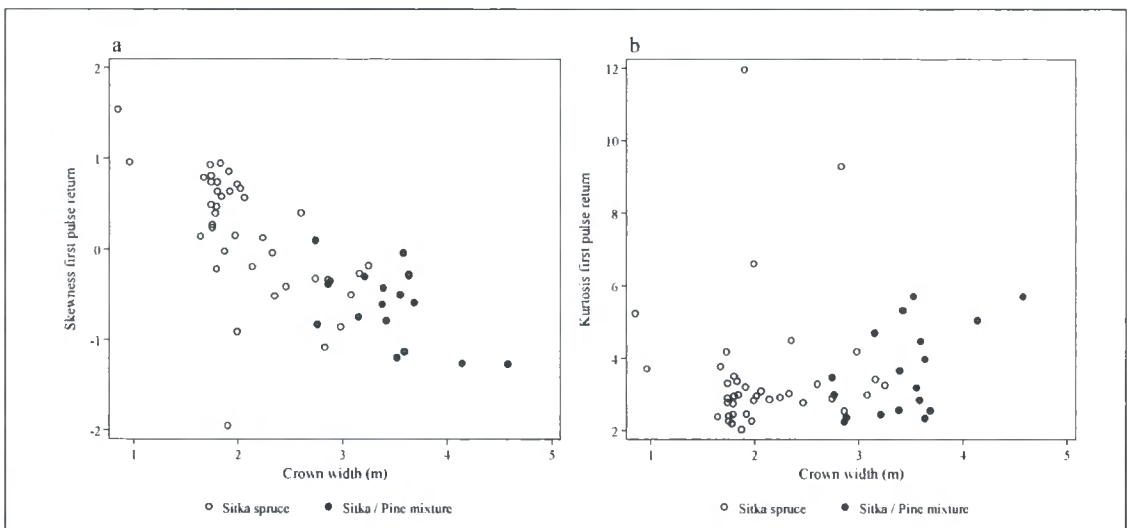

Figure 6.6 Skewness and kurtosis against crown width.

6.3 Modelling

Regression equations were fitted to predict top height, volume and density from laser measurements, using the 60 reference plots. For each variable, the laser height percentile with the highest R^2 and lowest RMS error values was used.

Multiple regression analysis was conducted to see if any further variation could be explained in the models by the inclusion of LiDAR-derived measures of canopy structure/density. Six predictor variables, described in section 6.1.2, were tested. These were: (1) percentage of ground returns (*pczero)*, (2) LiDAR-derived canopy length (Lk_l), (3) coefficient of variation (C_v), (4) LiDAR-derived crown volume (Lk_v), (5) skewness (*skewfp*) and (6) kurtosis (*kurtfp*). No variable was added to the model unless its contribution was significant at the 5% level. The presence of collinearity between variables was assessed by calculating the variance inflation factor (VIF). VIF measures the inflation in variance of the parameter estimate due to collinearity between the explanatory variable and other variables in the model (Equation 6.4).

Variance inflation factor	$VIF_j = \frac{1}{1-R^2}$

Equation 6.4

Here, VIF_j is the variance inflation factor for the explanatory variable and R^2 is the multiple coefficient of determination. According to Rabe-Hesketh and Everitt (2000) multicollinearity exists if VIF values are larger than 10 and if the mean VIF is larger than the VIF for individual variables.

The selected models were compared with top height, volume and density data measurements from 30 independent field plots. All samples were measured in pure Sitka spruce stands, because of a lack of plantation mixtures within the study area. Adjustments for tree growth were applied to top height and volume measurements, as these plots were recorded 1 year later than the dataset used to create the models. The adjustments were based on Forestry Commission (FC)-published annual increment data for Sitka spruce (Edwards and Christie 1981). Top height values were revised downwards by 0.58 m and volume increment by 12 m^3/ha. It should be noted that the corrections are based on average values.

6.3.1 Model selection criteria

In this research, a series of models were considered for the prediction of top height, volume and density. Commonly, model selection is based on assessing goodness of fit, using a single measure such as R^2. However, further insight can also be obtained by considering the RMS error of the model. This provides a measure of standard deviation of the data about the regression fit. The advantage is that RMS error has the same units as the response variable (e.g. height or volume). In addition to these measures, it is also important to consider other criteria. Cox et al. (*in review*) identify seven criteria that can assist in the model selection process (Table 6.3).

Table 6.3. Assessment criteria of models as suggested by Cox et al. (*in review*).

Criteria	Notes
Summary	Should capture the main features/behaviour in the system, which is relevant to the concerns of the investigation. In statistical terms a model should provide some measure of average components and a measure of variability.
Physical basis	Should ideally be based on physical principles.
Physical plausibility	If it is not possible to have a physically based model then it should at least be physically plausible.
Goodness of fit	The model should predict close to observations, but this can be problematic. For example, a closer fit may be achieved by increasing model complexity but this may not increase scientific insight. Also an improved fit may cause over-fitting, i.e. the relationship becomes too specific to the data it was derived from. Assessment generally done by examining single numbers, such as R^2, but residual plots should also be examined.
Simplicity	Should be simple enough to understand but complex enough to gain insight into the system characteristics.
Computability	Facilities to develop the model in the restricted time framework are required.
Comparability	The potential to compare the outcomes of models with other examples in the literature.

Similar criteria are also commonly cited in various forestry texts (Phillip 1998; Vanclay 1998) as a means of evaluating different models. Often, greater importance is placed on developing models that satisfy specific accuracy requirements, as well as providing realistic predictions over a range of ages and site conditions, since the predictions from such models are used to make management decisions. Unreliable predictions may lead

to sub-optimal decisions, so it is important that limitations are ascertained before use. The following section evaluates a series of LiDAR-derived models generated from the reference dataset (60 sample plots) to predict top height, volume and tree density.

6.4 Forest estimations

6.4.1 Top height

In Chapter 5, dominant height (i.e. height of the tallest trees in each plot) was used to assess accuracy of the LiDAR height estimation, because these trees are most prominent in the canopy and so are likely to provide LiDAR returns. However, in the UK the standard measurement used to provide a measure of a stand's productivity is top height[23]. Consequently, all Forestry Commission yield models are based on relationships between top height and age, and top height and volume. A description of how top height was derived from LiDAR data follows. Two models were assessed, one based on pure Sitka spruce plots (n = 38) and a second that included all sample plots regardless of tree species (n = 60).

6.4.2 LiDAR-derived top height

The percentile height with highest R^2 and lowest RMS error was selected as the predictor for estimation of top height. In this case, laser height values corresponding to the 99th percentile were used (Table 6.4). Between percentiles, differences in R^2 values are small, which implies that if separate models for each percentile were generated then each model would explain a similar amount of variance. However, if RMS error of each top height model is considered then differences between the percentiles become apparent (Table 6.4).

[23] Top height is the height of the tree with the largest breast height diameter in a 0.01 ha sample plot. This is not necessarily the tallest tree.

Table 6.4 Summary of LiDAR height percentiles used to estimate top height.

	Top height Sitka spruce $n = 38$		Top height All species $n = 60$	
Height percentile	R^2	RMSE (m)	R^2	RMSE (m)
10	0.960	1.70	0.978	1.18
20	0.970	1.49	0.983	1.02
30	0.975	1.35	0.986	0.93
40	0.979	1.24	0.988	0.86
50	0.982	1.16	0.989	0.84
60	0.984	1.09	0.989	0.82
70	0.985	1.03	0.989	0.82
80	0.987	0.96	0.990	0.79
90	0.989	0.87	0.992	0.72
95	0.990	0.83	0.993	0.67
99	0.991	0.80	0.995	0.57
Maximum height	0.989	0.90	0.995	0.58

The differences can also be seen in the associated scatterplots (Figure 6.7a to l). The most prominent trend is for scatter to decrease above the 80th LiDAR height percentile: if lower height percentiles are used, top height is underestimated. Whilst the 99th percentile was selected because of its low RMS error, the results suggest that any height percentile above the 80th percentile could be used to predict top height, without a substantial decrease in accuracy.

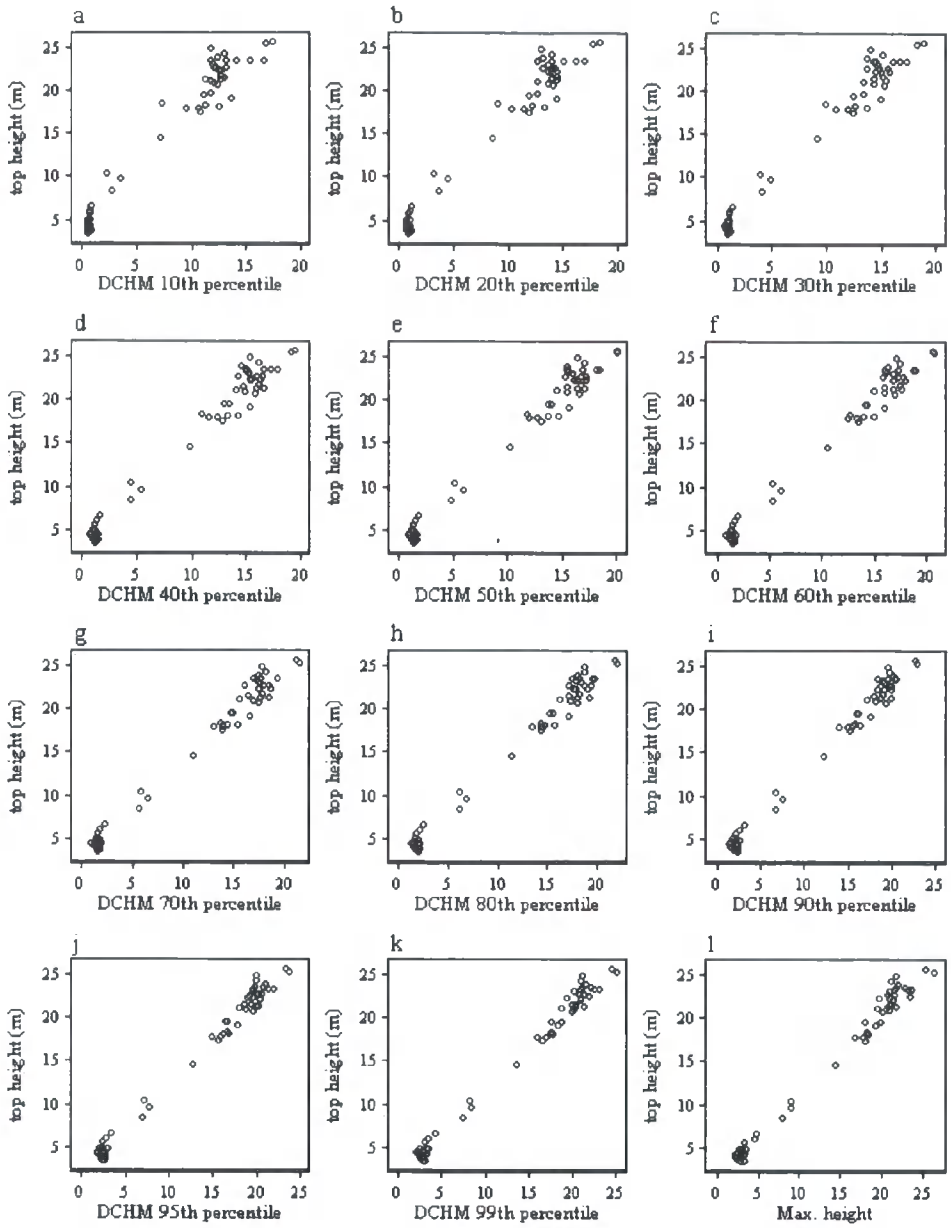

Figure 6.7 Top height against various LiDAR height percentiles.

The RMS error values for top height models, shown in Table 6.4, which are based on Sitka spruce and all species (Sitka spruce and mixture plots combined), also show that a single model that pools data from Sitka and Sitka spruce/lodgepole pine mixture plots provides a more accurate estimation of top height (RMS error = 0.57 m). Figure 6.8 illustrates the relationship between the 99th height percentile and field-measured top height, together with the two regression models, for Sitka spruce and all species. The same patterns identified in Chapter 5, where maximum tree height and LiDAR height

were compared, are also identifiable in Figure 6.8. Specifically, top height is underestimated in both open and closed canopy plantations. Variation increases as tree height increases; and sample plots comprising plantation mixtures show the largest variation. Figure 6.9 is a residual plot of the model fit for all species.

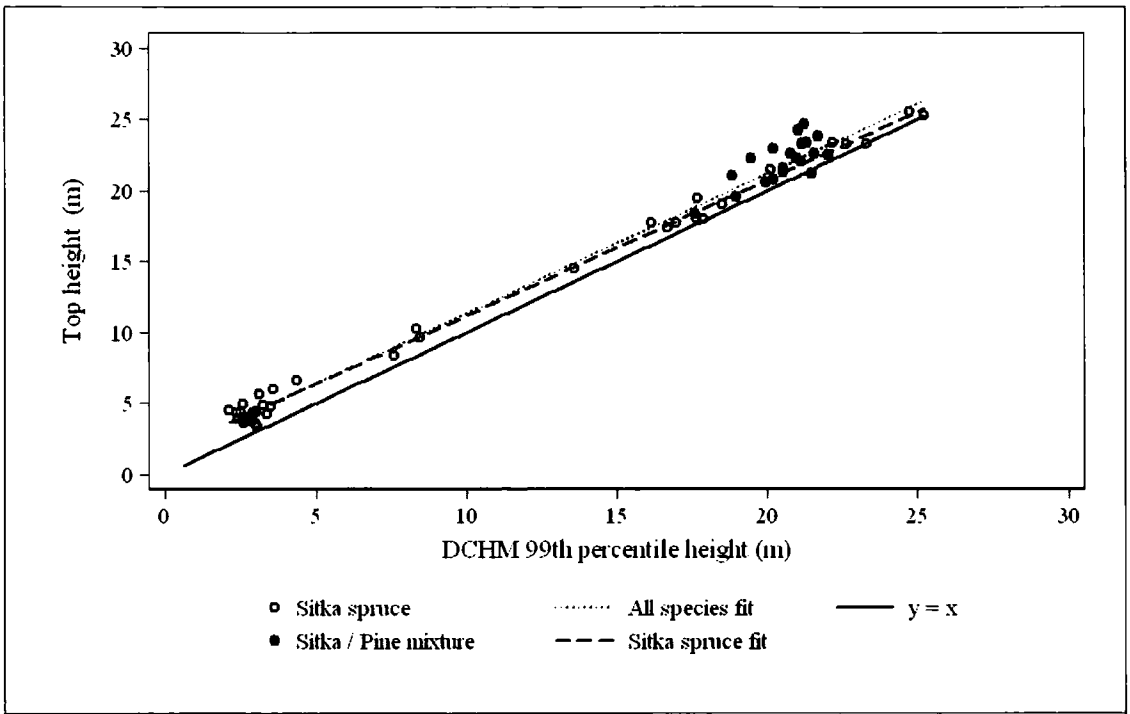

Figure 6.8 DCHM 99th height percentile against top height.

In the residual plot (Figure 6.9) the symbols P and M are used to indicate pure Sitka spruce crops and Sitka spruce/lodgepole pine mixtures, respectively. Absolute residual values increase with tree height, with a mild tendency for the outliers to be clustered in the plantation mixtures. It could be argued that recasting the model by applying a logarithmic transformation would reduce the variance in the residuals, an approach used in many studies (e.g. Naesset 1997; Means et al. 1999; Nelson 1997; Holmgren et al. 2003). However, the outliers in the untransformed model are genuine and are caused by a combination of field-measurement error (up to 1.3 m) and errors in the LiDAR DTM, so by transforming the data these outliers may well be hidden (Figure 6.10).

In this case, it is more important to note that top height estimates will be less accurate in plantation mixtures than in pure Sitka spruce crops. Identification of these crops would therefore be advantageous if top height were to be predicted at a wider scale using a

LiDAR-derived top height model. Methods of detecting plantation mixtures are further discussed in Chapter 7.

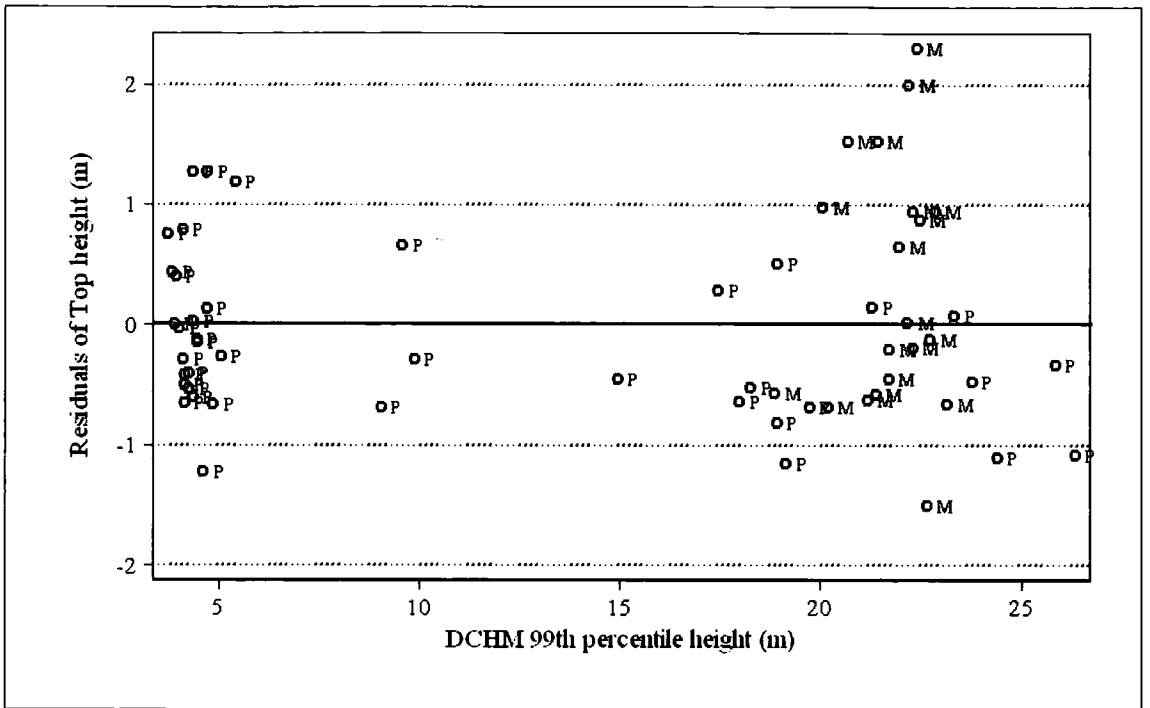

Figure 6.9 Residual versus fitted plot for top height.

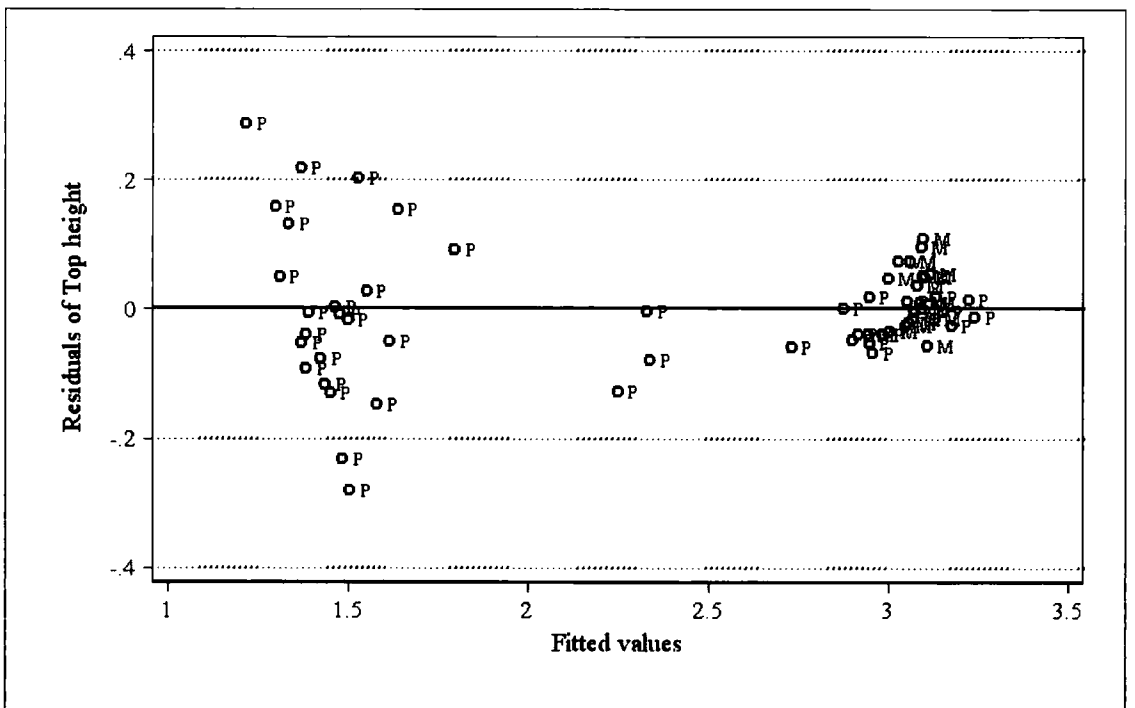

Figure 6.10 Residual versus fitted plot. Top height and DCHM 99th percentile, transformed using the natural logarithm.

6.4.3 Considering multiple predictors

The results show that top height is accurately estimated using a single predictor. However, the scatter of residuals in Figure 6.9 suggests that errors >1 m are possible in both younger crops and plantation mixtures. It was shown in Chapter 5 that canopy height in younger crops is systematically underestimated, because the laser pulse misses the tree apex. The underestimation in plantation mixtures is caused by a combination of factors, which makes it difficult to model the error

To investigate whether the top height model can be improved, particularly for younger crops, multiple regression, including other percentile heights and canopy structural variables, was used. Beginning with an empty model, all variables were considered but a variable was only added if the p-value fell below 5% (i.e. where inclusion of a variable was warranted because it significantly improved the fit of the model). In all, five variables were added to the model, including four LiDAR height percentiles and one measure of canopy density (Table 6.5).

Table 6.5 LiDAR variables considered in the prediction of top height

			R^2= 0.99	RMSE = 0.65	Prob > F = 0.00
Variable	Description	Coefficient	Standard Error	t- statistics	Prob >|T|
p99	99th height percentile	0.66	0.15	4.310	0.000
p20	20th height percentile	−1.50	0.34	−4.430	0.000
p80	80th height percentile	1.08	0.24	4.580	0.000
p10	10th height percentile	0.72	0.24	2.990	0.004
pczero	% ground returns	0.02	0.01	2.290	0.026
cons	Constant	0.40	0.45	0.900	0.373

Given the strong relationships between the different height percentiles and top height observed in the scatterplots in Figure 6.7, collinearity between percentiles is potentially

a problem. Table 6.6 shows that the 20 and 80th height percentiles exceed the recommended VIF level of 10 and also, individually, their VIFs exceed the mean VIF.

Table 6.6 Identification of multicollinearity between predictors using Variance Inflation Factors.

Variable	VIF
p20	635.91
p80	460.62
p10	278.56
p99	233.10
pczero	3.71
Mean VIF	322.38

If the 20 and 80th height percentiles are removed and the regression repeated then only the 99th percentile remains. The analysis suggests that a simple model that uses just the 99th percentile height is the most effective for estimating top height. This is because the different LiDAR percentiles are strongly inter-correlated so do not warrant inclusion and similarly uncorrelated variables, such as *pczero* do not add any additional value to the predictive model in terms of explaining the remaining variation.

6.4.4 Comparison with validation data

To determine accuracy of the top height predictions, they were compared against measurements made in the 30 validation sample plots. Figure 6.11 shows field-measured top height for both reference and validation datasets, against predicted top height. If the same accuracy levels observed in the dominant height dataset (See Chapter 5), of about 2 m (canopy error[24] ± 1.71 m and DTM error ± 0.17 m), are applied to this top height dataset then the model provides sensible predictions at the two extremes, but in between predictions are less accurate.

This pattern is more evident in the residual plot of Figure 6.12, which shows the difference between field measurements and model predictions. Three plots belonging to the validation dataset, which lie outside the expected accuracy of the top height estimate, are identified (circled).

[24] Included in canopy error is also field measurement error, which is thought to be as high as 1.22 m.

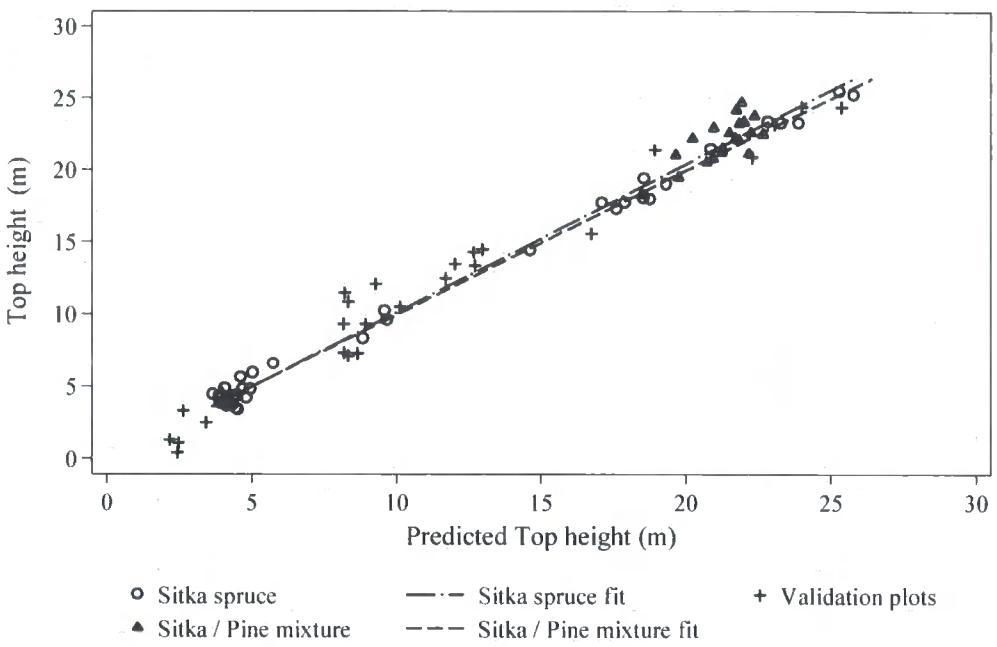

Figure 6.11 LiDAR-derived top height against field-measured top height from reference and validation datasets.

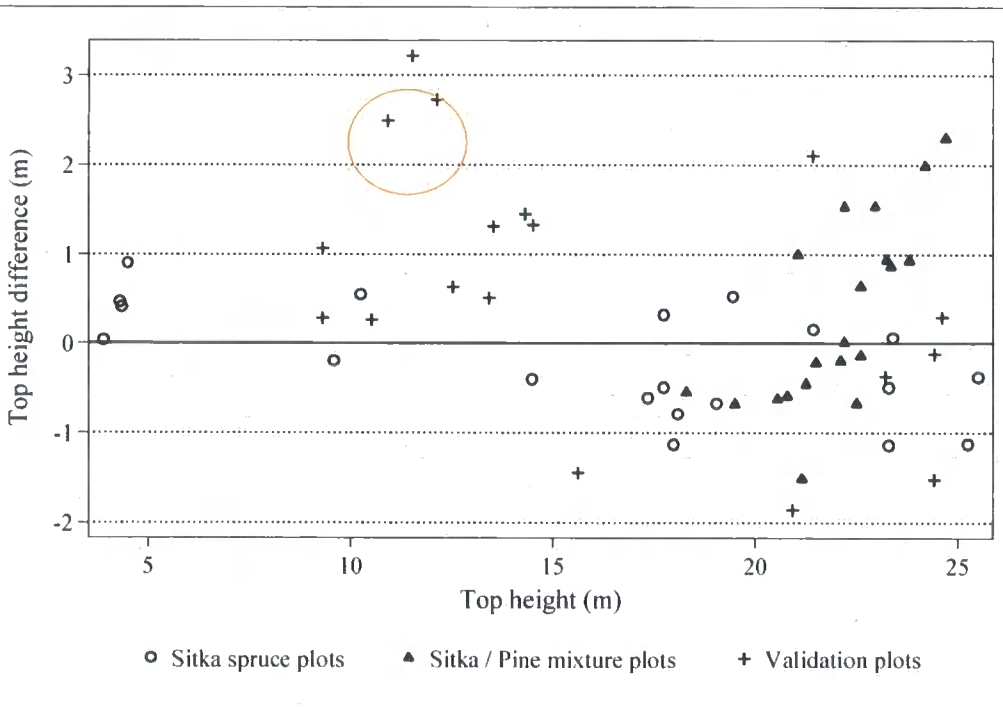

Figure 6.12 Height difference between LiDAR-derived top height and top height measured in the validation plots.

Despite a growth correction (0.58 m) being applied to account for the 1 year time lag between measurement of the reference and validation dataset, top height is underestimated by 2.4 to 3.1 m in the three plots that are circled. The most likely reason for the difference is that actual annual height growth has exceeded the Forestry Commission's expected annual height increment. Apart from this cluster of plots, the remaining validation plots show a similar distribution pattern to plots used to generate the top height model. This suggests that LiDAR-derived top height estimates can be used in place of field-measured top height.

6.4.5 Total Volume

In Britain, the standard method for estimating volume is to use top height as the predictor. In even-age conifer plantations the relationship between top height and volume is non-linear, with volume increasing slowly until the crop is established. Thereafter it increases quickly to a maximum value (asymptote), after which the rate of volume increment decreases. For this reason functions that have a sigmoid form (s-shaped), such as polynomials, logistic and Gompertz, are often used. The UK Forestry Commission uses polynomial models (Equation 6.5) to estimate measurable volume[25], Y, from top height, X, (Philip 1998).

$$Y = a + bX + cX^2 \qquad \text{Equation 6.5}$$

The Forestry Commission's models are based on measurements recorded in permanent sample plots[26] (PSPs) which, on the whole, have been established in single species, even-aged stands and thus are not fully representative of current forestry practice in the UK. Furthermore, the majority of these PSPs are located in more productive lowland conifer plantations, so there is a possibility that the results may differ when the models are applied to upland conifer plantations (PSP location map in Appendix 6.3). Nevertheless, using the top height–volume relationship a yield class system has been developed by the Forestry Commission, which is used to classify forest sites based on the annual rate of volume increment (measured in m^3/ha/yr). For a given site, yield class is determined by dividing total volume by crop age. This process is further

[25] Measurable volume is defined as stem wood of at least 7 cm diameter over bark.
[26] The permanent sample plots were established in the 1920s with the aim of providing data on which to base yield models for forest management and production forecasting. FC currently measures 509 PSPs on a 5 yearly cycle.

simplified by plotting the top height–age relationship, presented as a series of yield class curves, divided into intervals of 2 m^3/ha/year (Figure 6.13).

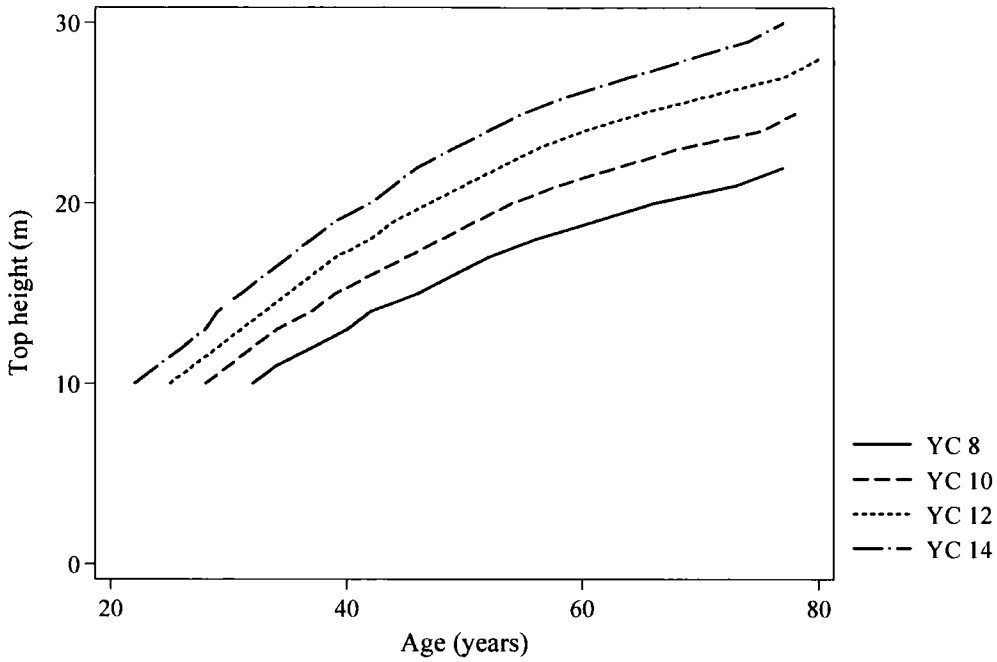

Figure 6.13 Forestry Commission yield class curves based on top height–age relationship.

For Sitka spruce species, yield class range is from 6 to 24, and for the slower growing lodgepole pine, from 6 to 14. In stands with more than one species, yield class is calculated separately for each species. The overall yield class of the stand is obtained by averaging the different components and weighting this by the proportion of the canopy each species occupies. For example, if one species occupies 40% of the canopy and has a yield class of 10 and a second species occupies the remainder and has a yield class of 14, then the yield class is (10 x 40 + 14 x 60)/100 = 12.4 (rounded to 12).

In this research, volume is estimated using LiDAR-derived top height (based on the 99th percentile). The current Forestry Commission yield class model is compared with estimates derived from fitting polynomial, logistic (Equation 6.6) and Gompertz (Equation 6.7) functions to field data.

$$Y = b_1 / [1+\exp\{-b_2(X-b_3)\}] \qquad \text{Equation 6.6}$$

$$Y = b_1 [-\exp\{-b_2(X-b_3)\}] \qquad \text{Eqiation 6.7}$$

Logistic and Gompertz[27] curves are similar in form with asymptotes at zero and the maximum value. The main difference is that the logistic function is symmetric about the point of inflection, whereas the Gompertz function is not. This means that using the logistic model, predicted volume might decrease once the maximum volume has been attained. The R^2 and RMS error values shown in Table 6.7 indicate that logistic and Gompertz models are superior to the polynomial model but, as discussed in section 6.2, this is not sufficient justification for discarding the model (regression output provided in Appendix 6.4).

Table 6.7 Comparison of regression models used to estimate total volume.

Model	Volume $n = 35$	
	R^2	RMSE (m)
Polynomial	0.934	71.365
Logistic	0.961	68.796
Gompertz	0.960	69.205

Figure 6.14 shows the sample data and fit for the polynomial, Gompertz and logistic models, with pure Sitka plantations plotted using circles and Sitka/ pine mixtures plotted using triangles. For comparison, the Forestry Commission (FC) yield class model for a crop with yield class 12 (also a polynomial) is shown (dotted red line). The FC model has a minimum volume of 63 m^3/ha (i.e. once the crop has a measurable volume) and is constrained by a maximum volume of 778 m^3/ha. If a higher yield class were selected, the fit of the model would be the same but the maximum volume would increase (i.e. YC 14 = 880 m^3/ha, YC 24 = 1,466 m^3/ha).

[27] This function is named after Benjamin Gompertz who created it in 1825.

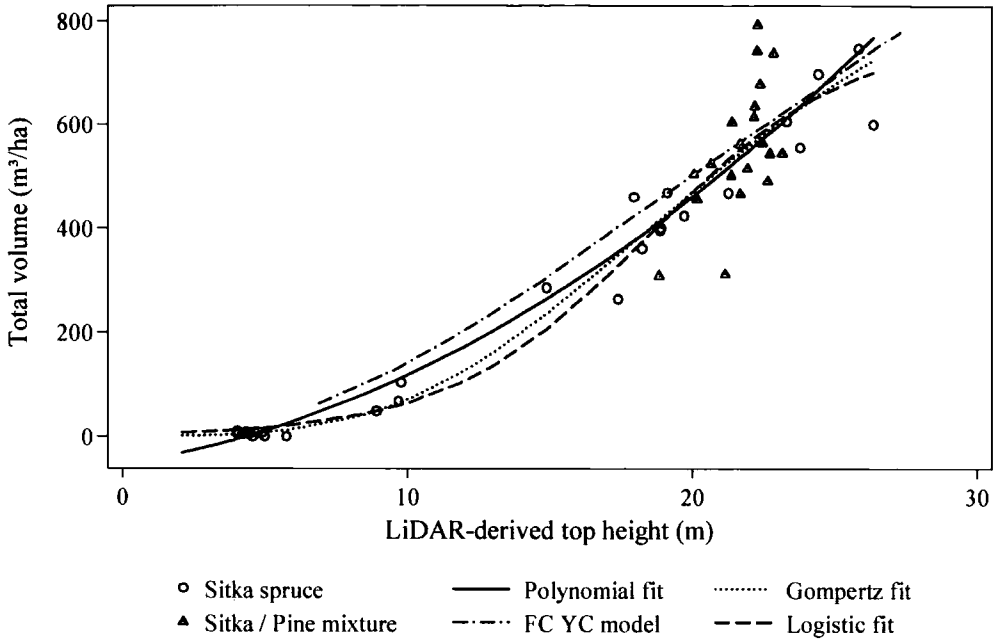

Figure 6.14 Sample data and fit of different volume models (n= 35).

All models pass through the middle of the main cluster of data points (500 to 650 m^3/ha), so predictions are similar in this region. However, at the extremes predictions vary, with some curvature in the residuals observed at lower volumes (200 m^3/ha) where there are less data (Figure 6.15). For reference, the residual plot for the linear model is also presented. As already observed in the top height residual plot (Figure 6.9), the main outliers include sample plots located in plantation mixtures. The plot volumes in the plantation mixtures are higher than those located in pure Sitka spruce because of the more open canopy structure which leads to an increase in the mean stem diameter, but not necessarily increases in the top height.

The fits of logistic and Gompertz models are similar, with curvature at lower volumes representing the sample plot data quite accurately. Despite this, these models cannot be used to reliably predict volume over the entire study area because the upper asymptotes (defined using the sample data) do not reflect the height values in the wider dataset: according to LiDAR data the maximum crop height is 38 m, whereas in the sample data the maximum is 25 m. Therefore, in areas where heights are encountered that are outside this range, logistic and Gompertz models will under-predict volume and consequently cannot be practically applied.

The polynomial model provides realistic predictions at lower and higher volumes if the negative intercept (−52) is ignored. Some differences are observed between the fit of the FC yield class model (Figure 6.14) and the empirically fitted polynomial model, especially at lower volumes (200 m^3/ha to 500 m^3/ha). It is unclear whether the difference is related to lack of data in this region, or whether there is a real difference in growth between upland and lowland conifer plantations. Above 500 m^3/ha the predictions from the polynomial model are similar, although the FC model provides more realistic volume predictions when extrapolated. For example, if top height is 35 m the FC model estimates a volume of 1,122 m^3/ha, whereas the empirically fitted polynomial estimates 1,295 m^3/ha.

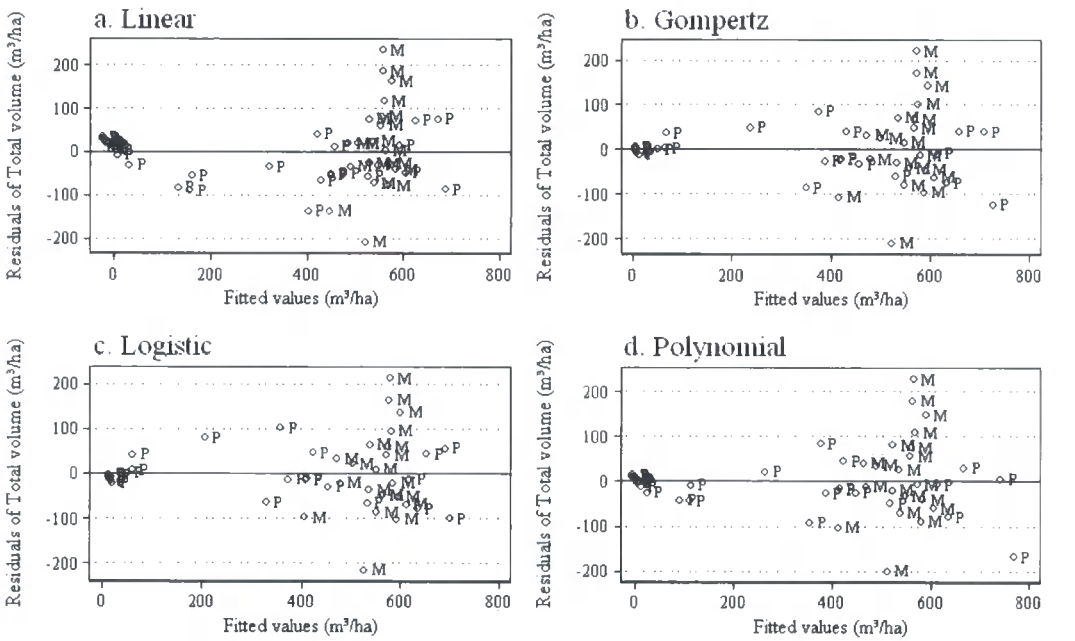

Figure 6.15 Residual plots for different volume models.

On this basis, the FC model is considered to be the most appropriate for application over a wider area. No improvement is made to the volume predictions by including other percentile values or LiDAR-derived canopy density measures, as none of these variables are significant at the 5% level (see Appendix 6.4).

6.4.6 Comparison with validation data

Figure 6.16 shows field-measured volume, for both reference and validation datasets, against predicted total volume. For the analysis, only validation plots with total volume

above the FC model minimum volume threshold, of 63 m^3/ha, were considered (14 sample plots). Differences are observed between validation plots and the FC model at volumes of less than 200 m^3/ha. However, more substantial differences in terms of volume over-estimations occur above this point. Two plots in particular stand out in both the scatter plot and the residual plot (circled), where volume is over-estimated by more than 290 m^3/ha (Figures 6.16 and 6.17).

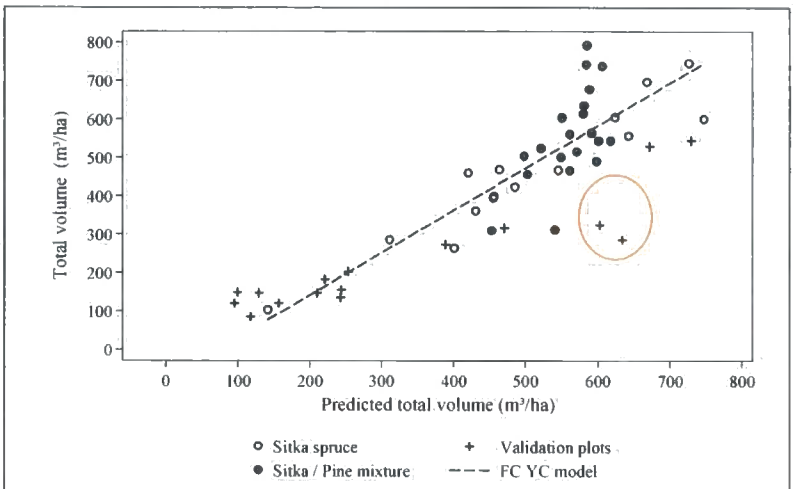

Figure 6.16 LiDAR-derived volume against field-measured volume from reference and validation datasets.

Both samples are located close together in an area with a planting density that exceeds 3,200 trees/ha. Consequently, tree diameters are reduced (<13 cm) because of increased competition, but top height measurements are similar to areas with high tree volume. While the rate of tree mortality is also considered in the FC model, predictions are predominately based on top height, so any areas of anomalous growth not associated with height are difficult to model.

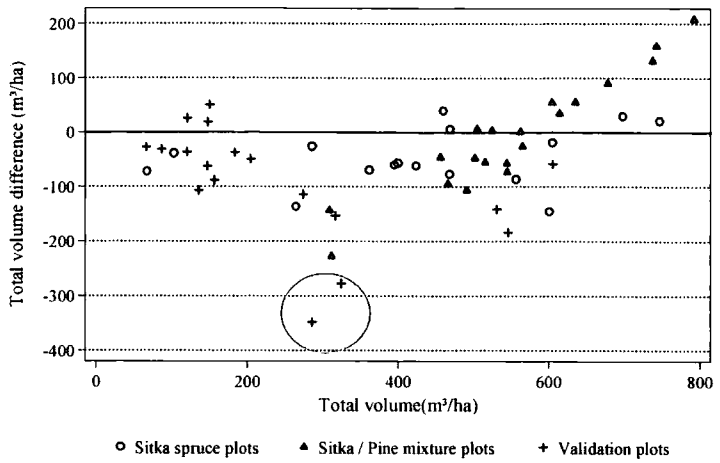

Figure 6.17 Volume difference between LiDAR-derived volume and volume measured in validation plots.

A key weakness of the FC model is that it assumes tree density and diameters are homogenous and that top height can be used to provide estimates of volume. As tree density appears to exert a strong influence on the accuracy of volume estimates, it would be advantageous if areas that show atypical crop development could be identified prior to applying the volume model (This is investigated further Chapter 7).

6.4.7 Tree density

Two approaches were tested in order to obtain estimates of tree density from LiDAR data. First, models that used the different DCHM height percentiles as predictor variables were assessed; and second, models that used combinations of canopy density measures were tested.

6.4.8 Tree density prediction using height percentiles

Analysis of tree density data indicates that density ranges from 1,150 to 12,300 trees/ha (Table 3.5). Areas of high tree density (caused by natural regeneration) are easily identified in Figure 6.18a, which plots maximum LiDAR height against tree density. Compared with other sample plots of a similar age tree density in these plots is up to five times higher. There is a weak relationship between LiDAR height and tree density if these plots are included in the model (R^2 = 0.31). Removal of these plots increases the R^2 value substantially, to 0.73. However, inspection of Figure 6.18b suggests that models based solely on height do not summarise the relationship very accurately. Here,

the R^2 value is inflated by the presence of sample plots (outliers) with high density and low canopy heights. Little variation is observed in tree density values (2,000 to 3,000 trees/ha) relative to changes in tree height. Simply, the model does not pass the model selection criteria identified in Table 6.3 and therefore is of limited use.

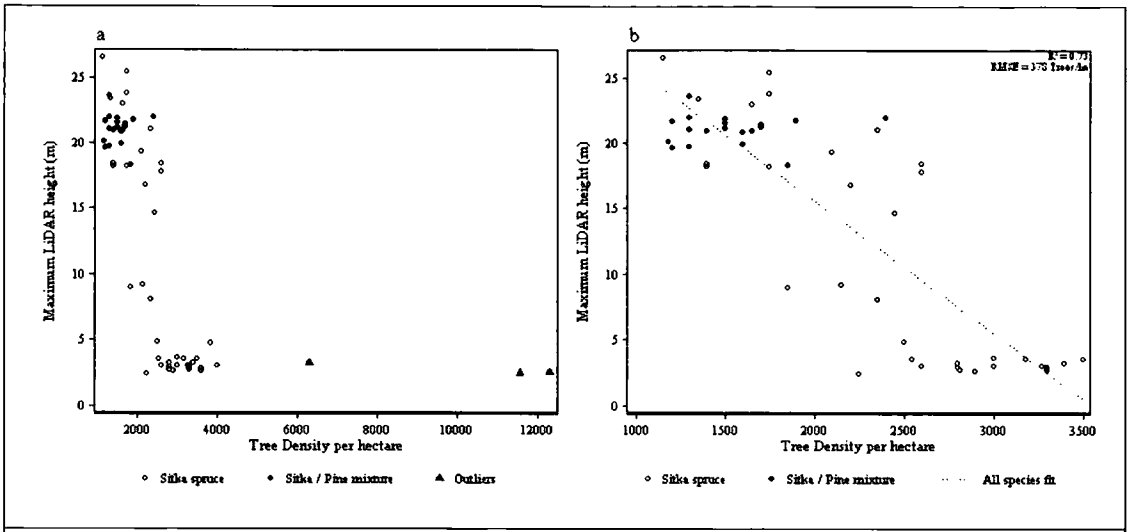

Figure 6.18 (a) LiDAR height against field-measured tree density and (b) same data after plots with high regeneration are removed.

6.4.9 Tree density prediction using canopy density measures

The second model tested was derived from regression (procedure used in section 6.3.1), and includes both height percentiles and the five canopy measures. None of the height percentiles are significant ($p > 0.05$), but two canopy measures, skewness and LiDAR canopy volume (Lk_v), warrant inclusion. Figures 6.19a and b show the relationship between tree density and skewness and Lk_v.

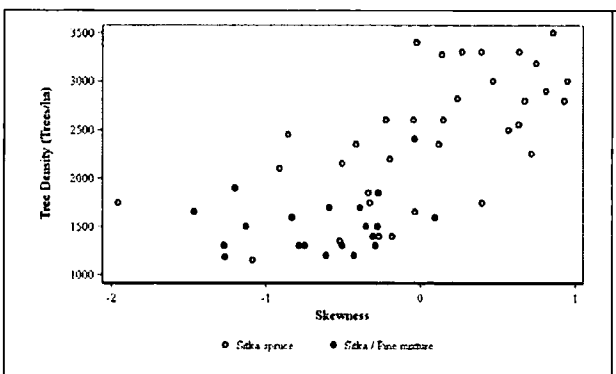

Figure 6.19a Tree density against skewness.

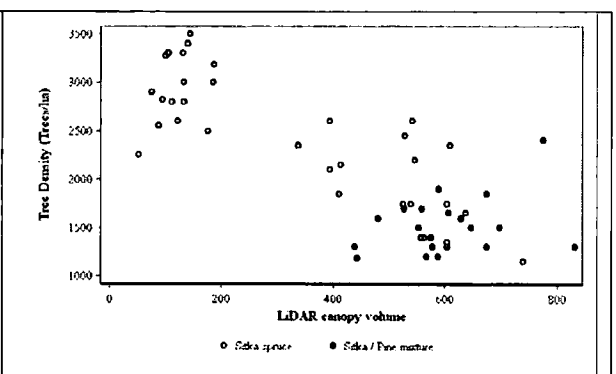

Figure 6.19b Tree density against LiDAR canopy volume.

Skewness is positively correlated with tree density, while LiDAR crown volume is negatively correlated. Consequently, no collinearity exists between the variables when they are included in the predictive model. Figure 6.20 shows the tree density model based on skewness and LiDAR crown volume (R^2 = 0.72 and RMS error = 434 trees/ha).

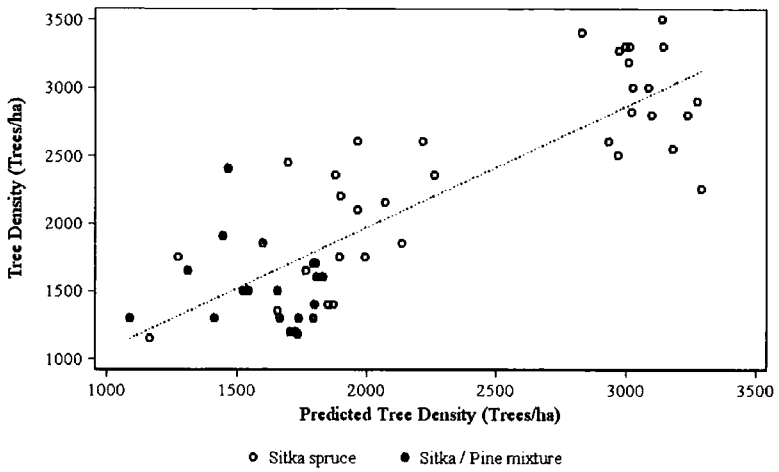

Figure 6.20 LiDAR-derived tree density against field-measured tree density.

Two distinct clusters are apparent in the residuals, which are caused by the distribution of the field samples (Figure 6.21). Despite this, there is no pattern or structure in the residuals, which indicates that the model predicts tree density equally well at both high and low tree densities; that is within the range of 1,000 to 3,500 trees/ha. However, the RMS error of the model is high (434 trees/ha or 17% of the mean tree density), limiting its practical use for providing estimates of tree density.

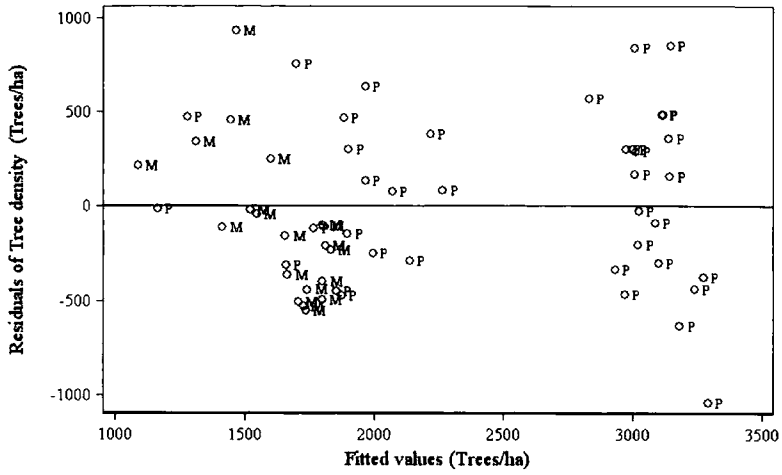

Figure 6.21 Residual plot for tree density.

6.4.10 Comparison with validation data

Figure 6.22 shows the difference between field-measured tree density and modelled tree density, against measured tree density, for both the reference and validation datasets. Here, a negative difference indicates that the model underestimates tree density. More variation is observed in the validation dataset compared with the reference dataset. There are five validation plots where the difference is greater than 1,000 trees/ha.

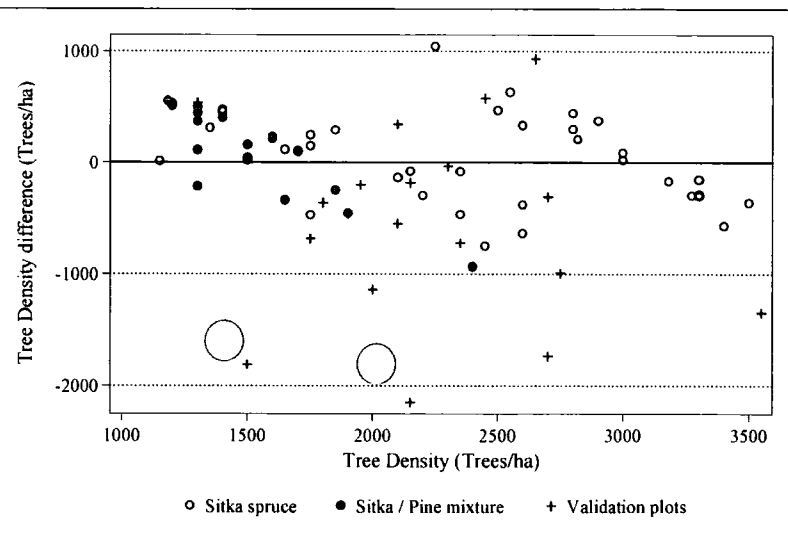

Figure 6.22 Tree density difference between LiDAR-derived tree density and tree density measured in the validation plots.

The two plots circled are the same plots identified earlier in Figure 6.17 which showed anomalous timber volumes. This suggests that even though the prediction is not

accurate enough to provide estimates of tree density, it could be used to highlight areas of anomalous growth.

6.5 Discussion

The objective of this chapter was to assess the accuracy of forest estimations such as height, volume and density derived from laser scanning data.

6.5.1 Effect of forest canopy on the first and last pulse distributions

Inspection of first and last pulse laser height distributions, and results of the *t* test presented in section 6.1.1, show that if ground returns are ignored (i.e. returns >0.5 m) the penetration into the forest canopy of the first pulse and last pulse returns is the same. This is related to the way in which the Optech ALTM 2033 LiDAR system separates the two pulses; the first return is registered when the return energy meets the predetermined threshold (usually the leading edge of the pulse), while after a short time delay the second return is registered. Therefore, the most likely explanation, in closed canopy crops, is that the forest canopy is so dense that the majority of laser pulses are unable to penetrate to the lower canopy. Consequently, no additional information on forest structure is gained by inclusion of last pulse data. In contrast, in studies conducted in European conifer-dominated forests, which are multi-storied and not as dense (typically <1,500 trees/ha), last pulse data is routinely used for the calculation of forest height, volume and tree density (Naesset 1997; Naesset & Økland 2002).

6.5.2 Top height predictions

Top height is accurately estimated using the 99th height percentile (R^2 = 0.995; RMS error = 0.57 m), with no substantial differences if separate top height models for pure Sitka spruce crops and plantation mixtures are considered. It was suggested in Chapter 5 that the estimation of canopy height might be improved with the inclusion of additional height percentiles or canopy density measures. However, this research finds that inclusion of these measures does not yield substantial improvement in the top height model. This is attributed to the strength of the relationship between 99th height percentile and field-measured top height, which explains 99.5% of the variance in the model. Overall, the model still under-estimates top height in younger stands and in plantation mixtures. The reasons for the under-estimation are the same as those in Chapter 5, and can be summarised as follows; in younger stands, the tree apex is missed

and in closed canopy mixtures, a combination of DTM and DCHM errors contribute to an underestimation of top height.

The results suggest that to predict top height from LiDAR some field-measured data are required to identify top height of trees. Once calibrated using these data, it should be possible to predict top height over a wide area using the LiDAR top height model at an accuracy (± 0.57 m) that is close to, or better than, traditional field measurement methods (± 0.50 m in crops <15 m and ~1.22 m in crops >15 m). The only exception is that top height estimates in plantation mixtures may not be as accurate.

6.5.3 Volume predictions

In the UK, forest volume predictions are made using top height measurements, and therefore, it should in principle be possible to replace field measurements with LiDAR-derived top height. The relationship is non-linear, so volume is best predicted with functions that allow some curvature. Of the four models assessed (Gompertz, logistic, polynomial and FC yield model) the polynomial model and the FC yield class model provide the most physically plausible estimates. The assessment is based on more than just R^2 and RMS error for each model. Also considered is the ability of the model to provide realistic estimates beyond the data. In this context the FC yield model is more appropriate than the empirically fitted polynomial because, when extrapolated beyond the range of the data, volume is constrained by an upper limit. It is worth noting that there is an offset between the polynomial model and the FC model (Figure 6.14), in the 200 to 500 m^3/ha range. Although the dataset used here is small (n = 35) and quite limited in geographical extent, the difference implies that the FC yield class model over-predicts volume within this range. The models converge at approximately 600 m^3/ha, which is at the limit of this dataset. To properly validate current yield models, additional sample plots that cover a range of sites and planting densities would be needed, which is beyond the scope of this research. The volume estimate is, once again, not improved by the inclusion of additional height percentiles or canopy density measures. Also, more variation in volume predictions for plantation mixtures than for pure Sitka spruce stands, is observed.

Analysis of validation plots shows that there are some deficiencies in the yield class model. The key weakness is that they are made using top height, alone. Problems arise

when crops do not develop in a uniform way e.g. have higher than average levels of mortality or contain a mixture of tree species. In these areas, it is difficult to make accurate volume predictions based on top height alone. Although not explicitly stated in section 6.1.2 it is possible that LiDAR crown density measures that are easily calculated (i.e. require no field measurements for calibration), such as coefficient of variation, percent ground returns and skewness could be applied spatially, to identify areas of anomalous growth, or the dominant species in a plantation mixture. This is the focus of Chapter 7.

6.5.4 Tree density predictions

Tree density is not reliably predicted using LiDAR height percentiles, as density does not necessarily change with increased height (Figure 6.18b). However, tree density can be predicted using canopy density measures. A model, based on skewness and LiDAR canopy volume, provides a realistic prediction (R^2 = 0.72 and RMS error = 434 trees/ha). However, application of the model is limited to areas that have tree densities between 1,000 and 3,500 trees/ha. Comparison with validation data indicates that predictions are erratic in situations where the canopy structure deviates from what is typically encountered in even-aged plantation crops. Potentially, this means that areas of abnormal tree density could be identified. However, it would probably be better to use LiDAR crown density measures that do not need any field calibration, instead of LiDAR canopy volume, which requires the calculation of LiDAR crown length using field-measured crown length.

6.6 Summary

It may be concluded that LiDAR can be used to make accurate estimates of top height (± 0.57 m), which in turn can be used to parameterise existing Forestry Commission yield class models. Additional findings include:

1. The density of the forest canopy impedes penetration of laser pulses to the lower canopy, which means that no additional information on the canopy structure is added by inclusion of last pulse data. This outcome is not the same as reported in LiDAR studies conducted in more open canopied forests.

2. Top height is accurately estimated using the 99th LiDAR height percentile (R^2 = 0.99 and model RMS error = 0.57 m). The inclusion of additional LiDAR

height percentiles, or canopy density measures, does not improve the estimation. The size of the RMS error suggests that accuracy of top height measurements obtained from LiDAR is equivalent to, or better than, those achieved using field-based techniques.

3. Volume can be estimated using LiDAR-derived top height. Comparison between the current FC yield class model and an empirically fitted polynomial suggests there are, however, some inconsistencies in volume predictions. These are observed below 500 m^3/ha, but above this the model predictions are similar. The model is not improved by inclusion of additional LiDAR height percentiles or crown density measures. Additionally, the results suggest that volume is more difficult to predict in plantation mixtures, owing to large variations in growth rate. Therefore, it is important to know where the mixtures are located and the outcome, or the success, of the mixture. Identification of plantation mixtures is the focus of Chapter 7. Also, the results from the validation plots indicate that volume is poorly predicted in crops that do not follow a 'normal' pattern of growth. Crown density measures may assist in the identification of these areas (also discussed in Chapter 7).

4. Tree density is difficult to predict using height data. Tree density estimates using LiDAR-derived canopy density measurements are more plausible as these measures are more sensitive to biophysical changes in canopy structure. Tree density predictions are relatively accurate (R^2 = 0.72 and RMS error = 434 trees/ha), but the RMS error is quite high, which limits the practical application of the model. Additionally, tree density cannot be predicted reliably in areas that exceed 3,500 trees/ha.

Chapter 7: Mapping plantation species using LiDAR

7.1 Introduction

The results presented in Chapters 5 and 6 indicate that LiDAR provides accurate estimates of tree height and volume. However, it is apparent that growth models developed for single species stands are not directly transferable to plantation mixtures. This chapter focuses on the detection of plantation mixtures and identification of areas of variable growth. A different study area located in Galloway forest district, Scotland is used, because it contains a wider range of plantation types than found in the Kielder study area. Remote sensing data collected over the Galloway study area is very similar to the Kielder data set and includes sample plot measurements, LiDAR, SPOT 5 HRG imagery and 1:10 000 aerial photography.

Using FC forest boundary information, three species groups are identified: areas of pure Sitka spruce, areas of pure lodgepole pine and areas where the two species have been planted together. Two approaches are assessed for detection of plantation mixtures: the first uses LiDAR intensity data to separate spruce and pine species and the second uses LiDAR-derived crown density measures, coefficient of variation (C_v), skewness (*skewfp*), percentage of ground returns (*pczero*) which provides a measure of canopy openness and the mean canopy height (*meanh*) which enables areas with height variations to be identified. The merits of each measure are initially assessed separately and then combined to produce classifications that both include and exclude LiDAR intensity. The accuracy of classification is compared with SPOT 5 HRG data and 1:10 000 aerial photography.

7.1.1 Plantation mixtures

During the 1960s the UK Forestry Commission established extensive areas of forest plantations in remote upland areas. Whilst a majority of plantations were established using Sitka spruce, some of the poorer waterlogged or heather infested sites were planted with structured species mixtures of Sitka spruce and lodgepole pine, either planted in alternate rows or intimately mixed in varying ratios and combinations. The rationale was that the pine species was planted as a sacrificial nurse to improve the site characteristics; over time the pine would die back from competition from the Sitka spruce. In practice, as these crops have matured, two possible outcomes have emerged:

(i) self-thinning crops dominated by one species, usually Sitka spruce or (ii) where both species compete equally. Figure 7.1 shows an example where the outcome in terms of species dominance is clear and therefore easily identified. However, the transition is harder to detect if it occurs in remote areas or within forest compartments. In these situations the challenge is firstly to identify and map these areas and secondly to produce reliable growth estimates.

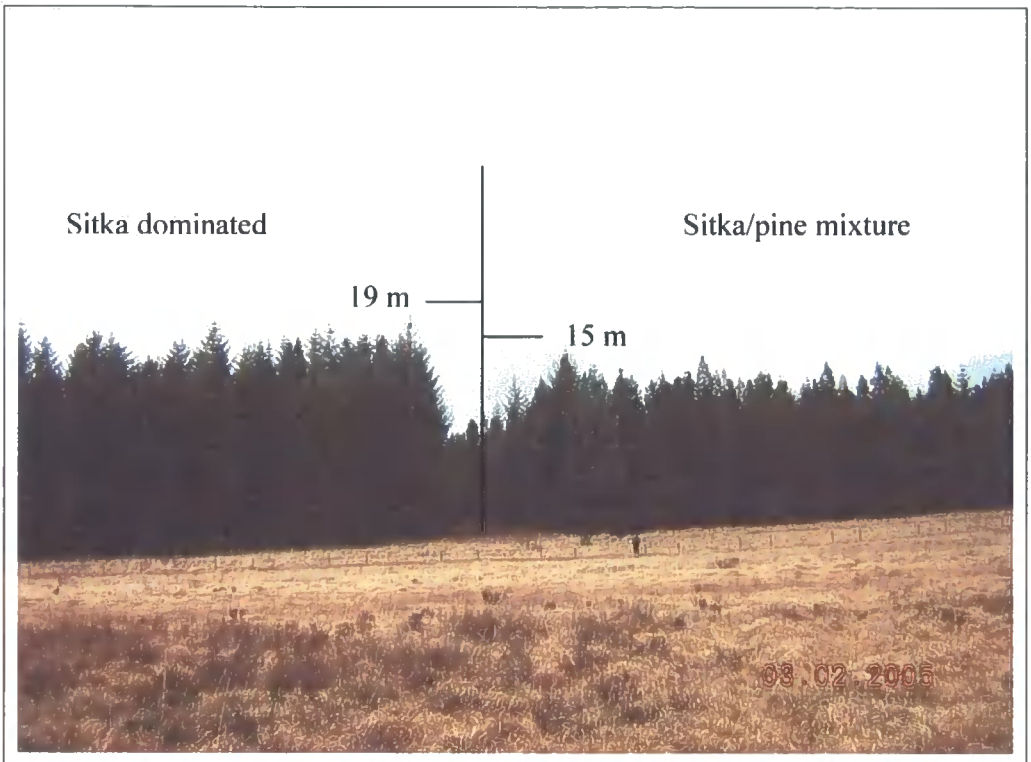

Figure 7.1 Forest compartment planted in 1960 showing two different outcomes. Left side is Sitka spruce dominated and right side Sitka spruce and lodgepole pine mixture.

Traditionally a combination of ground survey and aerial photography has been used to provide this type of information, with the ground survey component providing quantitative measurements and aerial photography used for crop stratification purposes. The accuracy of this method depends on how closely changes in crop structure on the ground can be matched with those observed in the aerial photography. The mapping process can be quite subjective being affected by a range of factors. These include timing, resolution and quality of the photography, size and shape of the area of mixture and analysis by the photo interpreter and/or field surveyor. Within this context, LiDAR is evaluated for its potential as an alternative, unbiased method of identifying tree species and mapping crop variability.

7.1.2 Study area, image and field data

The selected study area contains a range of tree species, from pure crops to plantation mixtures. The terrain is gently undulating with a maximum slope of 14° and a topographic range of 230 to 300 m above mean sea level (amsl).

LiDAR data was acquired on 15 June 2003 using an Optech ALTM 3033 system, operating at a flight altitude of 1,250 m amsl using a scan angle of <9°, with a point density of 4 returns/m^2. Other optical data available include a cloud-free SPOT 5 HRG multi-spectral scene acquired two months earlier on 17 April 2003 and 1: 10 000 aerial photography flown 12 days after the LiDAR flight. The NIR band of the SPOT 5 HRG image was used to check the radiometric consistency of the LiDAR intensity data. LiDAR was resampled to the spatial resolution of the SPOT 5 HRG data (10 m). Although the LiDAR and SPOT 5 HRG are processed at the same pixel resolution the LiDAR intensity is not directly comparable to the SPOT 5 HRG NIR response. The key differences are in the way in which passive and active sensors measure the NIR signal. SPOT 5 is a space-borne satellite and the response recorded by the HRG sensor is the average response for a 10 m cell. Since the data was not calibrated there are a number of factors that can affect the SPOT 5 HRG NIR response, these include; the atmosphere (i.e. cloud or haze), topographic shadowing sun elevation, sensor view angle and reflectance from neighbouring pixels. In comparison the LiDAR measures the response for each laser return, which represents the NIR signal for a small highly culminated beam of light. Factors that affect the intensity of the NIR can include pathlenght of the beam (i.e. the distance between the LiDAR and the target) the incidence angle of the beam and the composition of the target (i.e. vegetative or inert). To ensure the datasets were overlaid the SPOT data was clipped to match the LiDAR coverage and then geo-corrected, using the LiDAR data to provide GCPs. The reported RMS error of the geo-correction process was 0.5 pixel or 5 m.

Aerial photography was used only for reference purposes. Figure 7.2 a to c shows the area and the different images with species boundaries and sample plot locations overlaid.

Accurate top height, volume and species data were measured for 20 (0.02 ha) field

plots, 17 in pure Sitka spruce and three in Sitka spruce/lodgepole mixtures. Since no plots were measured in pure lodgepole pine, height measurements from two areas were extracted from the 10 m LiDAR height grid (62 pixels). Table 7.1 summarises the plot data for each crop type by top height and volume. Plots measured in the Sitka spruce show the highest variability in both top height and volume. This is because these plots cover a range of forest conditions. Variation in top height and volume is also observed in the Sitka spruce/lodgepole mixtures though in terms of volume lodgepole pine tends to be the dominant species.

Table 7.1 Summary of field plot measurements by crop type

Crop type	**Tree species**	**Obs**	**Top height (m)**				**volume (m^3/ha)**			
		No. field plots	Mean	S.D.	Min.	Max.	Mean	S.D.	Min.	Max.
Pure	Sitka spruce	17	19.5	3.1	13.5	23.9	500.7	160.6	184.2	697.4
Pure	Lodgepole pine*	(62)	15.8	0.9	13.0	18.0	n/a			
Species mixture	Sitka spruce	3	16.9	1.6	15.3	19.0	146.4	21.3	132.7	177.3
	Lodgepole pine		16.5	1.5	14.4	17.9	184.0	86.7	60.4	256.6

* Top height calculated from 62 pixels extracted from the 10 m LiDAR height grid.

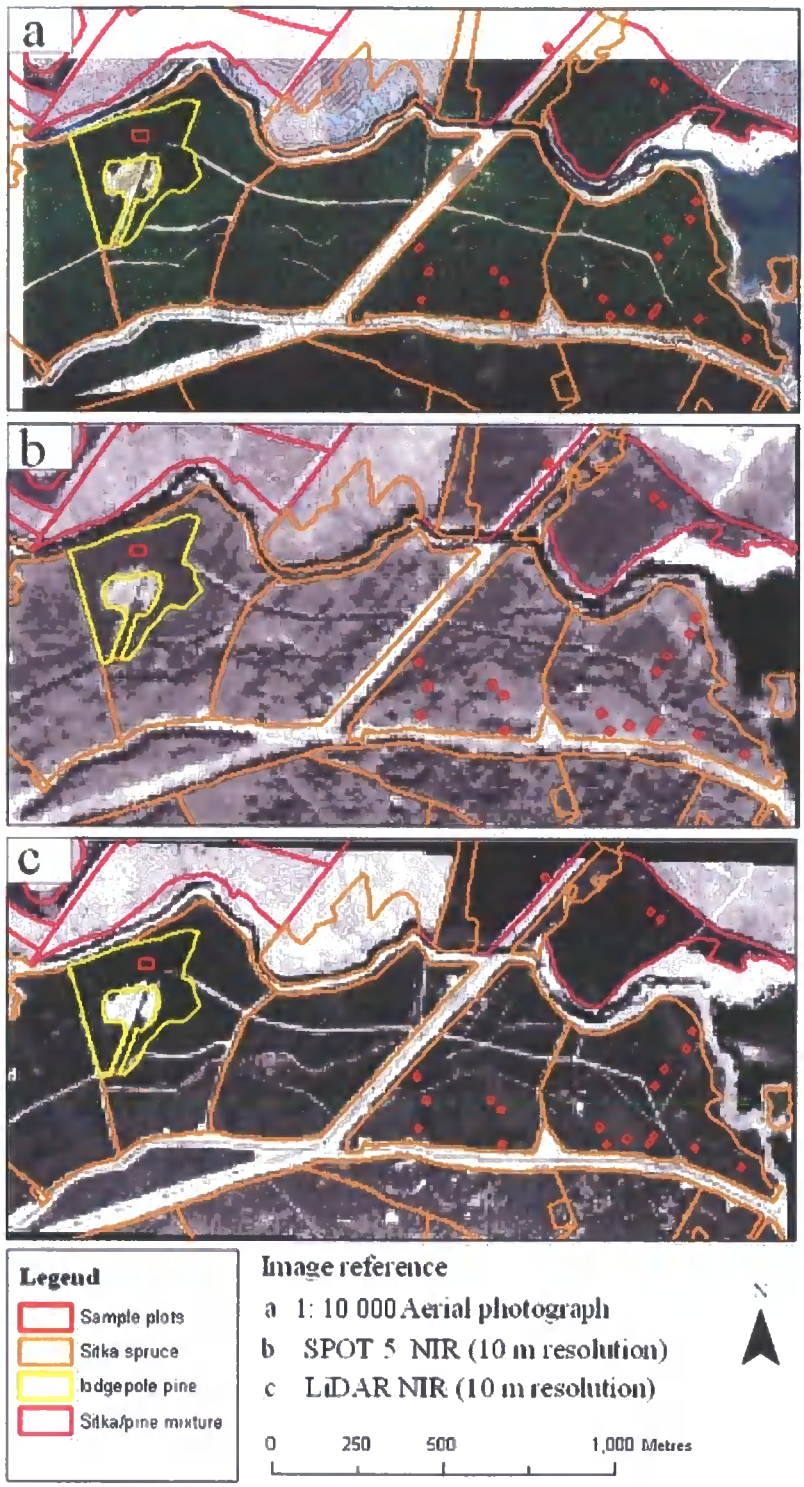

Figure 7.2 Forest compartment boundaries overlaid on: a.) 1: 10 000 aerial photography b.) SPOT 5 HRG NIR band and c.) LiDAR NIR band.

7.1.3 Spectral characteristics of lodgepole pine and Sitka spruce

Figure 7.3 shows a measured spectral reflectance profile for lodgepole pine and Sitka spruce needles collected from the study area and measured in the laboratory, using the GER 1500 spectroradiometer. While the shape of the spectral profile for both species is similar in the visible and NIR, there is clear separation in reflectivity between species suggesting that spectrally they are separable. Interestingly, the spectral reflectivity at the spectral band pass positions for the SPOT 5 HRG NIR band (plotted in grey) and LiDAR NIR (plotted in magenta) are similar (Figure 7.3), despite the broader spectral range sampled (780 nm to 890 nm[28]) and spectral separation of the two sensors.

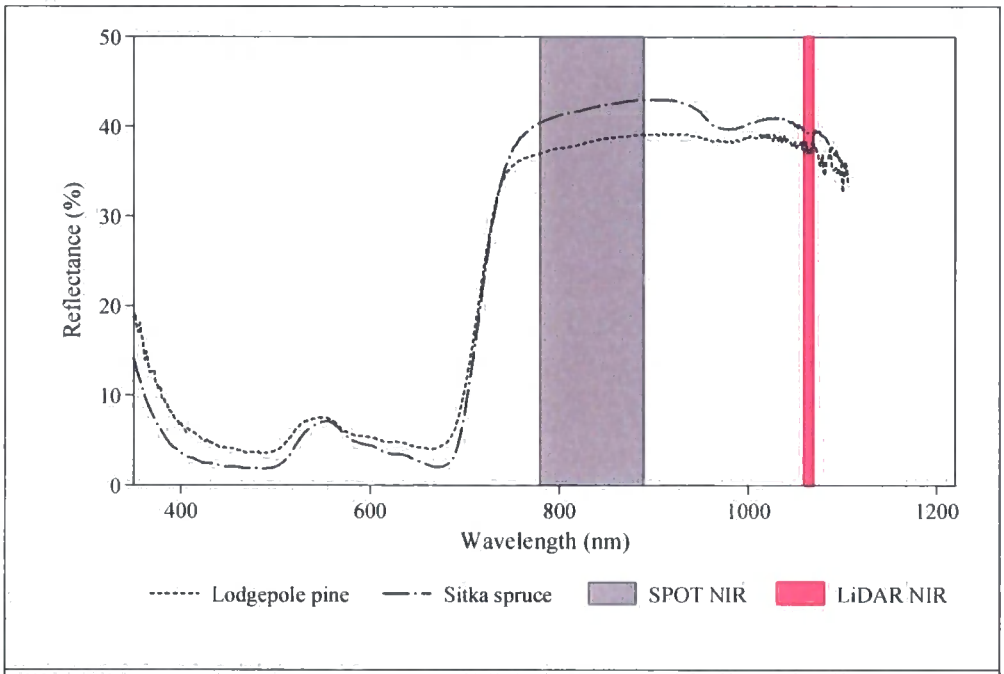

Figure 7.3 Spectral characteristics of Sitka spruce and lodgepole pine.

7.1.4 Spectral characteristics of LiDAR and SPOT 5 HRG data

While LiDAR systems are principally designed to record distance, many systems can also measure the intensity of the laser return. The ALTM 3033 uses a laser that can produce a monochromatic light in the near infrared (1064 nm) region with a very narrow spectral width of 10 nm (pers comm. Brent Smith, Optech Canada, 02/03/05). The intensity of each return represents the energy from a highly culminated beam of light (footprint size of ~0.20 m if the sensor's operating height is 1,000 m) reflected from a small part of the target, which provides a concentrated[29] measurement of the

[28] Source www.spotimage.fr
[29] Laser is an active system so the pulse is unaffected by shadow or occlusions.

object reflectivity. The intensity measurement is proportional to the voltage of the return signal, so a target with twice the reflectance ideally produces twice the intensity reading. For example, vegetative targets like dense forest canopies are highly reflective in the near infrared, while targets like black tarmac act as an absorption feature in this spectral region and therefore return very little energy (www.rieglusa.com). Typically, DN values are less than 255, but occasionally specular reflection from targets like glass, chrome and water can cause very high digital number (DN) values of over 1,000. Over forest the following factors may affect the recorded intensity: variations in laser path length, caused by changes in the distance between the sensor and target, orientation of the target relative to the sensor, which may change according to the laser scan angle or topography; laser beam divergence, which alters the footprint size; and attenuation of the signal by the atmosphere. However, provided that data are acquired over a short time spatial differences in attenuation by the atmosphere should be minimal (Luzum et al. 2004). It is also worth noting that there may be variations in intensity measurements between LiDAR systems due to differences in receiver gain and the type of laser used. Given this list of factors it is not surprising that few studies have used LiDAR intensity data. One of the main reasons cited is the difficulty of calibrating data, so that results might not be repeatable (pers comm. Paul Treitz, Queen's University, Canada, 2/09/03).

This issue of radiometric consistency can partially be addressed by comparing LiDAR intensity to a radiometrically-calibrated dataset. For this purpose the 10 m NIR band (780 nm to 890 nm[30]) on the SPOT 5 satellite, which records the average response over 110 nm range is considered appropriate. However, it is worth noting that the SPOT 5 HRG data was not calibrated to actual ground leaving reflectance so will contain noise due to atmospheric, topographic and sun elevation effects. Since the SPOT 5 HRG image was acquired two months earlier (under cloud-free conditions) it is not expected that the spectral response of closed canopy lodgepole pine and Sitka spruce will have changed substantially in the interim.

7.2 Processing methodology

Two approaches were used to identify plantation species composition. The first used LiDAR intensity data and the SPOT 5 HRG NIR band. In this instance, the SPOT 5

[30] Source www.spotimage.fr

HRG NIR band was used to check the radiometric consistency of the LiDAR data. The second approach used statistical summary measures, derived from distribution of the laser height data, namely the coefficient of variation (C_v), percentage of ground returns (*pczero*) and skewness of height (*skewfp*) to try to identify differences in forest canopy structure. Mean height (*meanh*) was also included to provide a measure of crop variability. Figure 7.4 summarises the processing steps involved in processing the LiDAR and SPOT 5 HRG data. The level of processing required for processing LiDAR intensity is more complex than the method based on canopy structural measures alone.

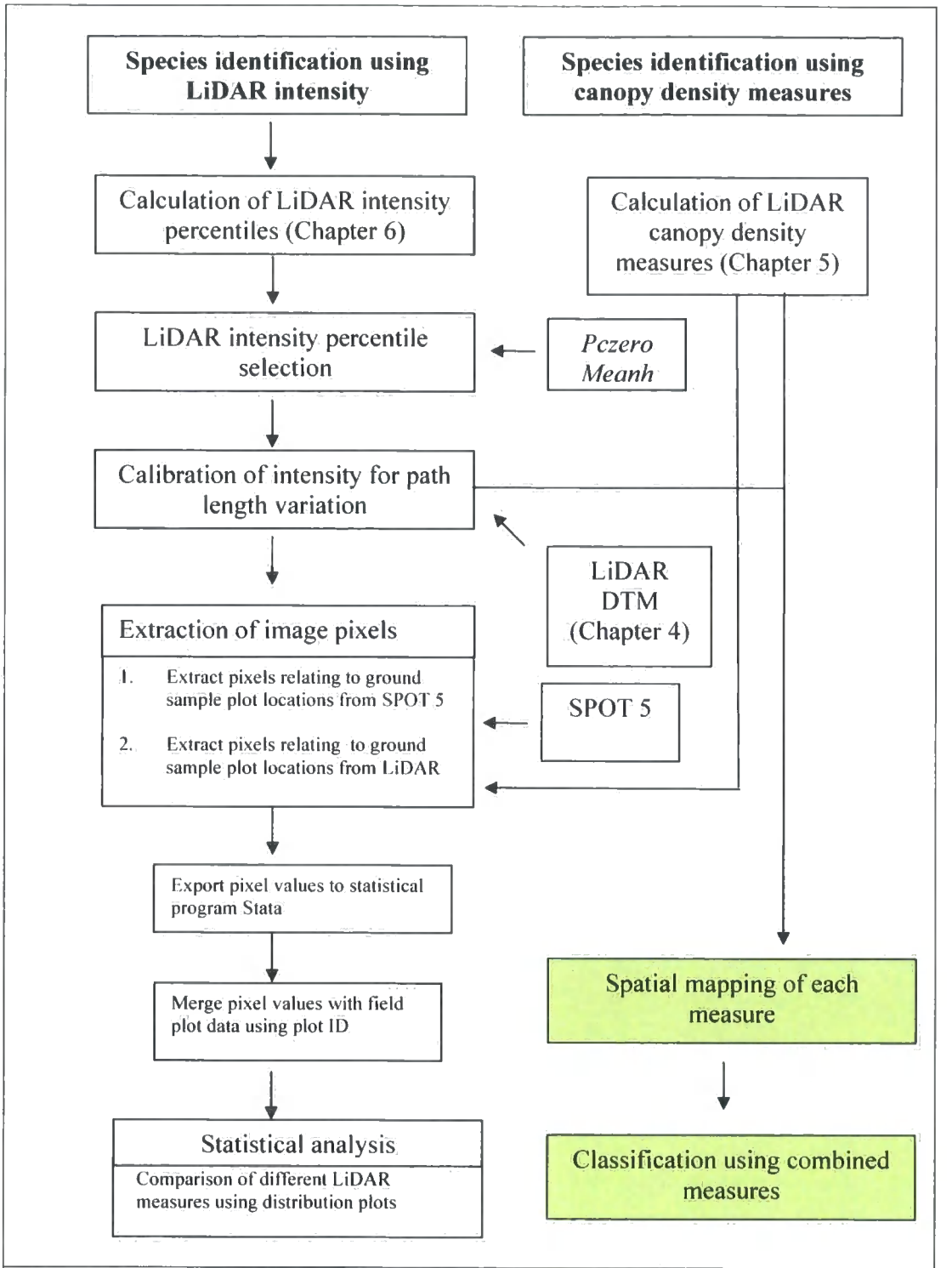

Figure 7.4 Summary of LiDAR image processing steps.

7.3 Species identification using LiDAR intensity

Although a number of studies have used LiDAR to provide estimates of height, volume and basal area (i.e. Naesset 2002; Means et al. 1999) relatively few studies have

assessed the potential of LiDAR for identifying and mapping forest species. In Swedish forests, Holmgren & Persson (2003) successfully identified individual trees from LiDAR data by using LiDAR firstly to delineate the tree crown and then secondly to identify the tree species using LiDAR intensity and measures of the laser distribution. In this instance laser data was collected using a helicopter-mounted LiDAR at high-resolution (>10 points/m^2) over forest stands with tree densities between 220 and 1,400 trees/ha. At stand level, Maltamo et al. (2004) identified suppressed trees in multi-layered spruce forests by summarising the height distribution of the laser data.

Two further studies are relevant to this research: Song et al. (2002) discussed the use of gridded LiDAR data for urban land use classification and Luzum et al. (2004) described a method of calibrating LiDAR intensity data. Both studies noted that intensity values are inconsistent between similar targets. Song et al. (2002) suggested that the variation in intensity is related to the reflection angle of the laser pulse from the target and used a median filter with a set window size (3 x 3) to reduce this effect. In contrast, Luzum et al. (2004) developed a method for correcting the raw LiDAR point data. This correction compensates for differences in flying height, changes in ground topography, and other variations in path length caused by the laser's scan angle (i.e. variations in laser footprint size). The algorithm does not correct for the effects of beam divergence or other factors that affect reflectivity. The method also requires that a time tag is recorded for each laser pulse. From this information the path length is calculated by finding the difference between the sensor's position and the reflected laser pulse position.

In this research, a combination of methods used by Song et al. (2002) and Luzum et al. (2004) was used. The data were converted to a grid format and intensity corrections were made to each pixel of the grid. There are, however, two main differences: no averaging filter was applied to the LiDAR grid and intensity values were not corrected for the effect of scan angle. This was because the time tag information for each pulse was not supplied[31].

[31] Time tag data is usually recorded, but is often discarded during post processing by the LiDAR contractor (pers comm. Dr. Simon Roberts, NERC Airborne Research Facility, 25/02/05).

7.3.1 Calculation of LiDAR intensity percentiles

The urban area classification conducted by Song et al. (2002) used mean intensity. When classifying vegetation the penetration of the laser pulse means that intensity can be separated by height, which enables returns that are not associated with forest vegetation, such as ground returns, to be removed.

The intensity data were divided into two groups, total intensity, which is the average of all intensity values, and vegetation intensity. Vegetation intensity was further divided into four classes representing the 25th, 50th, 75th and 90th height percentiles. Vegetation intensity therefore excludes any returns that may come from the ground surface. This concept is illustrated using a tree as an example in Figure 7.5, where it is assumed that laser pulses are equally distributed and penetrate to the ground.

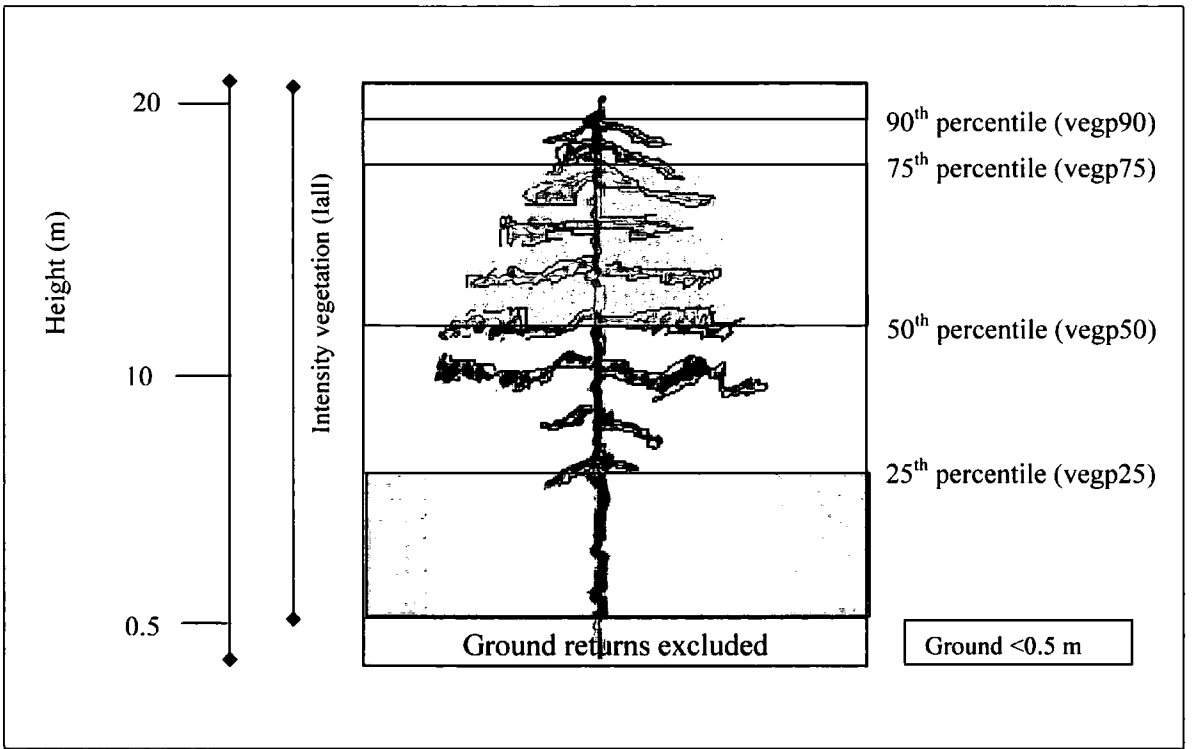

Figure 7.5 Calculation of intensity measures

7.3.2 Comparison of LiDAR intensity measures

To compare the different intensity measures, the pixel values corresponding to each intensity variable were extracted from a transect 100 m wide and 900 m long over the study area. A transect was placed perpendicular to the flight direction and positioned to span the topographic range of the data (70 m). The transect width corresponded to the

swath width of one LiDAR flight line, although given the 70% overlap additional returns from adjacent flight lines would also be included. Figure 7.6 shows the location of the transect overlaid on the DTM, with contour lines spaced at a 5 m interval also shown.

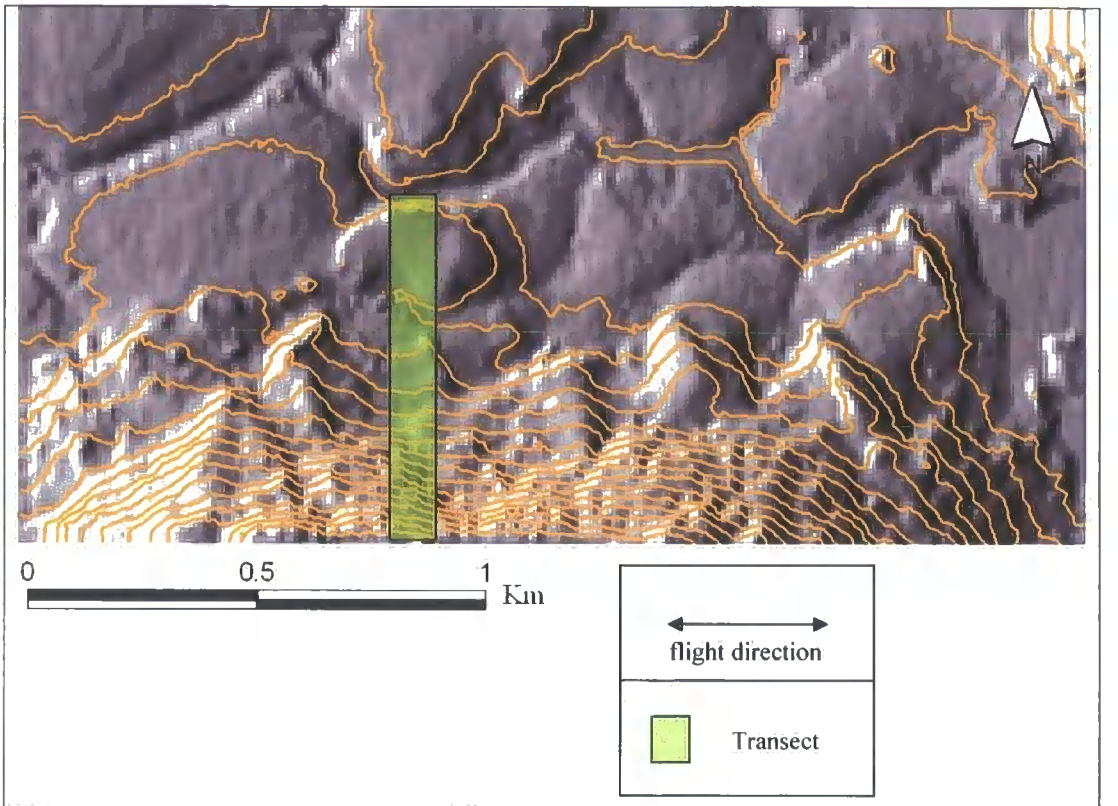

Figure 7.6 Transect overlaid on hill shade image. Contour lines drawn at 5 m intervals.

The transect was placed so that it only covered areas of pure Sitka spruce, to reduce the possibility of spectral variation caused by different species. The intensity data were filtered to exclude forest gaps and non-forest areas, using the percentage of last pulse ground returns (*pczero*). By setting a threshold of 50% these areas were successfully filtered out.

Figure 7.7 shows the distribution of each intensity measure using box plots (summary statistics presented in Appendix 7.1). The box represents the interquartile range, intersected by the median and the whiskers mark the upper and lower adjacent values, with points outside these indicated by dots. The greatest variation in LiDAR intensity is observed if all canopy and ground returns are considered (*Iall*). Variation decreases if

ground returns are eliminated, remains relatively constant above the 25th canopy percentile and increases below this point. Analysis suggests that intensity associated with the 50th vegetation percentile provides the most stable measure, as indicated by the box plot distribution. At this level most of the returns will originate from the upper canopy, which is predominantly needles. Lower percentile values are more likely to include more woody material, which has lower reflectivity in the near infrared; thus increasing the variation (Watt & Donoghue 2005).

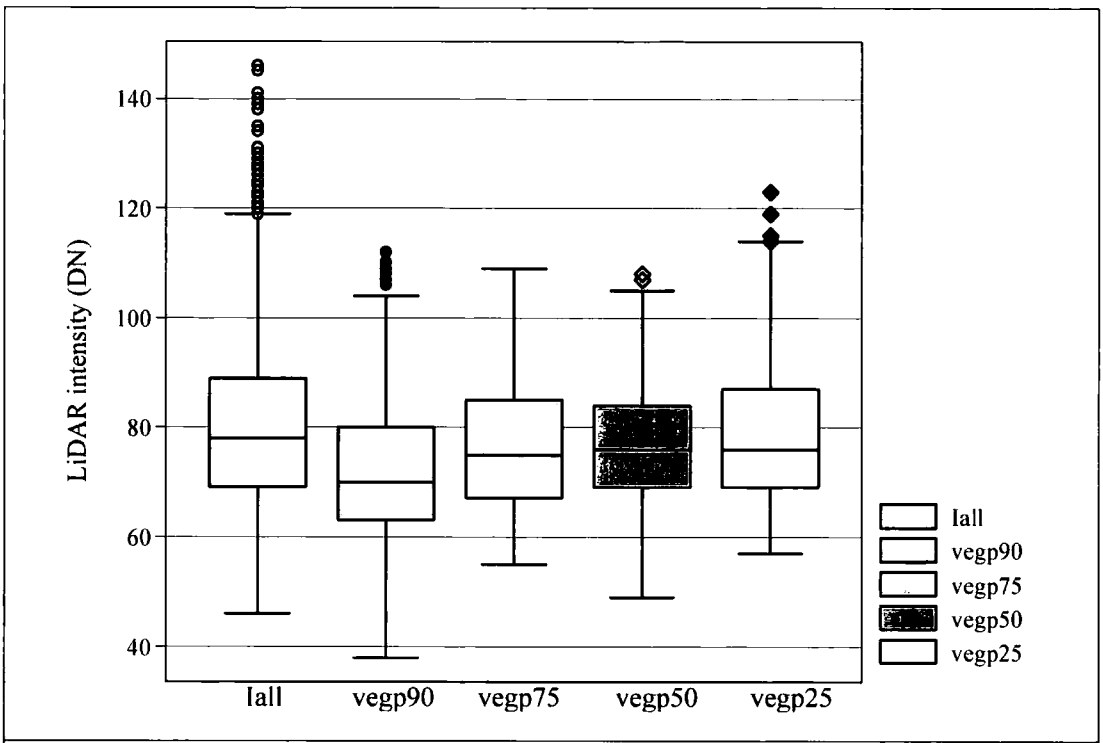

Figure 7.7 Variation in various LiDAR intensity percentiles across the forest transect.

7.3.3 Normalisation of laser path length

The topographic range over the study area is 70 m and therefore it is necessary to correct the intensity data (*vegp50*) for changes in laser path length. It is well known that the intensity recorded by the receiving optics of the LiDAR strongly depends on the range (path length) and reflectivity of the target. For homogeneous targets the intensity of the return is inversely proportional to the second power of the range (Baltsavias 1999a). The same principle is also true for diffuse targets such as forest canopy, as shown in Figure 7.8. In this example, path length is calculated by subtracting the average flight altitude (1,275 m) from the sum of DTM and the height of the vegetation 50th percentile. Again, the same filtering method is used to mask non-forest areas.

Despite the obvious scatter, the general trend is for intensity to decrease as path length increases (R^2 = 0.44), even over a range of 70 m. The high degree of scatter is most likely due to changes in path length caused by the laser incidence angle, as this is not accounted for.

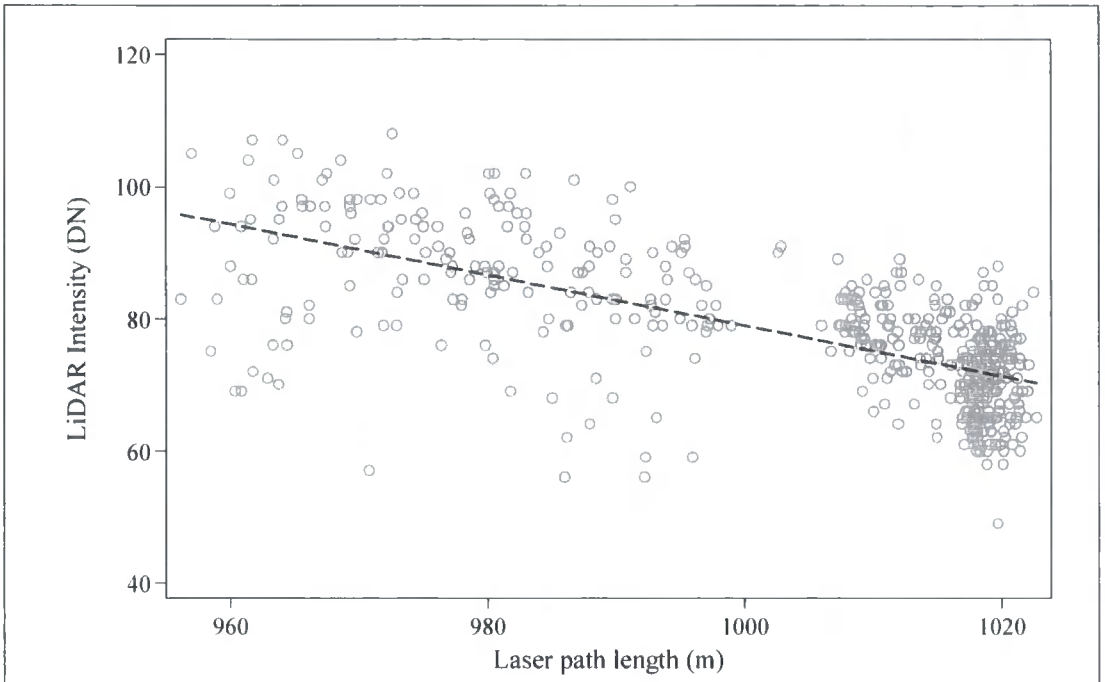

Figure 7.8 Effect of laser path length changes on LiDAR intensity (*vegp50*).

Path length was normalised by applying the equation published in Luzum et al. (2004), where path length is squared and then divided by the square of the average elevation (1,007 m) over the selected area.

$$N\,\text{int} = vegp50 \times \frac{path\ length^2}{elevation^2} \qquad \text{Equation 7.1}$$

Figure 7.9 presents the histogram of intensity before and after normalisation of path length and Figure 7.10 shows a spatial map of DN changes across the area of interest. The greatest reduction in intensity values (~10 DN) is observed in areas with higher elevation, which have a shorter laser path length.

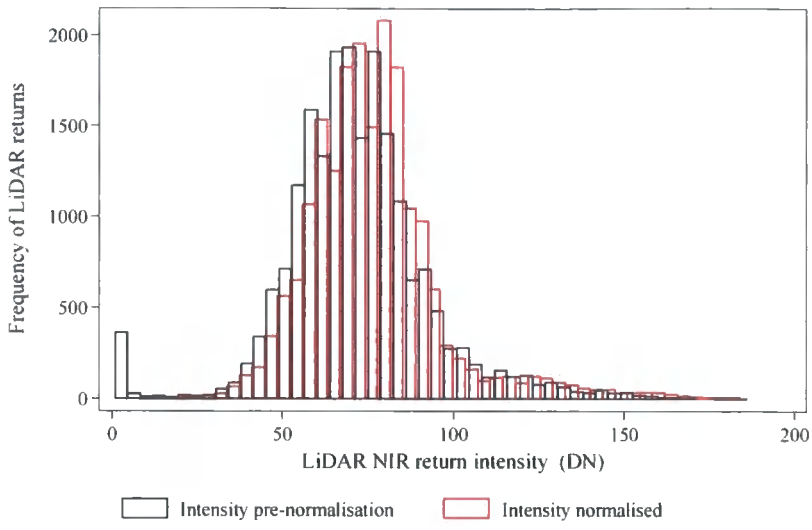

Figure 7.9 Distribution of LiDAR intensity values before and after path length normalisation.

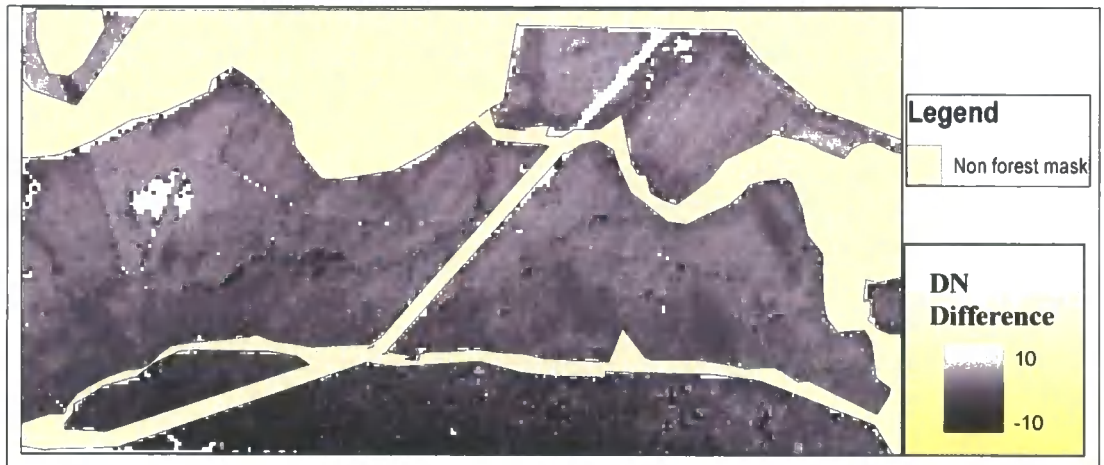

Figure 7.10 Change in LiDAR DN values after path length normalisation.

7.3.4 Extraction of intensity values

Once the intensity has been normalised for changes in path length it is possible to compare the NIR response for each species type between the SPOT 5 HRG and LiDAR data. For each target or plot, the pixel values were extracted using a 2 x 2 pixel window around each sample plot from the SPOT 5 HRG and LiDAR NIR data. At the same time, the canopy density measures (used in Section 7.3) were also extracted for the sample plots. To provide a relative scale, the minimum and maximum intensity values were identified and the corresponding DN values extracted. In both images, the

minimum value (darkest target) was water[32] and maximum value (brightest target) flying bent (*Molinia caerula*) see Figure 7.11.

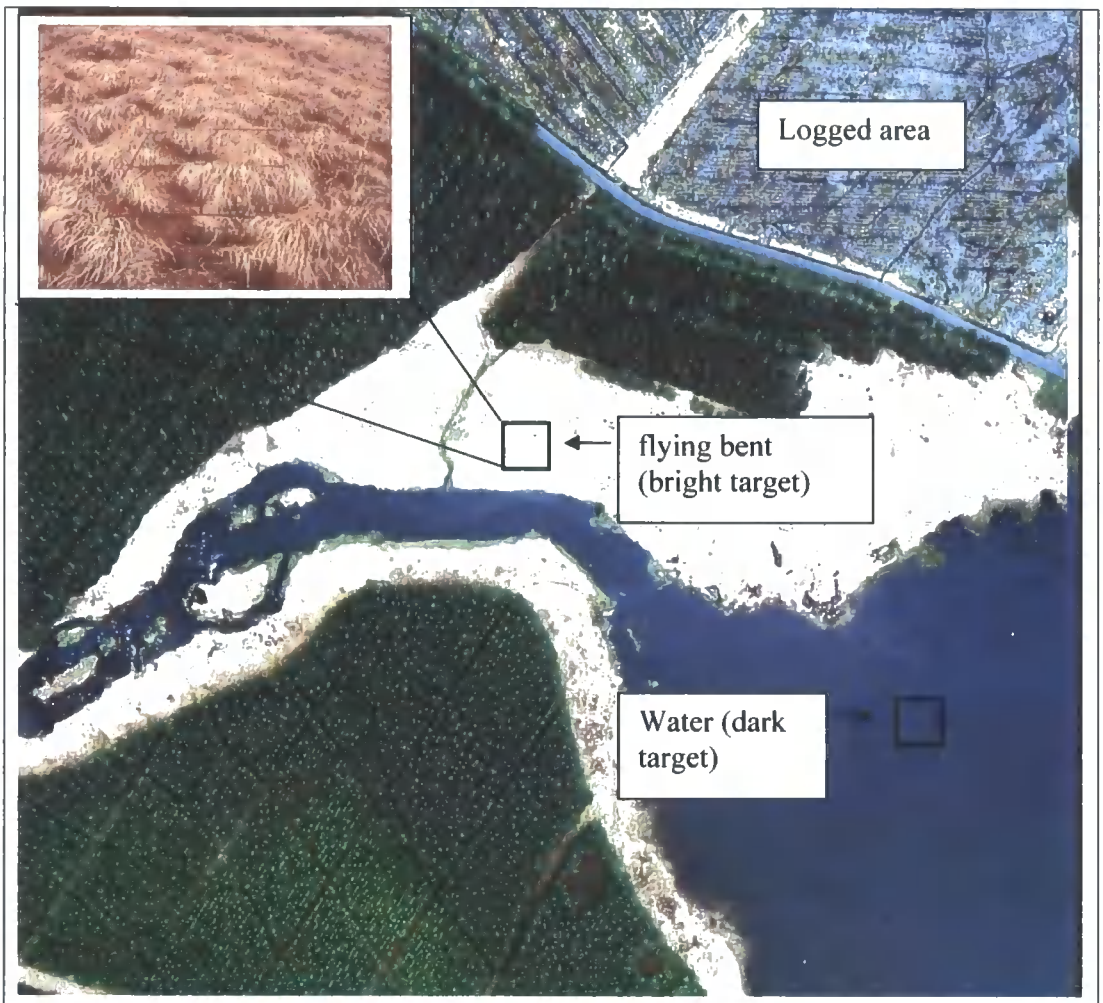

Figure 7.11 Selection of light and dark targets, (1:10 000 aerial photograph used for illustrative purposes only).

Ideally, these targets should be spectrally invariant and recorded close in time so the NIR response can be compared in absolute terms. Water is suitable (unless the laser return is specular), but vegetation such as grass is less suitable, as its reflectivity may vary according to the season. However, since there are no other invariant bright targets (i.e. concrete) within the study area, grass was used.

[32]Areas of specular reflectance were avoided.

(i) Comparison of LiDAR and SPOT 5 HRG NIR DN values between species types

The difference in the NIR DN values in the LiDAR and SPOT 5 HRG data indicates that pure lodgepole pine and Sitka spruce and species mixtures are separable. Table 7.2 provides a summary of the NIR values by sensor, for each species type/target. In the LiDAR intensity data, lower DN values (30 to 59) are observed in plots of lodgepole pine and also in plots that contain a mixture of lodgepole pine and Sitka spruce (47 to 63). The highest DN values are observed in pure Sitka spruce plots (48 to 96). These plots show highest variation in intensity (S.D of 9.2 DN), which is attributed to the field plots being measured over a range of forest conditions, including crops with low tree densities and poor growth. Therefore, the combined response will be the average of tree stem, branch and needle material intensities.

Table 7.2 Summary of SPOT 5 HRG and LIDAR NIR values for field plots and targets

Species type/ target	Sensor	Obs.	Mean	Std. Dev.	Min.	Max.
		(No. 10 m image pixels)	(Near infrared DN value)			
Lodgepole pine	SPOT 5 HRG	62	41	0.8	39	42
	LiDAR	62	46	6.5	30	59
Sitka spruce	SPOT 5 HRG	177	48	2.2	40	52
	LiDAR	177	78	9.2	48	96
Sitka spruce/ pine mixture	SPOT 5 HRG	10	43	0.4	42	43
	LiDAR	10	57	4.2	47	63
Dark target (Water)	SPOT 5 HRG	4	27	0.5	27	28
	LiDAR	4	14	3.3	10	18
Bright target (Grass)	SPOT 5 HRG	4	62	1.0	63	64
	LiDAR	4	153	3.0	155	159

These observations can be further tested statistically, using Analysis of Variance (ANOVA). In this case a one-way ANOVA was used to compare the mean NIR response between the three crop types (i.e. Sitka spruce, lodgpole pine and Sitka spruce/ lodgpole pine mixture). Two hypotheses were tested; H_o: there is no difference in NIR values between the three species types, and H_a: there is a difference in NIR values between the three crop types. The results of the ANOVA show that variability between crop types for both LiDAR and SPOT NIR response is significant at the 5% level,

indicating that the NIR responses, at least, are not the same between one of the three crop types. A second test is required to compare the mean NIR values between each crop type. For this purpose, the Bonferroni multiple-comparison test was used[33]. Again, the results showed that the NIR responses for the three crop types are significantly different at 5% level for both LiDAR and SPOT 5 HRG data (ANOVA results presented in Appendix 7.3). These results suggest that in closed canopy crops it is possible to use NIR response from either LiDAR or SPOT 5 HRG to identify different crop species.

Outside of the forest areas other differences are also noted between the NIR DN values for the two reference targets, water and grass. The standard deviation is higher in the LiDAR than the SPOT 5 HRG. The LiDAR response is the average of all returns within a 10 x 10 m area, so for diffuse targets like grass the higher standard deviation is most likely caused by the inclusion of responses from the ground as well as grass. Over water the response might have been affected by increased sediment from nearby logging operations (see Figure 7.11).

The difference in NIR response between sensors is shown in Figure 7.12, which plots average intensity values for each target/sample plot by sensor. For reference, a line is drawn between the dark and bright targets. Although the measurement scale of the sensors is not the same, and LiDAR data are not radiometrically calibrated to a standard, the relationship is nevertheless linear (R^2 =0.94). Over forest targets, the dynamic range is 4 times higher in LiDAR (41 to 84 DN) than in SPOT 5 HRG (41 to 51 DN). Discriminating between species, and identifying areas of poor growth within stands of the same species, is therefore potentially easier, using LiDAR.

[33] There are a number of possible tests available. In Stata the user may choose from the Scheffé and Šidák comparison tests; both provide similar results to the Bonferroni test.

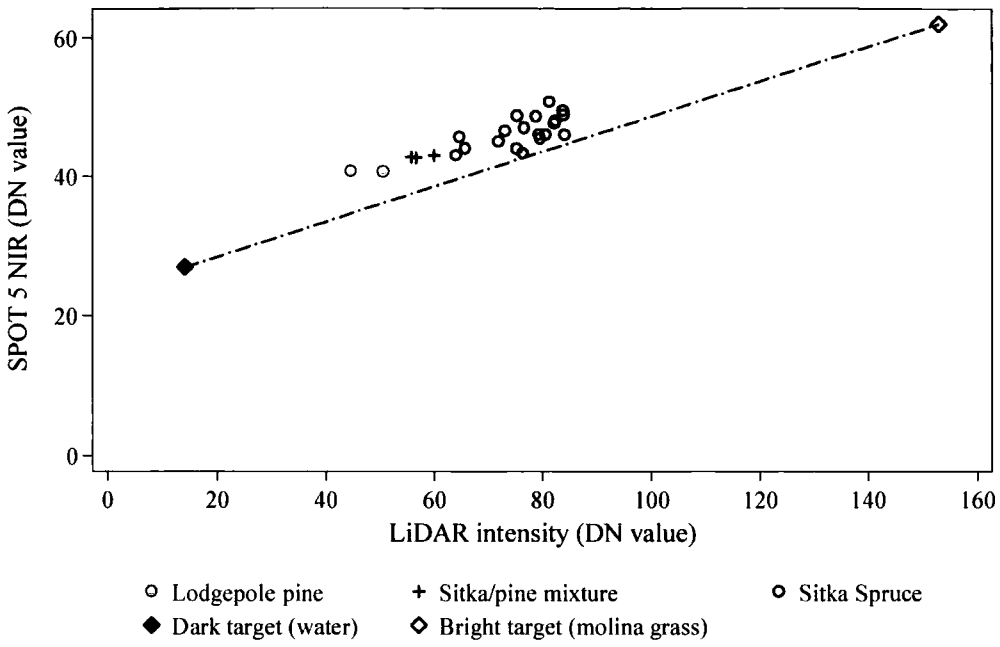

Figure 7.12 SPOT 5 HRG NIR values against LiDAR NIR DN values for different species combinations and reference targets. The straight line represents the response from dark and bright target in both sensors.

Differences in intensity can also be assessed visually; Figure 7.13 shows a map of LiDAR intensity at 10 m resolution generated using a density slice to highlight areas of Lodgepole pine and Sitka spruce, over the study area, with forest compartment boundaries overlaid. The intensity range (0 to 125 DN) is represented by a colour gradient. On Figure 7.13 a mask has been applied to exclude areas of non-forest. There are no data in the black areas and pink areas have high DN values, which are associated with wind damage and topographic effects. Between these limits lie forested areas.

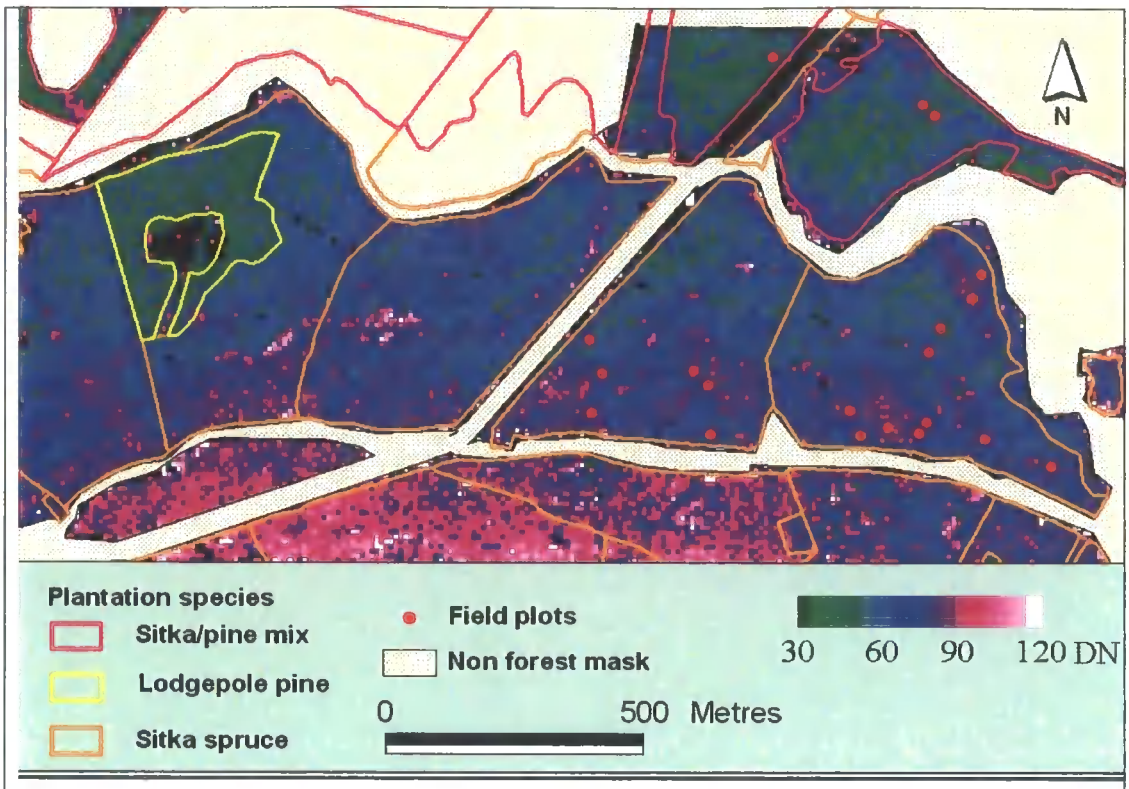

Figure 7.13 LiDAR intensity map generated using a density slice to highlight pine and Sitka crops.

Most of the green coloured areas (DN 30 – 50) are located in forest compartments that are identified in the GIS as pure pine or a mixture of Sitka spruce and pine. There are, however, some green areas located in pure Sitka spruce compartments that do not contain pine. Areas of pure Sitka spruce crops are coloured blue. Where lodgepole pine and Sitka spruce are planted as a mixture (GIS boundary colour magenta), the colours are a combination of green and blue tones. The map shows that intensity data can be used to separate pine and pine/spruce mixtures from pure Sitka spruce crops. However, some misclassification does occur, with areas of pine appearing in areas designated as Sitka spruce. Additionally, there is still some noise in the intensity data, which may be related to LiDAR scan angle, for which correction was not made. This problem is, however, confined to an area of sloping terrain.

To reduce this misclassification, other LiDAR measures that are based on laser pulse distribution, such as skewness, coefficient of variation, percentage last pulse ground returns and mean height, are evaluated in section 7.4.

7.4 Species identification using crown density measures

The results in Chapter 3 show that the growth characteristics of tree species in a plantation setting vary, depending on the species. For example, vigorous pure Sitka spruce crops form a dense forest canopy and reach canopy closure relatively early (approx 10 m). Whereas, pure lodgepole pine or Sitka spruce/lodgepole pine mixtures have more open, clumpy canopies. Figure 7.14 a to c shows that the different canopy structures of Sitka spruce, lodgepole pine and species mixtures affect the distribution of the laser pulse (first pulse) through the canopy. The largest variation is observed between pure Sitka spruce plots, and those containing lodgepole pine. The density of Sitka spruce canopy restricts laser penetration to the top third of the canopy, whereas the clumpy canopy of lodgepole, and species mixtures, allows the laser to penetrate almost to the ground. Pulse distribution from pure lodgepole pine is more homogeneous than from species mixture. It is worth noting that the same laser distribution patterns observed in these plots are replicated in the Kielder forest dataset (see Figure 5.17a and b). This means that the same laser distribution "signatures" are likely to be found in other conifer plantations in the UK that are managed using similar silvicultural regimes.

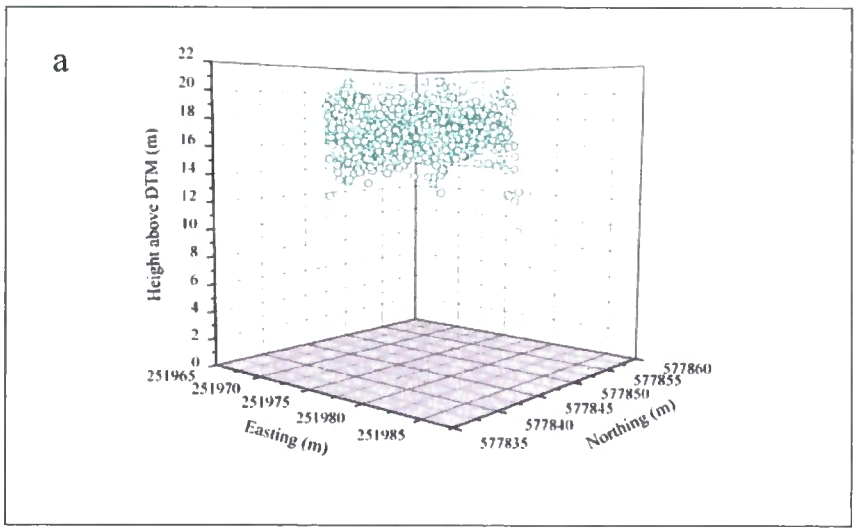

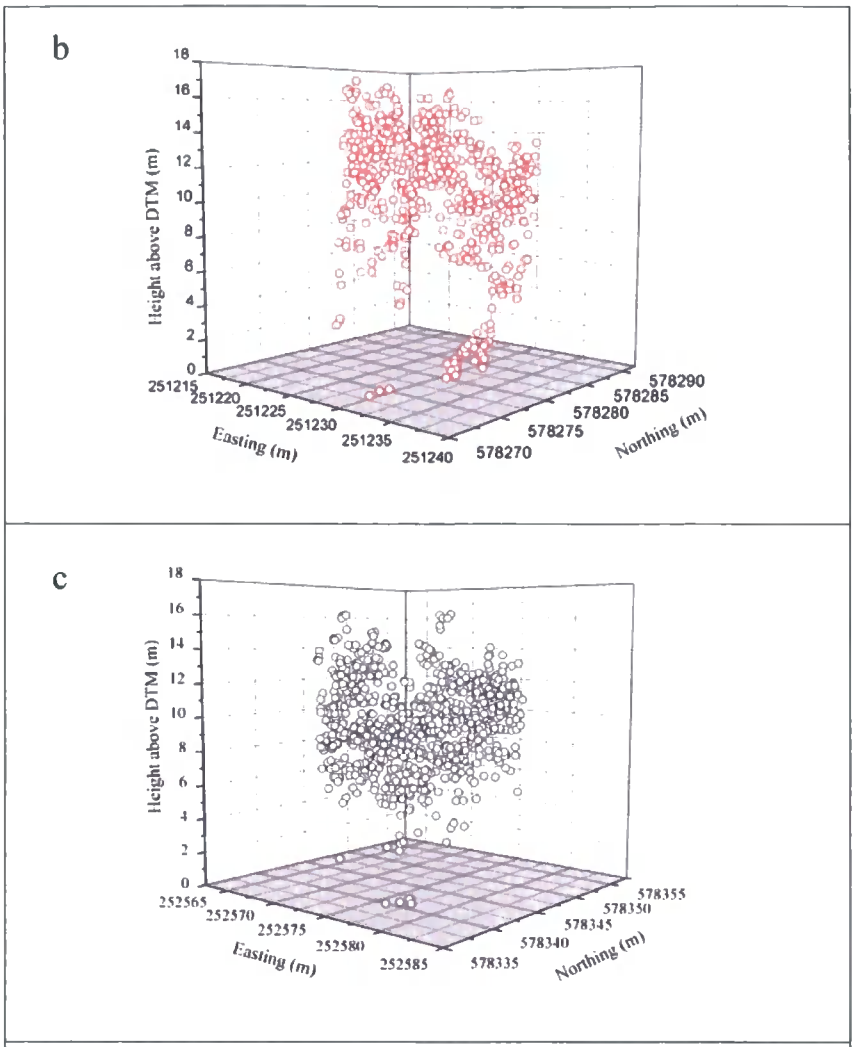

Figure 7.14 First pulse distribution for a) Pure Sitka spruce, b) Pure lodgepole pine and c) Sitka spruce/ lodgepole pine mixture.

Each LiDAR canopy density measure, C_v, *pczero*, *Skewfp* and mean height (*meanh*), were assessed using the same plot data and method applied to analyse intensity. The results are presented in sections 7.4.1 to 7.4.4.

7.4.1 Coefficient of variation

The coefficient of variation[34] (C_v) summarises the relative dispersion of the LiDAR-derived height distribution data. Dense forest canopies are associated with low LiDAR penetration rates and therefore have lower coefficients of variation (<15%). The dot plot (Figure 7.15) provides a quantitative representation of the 3D laser distribution plots for each species or species combination. It shows that 75% of the Sitka spruce

[34] The coefficient of variation is the ratio of the S.D. of height to mean height and is expressed as a percentage.

plots conform to this distribution pattern, having C_v of less than 15% (summary statistics in Appendix 7.2). The main outliers (C_v >15%) are located in plots that have open canopies or forest gaps. Overall, the coefficients of variation for pure lodgepole pine and Sitka spruce / lodgepole pine mixtures are higher than those for pure Sitka spruce, which indicates that the canopy is more open. The range of C_v values for lodgepole pine and Sitka spruce/lodgepole pine mixtures is similar, which makes it difficult to separate the two crop areas using this measure. This observation is also confirmed statistically using ANOVA, as C_v for lodgepole pine and Sitka spruce/lodgepole pine mixtures are not different at the 5% significance level. According to the results of ANOVA, the only crop types that can be separated with confidence are Sitka spruce and lodgepole pine, and also Sitka spruce and Sitka spruce/lodgepole pine mixtures (see ANOVA results in Appendix 7.3).

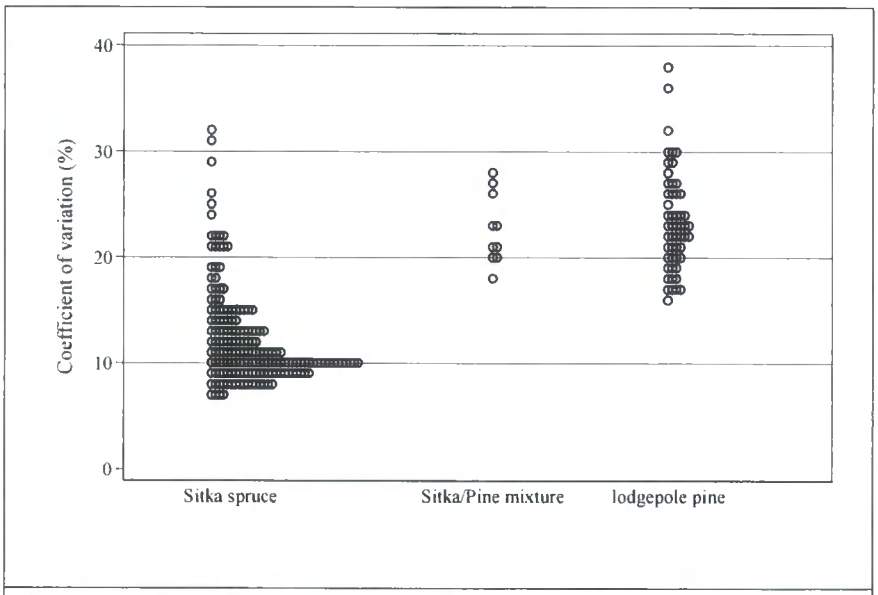

Figure 7.15 Coefficient of variation by crop type.

However, a more complex picture emerges when the coefficient of variation is mapped spatially (Figure 7.16). Colour transition from green to blue provides an indication of canopy or vegetation density. Areas of pine are a blend of blue and green tones, whilst Sitka spruce areas are solid green or blue, making it difficult without the assistance of a GIS to separate these areas. Within Sitka spruce crops, solid blue tone highlights areas of low tree density or forest rides. Detection of forest rides is due to 'pixel mixing' between forest areas and the rides, as during pre-processing, areas 0.5 m above the DTM were excluded. The mixing occurs because the rides are generally less than 15 m

wide, so the pixel values become a combination of forest and ride. Wind damaged areas have high C_v values and appear white or pink in the image.

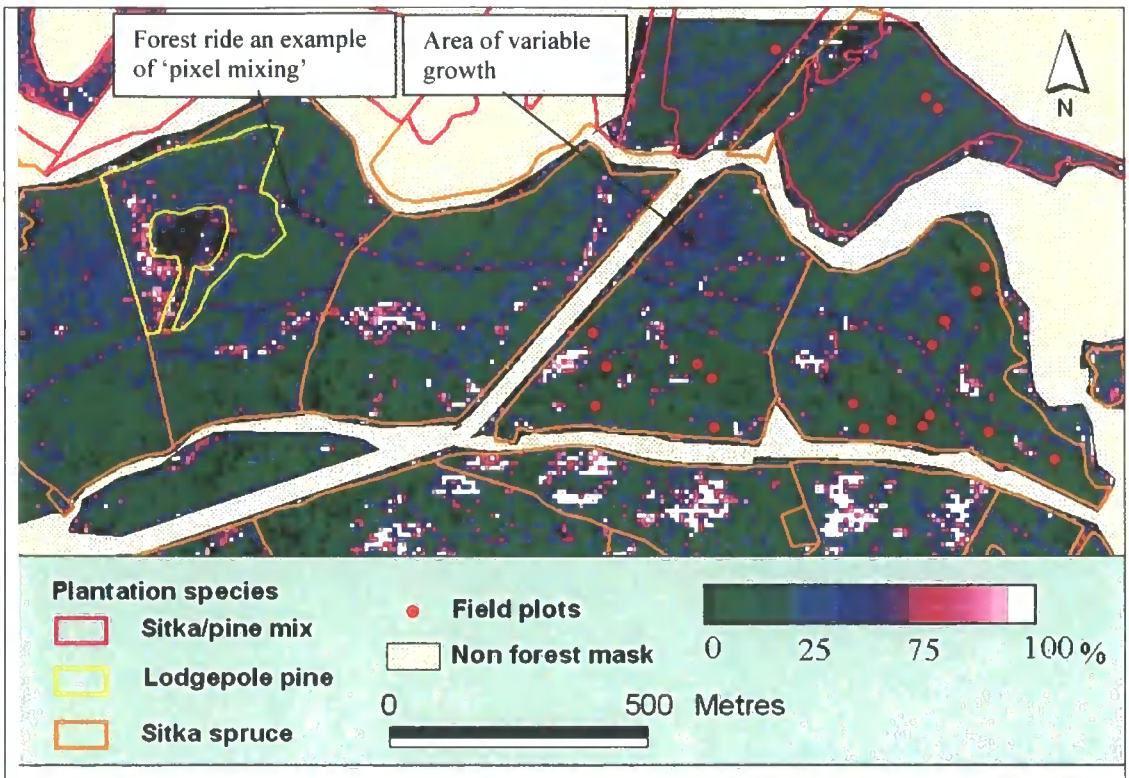

Figure 7.16 Coefficient of variation map generated using a density slice to highlight pine and Sitka crops.

7.4.2 Skewness of LiDAR height

The degree of canopy closure and height of the canopy influences skewness. Positive skewness values are associated with open sparse canopies and negative values, with closed canopies. Unlike C_v, there is no differentiation between skewness in pure Sitka spruce and in crops that comprise lodgepole pine (Figure 7.17). Furthermore, skewness distribution overlaps between species. Statistically, none of the species can be separated with confidence (see ANOVA results in Appendix 7.3) and therefore it would be difficult to use this measure to separate tree species.

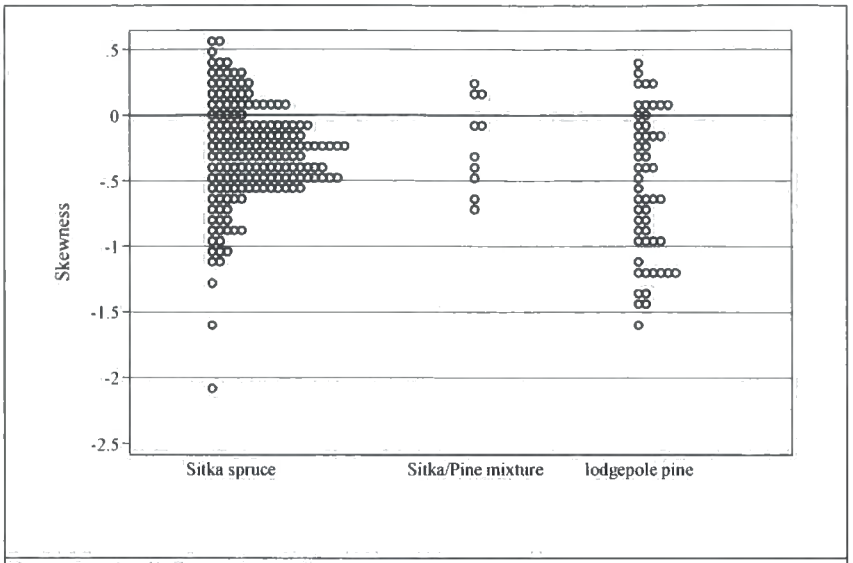

Figure 7.17 Skewness, by crop type.

The skewness map confirms these observations (Figure 7.18). On the map, skewness ranges from –2 to 1.2 (green to purple). Negative skewness occurs when the majority of returns are from the upper canopy, but the laser also penetrates to lower levels of the canopy. These areas are coloured green and are observed in pure pine, although similar patterns are also observed in Sitka spruce. As skewness shifts from –2 to 0, and the distribution becomes more symmetrical, the colour changes from green to blue. Blue areas, which are the majority of the area, also represent negative skewness. However, in these areas the denser canopy restricts the laser's penetration to the upper canopy, which decreases the skewness. Near zero skewness is observed in 'hard' areas like open and clearfelled areas (coloured purple), where there is no difference between laser heights. Skewness above zero is associated with crops that have sparse canopies, such as areas with low stocking densities (coloured magenta) and, at the extreme (values >1), areas of wind damage (coloured white).

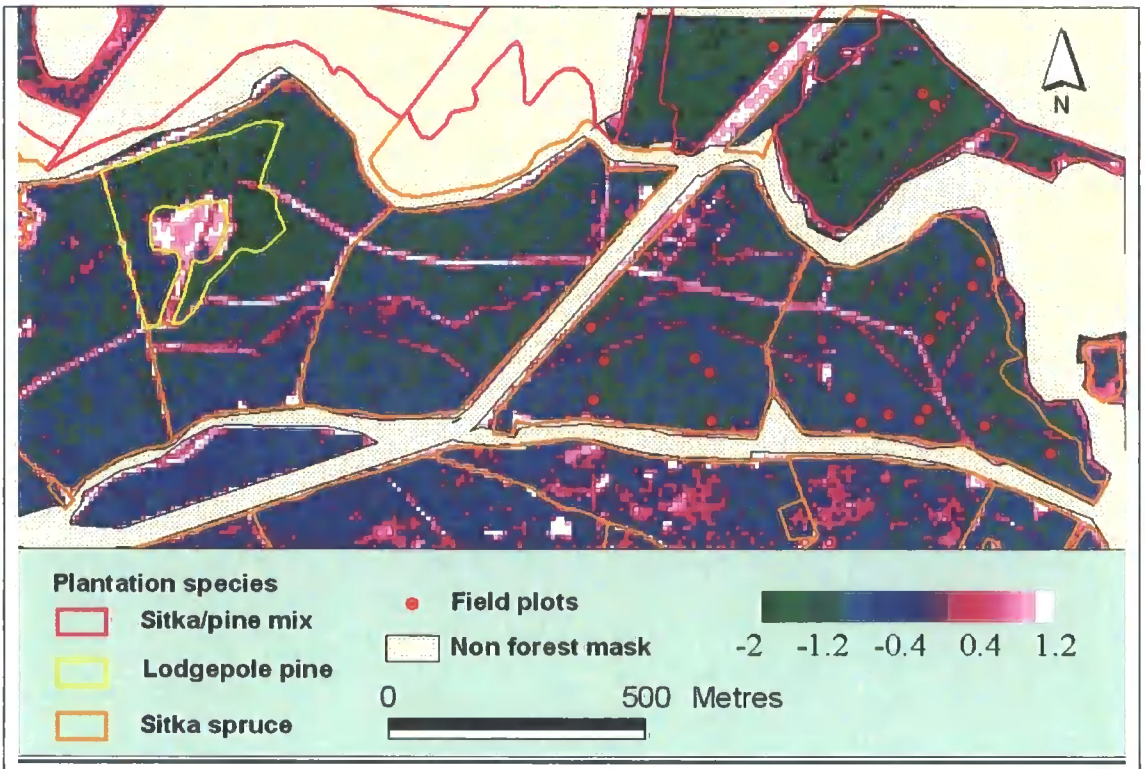

Figure 7.18 Skewness map generated using a density slice to highlight pine and Sitka crops.

7.4.3 Percent of last pulse ground returns

In forested areas the percent of last pulse ground returns (*pczero*) shows a similar pattern to the coefficient of variation; Sitka spruce can be differentiated from pine and Sitka spruce/lodgepole pine mixtures (Figure 7.19). This is predictable, as forest areas with high coefficients of variation (i.e. areas with dense canopies) will also have a low number of ground returns.

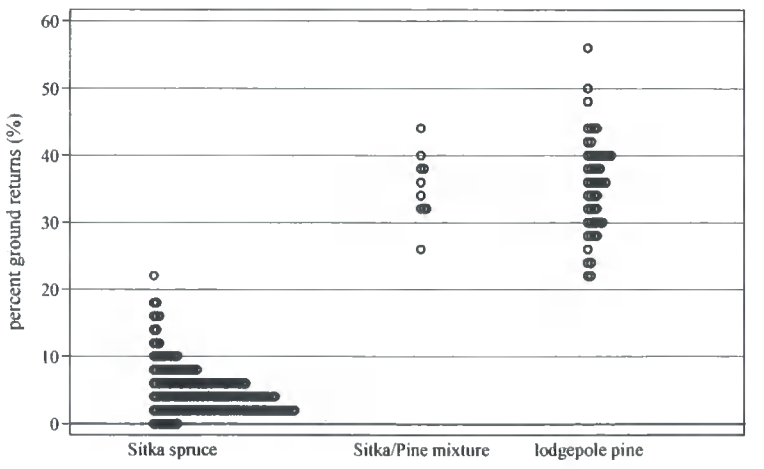

Figure 7.19 Percent last pulse ground returns by crop type.

Other non-

forest areas, such as forest gaps or rides, may also have high coefficients of variation, but these areas are separable from closed canopy forest by their high percentage of ground returns. Unlike coefficient of variation, differences between pure pine areas and Sitka spruce/lodgepole pine mixtures are more pronounced when percent of ground returns is mapped spatially (Figure 7.20). Black areas are those where no ground returns have been recorded because of very dense forest canopy. White areas show the opposite effect: the percentage of ground returns is very high because of the presence of roads and clear felled areas. Areas of forest are within the black to blue range (0% to 60%), with the colour transition providing an indication of canopy or vegetation density. Areas of pine are a blend of blue and green tones, whilst Sitka spruce areas are solid green or black. The larger blue areas within Sitka spruce represent wind damage, although *pczero* does not define these areas as well as

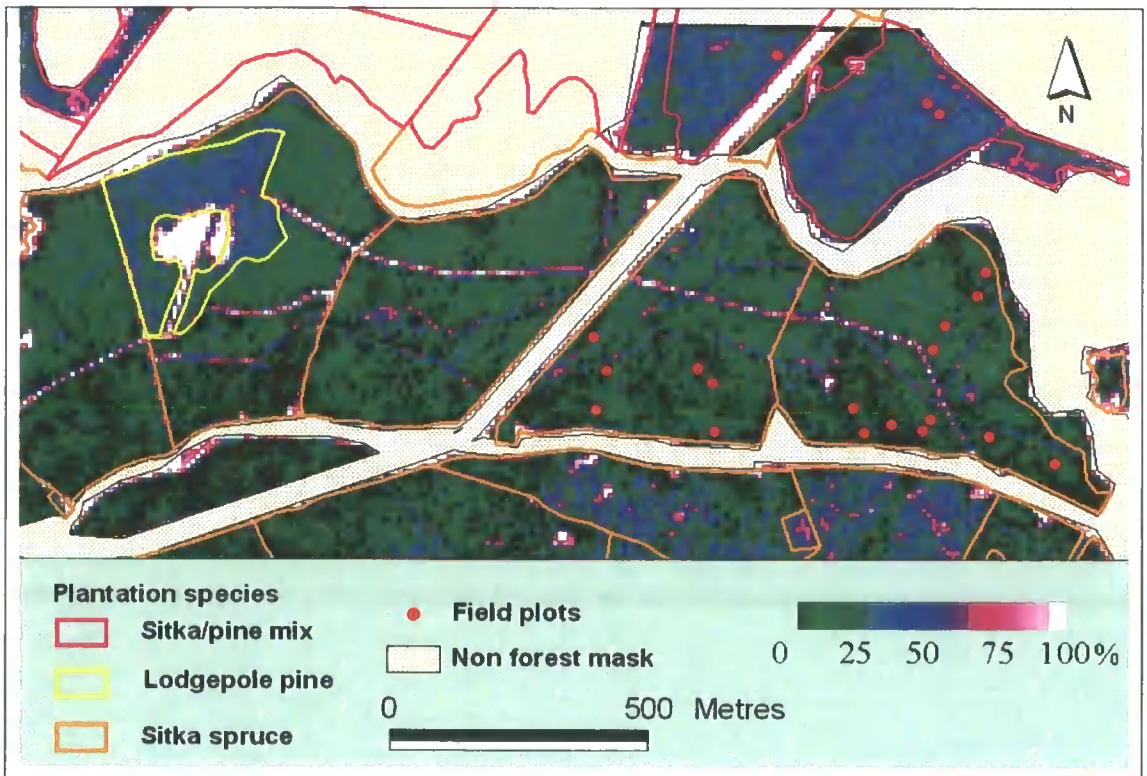

Figure 7.20 Percent of last pulse ground returns map generated using a density slice to highlight pine and Sitka crops.

7.4.4 Mean height

Mean height[35], like *pczero,* does not provide a measure that describes laser height distribution. Instead, it can be used to identify forest gaps, wind damage and variations in height within similar aged crops. Figure 7.21 shows that, overall, mean canopy height of Sitka spruce is greater than that of other crops. However, Sitka spruce height ranges from 8 to 18 m, which overlaps with the height range of pine and Sitka spruce/lodgepole pine mixtures. Height distributions of pine and Sitka spruce/lodgepole pine mixtures are similar.

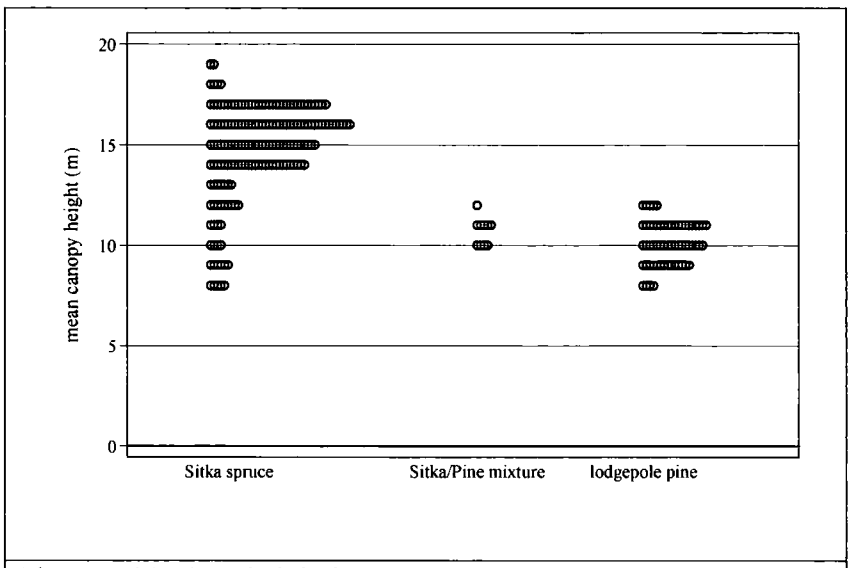

Figure 7.21 Mean height by crop type.

Figure 7.22 shows the mean height map. Mean height ranges from 0 to 18 m (black to white). The map suggests that mean height cannot be used to identify different species combinations. However, since the age range over the area is similar, it does provide a useful method for mapping variations in crop height. Additionally, height can be used to identify areas of wind damage, forest gaps and rides. In fact, when compared to the other measures, mean height is the most effective measure for this purpose.

[35] Mean height is based on the 50th percentile laser height and is calculated using the same method used in Chapter 6.

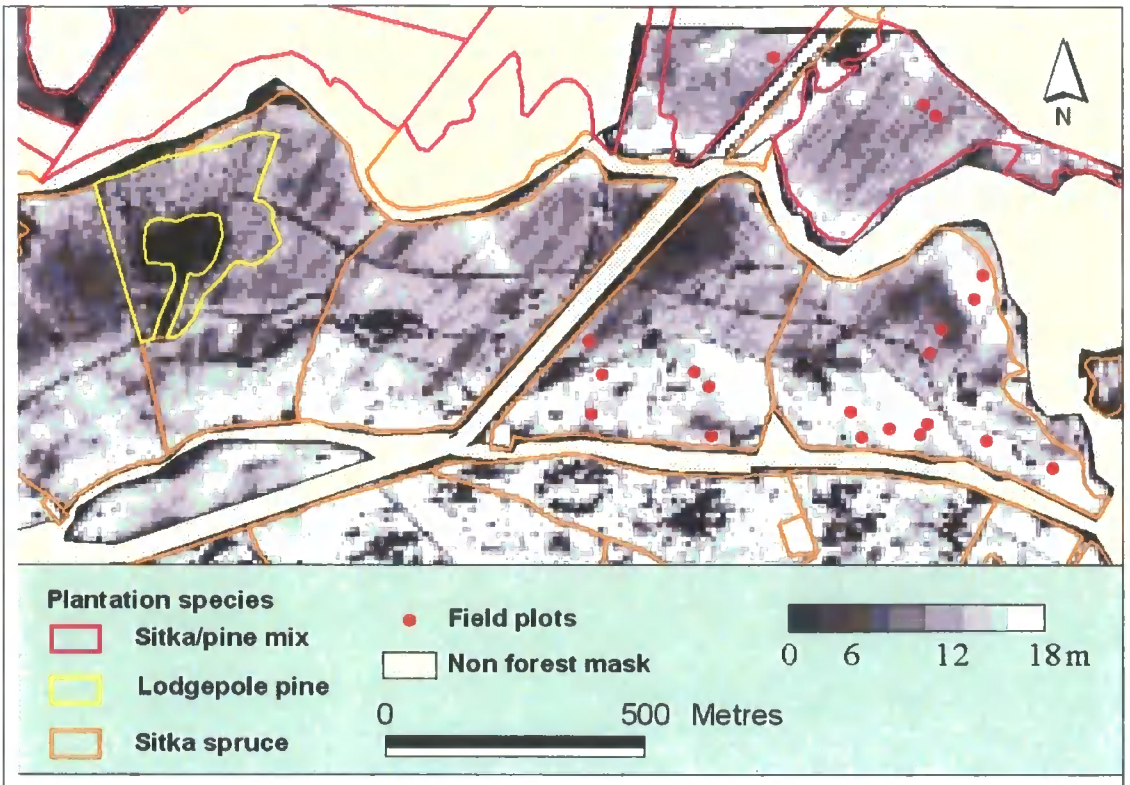

Figure 7.22 Mean height map.

7.5 Summary of LiDAR measures used to map plantation species

Graphical and spatial analyses of intensity, and other measures of canopy density and height, indicate that some measures are more effective than others at differentiating species type. While this can be confirmed statistically using one-way ANOVA, more insight is gained by extending the analysis beyond the sample plot data, by displaying the measures spatially. Table 7.3 provides a qualitative assessment of each measure considered. Despite the presence of noise in the data, LiDAR intensity is the best single measure for identifying different species and species mixtures. More variation is observed in physically based measures. Of all crop types, Sitka spruce is the easiest to identify because of its distinctive laser height distribution (refer to Figure 7.14a). The most promising measure, although not strictly a canopy density measurement, is the percentage ground returns, followed by the coefficient of variation. The result is not as definitive in lodgepole pine and Sitka spruce/lodgepole pine mixtures as it is in Sitka spruce. Skewness of height and mean height are less useful measures for discriminating between different tree species. However, of all measures assessed, mean height is the most effective for identifying wind damaged areas and areas of height variability.

Table 7.3 Qualitative summary of LiDAR measures used to identify plantation species.

Variable	Forest species			Non-forest	Comments
	Lodgepole pine	Sitka spruce	Lodgepole pine/Sitka spruce	Wind damage & forest rides	
Intensity	yes	yes	yes	partially	Identifies tree species but there is still noise in the intensity data, so use is limited in sloping areas.
Coefficient of variation	partially	partially	partially	yes	Identifies areas showing growth variability.
Percentage ground returns	partially	yes	yes	partially	Identifies areas of very dense forest (indicator of forest productivity), forest roads and rides. Wind damage is partially identified.
Skewness	partially	no	no	partially	Similar skewness is observed in many areas, although skewness does identify areas of pure pine and wind damage.
Mean height	no	no	no	yes	Identifies forest gaps, wind damage and areas with variable height, which provides an indicator of forest productivity.

Yes = useful measure No = not useful

7.6 Combined classification

To improve the accuracy of the species classification, all of the measures were combined and a supervised classification conducted. The following classes were defined using a combination of the GIS compartment boundaries and sample plot data: (i) pure areas of Sitka spruce divided into two productivity classes using mean height, (ii) areas of pure lodgepole pine (iii) species mixtures and (iv) areas of wind damage. Non-forest areas were not included in the classification, as these areas were excluded during pre-processing stage of the LiDAR data. Three classifications were generated using the ENVI maximum likelihood classifier[36] algorithm. The first classification included canopy density measures and height and the second included intensity data. As a check, the third compared the first two classifications with one generated from the

[36] Maximum likelihood classification routine in ENVI assumes that the statistics for each class in each band are normally distributed and calculates the probability that a given pixel belongs to a specific class.

SPOT 5 HRG multi-spectral satellite data using the same training areas used for the LiDAR classification incorporating all spectral bands. Figure 7.23 a to c shows the classification results for each run, with the Forestry Commission's GIS compartment boundaries overlaid. The classification, based on the SPOT 5 HRG imagery, shows the largest misclassification. In particular, areas of wind damage (not mapped in the FC's GIS), forest edges and forest rides are confused with lodgepole pine. Sitka spruce is accurately classified, although growth variations are not as clearly mapped when compared with the LiDAR classifications (also refer to the mean height map, Figure 7.22). Some of the smaller areas of wind damage are also misclassified as pine. Overall, there is little difference between the two LiDAR classifications. According to the Forestry Commission's GIS the area of pure pine area is correctly classified. In plantation mixtures the classification provides more detail than the GIS data, as it not only identifies the dominant species, but also maps the spatial extent of each species. Ideally, the accuracy of the species mixture classification would be best tested using validation plots, but unfortunately no such field data was available. As an alternative, the classification's accuracy can be compared with a 1: 10 000 aerial photograph[37] (Figure 7.24a) which indicates that the match is accurate, even at 10 m resolution (refer to Figure 7.23 for classification legend). Lastly, the inclusion of mean height enables areas to be classified according to height, which is a useful measure as it proves an indication of crop productivity.

[37] Aerial photography was flown 12 days after the LiDAR overpass, on the 27/06/03.

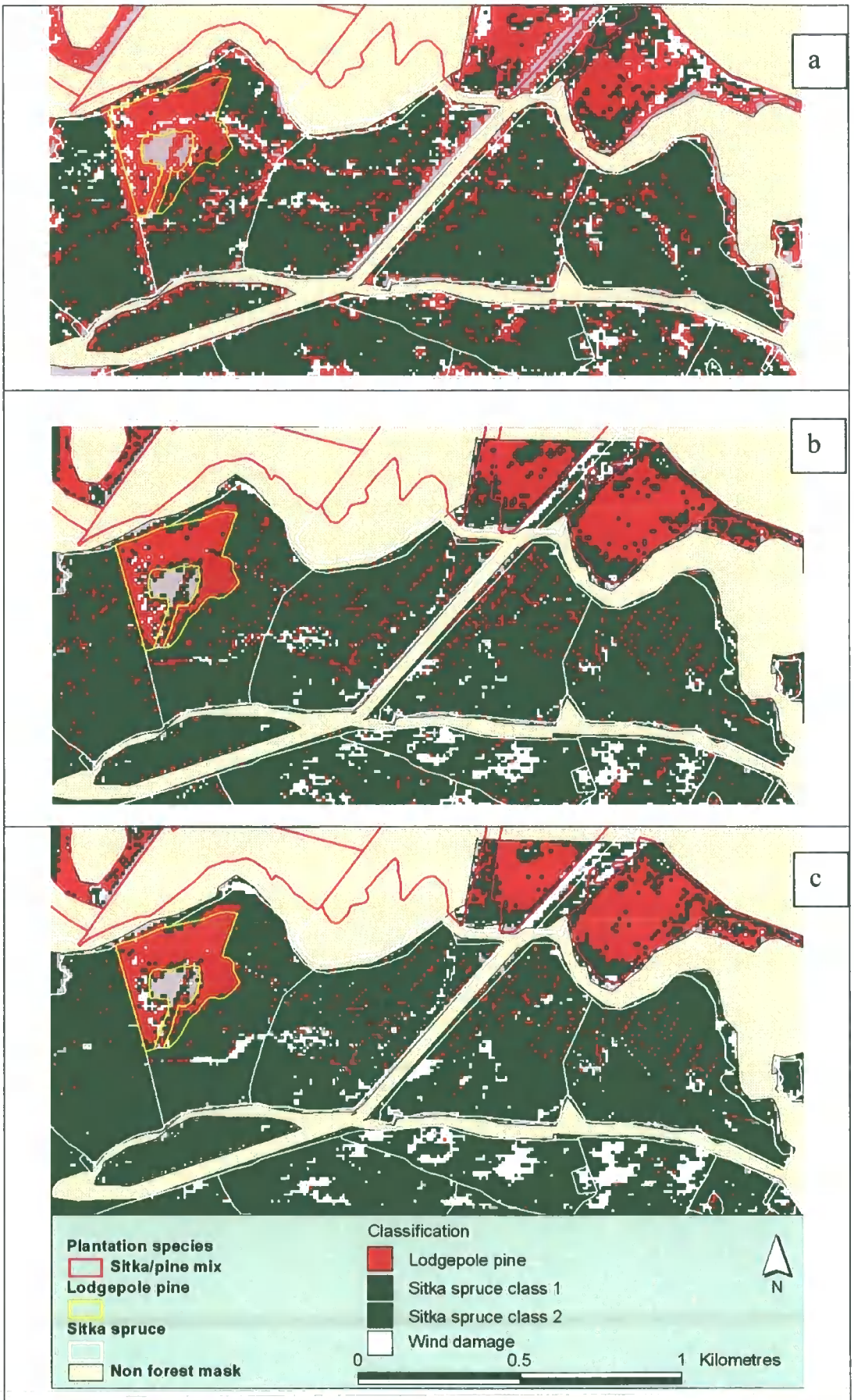

Figure 7.23 Forest species classification a.) SPOT 5 HRG b.) LiDAR density measures c.) LiDAR density measures and intensity.

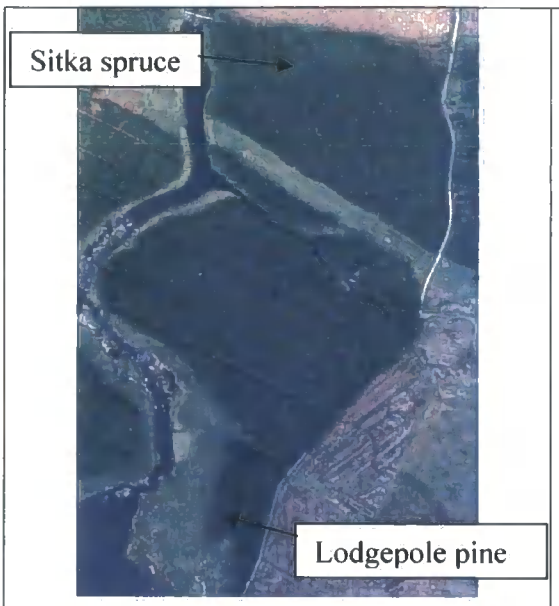

Figure 7.24a 1: 10 000 aerial photograph.

Figure 7.24b LiDAR classification.

7.7 Discussion

The objective of this chapter was to assess the potential of LiDAR intensity data and crown density measures for identifying plantation mixtures and areas of variable growth. Although the study area is small (300 ha), results strongly suggest that LiDAR data can be used to provide more than just estimates of forest height and volume. The methods developed show that, in UK conifer forests, species can be mapped using either LiDAR-derived crown density measures or LiDAR intensity data. Potentially, intensity is more problematic to use, as it is not radiometrically calibrated to a published standard. For the reasons outlined in section 7.1.4 it is to be expected that intensity values will vary between different LiDAR flights. However, if intensity of returns are calibrated against another source, then it offers considerable potential for forest mapping. Filtering intensity data further improves the classification, by removing unwanted noise after which it is possible to discriminate between different conifer species. The technique has limited potential in areas where topography is not constant (i.e. laser path length and footprint vary), although it appears that a more robust correction (i.e. using the method in Luzum et al. 2004) can be applied if the position and angle of the laser pulse is known. However, this uncertainty is reduced by using all the LiDAR variables in a statistical classification. In this context it is possible to resample the LiDAR data to any spatial resolution using the method developed in Chapter 4. This would allow LiDAR variables to be integrated with other remotely sensed data (e.g. IKONOS, SPOT, IRS or even RADAR data), which could be used to further refine

the classification, or to validate classifications/predictions made using other remotely sensed data/models. This is the focus of Chapter 8.

In addition to identifying and mapping forest species composition, it is also possible to map areas of anomalous growth. These areas are best identified using crown density measures coupled with forest height. When compared with conventional methods that use manual interpretation of aerial photography, the LiDAR-based method is more accurate because it is easier to identify areas of wind damage and variations in height that are not necessarily depicted on aerial photography.

These methods provide an accurate means of identifying different forest species, and areas of anomalous growth, at the stand level. It is clear that this sort of information would lead to improved forest yield estimations, as it is possible to exclude non-productive areas, identify areas of poor growth and identify and map species composition, so that the correct yield class model can be applied.

Chapter 8: Using LiDAR to compare forest height estimates from IKONOS and Landsat ETM+ data in Sitka spruce plantation forests

Chapters 5 and 6 demonstrated that LiDAR provides accurate estimates of forest height. The main limitation to wide-scale application of these data in the UK is their perceived cost (Donoghue & Watt *in review*). In comparison with LiDAR data, satellite imagery may provide a cheaper option for some mensuration and monitoring applications. However, despite the widespread availability of optical imagery at a variety of scales, including newly available fine spatial resolution satellite data, very few studies have tried to compare and contrast different scales of image data, especially for mapping forest structure (Hyyppä et al. 2000; Li and Strahler 1985; Woodcock and Strahler 1987).

This chapter compares and contrasts predictions of forest height in Sitka spruce plantations based on medium-resolution Landsat ETM+, high-resolution IKONOS satellite imagery and airborne LiDAR data. Regression analysis is used to evaluate the quality of predictions from each of these sensors, against measured tree heights. The first approach uses only tree height measured in the field as the dependent variable; the second approach uses tree height data derived from LiDAR to complement field measurements.

8.1 Field and image data

The forest mensuration dataset comprises 28 of 60 sample plots measured within Kielder forest study area, as summarised in Table 8.1. The sample plots exclude those measured in Sitka spruce/lodgepole pine mixture (16 plots), but include the 16 plots of 0.01 ha measured in the Sitka spruce. Because of their size and close proximity, these plots were amalgamated to form one plot: see Figure 3.7.

Table 8.1 Summary of 28 field survey plots

Variable	Age (years)	Density (trees/ha)	Basal area (m^2/ha)	Height (m)	Diameter (cm)
Mean	33.0	2,732	47.0	11.1	17.1
Standard Deviation	18.8	2,614	17.4	6.7	5.1
Minimum	8.0	1,150	4.5	1.5	4.3
Maximum	59.0	12,300	69.4	22.3	23.8

The LiDAR data were collected on 26 March 2003 using an Optech ALTM 2033 laser scanning system. The two satellite images were acquired in cloud-free conditions six months apart, with IKONOS data acquired on 13 March 2002 and Landsat ETM+ data on 2nd September 2002. The IKONOS data were collected at an off-nadir view angle of 30°. Spectrally, the band-passes of both sensors are very similar. For further details on image data and processing, please refer to Chapter 4.

8.2 Estimation methods

8.2.1 Image preparation

The satellite data were geo-corrected using LiDAR coverage. To match the pixel size of IKONOS data, the Landsat ETM+ data were resampled using nearest neighbour re-sampling, from a pixel size of 30 m to 4 m. This makes it easier to manage the data, as the image bands can be stacked into one file (including the LiDAR data). More importantly, resampling does not affect the radiometric characteristics of data (Figures 8.1a and b).

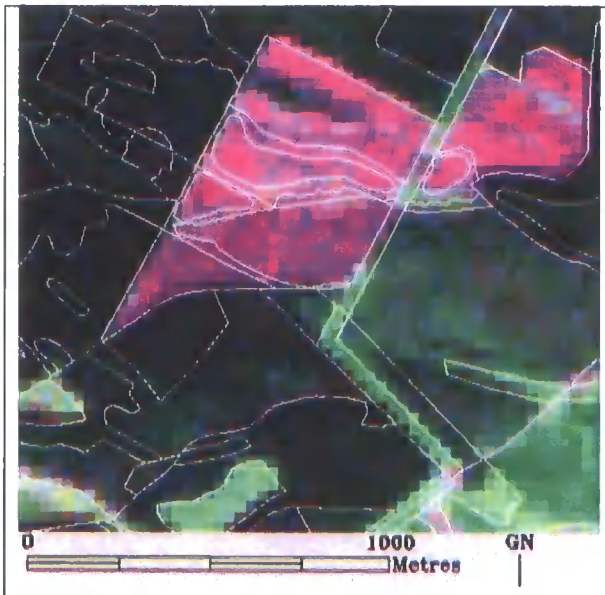

Figure 8.1a Geo-corrected Landsat ETM+ image displayed using band combinations: blue, near infrared and red.

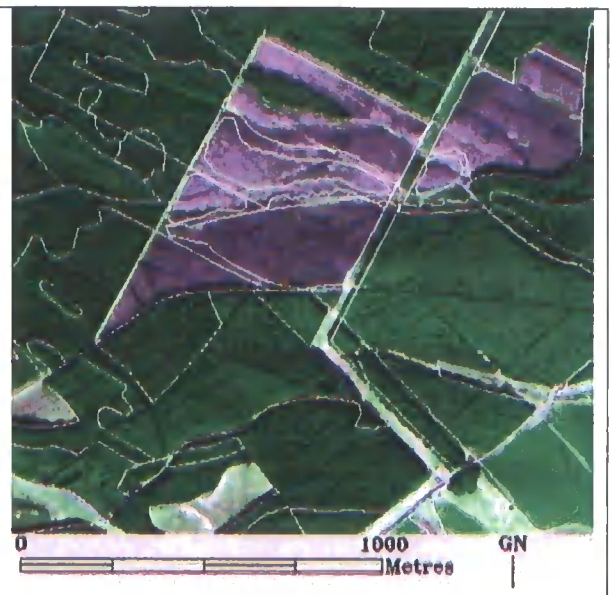

Figure 8.1b Geo-corrected IKONOS image displayed using band combinations: blue, near infrared and red.

8.2.2 LiDAR-derived height

To generate additional height samples, LiDAR data were used to provide estimates of mean height for each 4 m pixel. Using field sample plots, mean height was regressed against each LiDAR height percentile. From this analysis the 60th height percentile (*p60*) was selected based on its R^2 (0.99) and RMS error (0.88 m), as shown in Table 8.2. It is worth noting that R^2 and RMS errors are similar above the 50th height percentile, which suggests that any height percentile above this point could be used to predict mean height, without a substantial decrease in accuracy.

Table 8.2 Summary of LiDAR height percentiles used to estimate mean height

	Mean height Sitka spruce $n = 28$	
Height percentile	R^2	RMSE (m)
10	0.97	1.17
20	0.98	1.03
30	0.98	0.97
40	0.98	0.95
50	0.98	0.92
60	0.99	0.88
70	0.99	0.89
80	0.98	0.90
90	0.98	0.91
95	0.98	0.92
99	0.98	0.89
Maximum height	0.98	0.90

Figure 8.2 shows LiDAR-derived height values plotted against field-measured mean height at each of the ground sample plot locations.

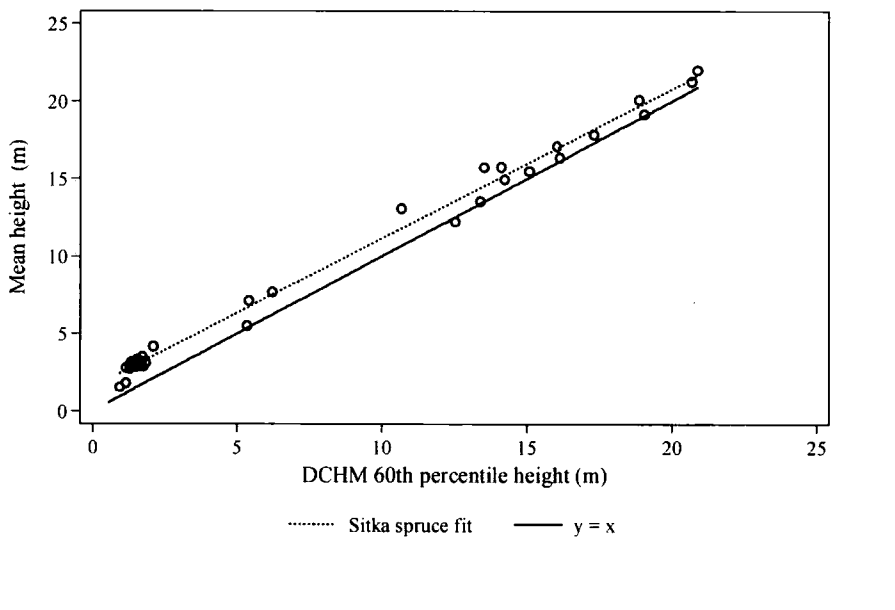

Figure 8.2 Relationship between mean height and LiDAR derived height.

From this relationship a regression (Equation 8.1) to predict mean height for each 4 m pixel on the LiDAR grid was derived:

$$\text{Mean height (m)} = 1.51 + 0.95\ p60 \qquad \text{Equation 8.1}$$

8.2.3 Extraction of plot data

For each sample plot, mean height was calculated from field data and compared with corresponding image pixel values extracted from the IKONOS and Landsat ETM+ data. This procedure was repeated for the four IKONOS and six Landsat ETM+ image bands. For each sample plot, the mean of these pixels was taken to represent the plot's canopy reflectivity. Using the LiDAR 'mean height' grid, a second dataset was constructed as a substitute for field data. This was achieved by generating a systematic sampling grid in a GIS at an interval of 100 m between samples. A circular buffer of radius 7.98 m was generated around each sample, to give it the same area as a 0.02 ha ground sample plot and the corresponding pixel values were extracted from the LiDAR grid. Samples were stratified into forest or non-forest using the forest compartment GIS layer and those points that were located within 30 m of forest compartment boundaries were discarded. This process generated 410 additional height data samples over the study area (Figure 8.3).

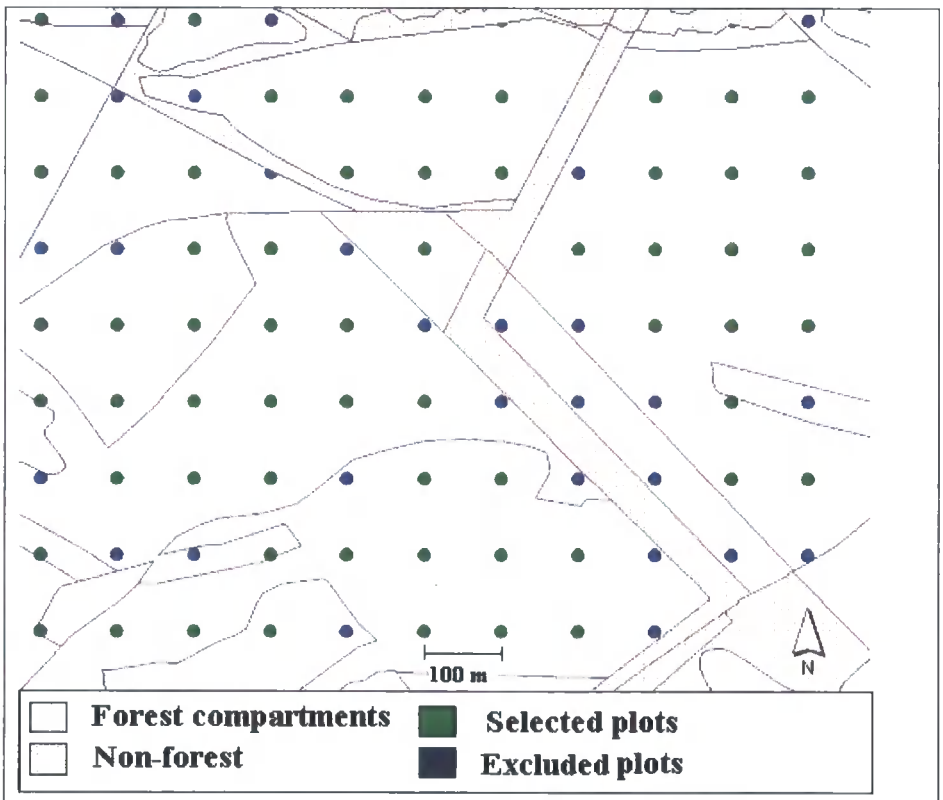

Figure 8.3 Selection of additional field plots used to extract height values from LiDAR 60th percentile height.

8.2.4 Regression models

The relationship between LiDAR derived height and measured height is linear, so a conventional least squares linear regression model is appropriate (see Figure 8.2). For IKONOS and Landsat ETM+ data, various single and multiple band regression models were tested. Inspection of the scatter plots for IKONOS, Landsat ETM+ and ground data shows that the relationship between reflectance and height is curvilinear.

[38]Common approaches to dealing with the curvilinear shape of the relationship include, (1) fitting something more complicated than a line (e.g. a quadratic or other polynomial) and (2) transforming the response (e.g. by taking logarithms) and working on a transformed scale, an approach used in many studies that have used optical (Ahern et al. 1998; Hyyppä et al. 2000; Puhr and Dongohue 2000) or LiDAR data (Naesset 1997; Means et al. 1999; Nelson 1997; Holmgren et al. 2003). Neither is problem-free. With (1), a more complicated curve may exhibit un-interpretable wiggles and it may also extrapolate very poorly beyond the range of the data, even to the extent of producing unacceptable predictions (such as negative tree heights). This is a key weakness for an approach based on fitting a relationship in a training data set and then extending it to the wider area covered by imagery. Such problems do not arise to the same extent with (2) an approach based on transformations, but the need to back-transform predictions to the original scale is at best awkward, and other difficulties can arise, such as the fact that R^2 and RMS error both refer to variations on the transformed logarithmic scale.

An approach which in many ways offers the best of both worlds, is that afforded by generalised linear models (GLMs). There are two main differences between GLMs and general linear models: first, the response may have a non-normal distribution and second, the transformation applied to the response variable is selected by applying the appropriate link function (e.g. logarithmic) in the software. One key advantage of using a GLM is that predictions are generated and presented on the original measured scale of the response and so there is no need for back-transformation or bias corrections (Cox et al. *in review*). In this thesis the logarithmic link function was used, which thus instructs the software to fit a relationship on a logarithmic scale, but to report results on the scale of the original response variable.

---

[38] This section draws on material adapted from Donoghue et al. (2004).

As an example, Figure 8.4 compares the fit of a power function, which is suggested by the curvilinear pattern and a GLM model using the field data (n =28) and Landsat ETM+ green band reflectance. The graph suggests that there are advantages and disadvantages attached to both model types. Superficially, the power function appears to be a better fit, as the model passes through the centre of the data points. In contrast, the GLM fits the upper range of the data (>10 m) but over-predicts tree height in the lower range (<10 m). The poor fit of the GLM over this range is probably due to the low number of field observations. Despite this limitation the GLM has less curvature than the power function and therefore, will provide more realistic height predictions when extrapolated. Although not so obvious in this example, if extrapolated, power functions have potential to behave erratically at tail end of the curve by decreasing and then increasing again.

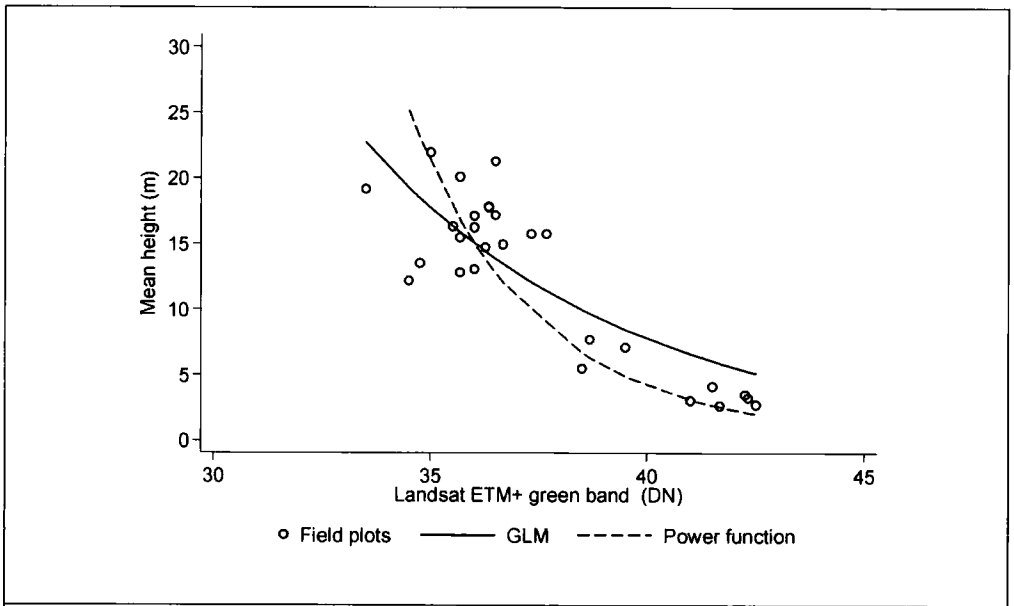

Figure 8.4 Comparison of model fit between a GLM (logarithmic link, log DN predictor) and power function using field-measured mean height predicted from Landsat ETM+ green band.

It is, therefore, difficult to model these data using a power function because of its sensitivity to outliers, which can drag the curve upwards at the tail. Figure 8.5, using the same spectral band, shows the effect on model fit of increasing the number of observations through inclusion of LiDAR height samples (n = 438).

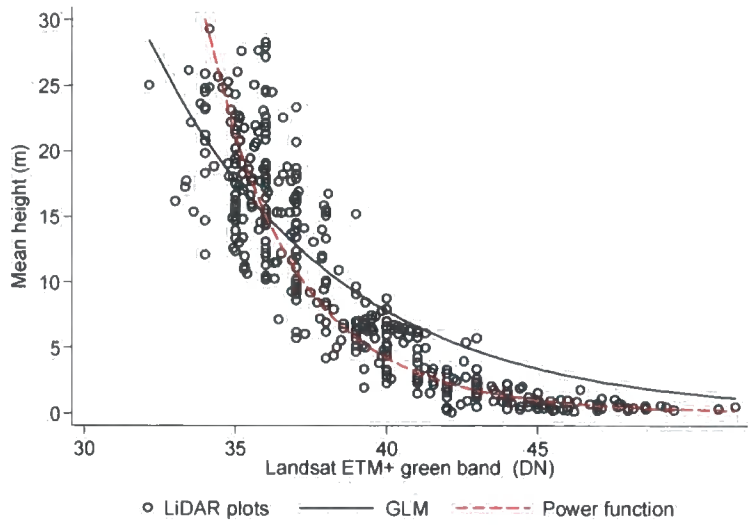

Figure 8.5 Comparison of model fit between a GLM (logarithmic link) and power function, using LiDAR-derived mean height predicted from Landsat ETM+ green band.

Here increasing the number of observations improves the fit of both models by extending the data range to include more newly established plantations. This has the effect of grounding both models close to or at zero. On balance, the GLM is a better choice of model as it provides more robust predictions than the power function. Consequently, GLMs are used for the rest of the analysis.

8.2.5 Height estimates using GLMs

For each spectral band and sensor, two linear regression models were generated. The first, referred to as Model A, included only the ground survey plot data (28 sample plots), and the second, referred to as Model B, used data derived from 410 LiDAR-measured sample plots. In both cases models based on single and multiple band combinations were also considered[39]. The suitability of each model was assessed using the criteria presented in Table 6.3. Model selection was based on two measures of goodness of fit, R^2 and RMS error, together with the physical or biological plausibility and simplicity of each model. The statistical relationships between the ground reference data and IKONOS and Landsat ETM+ spectral bands are presented in sections 8.2.5 and 8.2.7.

[39] This process was automated in Stata, so that all possible band combinations were considered.

8.2.6 IKONOS regression models

The relationship between height and IKONOS data was assessed using 15 possible band variations, extended to generate height predictions for the two datasets (Table 8.3). To improve interpretability, Table 8.3 is divided according to the number of spectral bands used to generate each model. For models (based on Model B) that use single spectral bands, R^2 ranges from 0.27 in the near infrared to 0.74 in the green band. It is also worth noting that the blue and red spectral bands correlate strongly with height with R^2 = 0.69 and 0.75, respectively. This suggests that height can be predicted using any spectral band located in the visible spectrum. Overall more complex models that include more than one spectral band tend to have higher R^2 and lower RMS error values. For example, on its own, the near infrared band is a poor predictor of height, but when combined with other spectral bands, R^2 and RMS error of the predictions improve. Models that show this pattern are highlighted in Table 8.3. Lower RMS errors for Model A, suggest that there is less variation in the data used to generate Model A than Model B. The higher RMS errors for Model B (the LiDAR-based sample) are probably caused by inclusion of samples located near to areas of non-forest, damaged areas or forest rides, causing the corresponding image pixels to comprise a mixture of spectral responses.

Table 8.3 Summary of regression models used to estimate forest height from IKONOS satellite data

No. predictors	Model	Image Band(s)	Height **Model A**: (n=28)		Height **Model B**: (n=438)	
			R^2	RMS error (m)	R^2	RMS error (m)
1	1	1	0.69	3.54	0.68	4.46
	2	2	0.79	2.96	0.74	4.03
	3	3	0.75	3.21	0.73	4.10
	4	4	0.35	5.16	0.27	6.78
2	5	1 2	0.80	2.91	0.75	4.01
	6	1 3	0.75	3.23	0.74	4.03
	7	1 4	0.79	3.00	0.83	3.31
	8	2 3	0.80	2.96	0.72	4.17
	9	2 4	0.89	2.20	0.74	4.03
	10	3 4	0.84	2.66	0.79	3.63
3	11	1 2 3	0.80	2.97	0.76	3.92
	12	1 2 4	0.89	2.24	0.83	3.29
	13	1 3 4	0.84	2.67	0.79	3.64
	14	2 3 4	0.89	2.21	0.83	3.31
4	15	1 2 3 4	0.89	2.23	0.83	3.29

8.2.7 IKONOS height estimates using a single predictor

Models based on a single predictor are attractive as the relationship is simple to apply and often more easily understood. From Table 8.3 it is clear that any of the visible bands could be used to predict height. Figure 8.6 shows the relationship between height and the IKONOS green band which has the highest R^2 and lowest RMSE. It also shows the fit of both height models; Model A, derived from the field sample plots, and Model B, derived from the additional height sample taken from LiDAR. The form of the relationship is very similar, despite differences in R^2 and RMS errors. The overall pattern is for reflectance to increase quickly below 10 m, while above 10 m little change in reflectance occurs as tree height increases (i.e. changes in DN values are <20 DN). The curves for height Model A and B are closely aligned, which suggests that increasing the number of height samples makes little difference to height estimates.

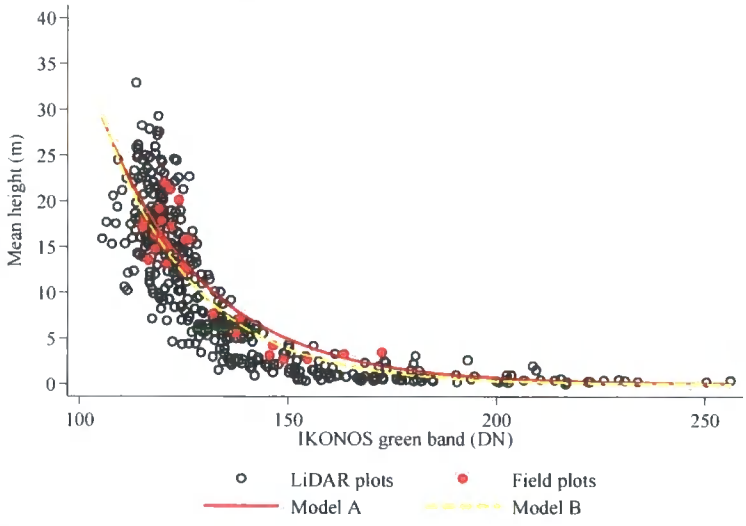

Figure 8.6 GLM height Models A and B used to predict height from IKONOS green band DN values, using field and LiDAR sample plot data.

8.2.8 IKONOS height estimates using multiple predictors

Results presented in Table 8.3 show that increasing the number of spectral bands in the model improves the R^2 and RMS error. Fitting a more complex model is justified if inclusion of additional bands improves the predictive ability of the model and if the

model also has a physical basis. To show this graphically, a series of predictions are created by sequentially adding spectral bands. As each prediction is made, the corresponding residual plot is produced to show impact on predictive ability of the model. Figures 8.7 and 8.8 compare height predictions and residuals for IKONOS band 2 and height models, 9, 12 and 15, based on multiple spectral bands. These are the best models, with 1, 2, 3 and 4 predictors respectively. The following series of plots show diminishing returns as predictors are added.

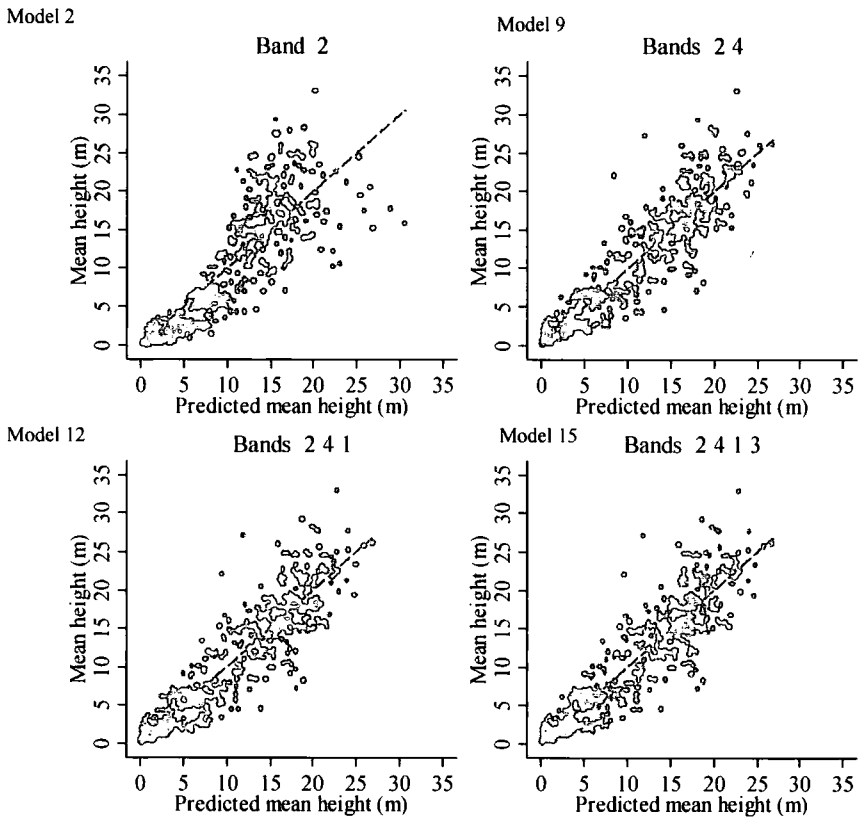

Figure 8.7 GLM height Model B, used to predict height from multiple IKONOS bands.

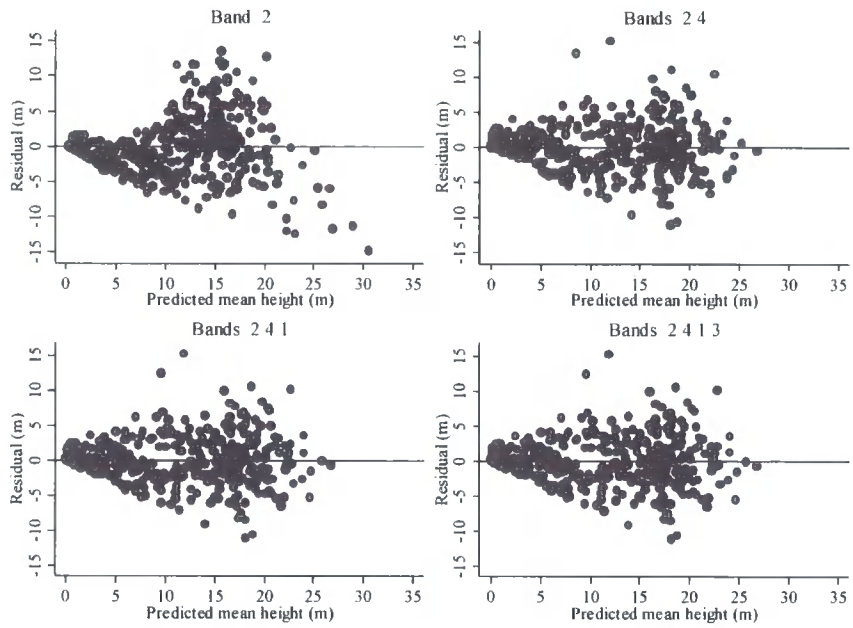

Figure 8.8 Residual plots for height Model B, using multiple IKONOS bands.

The height predictions and residual plots show that the relationship between height and IKONOS image bands improves with the addition of the near infrared band, but does not substantially improve as further bands are added to the model. Figure 8.8 shows that residual errors in all models increase as tree height increases, with residual errors exceeding 5 m once tree height reaches 10 m. In model 2 (the green band), some curvature is observed in the residual distribution above 10 m. This is corrected by adding an additional band, but at the same time this also increases the scatter of the residuals. Consequently, a simple model based on a single predictor, the green band (band 2), is preferred (R^2 =0.79), as the improved fit of models with more than one spectral band does not adequately compensate for their inherent complexity (R^2 =0.89).

8.2.9 Landsat ETM+ regression models

Since Landsat ETM+ has six spectral bands that record data in the visible, near infrared and shortwave infrared, it was possible to evaluate the relationship between different band combinations and height using 63 models. This could be expanded to 126 models, when height models A and B were considered (Table 8.4). The green and red

wavelengths show the strongest relationships, with R^2 of 0.79 and 0.71 respectively, and NIR the weakest relationship, with R^2 of 0.45. For reference, the same combination of spectral bands used in the IKONOS analysis is highlighted in Table 8.4. Analysis of Landsat ETM+ data is also extended, to include models with shortwave infrared bands (Landsat ETM+ bands 5 and 7).

Table 8.4 Summary of regression models used to estimate forest height from Landsat ETM+ satellite data

No. Predictors	Model	Image Band(s)	Height **Model A** (n=28)		Height **Model B** (n=438)	
			R^2	RMS error (m)	R^2	RMS error (m)
1	1	1	0.49	4.57	0.53	5.47
	2	2	0.69	3.58	0.79	3.63
	3	3	0.75	3.18	0.71	4.28
	4	4	0.46	4.68	0.45	5.86
	5	5	0.64	3.82	0.66	4.63
	6	7	0.66	3.74	0.59	5.06
2	7	1 2	0.69	3.65	0.79	3.63
	8	1 3	0.79	3.02	0.71	4.27
	9	1 4	0.51	4.56	0.64	4.80
	10	1 5	0.64	3.88	0.66	4.60
	11	1 7	0.66	3.81	0.62	4.87
	12	2 3	0.76	3.21	0.80	3.53
	13	2 4	0.69	3.65	0.79	3.63
	14	2 5	0.71	3.53	0.80	3.59
	15	2 7	0.73	3.40	0.80	3.56
	16	3 4	0.76	3.17	0.73	4.13
	17	3 5	0.75	3.24	0.72	4.18
	18	3 7	0.76	3.20	0.71	4.24
	19	4 5	0.68	3.65	0.68	4.48
	20	4 7	0.67	3.73	0.68	4.49
	21	5 7	0.66	3.81	0.66	4.63
3	22	1 2 3	0.79	3.06	0.80	3.53
	23	1 2 4	0.69	3.71	0.79	3.63
	24	1 2 5	0.71	3.56	0.80	3.59
	25	1 2 7	0.74	3.37	0.80	3.56
	26	1 3 4	0.79	3.08	0.73	4.13
	27	1 3 5	0.80	3.01	0.72	4.18
	28	1 3 7	0.81	2.87	0.71	4.23
	29	1 4 5	0.69	3.73	0.68	4.46
	30	1 4 7	0.67	3.80	0.68	4.47
	31	1 5 7	0.66	3.88	0.66	4.60
	32	2 3 4	0.77	3.16	0.80	3.53
	33	2 3 5	0.76	3.27	0.80	3.53
	34	2 3 7	0.76	3.24	0.80	3.52

	35	2 4 5	0.74	3.42	0.80	3.58
	36	2 4 7	0.76	3.28	0.80	3.56
	37	2 5 7	0.75	3.33	0.80	3.56
	38	3 4 5	0.78	3.14	0.73	4.12
	39	3 4 7	0.79	3.07	0.73	4.12
	40	3 5 7	0.78	3.15	0.72	4.18
	41	4 5 7	0.69	3.70	0.68	4.47
4	42	1 2 3 4	0.79	3.12	0.80	3.53
	43	1 2 3 5	0.80	3.07	0.80	3.53
	44	1 2 3 7	0.82	2.92	0.80	3.52
	45	1 2 4 5	0.74	3.49	0.80	3.58
	46	1 2 4 7	0.76	3.33	0.80	3.56
	47	1 2 5 7	0.76	3.36	0.80	3.56
	48	1 3 4 5	0.80	3.03	0.73	4.12
	49	1 3 4 7	0.82	2.90	0.73	4.12
	50	1 3 5 7	0.82	2.88	0.72	4.19
	51	1 4 5 7	0.69	3.78	0.69	4.46
	52	2 3 4 5	0.78	3.17	0.80	3.53
	53	2 3 4 7	0.80	3.06	0.80	3.52
	54	2 3 5 7	0.80	3.07	0.81	3.51
	55	2 4 5 7	0.76	3.33	0.80	3.56
	56	3 4 5 7	0.79	3.13	0.73	4.12
5	57	1 2 3 4 5	0.80	3.09	0.80	3.53
	58	1 2 3 4 7	0.82	2.94	0.81	3.52
	59	1 2 3 5 7	0.83	2.87	0.81	3.52
	60	1 2 4 5 7	0.76	3.39	0.80	3.56
	61	1 3 4 5 7	0.82	2.95	0.73	4.13
	62	2 3 4 5 7	0.80	3.07	0.81	3.52
6	63	1 2 3 4 5 7	0.83	2.94	0.81	3.52

8.2.10 Landsat ETM+ height estimates using a single predictor

The relationship between mean height and the Landsat green spectral band, using height models A and B is presented in Figure 8.9. The relationship is similar to that of IKONOS, with reflectance increasing quickly below 10 m and remaining relatively static above 10 m (i.e. alters by less than 5 DN). Increasing the number of height samples improves fit of the height model slightly below 5 m, but overall there is little difference between the two height models.

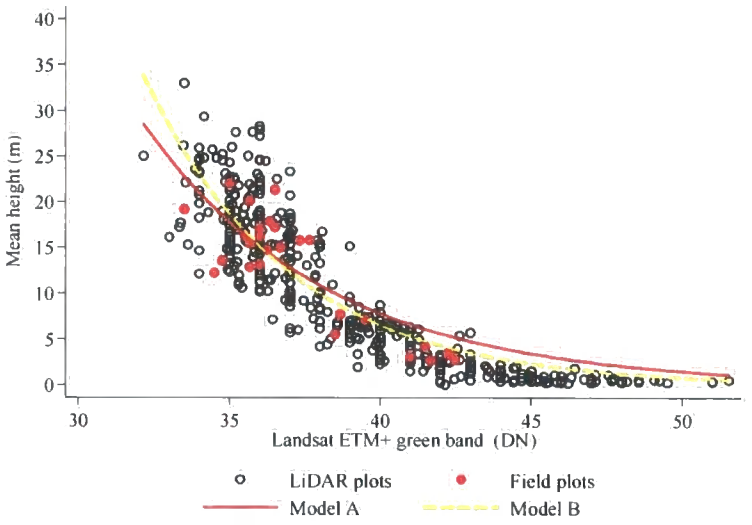

Figure 8.9 GLM height models A and B used to predict height from Landsat ETM+ green band DN values, using field and LiDAR sample plot data.

8.2.11 Landsat ETM+ height estimates using multiple predictors

Only small improvements in the R^2 and RMS error of the height model are achieved by including additional spectral bands (Table 8.4). This is shown graphically in Figures 8.10 and 8.11, which compare height predictions and residuals for Landsat ETM+ band 2 and height models, 13, 23, 42, 59 and 63, based on multiple spectral bands.

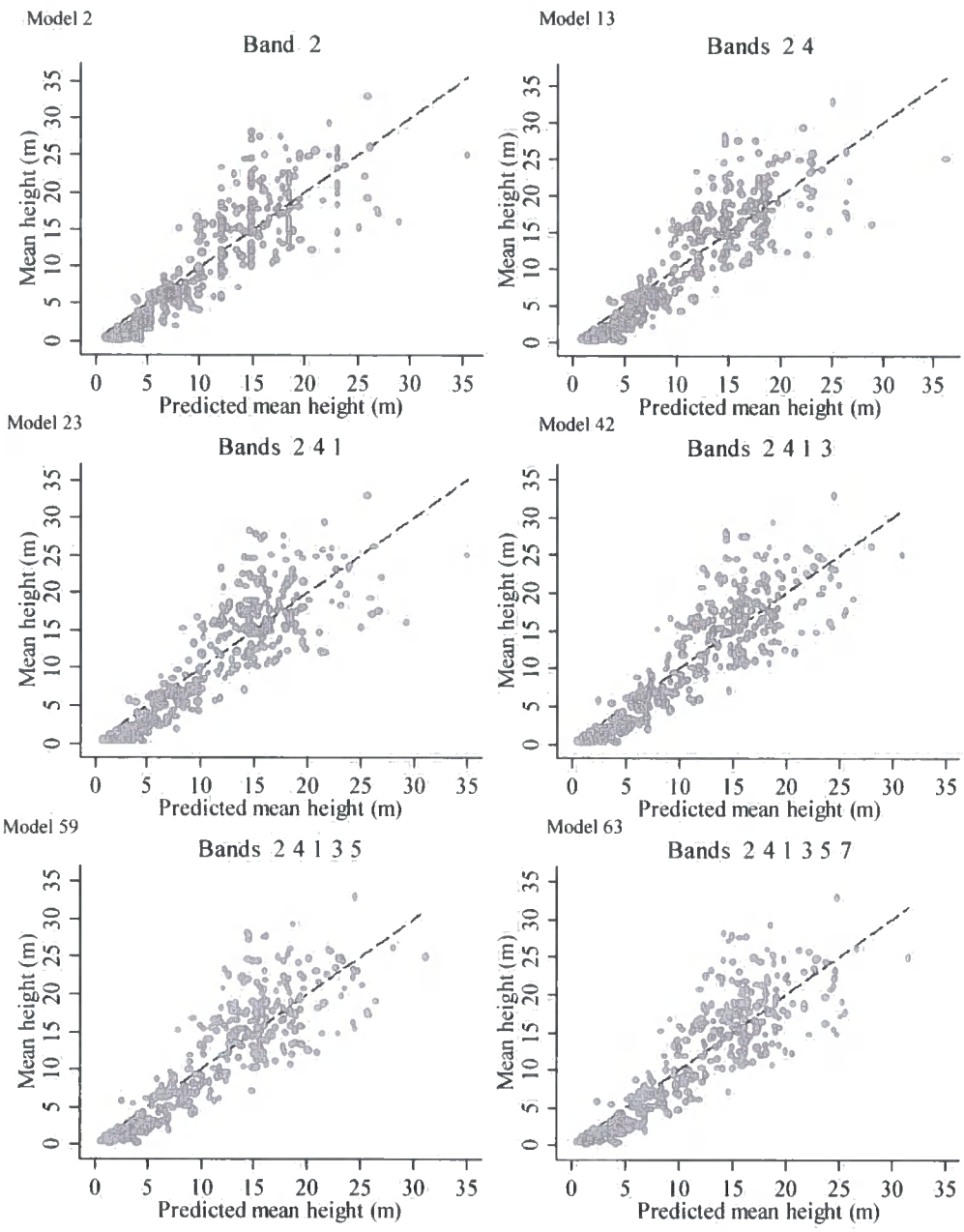

Figure 8.10 Height model B, used to predicted height from multiple Landsat ETM+ bands.

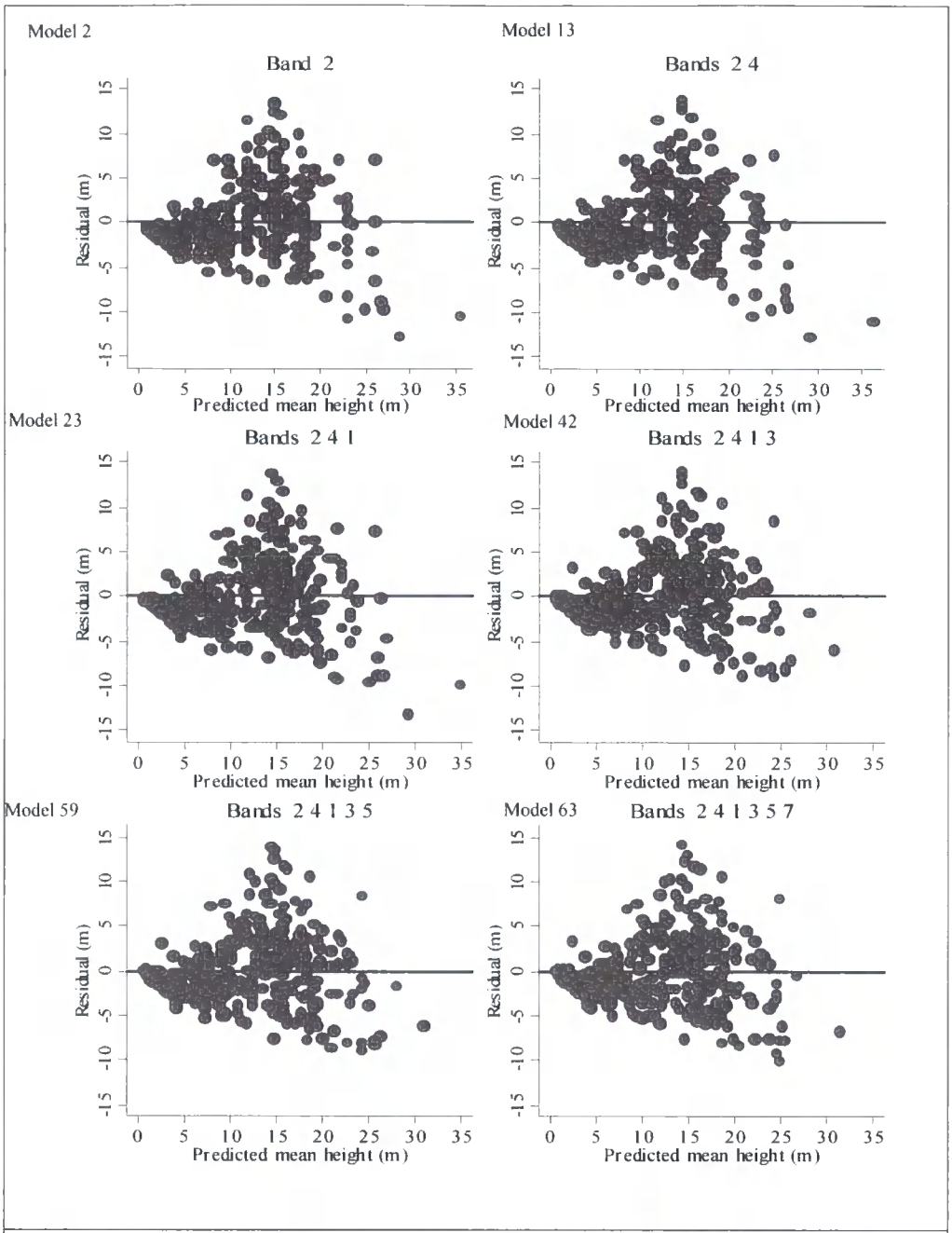

Figure 8.11 Residual plots for height Model B using multiple Landsat ETM+ bands.

The height prediction and residual plots show that, unlike IKONOS data, the relationship between height and Landsat ETM+ image bands does not improve with the addition of the near infrared band. Furthermore, increasing the number of spectral bands does not substantially improve the model. Figure 8.11 shows a similar pattern in the residual distribution to the IKONOS residual plot (Figure 8.8), with residual errors exceeding 5 m once tree height reaches 10 m. It is also worth noting the similarity in

the predictive ability of the same spectral bands between the two sensors, which suggests that the response is stable across a range of pixel resolutions. In this context any sensor with similar spectral band passes could potential be used to estimate height.

8.3 Validation of height estimates

Analysis of IKONOS and Landsat data shows that it is possible to use multiple spectral bands, or combinations of bands, as predictors. However, analysis of multiple band predictors shows that, at best, these provide only minor quantitative improvements in model fit. Furthermore, such benefits are outweighed by the risk of fitting a complex model that is not supported by a graphical analysis of the empirical data. Models based on single spectral bands are simple, but effective predictors. The inclusion of LiDAR height information is helpful because it is both time-consuming and difficult to measure height in the field. LiDAR-derived height data extend the range over which the statistical models are fitted because a greater number of both younger and older trees can be sampled than would be possible in the field. The additional number of samples provides more confidence that the empirical statistical models offer a sensible prediction of forest height (Wulder and Seemann 2003).

Figures 8.12 and 8.13 use the green spectral band of Landsat ETM+ and IKONOS to predict height, which is plotted against LiDAR-derived height. It is apparent from both scatter plots that beyond a height of approximately 10 m, the relationships deteriorate.

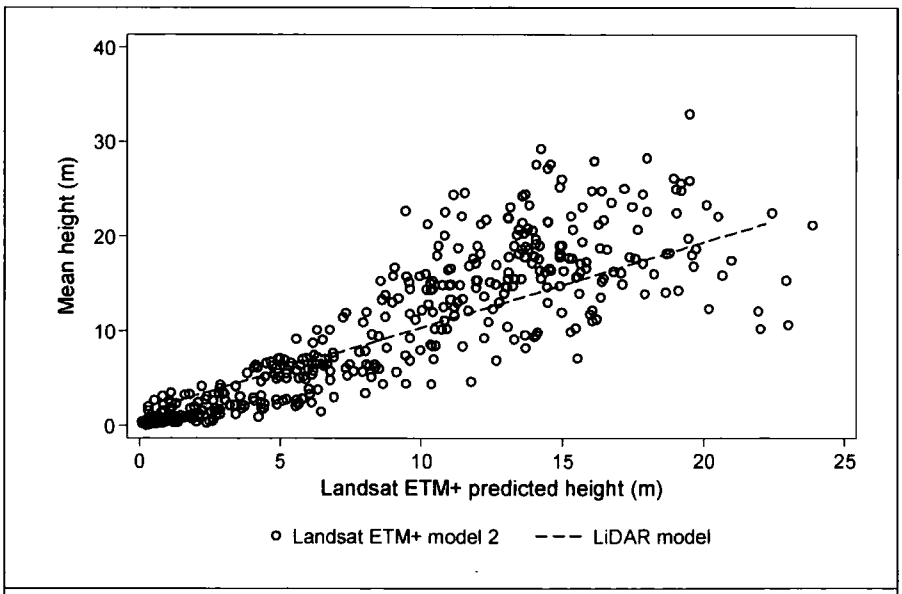

Figure 8.12 Comparison between Landsat ETM+ green band and LiDAR-derived and field-measured height (n=438).

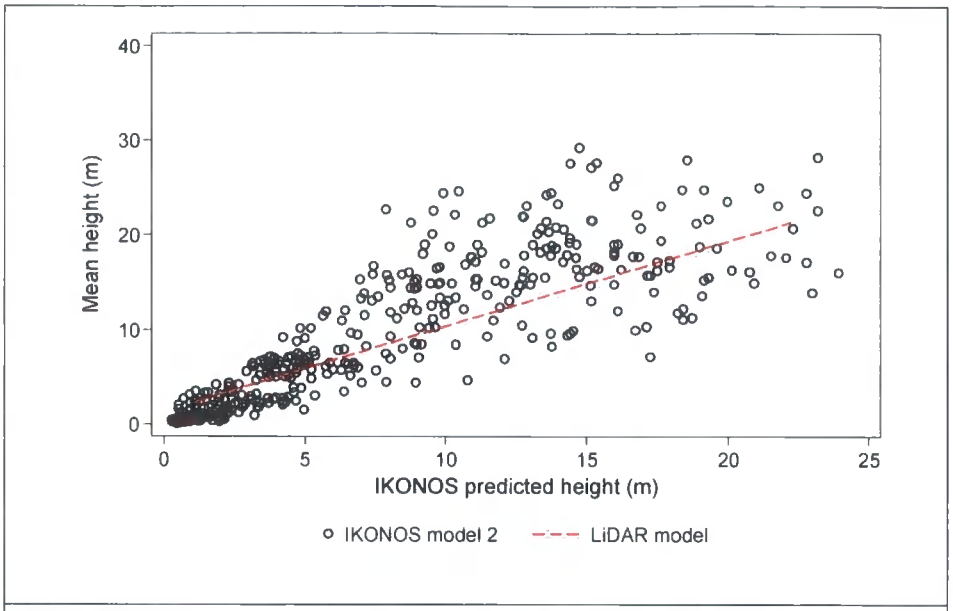

Figure 8.13 Comparison between IKONOS green band and LiDAR-derived, and field-measured, height (n=438).

8.3.1 Spatial comparison of height estimates

Since the estimates obtained from LiDAR and field-measured heights are comparable (R^2 = 0.99), the LiDAR height map is used as a benchmark against which to compare the IKONOS and Landsat height models. For comparative purposes, predictions of forest height were generated from the green wavelength band for both Landsat ETM+ and IKONOS data, using height Model B (based on the extra LiDAR samples). This was achieved by applying regression equations to each pixel of green band in the IKONOS and Landsat ETM+ data. Although the validation dataset is not independent as it is also used to construct the height model it does provide a useful method of identifying anomalous satellite-derived estimates. For each image pixel, Figures 8.14 and 8.15 show these predictions, classified into 2 m height increments.

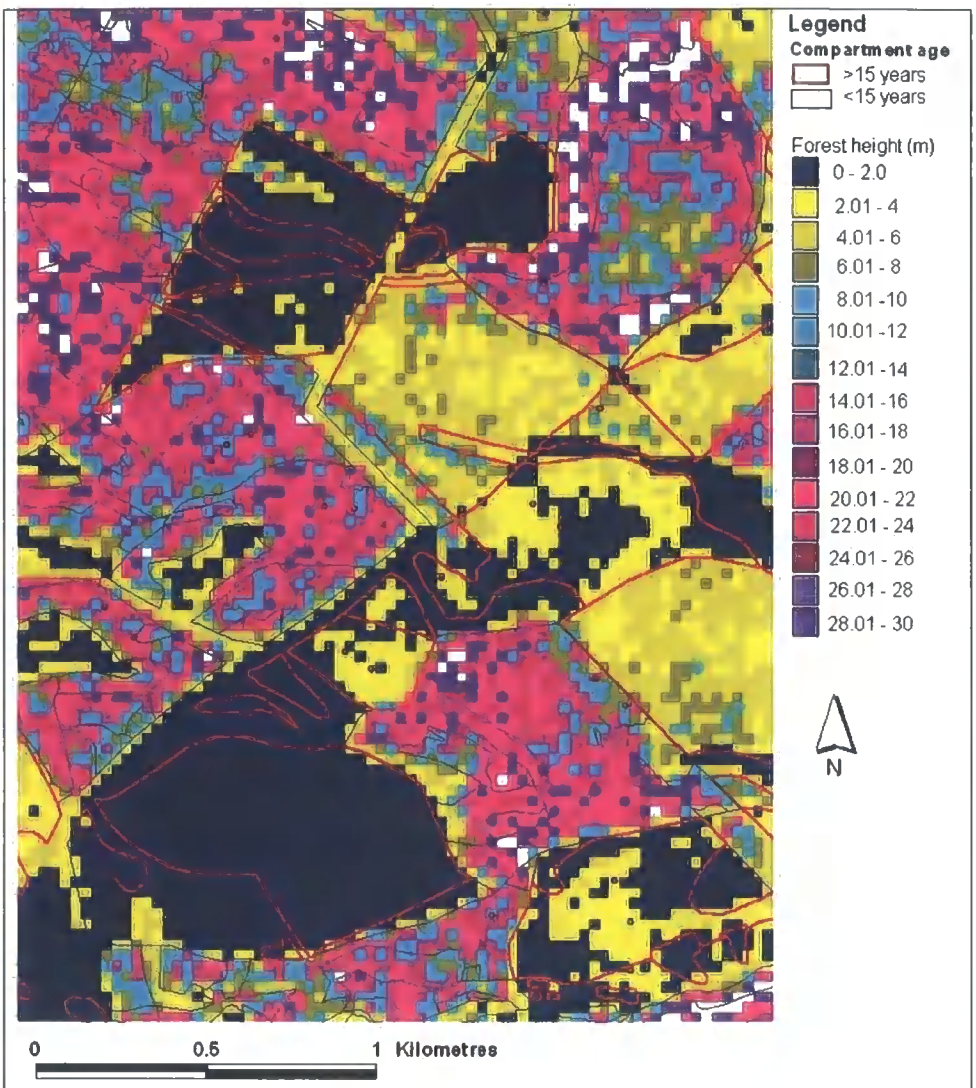

Figure 8.14 Height prediction image derived from Landsat ETM+ green band using height Model B.

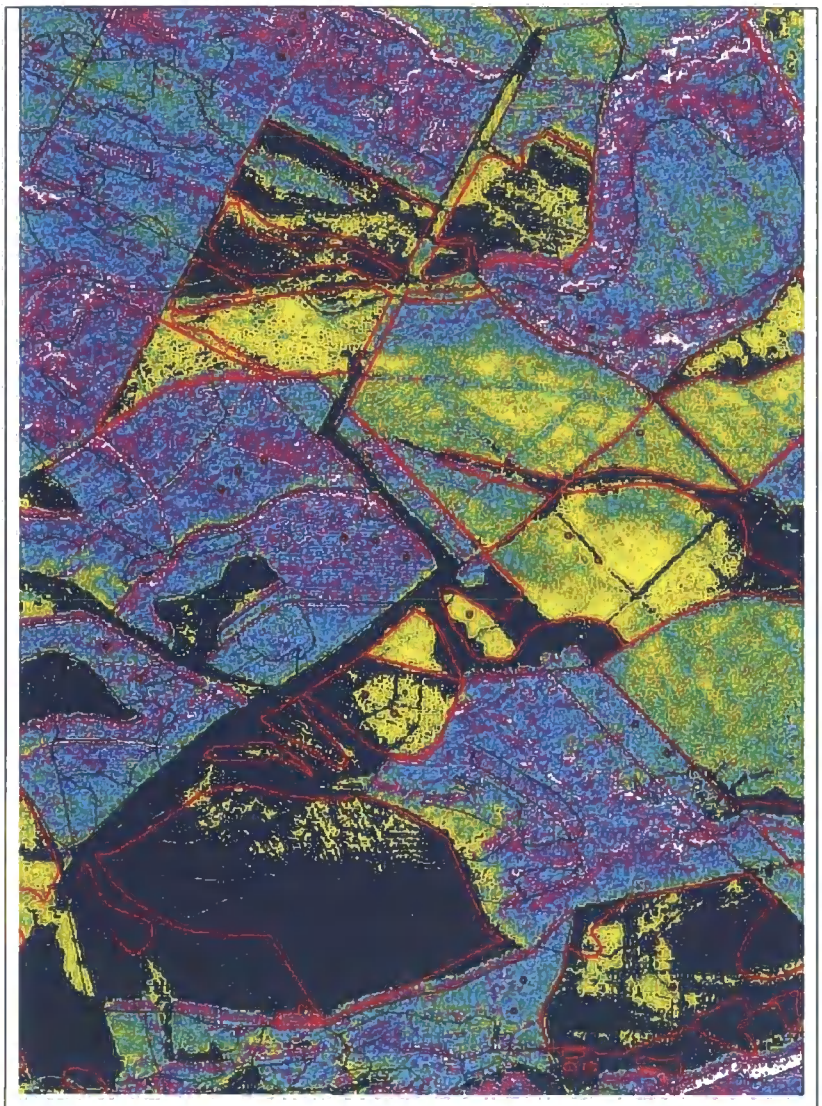

Figure 8.15 Height prediction image derived from IKONOS green band using height Model B.

The Landsat and IKONOS height models show good agreement for areas with trees less than 10 m in height. Although the coarser resolution of Landsat data produces a more generalised height map, a similar spatial pattern to the IKONOS model is observed.

To compare the differences between satellite estimates, two height residual maps were generated by subtracting LiDAR height estimates from IKONOS and Landsat models, using height Model B (see Figures 8.16 and 8.17). Data held in the FC's GIS were used to identify compartments where trees exceed 15 years in age, which corresponds to heights greater than 10 m. These areas are masked out and thereby excluded from the

analysis because the linear model shows limited ability to predict height beyond 10 m (refer to Figures 8.13 and 8.14).

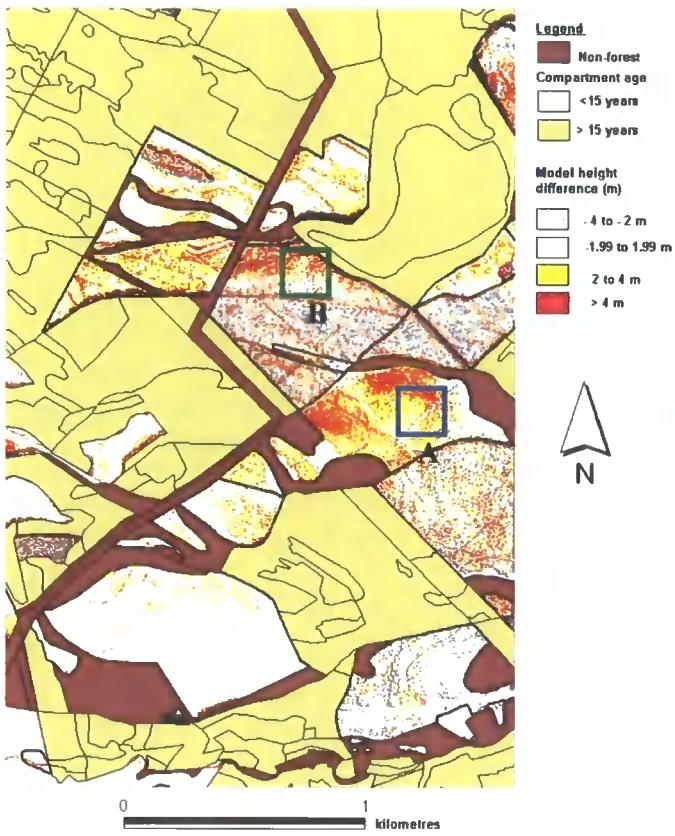

Figure 8.16 IKONOS height difference map: generated from band 2.

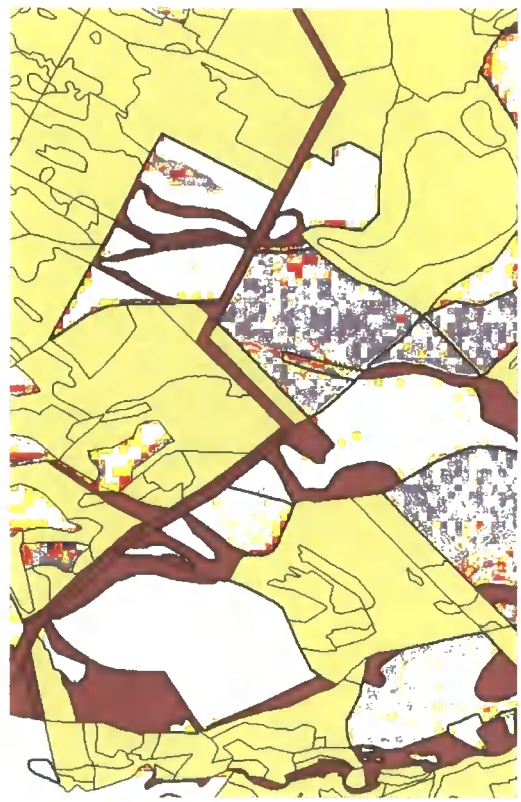

Figure 8.17 Landsat ETM+ height difference map: generated from band 2.

Inspection of residual height values reveals some interesting spatial patterns and highlights differences between predictions from the two sensors. Figure 8.16 shows residual height values for IKONOS categorised into four difference classes. In most parts of the study area the residuals are within the range ±2 m, which is acceptable for forest management purposes. However, a number of pixels show residual values greater than 4 m, which is unacceptable; these are coloured red on the residual height maps. In particular, there are two clusters of high residual values, where forest height is overestimated by the IKONOS model. Area A (identified by the blue box) contains high levels of natural regeneration causing tree density to exceed 12,000 trees/ha. Area

B (identified by the green box) is a north-facing valley side (10 to 15°) and the forest height over-estimate is most probably associated with interaction between the IKONOS sensor's off-nadir view angle of 30° and ground surface aspect and slope. This may have resulted in localised shadowing or depression of reflectance values compared with an equivalent stand of trees growing on flat ground. As a consequence, forest height values have been over-estimated. This effect is not observed in the Landsat model because ETM+ is a nadir-pointing sensor. Figure 8.17 shows residual height values for the Landsat ETM+ model. The area of high tree density, identified as area A on the IKONOS height difference map, is not detected by the Landsat model.

8.4 Discussion

When forest height predictions from the different image datasets are compared with ground-based observations, it is clear that LiDAR performs best, providing an accurate measurement over the full range of age classes studied (8-59 years). If the same IKONOS and Landsat 7 ETM+ band passes are compared then the green wavelength band, of IKONOS (4 m) multi-spectral and Landsat ETM+ (30 m) data, gave height predictions that are statistically very similar, despite the large difference in spatial resolution between the two sensors. Although regression models (Model B) using the green wavelength gave R^2 values of 0.74 and 0.79 for IKONOS and Landsat ETM+ respectively, these sensors do not make physical measurements of height; rather they display a strong negative correlation between forest height and reflectance. Similar patterns are also observed using Landsat 7 ETM+ SWIR spectral bands. The results achieved in this research are also observed other studies (Puhr and Donoghue 2000; Donoghue et al. 2004; Watt, 2002). In contrast to LiDAR, both satellite sensors can only predict height up to the point of canopy closure. This limitation of optical image data is well known and has been reported in several remote sensing studies of conifer forests (Danson and Curran 1993; Puhr and Donoghue 2000; Donoghue et al. 2004; Nilson and Peterson 1994).

The IKONOS green wavelength band is able to detect natural regeneration in young crops more readily than does Landsat. This is probably due to localised patterns of natural regeneration, which can be detected using a 4 m pixel size. These patterns are

not always detected by the Landsat 30 m pixels (as shown by the residual values in Figure 8.16) because areas without natural regeneration are incorporated in the reflectivity of the larger Landsat pixel. The 4 m pixel size of the IKONOS multi-spectral image therefore helps to pinpoint areas of anomalous growth that are not easily seen by either LiDAR height maps or the lower spatial resolution Landsat ETM+ sensor. Results from areas of steep terrain suggest, however, that off-nadir look angles can affect height predictions.

(i) Increasing ground samples using LiDAR

Interestingly, the results suggest that accuracy is not substantially improved by increasing the number of ground sample plots. This finding concurs with similar work conducted in upland Sitka spruce plantations in Galloway Forest District, Scotland (Donoghue et al. 2004; Puhr & Donoghue 2000; Watt 2002), which suggest that minimal field effort is required to parameterise such models. Alternatively, LiDAR data (if available) could be used in place of field sample plots as means of attaining height data to parameterise a reflectance-driven height model.

It is important to note that accuracy of LiDAR-derived height in closed canopy forests depends on obtaining a sufficient number of last pulse returns from the ground. If LiDAR poorly predicts ground elevation, then tree height measurements could be incorrect by ±1.5 m (section 5.1). Also, additional error, albeit more difficult to quantify, may occur if the percentile height used (i.e. the 60^{th} percentile) does not correspond to the mean canopy height in all areas. Holmgren (2003) noted that at larger scanning angles, and as tree density increases, the percentage of LiDAR canopy hits increases. This is because more canopy area is exposed to the laser at larger scanning angles, which reduces the penetration of the laser to the lower canopy.

(ii) Cost and Availability

The cost of Landsat data is very low (US$ 0.51/ km^2). The cost of IKONOS data is higher (US $20/$km^2$) but they are still very cost-effective compared with field sampling methods. Comparatively, LiDAR data are expensive[40] (US $100/$km^2$), but they offer a

[40] Figure based on the acquisition of data at the same specification used in this research. Cost of processing not included.

number of advantages over field inventory methods. First, LiDAR is able to provide spatially continuous estimates of height, over the entire forest height range, whereas field-sampling density is less intensive. Second, the quality of the survey data is enhanced because it is both continuous and accurate, which means it can identify areas of variability more easily than field-based methods.

Optical satellite data appear to provide an attractive alternative source of forest height information for forest stands less than 10 m in height, which could be used as a tool to monitor the success of forest establishment over extensive forested areas. Another important consideration is the availability of suitable image data. IKONOS data are difficult to obtain in the UK, even with pre-arranged tasking[41], due to cloud cover. For this reason, it is rare for these data to be acquired at nadir because this severely constrains the number of satellite overpasses that can be used to capture imagery. However, since prediction models are empirically based and use spectral data, other satellite data that have similar band-passes are also suitable for this application. This widens the choice to include other satellite sensors: Landsat 5 TM, Landsat ETM+, SPOT 4 HRV, SPOT 5 HRG, IRS LISS, Terra-ASTER, Quickbird.

In conclusion, LiDAR provides accurate forest height data at high spatial resolution, but it cannot detect areas of anomalous growth that are not related to height differences, such as natural regeneration. For this task it is important to have spectral information at green, red, near infrared or shortwave infrared wavelengths. Future LiDAR sensors will incorporate such image layers but for the moment it is clear that optical satellite data remain particularly suitable for monitoring the growth status of young crops in dense plantation forests.

8.5 Summary

The results from this chapter, and Chapters 5 and 6, show that in very densely stocked Sitka spruce crops (>2,000 trees/ha) LiDAR is able to provide an estimate of height over the entire range of age classes studied (8-59 years). Both IKONOS and Landsat ETM+ imagery can be used to generate accurate predictions of forest height in the range

[41] Since 2003 only two high-resolution images (IKONOS or Quickbird) have been acquired over the study area.

0-10 m, but above 10 m height predictions are very poor. The methodology developed in this research uses a combination of traditional criterion for evaluating different predictive models such as R^2 and RMS error, with the selection further refined by adding graphical interpretation of model predictions and residuals. This process assists in the selection of models that are both biologically and physically plausible. The results demonstrate the ability of optical satellite imagery to identify forest stands that display unexpected growth characteristics, such as areas of high natural regeneration and poor or incomplete stocking. The results also support the growing body of literature that highlights the potential of high-resolution airborne LiDAR imagery for accurate and detailed forest resource assessment. Unlike many other studies that have used satellite data to develop models for estimating forest parameters (i.e. Danson and Curran 1993; Puhr and Donoghue 2000; Nilson and Peterson 1994) this chapter shows the merits of spatially analysing the predictions to identify areas where the predictions appear spurious. Also, by integrating LiDAR data a much larger ground truth dataset can be attained to more rigorously evaluate the satellite-derived predictions. Furthermore, it also appears that LiDAR data can be used in place of, or to supplement, field-based height measurements.

Chapter 9: Discussion

9.1 Introduction

Very little research had been undertaken, until recently, into the application of remote sensing to forest management in the UK. Apart from conventional aerial photography, there are no examples nationally in the UK of remote sensing technology being applied to assist forest managers in decision-making. This is in stark contrast to countries such as Sweden, Finland, Norway and the U.S.A, where medium-resolution optical satellite data such as Landsat TM and/or SPOT images are routinely used to map forest areas and to provide forest stock estimates. Moreover, in Norway, with the assistance of government subsidies, LiDAR data are beginning to be used extensively to provide detailed forest estimates at stand level (Naesset et al. 2005).

This thesis has sought to evaluate the potential in UK upland conifer plantations of utilising some of the most promising commercially available, remotely-sensed data to provide estimates of forest variables at a range of scales. Results in preceding chapters have shown that LiDAR data can be used effectively in dense upland conifer plantations both to provide estimates of height and volume and to identify plantation species and species dominance in plantation mixtures. Additionally, these estimates have proved to be at least as accurate as conventional field measurement techniques. Canopy structure and tree species can also be mapped at compartment level, by using laser height distribution measures and/or spectral information recorded in the near infrared. Optical satellite data, which provide a cheaper alternative to LiDAR data, are able to provide estimates of forest height up to the point of canopy closure (10 m), which can be used to monitor the success of plantation establishment.

The discussion which follows is divided into two sections: firstly, the results of this thesis are compared with other research and secondly, these results are discussed to assess practical applications that would provide forest managers with up-to-date information on forest resources. Three potential applications are introduced that use data and/or techniques developed in this research. The first uses LiDAR-derived height and crown measures to improve forest compartment maps.

In the second LiDAR-derived top height is used to make yield class estimates from the revised forest compartment maps, which are compared with existing FC yield class predictions. The third uses the Landsat ETM+ height model and applies this to a time-series of Landsat TM and ETM+ scenes, to monitor forest growth and establishment. The chapter concludes by discussing potential future advances for remote sensing systems and how they could assist to meet information requirements for forest management.

9.2 Comparisons with related research

9.2.1 Accuracy of LiDAR measurements under the forest canopy

If laser canopy heights are to provide accurate measurements of canopy height and, through its allometric relationship with height to forest volume, a key requirement is adequate characterisation of the ground surface. Since tree densities in upland conifer plantations commonly exceed 2,500 trees/ha, a major concern was that the density of the forest canopy would restrict the distance the laser pulse penetrated into the lower canopy, thereby leading to height being underestimated. While results show that the percentage of returns reaching the ground surface decreases to about 5% after canopy closure (a canopy height of 10 to 15 m), the calculated ground height is still very accurate (± 0.46 m). This level of accuracy compares favourably with two studies that have been conducted in more open conifer-dominated or semi-natural forests. In the first, Kraus and Pfeifer (1998), using an Optech ALTM 1020 laser scanner at 3 pulses/m^2, reported an RMS error in a laser-derived Digital Terrain Model (DTM) of 0.57 m in a sloping forested area ranging from 3° to 34°. Similar levels of error were also noted in the second study by Reutebuch et al. (2003) in which the data were acquired by helicopter, at a density of 4 pulses/m^2. Over the range of forest conditions investigated, vertical error (z) was highest for uncut forest stands at 0.31 m, decreasing to 0.16 m for clearcut sites. Error margins for the clearcut site are comparable to those reported for flat hard surfaces by Baltsavias (1999a), Pereira and Janssen (1999) and Huising and Pereira (1998). In this research results suggest that even though the tree density restricts the penetration of the laser, there are still an adequate number of returns at 2 returns/m^2 to generate the DTM. Furthermore, once the laser penetrates the canopy it is more likely to reach the ground surface, because of the lack of understorey

vegetation. Errors in the DTM are expected to be higher in species mixtures dominated by Sitka spruce (illustrated in Figures 9.1 and 9.2: note figures taken from Chapter 5). In these areas the laser points that reach the ground are clustered rather than irregularly distributed, due to the spatial arrangement of the forest canopy, which may well decrease the accuracy of the interpolated ground surface.

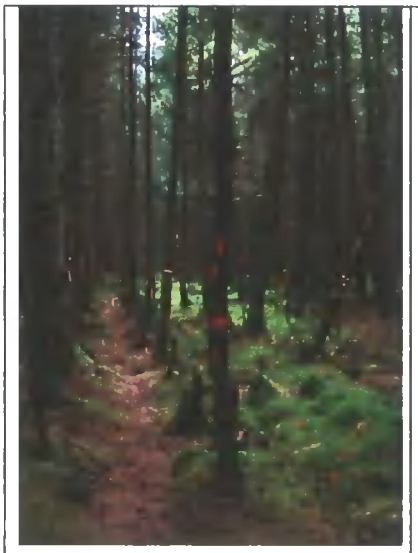

Figure 9.1a Photograph of a structured Sitka spruce/lodgepole pine mixture.

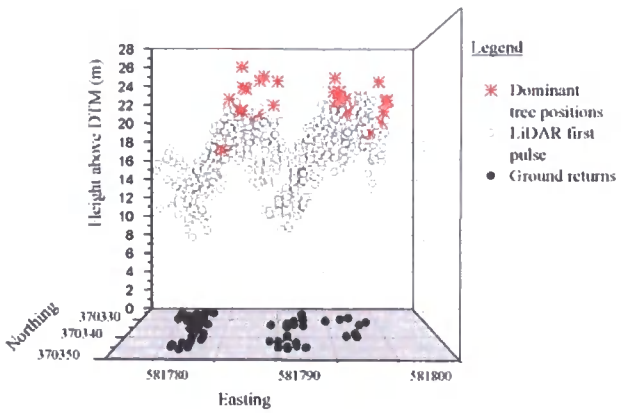

Figure 9.1b 3D plot showing tree locations, LiDAR first return and classified ground returns for an 20 x 20 m square sample plot located in a structured Sitka spruce/lodgepole pine mixture.

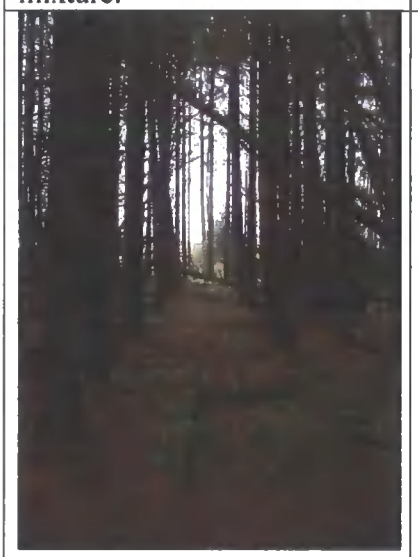

Figure 9.2a Photograph of a pure Sitka spruce crop.

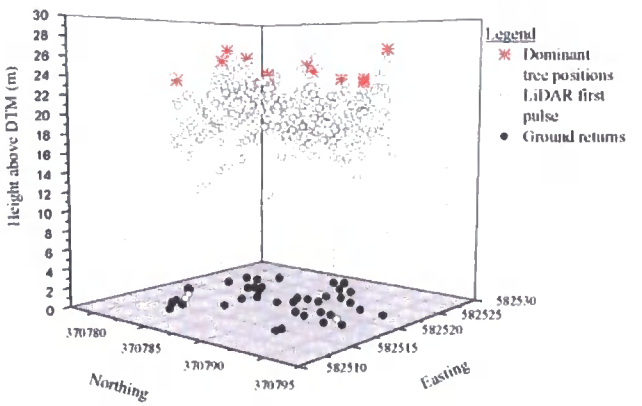

Figure 9.2b 3D plot showing tree locations, LiDAR first return and classified ground returns for an 8 m circular sample plot located in a pure Sitka spruce crop.

Results show that increasing the number of returns from 1 to 8 returns/m^2 did not lead to a reduction in overall canopy height error (i.e. combined DTM and DCHM errors). Therefore, in order to improve DTMs in species mixtures, it may be necessary to further reduce the laser scan angle, so that the sensor's view of ground is much narrower. This would increase the probability that a laser pulse penetrates to the ground surface. Additionally canopy penetration may be improved by lowering the flying height, thus reducing the laser's footprint size (i.e. a reduction in laser beam divergence). There is, however, a cost implication associated with this strategy, as more flight lines would be needed to provide the same area of coverage.

Most LiDAR research reports a combined measurement error that includes height errors, in both the DTM and DCHM (e.g. Naesset 1997b and Means et al. 1999). A key finding of this research is that separating the two surfaces is beneficial, as this provides an understanding of how forest canopy development affects the way in which the laser interacts with the ground and canopy surfaces. As forest canopy height increases and closes, laser height distribution changes, so that proportionally more returns are reflected from the upper canopy than from the lower canopy. Results in Chapter 5 show that under-estimates in laser canopy height for young open canopied crops (i.e <10 m in height) are similar to those for closed canopies (± 1.4 m). At this stage, in young crops, the maximum laser height is less accurate than can be achieved using field-based height measurement methods (expected to be about ± 0.5 m). However, since the underestimation in young crops is systematic, it is possible that, by applying a regression equation derived from field height measurements, this error is reduced to below 0.5 m. Other researchers approach this issue by stratifying the forest by growth quality, with each stratum taken to represent a different laser point distribution. For example, Naesset (2002) and Naesset and Økland (2002), in semi-natural mixed species plantations, divided forest areas into three growth stages, young forest, mature forest, mature forest with good growth, developing separate predictive models for each. However, the U.K simple management regime means that the majority of plantations are even-aged, planted at a high tree density and comprise single species or combinations of different conifer species. This leads to less variation in laser point distributions and penetration rate, as the forest canopy is relatively homogeneous in

terms of shape, density and coverage. This homogeneity means that, provided system parameters (i.e. LiDAR system, laser point density, scan angle and sensor altitude) are constant between surveys, then the LiDAR response and therefore accuracy should be consistent within similarly managed conifer forests.

9.2.2 Forest estimates from LiDAR data

This research concurs with the results of other studies, which have shown that the accuracy of LiDAR-derived height, after calibration to field height measurements, is comparable to that of manual field survey methods (Holmgren 2003; Hyyppä et al. 2000; Naesset 1997b; Persson et al. 2002). It showed a strong relationship between mean top height and laser heights above the 80th percentile; within this range little difference was observed between the percentiles, with R^2 of ≤ 0.99 and RMS error $\leq$ 0.79 m. This indicates that between the percentiles there are only minor differences in the distance the laser penetrates the canopy, which reflects the density and homogeneity of the forest canopy. Similar relationships have also been recorded in Naesset (1997b) and Naesset and Økland (2002). Figures 9.3 and 9.4 show a comparison of top height predictions from this research against the model predictions obtained by Naesset (2002).

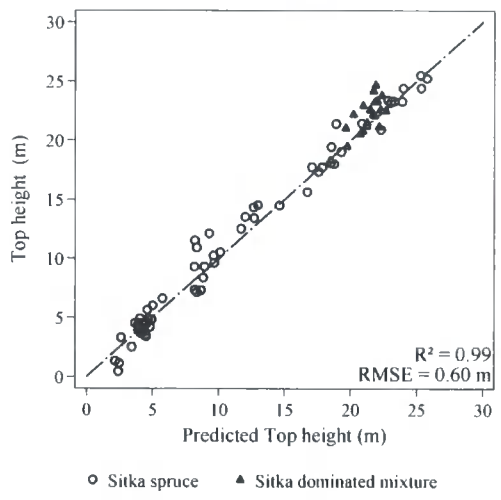

Figure 9.3 Top height against laser-derived top height (n = 90 sample plots). This study.

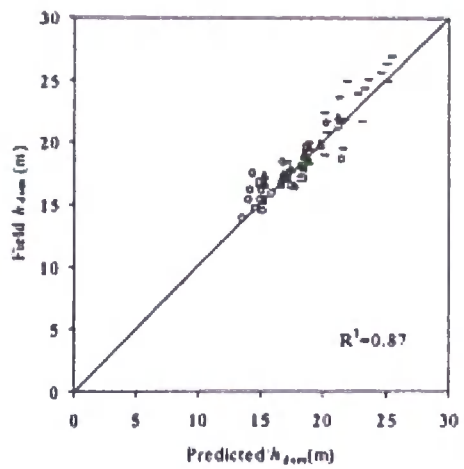

Figure 9.4 Top height against laser-derived top (n = 61 forest stands). Source: Naesset (2002).

Although the relationships are similar to Naesset's (2002) study, there are key differences in the way predictions are made; these differences can be linked to differences in forest structure. For example, Naesset (2002) generated separate regression equations for each stratum, used more than one predictor to estimate top height (i.e. coefficient of variation, last pulse percentiles and multiple first pulse percentiles) and summarised estimates at stand level, rather than plot level. Other laser-derived variables, apart from percentile heights, are also widely used in the prediction of volume or tree density (Holmgren 2003; Means et al. 1999; Popescu et al. 2002). In UK upland conifer plantations it appears that models based on a single predictor (e.g. the 99^{th} laser height percentile) can be used to predict top height, which in turn, by using it as an input into the FC's yield model, can be used to provide volume estimates. The use of an established model, which has been developed specifically for different UK conifer species, means there is less reliance on LiDAR data to provide the volume estimate. However, the validation data highlight the fact that the usefulness of current yield class models is limited when crops do not develop in a uniform way (e.g. have higher than average levels of mortality or contain a mixture of tree species). In these areas it is difficult to make accurate volume predictions based on top height information alone. Tree density is one variable that is difficult to estimate using LiDAR; even though the R^2 of 0.72 suggests that the model is able to predict tree density reasonably accurately, the RMS error is too high (434 trees/ha) to be useful for management purposes. The root cause is that, once the canopy has established and closed, the tree density still remains high through to the end of the forest rotation. Furthermore, trees tend to die standing and the crowns of surrounding trees fill any gaps created.

However, LiDAR-derived crown density measures (coefficient of variation and skewness) and percentage of ground returns are sensitive to changes in canopy structure. So, if relationships developed at the plot level scale (i.e. 0.02 ha) were converted to a raster layer, with a cell resolution equivalent to the plot level field samples, these areas could be identified and mapped. This information could be summarised to provide up-dated estimates at stand level, used to redefine new stand boundaries or further stratify stands into more homogeneous units (demonstrated in section 9.2). This approach has also been advocated by Naesset (2002), Holmgren (2003) and Holmgren and Jonsson (2004) for providing estimates of tree height, basal

area and volume at stand level. Naesset (2005) makes the point that, to extrapolate the estimations to cover a wider area, it is important that training datasets are used to provide a representative sample of the range of forest types likely to be encountered.

Additionally, other studies have noted that it is important to consider the possible effects on accuracy of forest height estimations caused by variations in (i) the laser sampling density (Naesset 2002) (ii) laser scan angle, which affects the height of different laser height percentiles (Holmgren 2003), and (iii) laser footprint size, which varies according to range from the sensor (Naesset 2004; Nilsson 1996). Consequently, these factors are important if LiDAR-derived estimates were to be expanded from a local scale to a larger regional scale.

(i) Laser sampling density

Indications from this research (Figure 5.13) show that, for young open canopied forest, the accuracy of raw LiDAR height estimates increases (to within 1 m of field measurements) as the laser sampling density increases from 2 to 8 returns/m^2. However, this pattern is not as obvious in closed canopy conifer plantations. Overall, increasing the number of returns from 2 to 8/m^2 does not result in a substantial increase in accuracy

(ii) Laser scan angle

In this study the effect of different laser scan angles on laser percentile height is expected to be minimal, due to the low scan angles used $\leq 10^{o}$ in both LiDAR surveys and the high tree density (> 2,500 trees/ha). The small differences in RMS errors above the 80^{th} laser percentile also appear to confirm this is the case.

(iii) Footprint size

Any changes in footprint size will affect penetration of the laser through the forest canopy. In both surveys divergence of the laser was set at 0.2 mrad, which was equivalent to a 0.20 m laser footprint diameter on the ground for the Kielder study area and a 0.25 m footprint diameter in the Galloway study area. Since the topographic range over both areas is less than 110 m, the change in laser range on footprint diameter is negligible (approximately 0.01 m).

Overall, the results from this research show that LiDAR is able to provide a robust estimate of top height. Furthermore, because the canopy structure in Sitka spruce is similar between different forest sites (Figure 9.5), the same methodology adopted for the Kielder study area will also be applicable in the Galloway test area. It also appears that the relationship between field-measured top height and laser-derived top height is stable across different conifer species, if plot data recorded in pure crops and species mixtures are pooled.

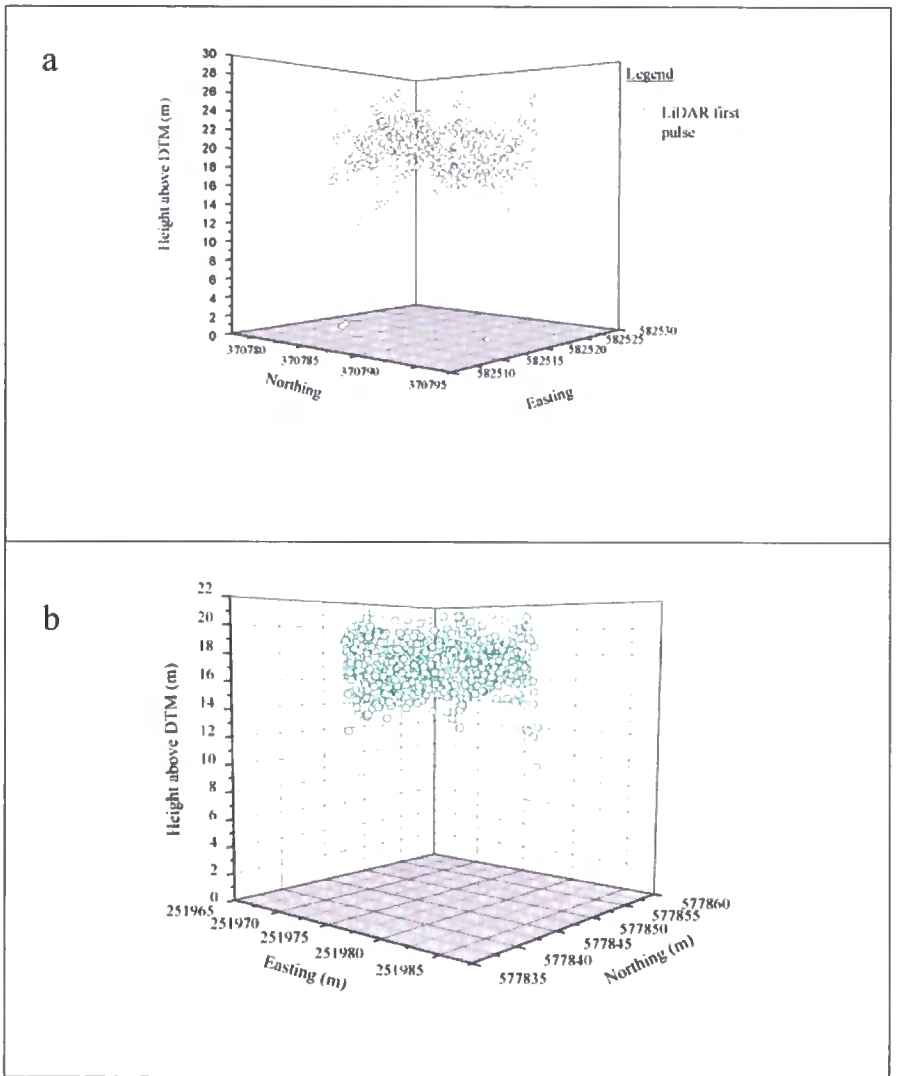

Figure 9.5 First pulse distribution for a.) Pure Sitka spruce Kielder study area, N.E England b.) Pure Sitka spruce Galloway, S.W. Scotland.

This is clear from Figure 9.6, which shows predicted top height for the Kielder and Galloway study areas. Here, the top height prediction for the Galloway dataset was generated using additional LiDAR areas and a further 112 field plots. These plots also cover a range of species, including pure Sitka spruce and mixtures of Sitka spruce and lodgepole pine.

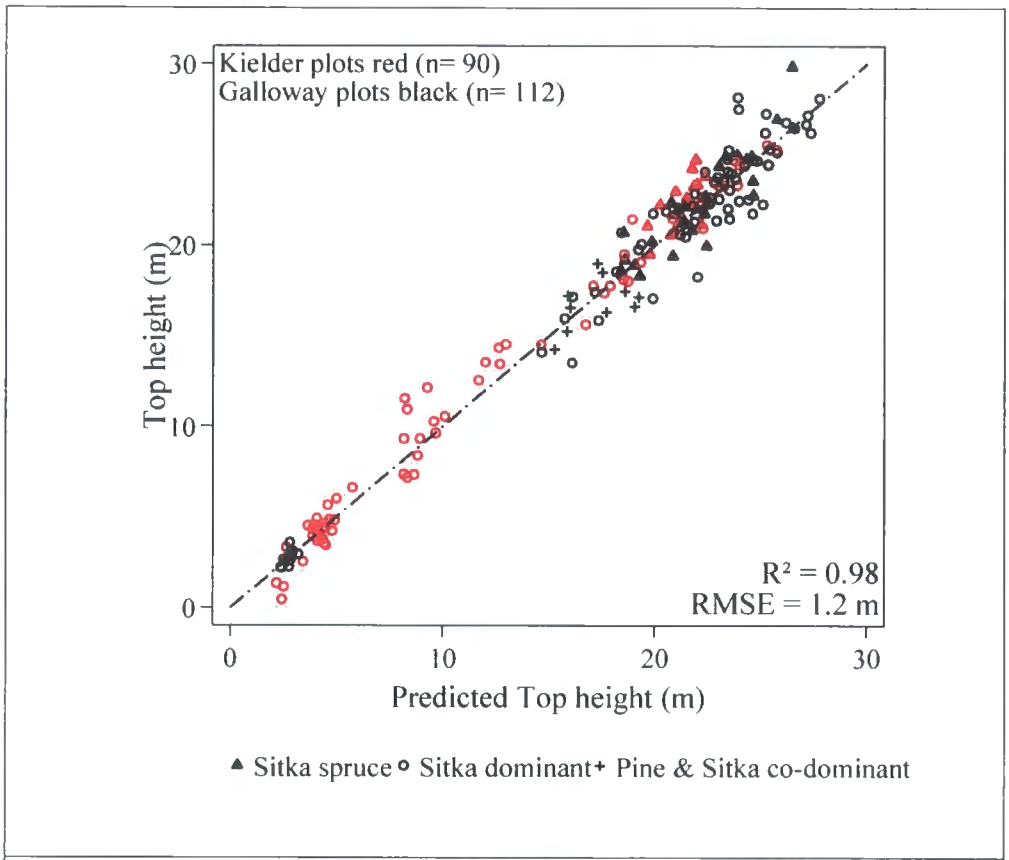

Figure 9.6 Top height against laser-derived top height for Kielder and Galloway study areas (n = 202 sample plots).

The line of best fit used to predict dominant height from the 99th percentile height, derived using least-squares, has an intercept of .089 m, with an RMS error of 1.2 m and R^2 = 0.98. These results open up the potential to develop a standard top height equation for both pure crops and plantation mixtures, which could be applied to any new LiDAR acquisition. If volume is estimated using the FC's yield model, with LiDAR-derived top height, it is then important to match the appropriate yield model with the correct conifer species. This is not an issue for single species stands because stand boundary and species information held in the GIS identify these areas. However, the situation

becomes more complex when stands contain a combination of species. In these areas the methods developed in Chapter 7 for identifying species' dominance assist in mapping the different components.

9.2.3 Mapping plantation species using LiDAR

Results presented in Chapter 7 show that it is possible to identify different conifer species and areas of anomalous growth at stand level. Although the method was only applied over a small area, in this research, results strongly suggest that crown density measures could be transferred successfully to other UK conifer plantations. In relative terms, there are differences in spectral response in the near infrared between closed canopy Sitka spruce and lodgepole pine; but a classification based on intensity is still potentially problematic. A number of factors may affect the strength of the near infrared response, leading to uncertainty that response will be consistent between LiDAR surveys, systems or forest sites. Each area may therefore need to be calibrated separately for intensity information to be used.

It is encouraging to note that Holmgren and Persson (2003) located and identified individual conifer species (Scots pine (*Pinus sylvestris*) and Norway spruce (*Picea abies*)) in a mixed species forest with low tree densities (280 to 1,430 trees/ha: calculated from Persson et al. 2002), using LiDAR intensity data without applying any form of calibration. The narrow laser scan angle used (10°), low flying height of the sensor (130 m) and small range in topography of the site (20 m) probably contributed to the result, therefore any variation in intensity values, introduced by changes in laser path length, would have been minimal.

In upland areas, a greater range of topography is expected, but in these areas it is useful to compare LiDAR near infrared response with a radiometrically-calibrated source. In this context, satellite data that have spectral bands in the near infrared (SPOT, Landsat TM, IKONOS and Quickbird) offer a way of checking the radiometric consistency of LiDAR response. Additionally, any spectral data with a spatial resolution of approximately 10 m could also be integrated into the classification by re-processing LiDAR variables to the same spatial dimension. This additional spectral information may well improve the accuracy of the identification process. However, even without

spectral data, the other LiDAR measures, derived from laser height distributions, can be used as a means of identifying and mapping species dominance. These measures are particularly well suited to identifying areas of wind damage, anomalous growth and forest gaps. When all this information is combined, the three components necessary to make a volume production forecast are assembled, namely (i) the area and proportion of each conifer species, (ii) volume for the different species, derived using the top height information and applying the appropriate FC yield model (iii) the stocked area, through eliminating areas such as wind damage and gaps. This process is demonstrated, using a sample dataset, in section 9.3.

9.2.4 Forest height estimates from satellite data

In managed forest plantations the biophysical and structural variables change in a predictable way over the forest growth cycle, so that reflectance is indirectly a function of these forest variables. The main mechanism controlling reflectance in all Landsat ETM+ and IKONOS bands appears to be the amount of understorey vegetation visible to the sensor and shadow, as the forest canopy closes (Danson and Curran 1993; Franklin 1986; Nilson and Peterson 1994; Donoghue et al. 2004; Donoghue & Watt 2005; Puhr & Donoghue 2000). During this early growth phase satellite data can be used to estimate forest variables. It should be noted that past research has identified a number of factors that can affect radiance values recorded by the sensor, such as localised atmospheric haze (Spanner et al. 1990), topographic shadowing (observed in this study) and silvicultural operations such as thinning (Nilson et al. 2001). All of these factors can be accounted for, if needed. For example, atmospheric effects are minimised if cloud-free imagery and bands with longer wavelengths are used; topographic corrections can be applied to off-nadir data if a DTM is available; and, using the FC's GIS, any areas that have been thinned could be identified and masked out.

Results from this research show that forest height estimates can be derived over large areas from a range of satellite data, i.e. Landsat ETM+ or IKONOS, using a range of optical wavelengths. Additionally, results suggest that to parameterise reflectance-driven models only a small number of field samples are required. These findings also concur with other research that has used SPOT and Landsat data to estimate height,

volume and basal area in other upland conifer plantations in the UK (Donoghue et al. 2004; Donoghue & Watt, 2005; Puhr & Donoghue 2000; Watt 2002). A common theme found in all these studies is that the relationship between image data and a particular forest variable is consistent between forest areas and sensors (see Figures 9.7a to d). For height, the strongest relationships are consistently observed in spectral bands located in the green, red ($R^2 \geq 0.70$) and shortwave infrared ($R^2 \geq 0.80$) wavelengths. Figure 9.7 a to d shows the relationship between mean height and green spectral wavelength for IKONOS, SPOT 4 HRVIR and Landsat ETM+ between two forest areas, one located in Kielder Forest District, England and the other in Galloway Forest District, Scotland.

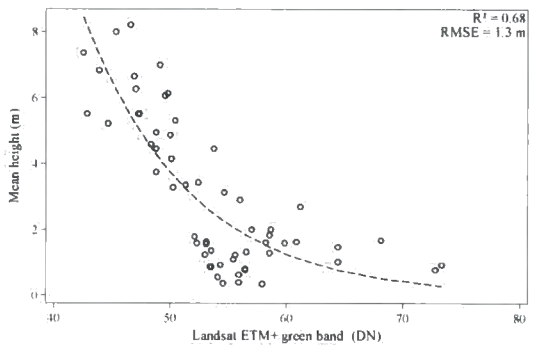

Figure 9.7a Mean height predicted from SPOT 4 HRVIR green band DN values using field plot data: Galloway dataset 2002: Source: Donoghue et al. (2004).

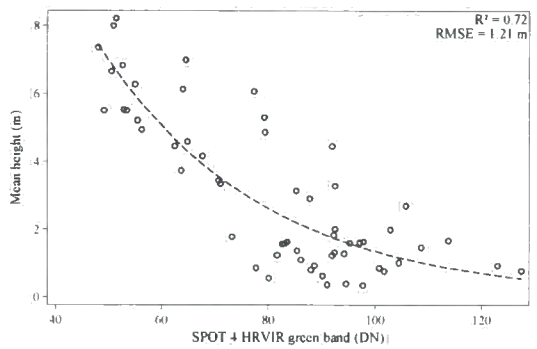

Figure 9.7b Mean height predicted from Landsat ETM+ green band DN values using field plot data: Galloway dataset 2002. Source: Donoghue et al. (2004).

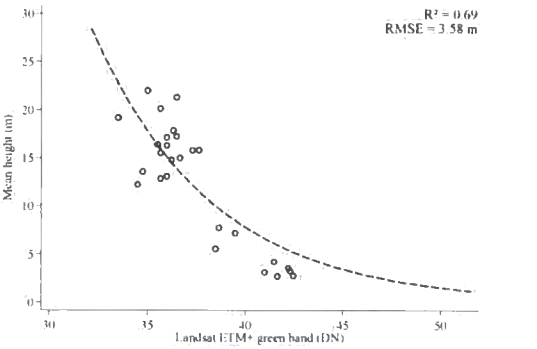

Figure 9.7c Mean height predicted from Landsat ETM+ green band DN values using field plot data: Kielder dataset 2003. This study.

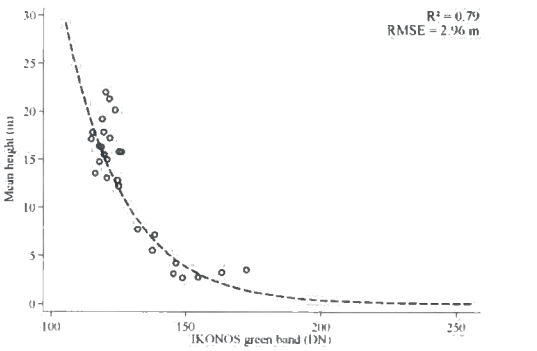

Figure 9.7d Mean height predicted from IKONOS green band DN values using field plot data: Kielder dataset 2003. This study.

Although the satellite data used in this example have not been radiometrically normalised to top of atmosphere reflectance, the different sensors all show a negative curvilinear relationship with mean height in the green spectral band. This suggests that the relationship in pure Sitka spruce stands is similar at a range of sensor resolutions and is also temporally and spatially stable. The RMS error of these models ranges from 1.3 m to 3.6 m, but perhaps a more robust assessment is provided when the prediction is mapped spatially and compared with height measurements made using the LiDAR. In this study, the IKONOS and Landsat pixel-level estimates were within the range of (±2 m), which is lower than can be achieved using field-based methods in forests of this height (±0.5 m). Nevertheless, the pixel-wise estimates from this research are better than reported in general literature made at stand level, which can be as high as ± 6 m (Hyyppä et al 2000). Accuracy could well be improved if pixel values were aggregated to stand level, using stand boundary information held in a GIS, assuming that the forest boundary is correctly mapped and does not contain substantial areas of non-forest. Further, if the image normalisation methods described in Hall et al. (1991) are applied to a time-series of images acquired over the same area, then the reflectance-driven height model can be applied either retrospectively or to future image acquisitions, thereby monitoring temporal changes in forest height in crops that are managed under similar silvicultural regimes (Donoghue et al. 2005). This is demonstrated in section 9.3. By combining LiDAR survey with satellite observation it is clear that the need for accurate ground measurements, which are expensive to obtain, could be substantially reduced and so it would be possible to generate an empirical prediction of height, based largely on carefully targeted LiDAR survey.

9.3 Application of remote sensing for forest management

Remote sensing has not been widely applied in the UK to assist with forest management. Malthus et al. (2002) and Suárez et al. (2005) list a range of factors that have contributed to the slow uptake of remote sensing approaches. These include the cost and spatial resolution of satellite data, lack of expertise in remote sensing and, interestingly, lack of direct relationships between optical satellite data and forest parameters. Additionally, the expansion of the state-owned resource has been planned and controlled for the past 80 years. This has led to investment in mapping the forest resource, using aerial photography and GIS. If compared with current methods, remote sensing is able to provide valuable information, at a range of scales, to assist managers

to make more informed resource management decisions.

Three applications that illustrate this are presented in the next section. These are based on data and methods used in this thesis or as part of the ForestSAFE project. In the first example, using data over Kielder Forest, the LiDAR-derived measures of forest structure are used to identify areas of wind damage and variations in crop growth. In the second, LiDAR-derived top height is used to calculate an estimate of yield class, which in turn is compared with the FC's yield class estimates held in the GIS. The third example looks at the larger scale application of monitoring plantation establishment in Galloway forest district. The first two examples use an image segmentation routine to further stratify forest compartments; this is used operationally in Sweden for mapping forest boundaries. The third example uses the method developed to create the reflectance-based height model for Kielder forest; this is applied to Landsat TM and ETM+ data acquired over Galloway Forest District.

9.3.1 Using LiDAR-derived height and crown density measures to improve forest compartment maps

Figure 9.8 shows a 1: 10 000 aerial photograph of a forest area, approximately 100 hectares in size, located in Kielder Forest District, with the FC's forest compartment boundaries overlaid. For each area the GIS also holds information on tree species, tree density and yield class. In this example, the areas of Norway and Sitka spruce are mapped, but areas of internal and external wind damage are not mapped. Figure 9.9 shows a composite image generated using the three laser distribution measures derived from the LiDAR point cloud and gridded to a 4 m resolution. Each display band represents a different measure, with the percentage of ground returns projected in blue, mean top height in green and the coefficient of variation in red. The associated legend roughly divides the area into a series of classes. Without additional information it is probable that some of the classes would not be properly differentiated (for example, wind-damaged areas and areas of closing canopy). However, the irregular shape and spatial distribution of wind-damaged areas suggests this would be unlikely. As a check, spectral data from aerial photography[42], IKONOS or Quickbird could be substituted for one of the LiDAR measures to assist in the classification.

[42] The aerial photography would need to be re-sampled to match the spatial resolution of the LiDAR-derived measures.

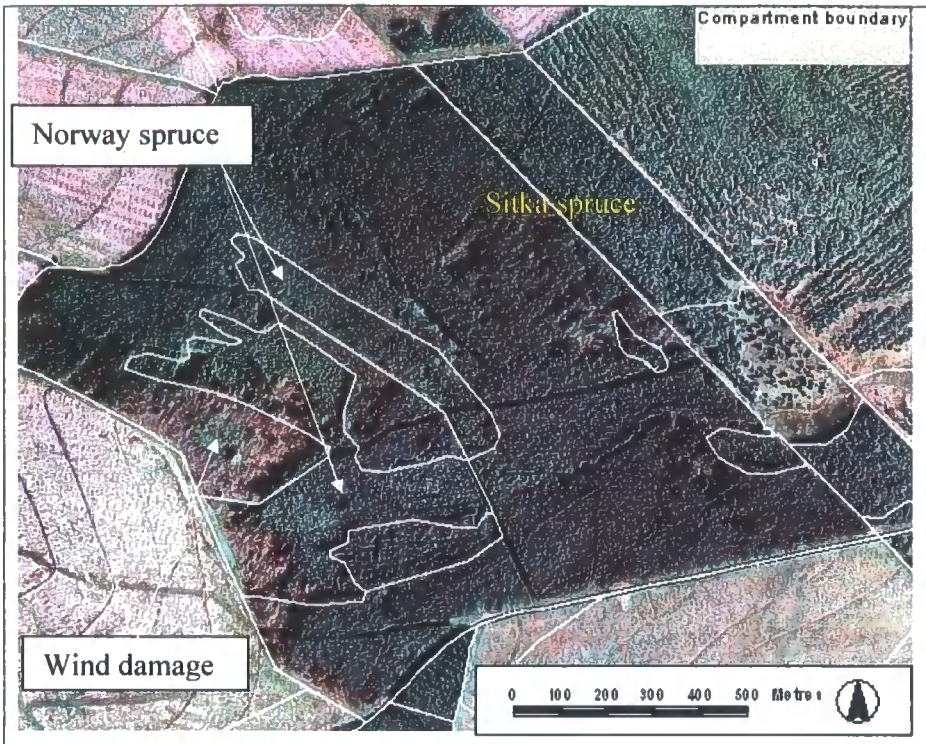

Figure 9.8 1:10 000 aerial photograph with existing forest compartment boundaries overlaid.

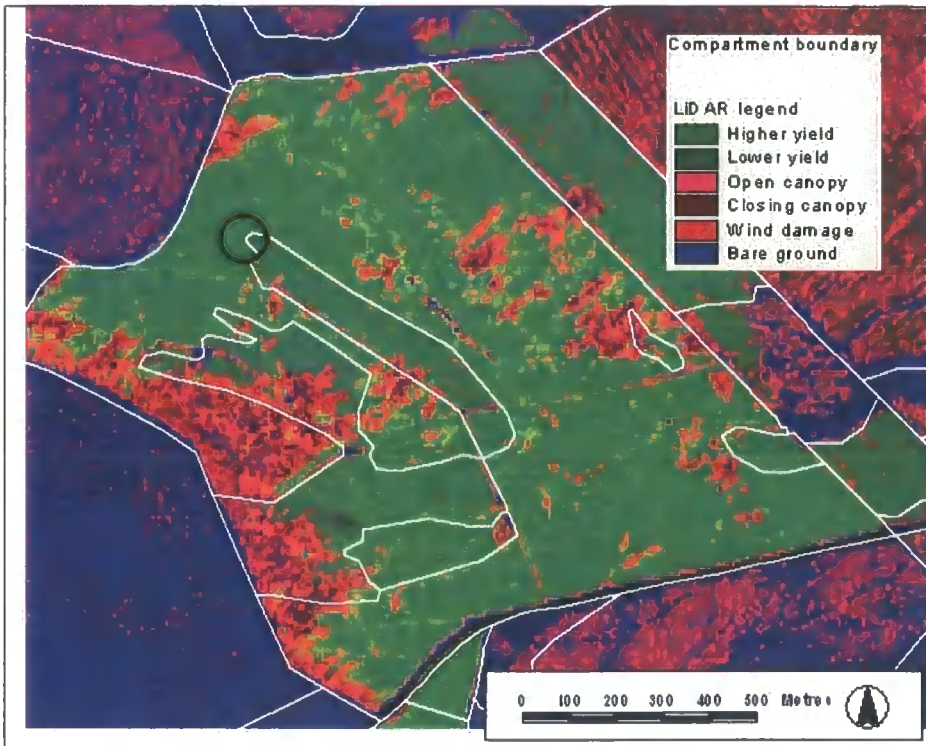

Figure 9.9 LiDAR composite image. Display bands, Red: Coefficient of variation, Green: LiDAR-derived top height, Blue: Percent ground returns.

In addition to providing height information, the LiDAR composite also highlights features that are not easily identified on the aerial photograph, in particular areas of small internal wind damage that are masked by shadow. While a pre-harvest inventory may identify some of the larger wind-damaged areas, it is likely that some would remain undetected. Identification of these additional areas would assist in determining the stocked area, which forms the basis of the production forecast. Small irregularities in GIS boundaries are also identified (as circled).

However, before making the production forecast, the stocked and non-stocked areas need to be mapped. In the UK this is done manually, by digitising around each area. Alternatively the delineation of these areas can be achieved by using an image segmentation method. Image segmentation works by dividing the image into spatially continuous and homogeneous regions (Mäkelä and Pekkarinen 2001). There are a number of segmentation routines available, but in this research the "t-ratio segmentation" method developed by Hagner was used (Hagner 1990). This is a type of region-growing algorithm, where spatially adjacent regions are merged if they cannot be separated with a given certainty. Similarity between segments is identified by means of the user-defined t-ratio value. The process is iterative, with the most similar regions merged first. Figure 9.10 shows the result of segmentation performed on the composite LiDAR image, overlaid on the 1: 10 000 aerial photograph. The segmentation is further refined by manually classifying each segment, in a GIS, into wind damaged, non-stocked and forest areas.

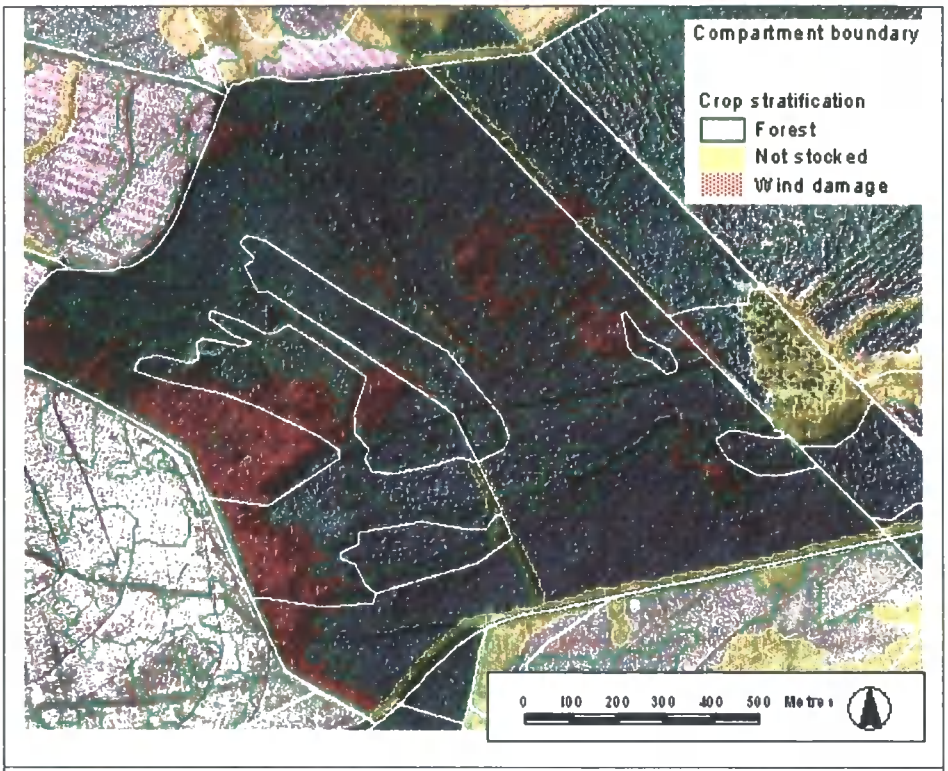

Figure 9.10 Segmented LiDAR measures classified and overlaid on the 1: 10 000 aerial photograph.

The results show that segmentation is able to provide an efficient method of mapping these areas. When compared with the FC's compartment boundaries, the classified segments provide a more accurate representation of the area of wind damage and forest gaps.

9.3.2 Using LiDAR-derived top height to make yield class estimates from revised forest compartment maps

The second example uses the outputs from section 9.2.1 to provide a revised estimate of yield class[43]. A five-step process (Figure 9.11) can be followed to create a yield class estimate from revised forest compartment maps. In step 1, the segmented areas generated in section 9.2.1. are used as a base map In step 2, each forest segment is allocated a mean top height value extracted from the LiDAR composite image. In Step 3, the FC sub-compartment GIS is intersected with each segment, to provide information on species, tree density and yield class. In step 4, the updated top height

[43] Yield class is a measure of forest productivity for single-species, even-aged plantations. It is derived from empirical models developed from extensive ground-based forest mensuration as is expressed in terms of annual volume increment (m^3/ha yr).

and forest attribute data are entered into the FC yield class models, to re-calculate the yield class for each segment. Lastly, in step 5 the revised estimates are compared with current yield class estimates, held in the FC's GIS.

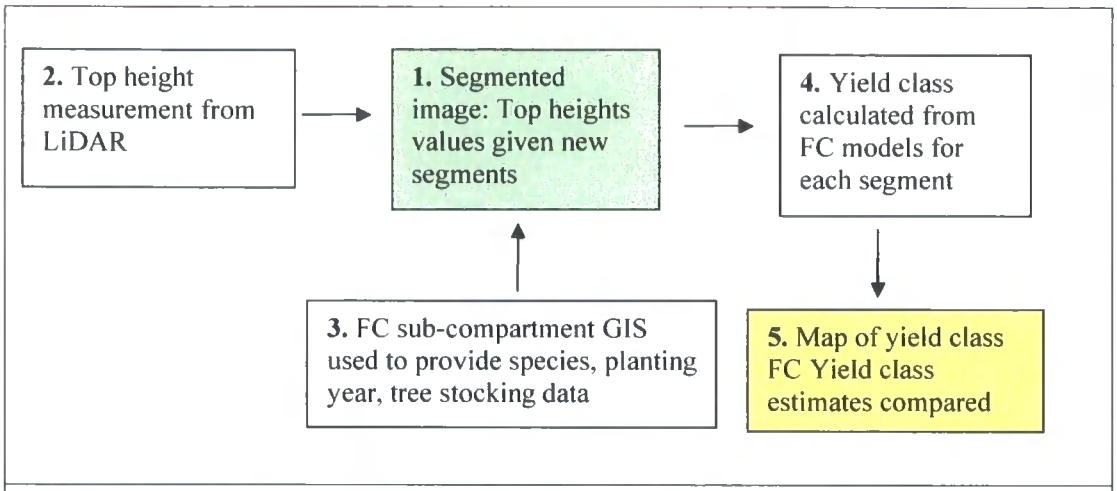

Figure 9.11 Processing steps used to estimate yield class.

Figure 9.12 shows the difference between that derived from LiDAR and the FC in terms of over- and under-estimations of yield class. The legend is divided into over- and under-estimates of yield class. An under-estimation occurs when the FC yield class is lower than the LiDAR estimate, with the opposite true of an over-estimation. The white areas represent small differences in growth rate e.g. ± 2 m^3/ha/yr, which is acceptable for forest management purposes. However, errors greater than this, if carried through a typical rotation length of 60 years, would exceed 15% of the average volume/ha. For example, if the yield class is estimated to be 12 m^3/ha/yr the total expected yield would be 720 m^3/ha. However, if the yield class were underestimated by 4 m^3/ha/yr, the total yield would be 480 m^3/ha (i.e. 60 x 8 m^3/ha/yr): an underestimation of 33%.

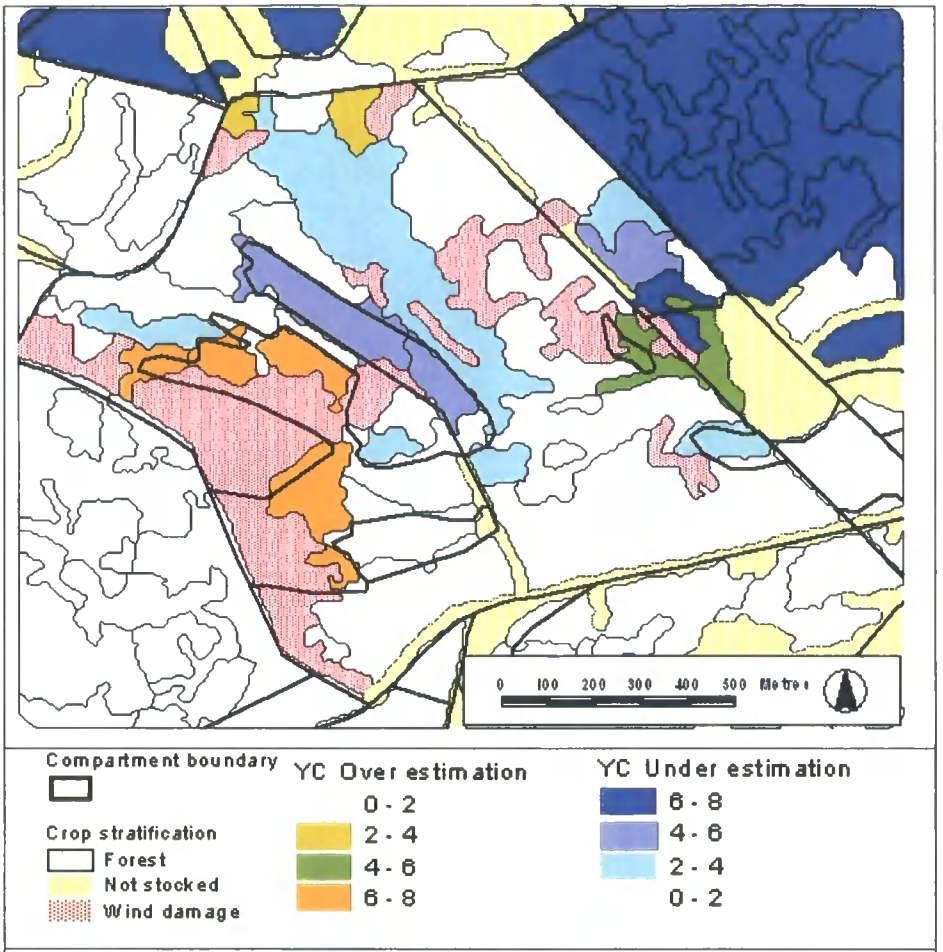

Figure 9.12 Forest compartment classified by yield class difference.

This simple analysis shows that LiDAR data, coupled with segmentation, enables more accurate mapping and stratification of forest areas than current methods based on ground survey and aerial photography. This technology could be used by foresters to identify areas of anomalous growth, leading to more precise production forecasts.

9.3.3 Height model applied to a time-series of Landsat TM/ETM+ to monitor forest growth and establishment.

The third application uses a time-series of Landsat TM and ETM+ scenes over Galloway Forest District. The methodology uses three images, acquired at approximately five-year intervals from 1989 through to 2001, to track changes in forest management and forest growth. The 2001 Landsat ETM+ is used as a base image, to which the other images are radiometrically normalised. The method, as described in Donoghue et al. (2005), uses the normalisation technique developed by Hall et al.

(1991), after which the image data appear as if they have been imaged under the same atmospheric and irradiance conditions. Height predictions are made by relating field height measurements, collected in 2002, to the 2001 Landsat ETM+ SWIR band (band 7). Applying the same height equation retrospectively to earlier images creates a quantitative change image. In this example the SWIR band (band 7) is used from each image. Figure 9.12 shows an example of the image time-series over the same area and the processed change/height image. The change image can be used to identify areas of change (represented by primary colours), such as clearfelled (red or yellow colours) or replanted areas (dark blue to light blue colours). Also apparent are areas of no change, such as moorland or closed canopy forest (identified as dull colours).

Overlaid on the change image (Figure 9.13) are the FC forest boundaries (White polygons) and the Woodland Grant Scheme (WGS) boundaries (Green polygons). WGS plantings are established using government grant funding, so there is a need to ensure that these plantings comply with the terms and conditions of the grant. For example, in the UK landowners who wish to receive a grant under the WGS must establish conifer plantations at a minimum density of 2,250 trees/ha and ensure the crop is maintained for a 10 year period (WGS 2003).

The example shows that changes in forest management can be monitored over large areas by integrating time series images. This, coupled with the height model, allows changes in forest height to be monitored up to the point of canopy closure (as shown by the graph in Figure 9.13). In terms of applications, the change/height image could be used to monitor large-scale changes in forest resources such as wind damage or harvesting and to ensure compliance with woodland establishment grants.

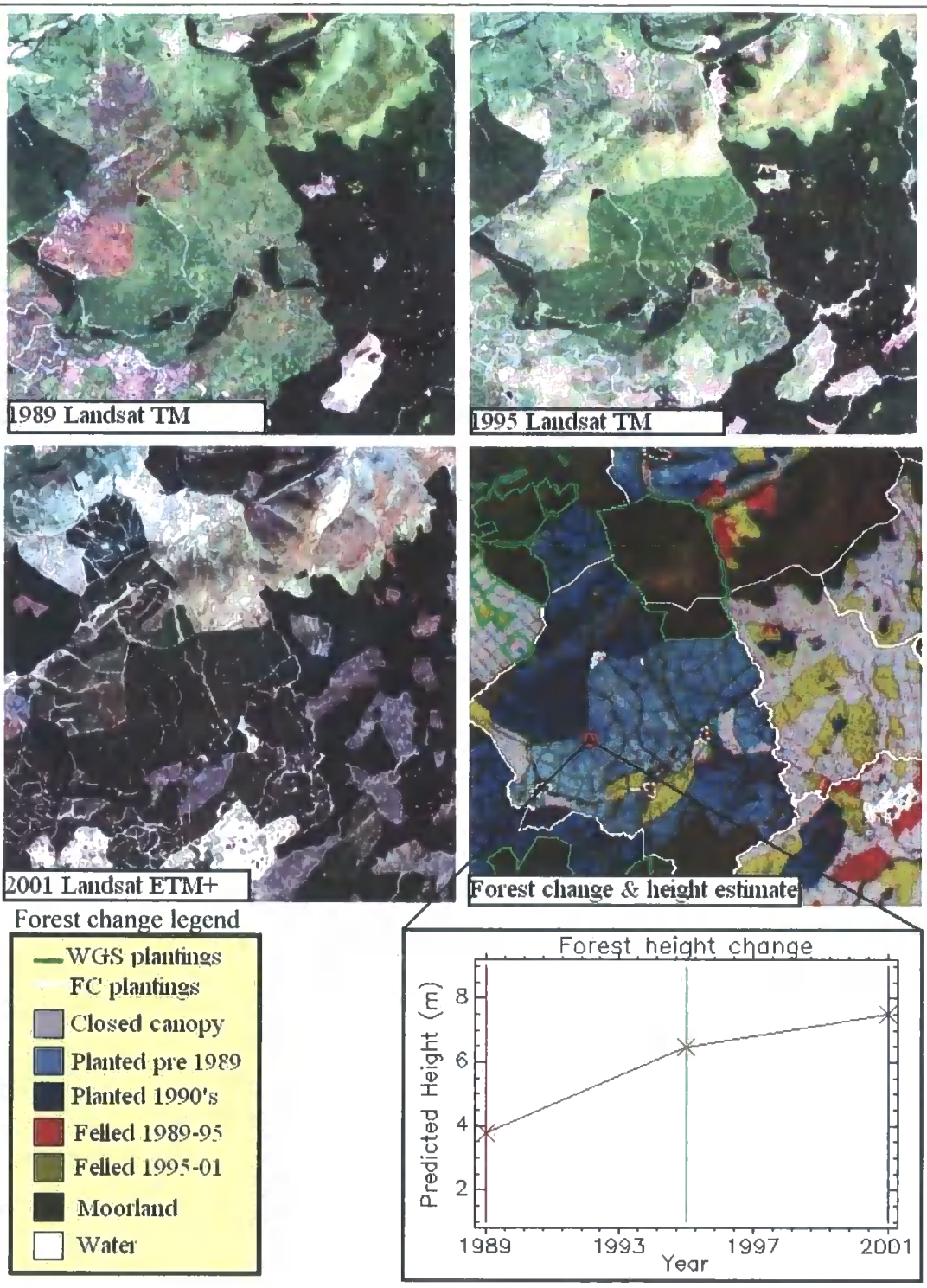

Figure 9.13 Example of forest change image processed to provide temporal height estimates.

Using medium resolution satellite imagery to monitor forest growth and establishment offers a range of advantages. These include the ability to survey extensive forested

areas using a single image, the instantaneous nature and replicability of the survey, the fact that each image requires very little computer processing and the simplicity of the predictive models, which are easily understood. Furthermore, the predictions do not require a large ground survey effort and an operational system would not have to rely on a single source of image data (i.e. SPOT, Landsat, IRS, Quickbird or IKONOS could be used). If implemented operationally, cost per unit area of a height map derived from satellite imagery could be less than £0.01 per hectare (calculation based on the current cost of Landsat TM data).

9.4 Further applications

In addition to the three examples focussed on forest estimates, it is also possible to use the methods and remote sensing data presented in this thesis for other purposes. Two potential applications are discussed.

(i) Integrated catchment management planning

The time-series/height change map provides a means of monitoring afforestation levels in upland river catchments. According to current EU Water Framework Directive (WFD) guidelines adapted for the UK, catchments over 300 m should not contain greater than 30% forest cover (European Parliament 2000). Since predictions from optical data saturate, once the forest canopy has closed, it is relatively easy to identify open and closed canopy areas, within a river catchment, using regression methods adopted in this thesis (see Figure 9.13). Such canopy closure maps can easily be integrated into a GIS system, to provide forest and environmental managers with a tool enabling accurate and rapid identification of afforestation levels in river basins. This is particularly important in areas of acid sensitivity, such as Galloway, south-west Scotland, where conifer afforestation may act to exacerbate acid levels.

(ii) Model validation

One of the key strengths of LiDAR is its ability to provide information on forest height and forest canopy characteristics. A number of studies, including this research, have shown that tree height and volume can be estimated with the same level of accuracy as field-based measurements (Holmgren 2003; Hyyppä-et al. 2000; Naesset 1997; Persson

et al. 2002). Therefore, there is considerable potential to use LiDAR both as a tool to validate predictions from models used to estimate volume and to use volume or height data to predict other variables (Nelson et al. 1984; Means et al. 1999; Naesset & Økland 2002). One topical application would be the use of LiDAR to validate above-ground carbon estimates. For example, field measurements of stem volume or basal area are often used in models, to determine above-ground carbon content; these parameters are then related to satellite data (i.e. RADAR backscatter or reflectance). A widely reported weakness of current approaches, using optical or RADAR data, is insensitivity in estimates, once the forest canopy has formed (Patenaude et al. 2004; Wagner 2003). It is therefore possible that estimates relying on satellite-derived relationships might also contain error. The likelihood of this is increased if models developed over relatively simple forests are extrapolated to areas containing more heterogeneity. In this context, because LiDAR data is able to penetrate the forest canopy layer and shows no apparent saturation, it could be used to provide independent verification of key parameters, like volume and height, and through this improve larger-scale estimations of above-ground carbon stocks. Additionally, considerable uncertainty still exists about estimates of CO_2-carbon fixation in conifer plantation forests. This is confounded by difficulties in estimating carbon stored in forest soil and litter. Many forests in upland Britain are planted on deep and shallow peatland and these soils can contribute to (i) poor growth leading to low yield, and (ii) an unstable root mat, leading to susceptibility to wind and snow damage (Cannell et al. 1993). LiDAR has the capability to identify areas of low yield and damage, with a high degree of precision. If the carbon stock in standing timber is assessed without accounting for stocked area and the quality of the crop, it will be considerably overestimated.

9.5 Meeting forest management needs using remote sensing

To manage forest resources effectively, forest planners require accurate and timely information on the growth and area of forests. It is clear that remote sensing can satisfy these requirements and provide information, to help meet the needs of forest planners. In this context, choice is not limited to sensors evaluated in this thesis and can be expanded to include RADAR or other optical systems such as hyperspectral optical data. Furthermore, there are advantages to be gained from combining these data as different sensors can provide complementary information on forest structure, which can

lead to more accurate forest estimates. For example, RADAR and optical data have been successfully combined to improve estimates of forest volumes in Sweden (Holmström and Fransson 2003). This type of research highlights the advantages of combining optical data, which provides spatial and spectral information, with active sensors like RADAR or LiDAR which have the ability to provide both horizontal and vertical information on vegetation structure. In the future there will be a demand for sensors capable of providing a range of measurements at different scales at a cost that is acceptable to the forest industry.

(i) Forest management applications from this research

The sensors investigated in this thesis cover a range of resolutions that can be used to provide forest estimates a compartment level through to the stand level. Small footprint airborne LiDAR is seen as offering detailed height estimates that can be used effectively to predict forest canopy height. Top height, which is a forest measurement often used to parameterise forest prediction models (i.e. stem volume models) can be estimated by selecting the relevant laser percentile height. In addition to height, laser intensity can be used to identify and map forest species. The level of detail in terms of separating mixed conifer plantations is better than any currently available satellite data. Laser height and intensity data can also be used to prove detailed stock maps by mapping out areas of wind damage, poor tree stocking, poor growth and other forest gaps. It is important however, to realise that LiDAR data is currently expensive and to justify its use the potential of the data must be maximised. Current practise favours the use of aerial photography as the data is widely available and it is a well established method of mapping forest areas and providing photogrammetrically-derived height. LiDAR, however, has the advantage of providing direct measurement of height unlike photogrammetric methods which require that the ground surface is visible. LiDAR is also capable of providing more accurate stocked area estimates as the laser is able to penetrate the forest canopy and unlike aerial photography is not affected by shadowing caused by cloud and sun angle. Shadowing makes it more difficult to identify forest gaps in densely planted forest. At a larger compartment/regional scale satellite data is able to provide a rapid overview of changes over forest areas. High resolution data such as Quickbird or IKONOS are able to provide sufficient detail to identify areas of wind damage, forest gaps and to differentiate different forest species. Medium resolution

data such as SPOT or Landsat provide a larger overview and a way of identifying broad scale forest changes, such as forest clearfells and larger areas of wind damage. This research has shown that the spectral information can be used to predict forest height up to the point of forest canopy closure (10 m). This offers a relatively inexpensive method of monitoring the development of forest crops up to the point of canopy closure. Additionally, if a time series of image data is available, then the same predictive models can be applied retrospectively to enable forest height development to be tracked through time.

(ii) Advances in LiDAR systems

Over the past 10 years there have been substantial advances in the capabilities of airborne LiDAR systems. It can be expected that the new generation of sensors will produce higher pulse rates and operate at higher altitudes. Both attributes reduce the number of flight lines required to survey an area, which potentially reduces the cost of LiDAR survey. Recently two commercial full-waveform LiDAR systems the Optech ALTM 3100 and TopEye MK II have emerged, enabling full digitisation of the laser pulse return. These systems can help to characterise the entire vertical profile of a forest canopy, which leads to the possibility of reconstructing forest structure in three dimensions. As laser technology continues to advance, it is possible that airborne LiDAR systems will emerge, with multi-spectral capability similar to optical systems. Such a development would lead to enhanced use of LiDAR data for better identification of tree species and landuse classification. The advantage of a multi-spectral LiDAR over a LiDAR and optical multi-spectral scanner is that the resolution of observation would be same, and also each pulse would also have an elevation value associated with it. This information could potentially allow different vegetative components (i.e. needles and trunk) to be separated by height above the ground. As these new sensors become commercially available, the current cost of LiDAR surveys using older discrete-return LiDARs should decrease, encouraging greater uptake. Furthermore, if a satellite-based LiDAR system is launched, with similar characteristics to the discontinued Vegetation Canopy LiDAR (VCL) programme, then low-cost wide-swath measurements of vegetation height and structure will be possible (Blair et al. 2001).

(iii) Advances in optical systems

Currently, airborne optical systems, such as digital cameras, provide the highest spatial resolution, while specialist instruments, such as the Compact Airborne Spectrographic Imager (CASI), provide data with the high spectral resolution. However, as the design of optical sensors improves, it is likely that airborne systems with these characteristics will become standard. It is probable that new systems will be developed, integrating other active sensors such as LiDAR or RADAR systems. Future improvements to space-borne optical sensors are also likely to include greater integration of sensors that allow simultaneous data acquisition (i.e. RADAR and optical sensor on the same platform). In the near future the spectral and spatial resolution of space-borne sensors will continue to improve, to include multi-spectral sensors, which are capable of measuring a wider range of spectral wavelengths.

Chapter 10: Summary and Conclusions

10.1 Summary of thesis

The objective of this thesis was to evaluate the potential of LiDAR, IKONOS and Landsat ETM+ data to provide estimates of forest variables, at a range of scales, in British upland conifer plantations. Results have shown that remote sensing can be used to improve forest resource management, by providing additional information. LiDAR data, in particular, provide accurate height information that can be easily integrated into existing models, to predict volume. Forest variability, wind damage and species composition can be identified and mapped, to provide up-to-date forest compartment maps. Optical satellite data can be used to estimate height, which provides a rapid tool for assessing the success of plantation establishment over large areas. Both methods demonstrate apparent repeatability and transferability to other forest areas. If combined, these data and methods complement existing current forest management systems and provide the potential for targeting existing resources more efficiently.

The following section summarises the research findings, in relation to the primary research aims, key scientific findings and practical forest applications and outlines potential areas for future research.

10.2 Research findings

Aim 1: assess the effect of canopy structure, topography and laser point density on the accuracy of measures extracted from LiDAR data in dense upland conifer plantations.

Results indicated that, despite the dense nature of the forest canopy, sufficient laser pulses penetrated to the ground to generate an accurate DTM. Consequently, the main source of error in height estimation, made by the laser, was associated with the canopy surface, rather than with the ground surface. No evidence was found of LiDAR accuracy being affected by changes in topography, although the topographic range within the study area is limited (0 to 17°). The accuracy of laser height measurement over the forest improved as the point density increased. However if the ground model is accurately defined, a point density of 2 returns/m^2 is sufficient to measure canopy height.

Aim 2: assess the potential of LiDAR data to provide estimates of forest variables used in forest management (i.e. top height, volume and density)

After calibration, LiDAR-derived top heights were found to be as accurate as field-based measurements. Top height is accurately predicted using the appropriate percentile height (99^{th} laser percentile; R^2 =0.99 and RMSE = 0.56 m). Accuracy is not improved by including additional variables calculated from the laser height distribution. Further, since there is no statistically significant difference in the penetration of the forest canopy by first and last pulses, no additional information on canopy structure is gained by including the last pulse returns.

Volume can be estimated by using LiDAR-derived top height (RMSE ~70m^3/ha), although there are some inconsistencies between the LiDAR prediction and the current FC model. Further research is required to determine the cause of these inconsistencies. Despite these differences, LiDAR-derived top height is easily integrated with established FC models to provide volume estimations. Potentially, this approach, taking accurate height estimates from LiDAR and matching these with models specific to UK management regimes and tree species, derives benefits from both. Tree density was not accurately estimated using LiDAR data in this study using this particular LiDAR configuration. This is because the canopy structure remains fairly static through the forest rotation cycle, making any change in tree density difficult to detect using LiDAR flown at this point density.

Results also strongly suggest that predictive equations, developed for top height over the Kielder study area, can be transferred to other UK conifer forests. Furthermore, the relationship between field-measured top height and laser-derived top height appears to be stable across different conifer species.

Aim 3: assess the potential of LiDAR-derived crown density variables and near infrared data to identify plantation species and areas of anomalous growth

Field measurements and laboratory spectral measurement of conifer needles show that the physical canopy structure and spectral characteristics of Sitka spruce and lodgepole pine are different. Consequently, LiDAR data could be used to differentiate between

species at stand level. Additionally, where mixed conifer species have been planted, the dominant species can be identified. Two methods were developed: the first generates summary measures based on the laser height distribution and the second summarises the near infrared intensity data by dividing the laser returns by height percentiles. When the different measures are mapped, detailed maps of forest stands can be produced. These enable classification of areas by species, identification of anomalous growth areas and detection of wind damage.

The methods developed are transferable to other similarly managed conifer forests. However, if LiDAR near infrared intensity data are used, a secondary data source is required to validate the radiometric consistency; satellite or airborne optical image data, recording radiance in the near infrared, would be appropriate.

Aim 4: examine the potential of Landsat ETM+ and IKONOS sensors for providing forest height estimates in upland conifer plantations.

Landsat ETM+ and IKONOS data can provide height estimates up to the point of canopy closure, which in UK conifer forests is about 10 m. This is because, at the scale of observation once the canopy has closed, there is little change in the canopy's spectral response. Generalised linear models allow current relationships to be handled well and avoid problems associated with other methods. Encouragingly, little difference is observed in the predictive ability of the height models as the spatial resolution increases from 4 m to 30 m. Landsat or SPOT data is cheaper per unit area than the IKONOS data. The higher spatial resolution of the IKONOS data does, however, enable easier identification of areas of high natural regeneration or incomplete stocking. If the satellite data are collected at high off-nadir angles (probably above >20°) and over areas of undulating topography, corrections will need to be applied to normalise the image data for illumination differences caused by topographic shadowing.

Results achieved over the Kielder area concur with findings from previous research conducted in upland conifer plantations, located in Galloway Forest District. This indicates that the methods and potential height prediction models are transferable between regions. Furthermore, since the height–reflectance relationship is stable between sensors and spectral bands, an operational system could use high- or low-resolution satellite data, obtained from a range of sensors.

Aim 5: assess the potential of LiDAR for providing additional height samples and validating forest height estimates derived from Landsat ETM+ and IKONOS models. LiDAR–derived height is as accurate as field-based measurements therefore reflectance-based height estimates can be made using the LiDAR data. Results from this research show that only a small number of height samples are required to apply parameters to these models. A carefully targeted LiDAR survey, ranging from newly established plantations to closed-canopy plantations, could provide these measurements. Similarly, LiDAR could be used as means to validate these height predictions.

10.3 Key scientific findings

(i) Accuracy of small footprint LiDAR in dense conifer plantations

Previous research has primarily focussed on evaluating commercially available small footprint LiDAR systems in relatively open semi-natural or boreal forests. Only one other study in the UK by Suárez et al (2005) has assessed the accuracy of LiDAR in densely planted coniferous plantations where tree densities exceed 2,500 trees/ha. Since a majority of the UK plantation resource is currently managed in this manner it is important to determine if LiDAR can be used to provide accurate method of measuring height in this environment. The following provides a summary of the key findings from this thesis.

- Small foot-print discrete laser systems operating at a pulse rate of 33,000 returns/sec at a density of 2 returns/m^2 penetrate the forest canopy to provide an accurate DTM.
- The main source of error in the measurement of maximum height is associated with the forest canopy as the laser pulse tends to miss the tree apex and is returned from the lower canopy.
- No evidence was found of LiDAR accuracy being affected by changes in topography, although the topographic range within the study area is limited (0 to 17°).
- The accuracy of laser height measurement over the forest improved as the point density increased. However if the ground model is accurately defined, a point density of 2 returns/m^2 is sufficient to measure canopy height.

(ii) Measurement of forest height, volume and tree density using small footprint LiDAR

Certain forest variables that are of interest to forest managers for the purpose of resource planning can be derived from LiDAR. Principally, this thesis focused on the measurement of top height, stem volume and tree density. Key findings from this thesis include:

- After calibration against field-measured height, LiDAR-derived top heights were found to be as accurate as field-based measurements. Top height is accurately predicted using the appropriate percentile height (99^{th} laser percentile; R^2 =0.99 and RMSE = 0.56 m). Accuracy is not improved by including additional variables calculated from the laser height distribution. Statistically there is no significant difference in the penetration of the forest canopy between first and last pulses. This means that no additional information on canopy structure is gained by including the last pulse returns. This finding differs from research conducted in less dense boreal or semi-natural forest types where often the metrics derived from the height distribution of first and last pulse data are used to estimate forest estimates (Naesset 2002).

- Stem volume can be estimated by using LiDAR-derived top height (RMSE ~70m^3/ha), although there are some inconsistencies between the LiDAR prediction and the current FC model. Further research is required to determine the cause of these inconsistencies. Despite these differences, LiDAR-derived top height is easily integrated with established FC models to provide volume estimations. Potentially, this approach, taking accurate height estimates from LiDAR and matching these with models specific to UK management regimes and tree species, derives benefits from both. Tree density was not accurately estimated using LiDAR data in this study using this particular LiDAR configuration. This is because the canopy structure remains fairly static through the forest rotation cycle, making any change in tree density difficult to detect using LiDAR flown at this point density.

- Results also strongly suggest that predictive equations, developed for top height over the Kielder study area, can be transferred to other UK conifer forests. Furthermore, the relationship between field-measured top height and laser-derived top height appears to be stable across different conifer species. It should however be noted that further ground measurements are necessary to fully evaluate this hypothesis.

(iii) The use of intensity data and canopy derived measures to identify conifer species.

The LiDAR near infrared response from the forest canopy can be used to differentiate between tree species at stand level. Previous research by Holmgren & Persson (2003) has also shown this to be possible at a single tree level in mixed species plantings. The research in this thesis highlights the benefits of using both spectral and metrics derived from the first pulse height distribution, namely coefficient of variation (C_v), mean laser height (*meanh*), first pulse skewness (*skewfp*) percent ground returns (*pczero*) for identifying and mapping the distribution of tree species in mixed conifer stands at the stand level. Additional key findings from this thesis include.

- The noise in the intensity data caused by variations in laser incidence angle and the targets composition can be reduced by dividing the laser returns by height percentiles so that only vegetative returns are considered.
- If the laser time tag information is available then it is possible to correct for variations in laser's incidence angle and path length.
- Variation in intensity values are further decreased by aggregating and averaging intensity values to a larger spatial scale (say 5 m or 10 m).
- Canopy density metrics derived from the first pulse laser distribution provide additional method of differentiating conifer species. In a plantation setting Sitka spruce and lodgepole pole have different laser height distributions with Sitka spruce producing a denser canopy than lodgepole pine. This is reflected in the laser height distribution. The most useful distribution measure for differentiating between species is coefficient of variation.

- Other measures such as skewness, mean laser height, and percent ground returns are effective for identify gaps and areas of wind damage. Mean laser height is also useful for identifying variations in height, which in turn provides an indication of crop performance.

(iv) Potential of Landsat ETM+ and IKONOS sensors for providing forest height estimates in upland conifer plantations.

The results obtained in this thesis for predicting forest height from medium resolution sensors such as Landsat and SPOT broadly concur with other research conducted in conifer forests (Danson and Curran 1993; Franklin 1986; Nilson and Peterson 1994; Donoghue et al. 2004; Donoghue & Watt 2005; Puhr & Donoghue 2000). It is important to note that the strength of relationships varies between studies as does the spectral band(s) selected. These differences in relationships can be caused by the structure of the forest canopy and by forest management practices, such as thinning. In contrast Britain's upland conifer plantations are densely planted with a simple management regime (no thinning or pruning), which causes the canopy to close at a young age. Therefore the main limitation of the method is that spectral response tends to decrease as the forest canopy closes; consequently predictions are only valid for the first part of the forest rotation. Original research conducted in this thesis evaluates the potential of IKONOS and compares a predictive model developed to estimate height against one derived from Landsat ETM+ data. Additionally, GLMs are introduced as an alternate regression technique for modelling these relations. Other key findings from this thesis include.

- Landsat ETM+ and IKONOS data can provide height estimates up to the point of canopy closure, which in UK conifer forests is about 10 m. This is because, at the scale of observation once the canopy has closed, there is little change in the canopy's spectral response. Consequently, little difference is observed in the predictive ability of the height models as the spatial resolution increases from 4 m to 30 m.

- Generalised linear models are used as an alternative for modelling the relationship between height and reflectance. Unlike many regression methods

GLMs are able to handle curvilinear without the need for fitting more complex curves or applying transformations to the response and working on a transformed scale, an approach used in many studies that have used optical (Ahern et al. 1998; Hyyppä et al. 2000; Puhr and Dongohue 2000) or LiDAR data (Naesset 1997; Means et al. 1999; Nelson 1997; Holmgren et al. 2003). An approach which in many ways offers the best of both worlds, is that afforded by generalised linear models (GLMs).

- There are two main differences between GLMs and general linear models: first, the response may have a non-normal distribution and second, the transformation applied to the response variable is selected by applying the appropriate link function (e.g. logarithmic) in the software. One key advantage of using a GLM is that predictions are generated and presented on the original measured scale of the response and so there is no need for back-transformation or bias corrections (Cox et al. *in review*). In this thesis the logarithmic link function was used, which thus instructs the software to fit a relationship on a logarithmic scale, but to report results on the scale of the original response variable.

- Since the IKONOS can be collected at off-nadir angles corrections will be necessary to normalise the image data for illumination differences caused by topographic shadowing prior to applying any reflectance-based model.

- Results achieved in this thesis using medium resolution satellite data concur with findings from previous research conducted in upland conifer plantations. Indicating that the relationships and mechanisms controlling these relationships are stable across similarly managed forests.

(v) Potential of LiDAR for providing additional height samples and validating forest height estimates derived from Landsat ETM+ and IKONOS models.

A common issue with many empirically based models is the need to test the robustness of predictions against an independent data source. In forestry this usually means that additional field measurements must be collected, which is both

time-consuming and expensive. LiDAR data is seen as an alternate data source that can be used to validate height predictions over a larger and wider sample.

- Increasing the number of height samples using LiDAR from 28 to 410 did not improve the height prediction model substantially.

- The mode of measurement and spatial coverage of LiDAR means that it can be used to provide supplementary data to validate estimates make using broader-scale optical sensors. In this context it identifies areas with incomplete tree stocking or poor growth.

10.4 Key forestry applications

The sensors investigated in this thesis cover a range of resolutions that can be used to provide forest estimates a compartment level through to the stand level. Small footprint airborne LiDAR is seen as offering detailed height estimates that can be used effectively to predict forest canopy height at the stand level while optical data are able to provide broader estimates at the regional/compartment level.

(i) LiDAR Applications

Small footprint discrete LiDAR systems were originally developed to provide high quality DTM information. However, over the past 10 years a large body of research has also assessed the potential of these systems to make forest measurements, such as height, basal area, stem volume and tree density. Many of these studies have focused on forests that are not as densely planted as UK conifer plantations. The following section highlights particular applications from this thesis that are seen to be particularly relevant to UK forests that could be used operationally should the datasets become more readily available.

- Top height, which is a forest measurement that can be estimated by selecting the relevant laser percentile height more accurately than field-based methods. This research also suggests that if the ground surface is correctly identified then variables such as top height estimates are transferable to different forest areas under similar management regimes.

- Top height information can be used to parameterise existing stem volume models. The use of an established model, which has been developed specifically for different UK conifer species, means there is less reliance on LiDAR data to provide the volume estimate. However, the validation data used in this thesis highlight the fact that the usefulness of current yield class models is limited when crops do not develop in a uniform way (e.g. have higher than average levels of mortality or contain a mixture of tree species). In these areas it is difficult to make accurate volume predictions based on top height information alone.

- Additional measures derived from the LiDAR height distribution such as Coefficient of variation (C_v), percent last pulse ground returns (*pczero*) and mean laser height (*meanh*) the can be used to identify areas of abnormal growth, gaps and wind damage. In turn this allows forest areas to be stratification and mapped to produce more accurate stand maps, either manually or by semi-automated methods (i.e. using the t-ratio segmentation routine as described in Chapter 9).

- In mixed conifer plantations laser near infrared intensity can be used to separate different species conifers. In this respect some of the LiDAR height measures also provide complementary information that assist with mapping these areas. It is worth noting that raw LiDAR intensity is sensitive to changes in topography and may require calibration to normalise for topographic effects.

- It is important however, to realise that LiDAR data is currently expensive and to justify its use the potential of the data must be maximised.

(ii) Potential applications using optical satellite data

Optical satellite data obtained from platforms such as Landsat and SPOT is used routinely in Scandinavia and the US at a larger compartment/regional scale to provide a rapid overview of changes over expansive forest areas. In comparison less work has

been done to evaluate the operational use of high resolution datasets such as Quickbird or IKONOS. This thesis has evaluated both medium resolution and high resolution datasets to assess their potential to estimate forest height over densely planted forest such as those found in the UK.

- Medium resolution data such as SPOT or Landsat provide a larger overview and a way of identifying broad scale forest changes, such as forest clearfells and larger areas of wind damage. This research has shown that the spectral information can be used to predict forest height up to the point of forest canopy closure (10 m). This offers a relatively inexpensive method of monitoring the development of forest crops up to the point of canopy closure. Additionally, if a time series of data is available the same predictive models can be applied retrospectively to enable forest height development to be tracked through time.

- Height models of a similar form can also be applied to higher spatial resolution of IKONOS. Overall the improved spatial resolution allows better discrimination of areas showing abnormal growth characteristics. Again height predictions can only be made up to the point of canopy closure.

10.5 Future research

A number of areas warranting further research have been identified during this research.

- Results from this research suggest that current FC yield models are accurate in homogeneous forest crops, but less accurate in crops that show growth variability. Since LiDAR can be used to estimate volume, it could be used to test the accuracy of FC's yield class models over a wider range of forest sites, silvicultural regimes, tree species and species mixtures. This would require additional field sampling, so that LiDAR-derived volumes could be compared with field-measured volumes. The outcome may enable refinements to current yield models.
- This research has shown that LiDAR-derived top height is as accurate as field-based measurement, at a laser pulse density of 2 returns/m^2. If the laser pulse density were reduced, substantial cost savings are possible, because of the lower number of flight lines required. More research needs to be conducted in UK forests to assess whether this approach would adversely affect the accuracy of LiDAR-derived estimates of height and volume. This would also require additional field

samples. Ideally, these should be distributed over a range of forest and topographic conditions.

- Results from this research strongly suggest that LiDAR-derived predictions of top height can be extended to other UK conifer forests. However, more research is required to evaluate the stability of these estimates over other forest regions. This could be tested by analysing additional field and LiDAR datasets, collected by Forest Research in Aberfoyle Forest District, Scotland. If the results are positive then it should be possible to establish a methodology for future LiDAR acquisitions and to establish generic equations for estimating top height and volume.
- Results also showed that the intensity of the LiDAR return is able to separate tree species. However, more research is required to establish a method for normalising laser intensity for topographic and scan angle effects. There is also a need to evaluate the stability of the near infrared response between sensors and other forest areas.
- Tree density was not accurately estimated in this research, using LiDAR (± 434 trees/ha). Although tree density was not estimated using the optical data, areas of high tree density were detected using IKONOS data. It possible that by integrating LiDAR-derived measures and spectral information from IKONOS a more accurate estimate of tree density could be obtained.
- Further research is also required into what additional information can be derived from full waveform small footprint LiDAR systems.
- Topographic shadowing was shown to affect height estimates from IKONOS data. More work needs to be undertaken, to evaluate normalisation routines, so these data can be used more widely. This is particularly important given that all of Britain's upland conifer forests are located on sloping terrain and that imagery suppliers appear reluctant to provide nadir-looking data, as it restricts sensor's swath width and increases the number of over-passes required to collect the data.

10.6 Conclusions

This thesis has established a working methodology, applicable across UK coniferous forest sites, for processing LiDAR data. This can be used to predict key forestry parameters and to identify and map conifer species. Transferable methods, using optical data, have also been developed, enabling foresters to rapidly appraise the success of forest establishment and to monitor compliance.

References

Ahern, F.J., Erdle, T., Maclean, D.A., and Kneppeck, I.D. 1991. A quantitative relationship between forest growth rates and Thematic Mapper reflectance measurements. *International Journal of Remote Sensing* (12) 387–400.

Aldred, A.H. & Bonner, G.M. 1985. Application of airborne lasers to forest surveys. Canadian Forestry Service Petawawa National Forestry Centre, Information Report PI-X-51, 62 pp.

Axelsson, P. 2000. DEM Generation from Laser Scanner Data Using Adaptive TIN Models. The International Archives of Photogrammetry and Remote Sensing, Amsterdam, The Netherlands, Vol. XXXIII, Part B4/1, pp. 110–117.

Baltsavias E. P. 1999a. Airborne laser scanning: basic relations and formulas. *ISPRS Journal of Photogrammetry and Remote Sensing* (54) 199–214.

Baltsavias, E. P. 1999b. Airborne laser scanning: existing systems and firms and other resources. *ISPRS Journal of Photogrammetry and Remote Sensing* (54) 164–198.

Bechtold, W. A. 2003. Crown position and light exposure classification-an alternative to field-assigned crown class. *Northern Journal of Applied Forestry* (20) 154–160.

Blair, B.J., Hofton, M., Luthcke, S.B. 2001. Wide-swathe imaging LiDAR development for airborne and spaceborne applications. In *proceedings of International Archives of Photogrammetry and Remote Sensing, Volume XXXIV-3/W4* Annapolis, MD, 22-24 Oct. 2001.

Cannell, M.G.R., Dewar, R.C., Pyatt, D.G. 1993. Conifer plantations on drained peatlands in Britain: a net gain or loss of carbon? *Forestry* (66) 353–369.

Cox, N.J. Warburton, J., Armstrong, A., and Holliday, V.J. *in review.* Fitting concentration and load rating curves with generalised linear models. *Earth Surface Processes and Landforms.*

Danson, F.M., and Curran, P.J. 1993. Factors affecting the remotely sensed response of coniferous forest plantations. *Remote Sensing of Environment* (43) 55-65.

Di, K., Ma, R., Li, R. 2003. Rational functions and potential for rigorous sensor model recovery. *Photogrammetric Engineering and Remote Sensing* (60) 33–43.

Donoghue, D.N.M., Watt, P.J., Cox, N.J., Dunford, R.W., Wilson, J., Stables, S. and Smith, S. 2004. An evaluation of the use of satellite data for monitoring early development of young Sitka spruce plantation forest growth. *Forestry* (77) 383–396.

Donoghue, D.N.M., Watt, P.J., McManus, K.B. 2005. Remote sensing of growth dynamics of Sitka spruce forests in upland Britain. In Proceedings of ForestSAT Conference, Borås, Sweden, May 31 - June 3, 2005.

Donoghue, D.N.M., Watt, P.J. *in review*. Using LiDAR to compare forest height estimates from IKONOS and Landsat ETM+ data in Sitka spruce plantations. *Remote Sensing of Environment.*

Donoghue, D.N.M., Watt, P.J., Cox, N.J., Wilson, J. *in review*. Remote sensing of species mixtures in conifer plantations using LiDAR height and intensity data. *Remote Sensing of Environment.*

Dye, S., Baylin, F. 1997. The GPS Manual Principles and Applications. Baylin Publications, Boulder, Colorado, USA.

Eid, T., Gobakken, T., Naesset, E. 2004. Comparing stand inventories for large scale areas based on photo-interpretation and laser scanning by means of cost-plus-loss analyses. *Scandinavian Journal Forest Research* (19) 512–523.

Edwards, P.N., Christie, J.M. 1981. Yield models for forest management. Forestry Commission Booklet 48. Forestry Commission, Edinburgh.

European Parliament, 2000. Directive of the European parliament and of the council 2000/60/EC establishing a framework for community action in the field of water policy 2000/60/EC.

Forestry Commission, 2004. Forestry Facts and Figures 2004.

Franklin, J. 1986. Thematic mapper analysis of coniferous forest structure and composition. *International Journal of Remote Sensing* (7) 1287–1301.

Gaveau D. L.A., and Hill R.A. 2003. Quantifying canopy height underestimation by laser pulse penetration in small-footprint airborne laser scanning data *Canadian Journal of Remote Sensing* (29) 650–657.

Haglöf Sweden www.haglofsweden.com

Hall, F.G., Strebel, D.E., Nickeson, J.E., and Geotz, S.J. 1991. Radiometric rectification: toward a common radiometric response among multidate, multisensor images. *Remote Sensing of Environment* (35) 11–27.

Hamilton, G.J. 1975. Forest Mensuration Handbook Forestry Commission Booklet No. 39. HMSO, London.

Hibberd, B.G. 1991. Forestry Practice No. 6. HMSO, London.

Holmgren, J. 2003. Prediction of tree height, basal area, and stem volume in forest stands using airborne laser scanning. Doctoral thesis. Acta Universitatis

Agriculturae Sueciae, Silvestria 278. Swedish University of Agricultural Sciences, Department of Forest Resource Management and Geomatics, Umeå, Sweden.

Holmgren, J., and Persson, Å. 2004. Identifying species of individual trees using airborne laser scanning. *Remote Sensing of Environment* (90) 415–423.

Holmgren, J., Nilsson, M., and Olsson, H. 2003. Simulating the effects of lidar scanning angle for estimation of mean tree height and canopy closure. *Canadian Journal of Remote Sensing* (5) 623–632.

Holmgren, J., Jonsson, T. 2004. Large scale airborne laser scanning of forest resources in Sweden. In *Proceedings of the ISPRS working group VIII/2, Laser-Scanners for Forest and Landscape Assessment*, 3-6 October 2004, Freiburg, Germany.

Holmström, H., Nilsson, M., Ståhl, G. 2001. Simultaneous estimations of forest parameters using aerial photograph interpreted data and the k Nearest Neighbour method. *Scandinavian Journal of Forest Research* (16) 67–78.

Holmström, H., Fransson, J.E.S. 2003. Combining remotely sensed optical and radar data in *k*NN-estimation of forest variables. *Forest Science* (49) 409–419.

Hudak, A.T., Lefsky, M.A., Cohen, W.B., and Berterretche, M. 2002. Integration of LiDAR and Landsat ETM+ data for estimating and mapping forest canopy height. *Remote Sensing of Environment* (82) 397–416.

Huising, E.J., and Pereira, L.M.G. 1998. Errors and accuracy estimates of laser data acquired by various laser scanning systems for topographic applications. *ISPRS Journal of Photogrammetry and Remote Sensing* (53) 245–261.

Hyyppä, J., Hyyppä, H., Ikinen, M., Engdahl, M., Linko, S., and Zhu, Y-H. 2000. Accuracy comparison of various remote sensing data sources in the retrieval of forest stand attributes. *Forest Ecology and Management* (128) 109–120.

Hyyppä, J., Hyyppä, H., Litkey, P., Xiaowei, Y., Haggrén, H., Rönnholm, P., Pyysalo, U., Pitkänen, J., Maltamo, M. 2004. Algorithms and methods of airborne laser scanning for forest measurements. In *Proceedings of the ISPRS working group VIII/2, Laser-Scanners for Forest and Landscape Assessment*, 3-6 October 2004, Freiburg, Germany.

IKONOS product guide, Spaceimaging, 2004. www.spaceimaging.com accessed 20th December 2004.

Iliffe, J.C. 2003. Datums and map projections for remote sensing GIS and surveying. 3rd ed. Whittles Publishing, Glasgow, Scotland.

Katila, M., and Tomppo, E. 2001. Selecting estimation parameters for the Finnish multisource National Forest Inventory, *Remote Sensing of Environment* (76)16–32.

Kraus, K., and Pfeifer, N. 1998. Determination of terrain models in wooded areas with airborne laser scanner data. *ISPRS Journal Photogrammetry and Remote Sensing* (53) 193–203.

Li, X., and Strahler, A.H. 1985. Geometric-optical modelling of a conifer forest canopy, *IEEE Trans. Geosci. Remote Sensing* (23) 705–721.

Lim, K., Treitz, P., Wulder, M., St-Onge, B., and Flood, M. 2003. LiDAR remote sensing of forest structure. *Progress in Physical Geography* (27) 88–106.

Lutes, J. 2004. Accuracy analysis of rational polynomial coefficients for IKONOS imagery. In *proceedings ASPRS Annual Conference.* Denver, Colorado. May 2004.

Luzum, B., Starek, M., Slatton, K.C. 2004. Normalizing ALSM Intensities GEM Center Report No. Rep_2004-07-001. University of Florida, U.S.A.

Magnussen, S., and Boudewyn, P. 1998. Derivation of stand heights from airborne laser scanner data with canopy-based quantile estimators. *Canadian Journal of Remote Sensing* (28) 1016-1031.

Mäkelä, H., Pekkarinen, A. 2001. Estimation of timber volume at the sample plot level by means of image segmentation and Landsat TM imagery. *Remote Sensing of Environment* (77) 66-75.

Maltamo, M., Packalén, P., Yu, X., Eerikäinen, K., Hyyppä, J., Pitkänen, J. 2004. Identifying and quantifying heterogeneous boreal forest structures using laser scanner data. In *Proceedings of the ISPRS working group VIII/2, Laser-Scanners for Forest and Landscape Assessment*, 3-6 October 2004, Freiburg, Germany.

Malthus, T.J., Suárez-Minguez, J., Woodhouse, I.H., Shaw, D.T. 2002. Review of remote sensing in commercial forestry. Forest Research internal report. October, 2002.

Means, J.E., Acker, S.A., Fitt, B.J., Renslow, M., Emerson, L., and Hendrix, C.J. 1999. Predicting forest stand characteristics with airborne scanning lidar. *Photogrammetric Engineering and Remote sensing* (66) 1367–1371.

Naesset, E. 1997a. Determination of mean tree height of forest stands using airborne laser scanner data. *ISPRS Journal of Photogrammetry and Remote Sensing* (52) 49–56.

Naesset, E. 1997b. Estimating timber volume of forest stands using airborne Laser scanner data *Remote Sensing of Environment* (61) 246–253.

Naesset, E., and Bjerknes, K.O. 2001. Estimating tree heights and numbers of stems in young forest stands using airborne laser scanner data. *Remote Sensing of Environment* (78) 328-340.

Naesset, E. 2002. Predicting forest stand characteristics with airborne laser using a practical two-stage procedure and field data. *Remote Sensing of Environment* (80) 88–99.

Naesset, E., and Økland, T. 2002. Estimating tree height and tree crown properties using airborne scanning laser in a boreal nature reserve. *Remote Sensing of Environment* (79) 105–115.

Naesset, E. 2004. Effects of different flying altitudes on biophysical stand properties estimated from canopy height and density measured with a small-footprint airborne scanning laser. *Remote Sensing of Environment* (91) 243–255.

Naesset, E., Bollandsås, O.M., and Gobakken, T. 2005. Comparing regression methods in estimation of biophysical properties of forest stands from two different inventories using laser scanner data. *Remote Sensing of Environment* (94) 541–553.

Nelson, R.1997. Modeling forest canopy heights: the effects of canopy shape. *Remote Sensing of Environment* (60) 327–334.

Nilson, T., and Peterson, U. 1994. Age dependence of forest reflectance: analysis of main driving factors. *Remote Sensing of Environment* (48) 319–331.

Nilson, T., Olsson, H., Anniste, J., Lükk, T., Praks, J. 2001. Thinning-caused change in reflectance of ground vegetation in boreal forest. *International Journal of Remote Sensing* (22) 2763–2776.

Nilsson, M. 1996. Estimation of tree heights and stand volume using an airborne lidar system. *Remote Sensing of Environment* (56) 1–7.

Patenaude, G., Hill, R.A., Milne, R., Gaveau, D.L.A., Briggs, B.B.J., and Dawson, T.P. 2004. Quantifying forest above ground carbon content using LiDAR remote sensing. *Remote Sensing of Environment* (93) 368–380.

Pereira, L.M.G., and Janssen, L.L.F. 1999. Suitability of laser data for DTM generation: a case study in the context of road planning and design. *Photogrammetry and Remote Sensing* (54) 244–253.

Persson, Å., Holmgren, J., Söderman, U. 2002. Detecting and measuring individual trees using an airborne laser scanner. *Photogrammetric Engineering and Remote Sensing* (68) 925–932.

Philip, M.S. 1998. Measuring Trees and Forests. 2nd ed. CABI Publishing, Oxon.

Popescu, S.C.,Wynne, R.H., and Nelson, R.F. 2002. Estimating plot-level tree heights with lidar: local filtering with a canopy-height based variable window size. *Computers and Electronics in Agriculture* (31) 71–95.

Puhr, C.B., and Donoghue, D.N.M. 2000. Remote sensing of upland conifer plantings using Landsat TM data: a case study from Galloway, south-west Scotland. *International Journal of Remote Sensing* (21) 633-646.

Pyysalo, U., & Hyyppä, H. 2002. Reconstructing Tree Crowns from Laser Scanner Data for Feature Extraction. In *ISPRS Commission III, Symposium 2002 September 9 - 13, 2002,* Graz, Austria.

Rabe-Hesketh, S., and Everitt, B. 2000. A handbook of statistical analysis using Stata. 2nd ed. Chapman and Hall, Boca Raton, Florida.

Reutebuch, S.E., McGaughey, R.J., Anderson, H., and Carson, W.W. 2003. Accuracy of a high-resolution lidar terrain model under a conifer forest canopy. *Canadian Journal of Remote Sensing* (29) 527–535.

Riaño, D., Chvieco, E., Condés, S., González-Matesanz, J., Ustin, S.L. 2004. Generation of crown bulk density for *Pinus sylvestris* L. from lidar. *Remote Sensing of Environment* (92) 353–363.

Sithole, G., and Vosselman, G. 2003. Report: ISPRS Comparison of Filters. Commission Working Group III/3, August 2003.

Sithole, G., and Vosselman, G. 2004. Experimental comparison of filter algorithms for bare-Earth extraction from airborne laser scanning point clouds. *ISPRS Journal of Photogrammetry & Remote Sensing* (59) 85–101.

Soininen, A, 2002. Terrascan for Microstation, user's guide. Terrasolid Ltd., Helsinki, Finland. Available from www.terrasolid.fi

Song, J., Han, S., Yu, K., Kim, Y. 2002. Assessing the Possibility of Land-Cover Classification Using LiDAR Intensity Data. ISPRS Commission III, September 9-13, 2002, Graz, Austria.

Spanner, M.A., Pierce, L.L., Peterson, D.L., Running, S.W. 1990. Remote sensing of temperate coniferous forest leaf index. The influence of canopy closure, understorey vegetation and background reflectance. *International Journal of Remote Sensing* (11) 95–111.

Suárez, J.C., Ontiveros, C., Smith, S., Snape, S. 2005. The use of airborne LiDAR and aerial photography in the estimation of individual tree heights in forestry. *Computers and Geosciences* (31) 253 –262.

Woodcock, C.E., and Strahler, A.H. 1987. The factor of scale in remote sensing, *Remote Sensing of Environment* (21) 311– 332.

Woodland Grant Scheme [Online] url - http://www.forestry.gov.uk/

Vanclay, J.K. 1998. Modelling forest growth and yield applications to mixed tropical forests. 2nd ed. CABI Publishing, Oxon.

Watt, P.J. 2002. An investigation of the potential of Landsat TM & Synthetic Aperture Radar (SAR) for deriving timber volume in Britain's upland conifer plantations, In *Proceedings of ForestSat 2002 Conference, Operational Tools in Forestry using Remote Sensing Techniques*, 5-9 August 2002, Edinburgh, U.K. [CD-ROM].

Watt, P.J., and Donoghue, D.N.M. 2005. Measuring forest structure with terrestrial laser scanning. *International Journal of Remote Sensing* (26) 1437–1446.

Wehr, A., and Lohr, U. 1999. Airborne laser scanning – an introduction and overview. *Photogrammetry and Remote Sensing* (54) 68–82.

Wagner, W., Luckman, A., Vietmeier, J., Tansey, K., Balzter, H., Schmullius, C., Davidson, M., Gaveau, D., Gluck, M., Le Toan, T., .Quegan, S., Shvidenko, A., Wiesmann, A., Yu, J.J. 2003. Large-scale mapping of boreal forest in SIBERIA using ERS tandem coherence and JERS backscatter data. *Remote Sensing of Environment* (85) 125–144.

Haglöf Sweden www.haglofsweden.com

Xiaowei, Y., Hyyppä, J., Hyyppä, H., Maltamo, M. 2004. Effects of flight altitude on tree height estimation using airborne lasers scanning. In *Proceedings of the ISPRS working group VIII/2, Laser-scanners for forest and landscape assessment*, 3-6 October 2004, Freiburg, Germany.

Zarnoch, S.J., Bechtold, W.A., and Stoke, K.W. 2004 Using crown condition as indicators of forest health. *Canadian Journal of Forest Research* (34) 1057–1 070.

Appendix 4.0 Spatially registering field and LiDAR datasets in a GIS

Before import into Stata the plot IDs for each sample plot need to be allocated to the laser points within each plot. This is a 4 step process as detailed below:

1. LiDAR data imported into the GIS as an ASCII table and point theme generated using x,y coordinates. Figure 4.0 shows laser points over the study area.

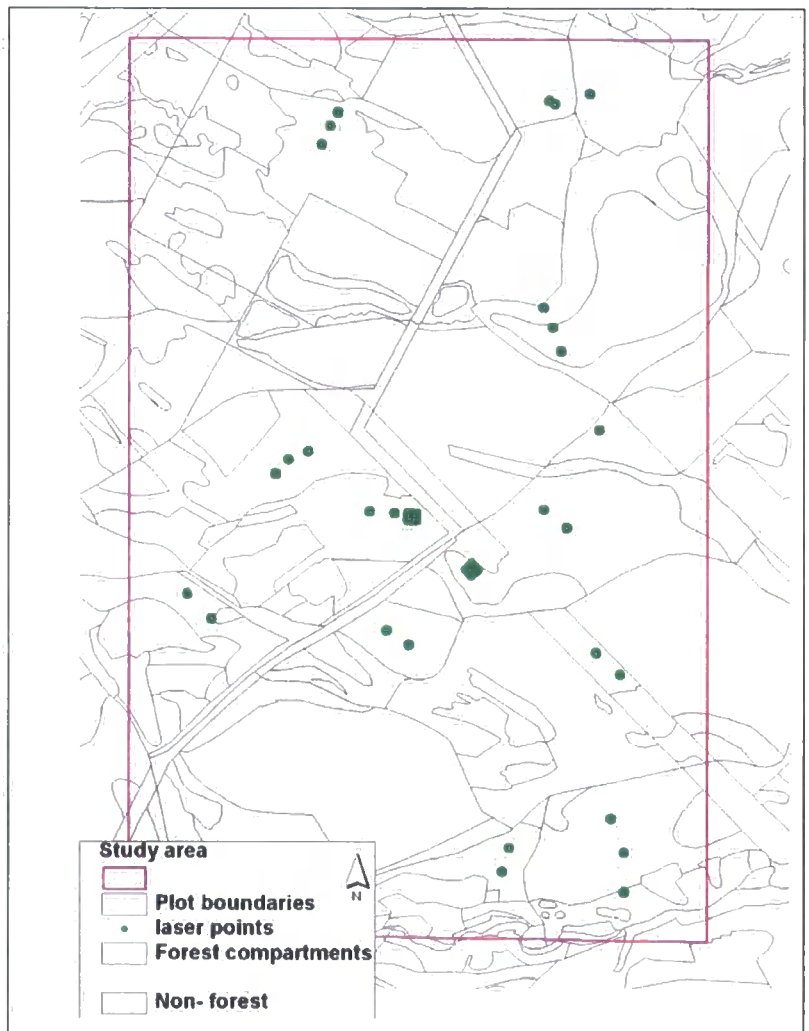

Figure 4.0 Sample plot location

2. Table 4.0 shows the laser point attribute table prior to the spatial join. Fields are Easting (x) Northing (y) Elevation (z) H normalised (point elevation values subtracted from the DTM)

Table 4.0 Laser point attribute table

Easting	Northing	Elevation	H (normalised)
370981.94000	582090.50000	326.25000	4.65
370982.66000	582090.56000	328.51000	6.94
370983.84000	582090.44000	327.14000	5.57
370984.94000	582090.31000	326.80000	5.23
370986.03000	582090.13000	324.91000	3.31
370987.03000	582090.13000	325.71000	4.11
370987.84000	582090.13000	326.80000	5.20
370988.19000	582089.56000	325.90000	4.57
370987.19000	582089.56000	325.18000	3.85
370986.44000	582089.50000	323.28000	1.95
370985.06000	582089.75000	326.63000	5.33
370984.06000	582089.88000	327.65000	6.35
370983.19000	582089.94000	327.00000	5.70
370982.06000	582090.00000	327.85000	6.55
370981.28000	582090.00000	326.12000	4.69
370979.16000	582088.94000	325.40000	3.97
370980.00000	582089.00000	328.06000	6.63
370981.09000	582088.94000	327.78000	6.35
370982.09000	582088.81000	326.73000	5.43
370983.00000	582088.88000	328.64000	7.34
370984.19000	582088.69000	327.06000	5.76
370985.13000	582088.63000	327.03000	5.73
370986.59000	582088.31000	322.68000	1.35
370987.50000	582088.31000	324.36000	3.03
370988.41000	582088.25000	324.59000	3.26
370989.09000	582088.50000	328.68000	7.35
370989.97000	582088.44000	329.15000	7.82
370990.31000	582087.75000	326.37000	4.90
370989.31000	582087.81000	327.10000	5.77
370988.59000	582087.75000	325.20000	3.87
370987.38000	582087.94000	326.80000	5.47
370986.63000	582087.88000	324.72000	3.39
370985.56000	582087.94000	324.88000	3.58
370984.34000	582088.19000	328.17000	6.87
370983.34000	582088.31000	329.15000	7.85

3.

Using geoprocessing wizard plot ID held for each field measured plot assigned to laser points (Figure 4.1)

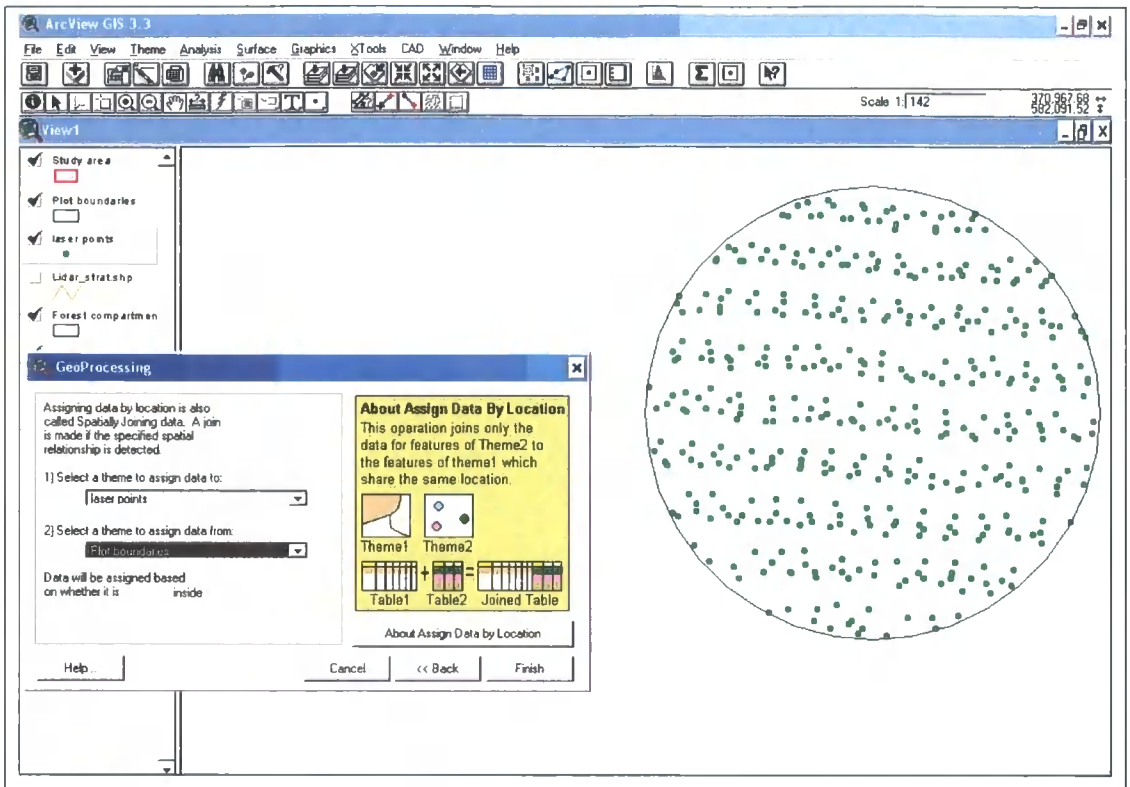

Figure 4.1 Spatial data join using geoprocessing wizard.

4. Table 4.1 shows the Laser point attribute table after to spatial join. Fields are: Plot ID taken from sample plot table, Easting (x) Northing (y) Elevation (z) H normalised (point elevation values subtracted from the DTM)

Plot ID	Easting	Northing	Elevation	DTM	H (normalised)
10	370981.94000	582090.50000	326.25000	321.60	4.65
10	370982.66000	582090.56000	328.51000	321.57	6.94
10	370983.84000	582090.44000	327.14000	321.57	5.57
10	370984.94000	582090.31000	326.80000	321.57	5.23
10	370986.03000	582090.13000	324.91000	321.60	3.31
10	370987.03000	582090.13000	325.71000	321.60	4.11
10	370987.84000	582090.13000	326.80000	321.60	5.20
10	370988.19000	582089.56000	325.90000	321.33	4.57
10	370987.19000	582089.56000	325.18000	321.33	3.85
10	370986.44000	582089.50000	323.28000	321.33	1.95
10	370985.06000	582089.75000	326.63000	321.30	5.33
10	370984.06000	582089.88000	327.65000	321.30	6.35
10	370983.19000	582089.94000	327.00000	321.30	5.70
10	370982.06000	582090.00000	327.85000	321.30	6.55
10	370981.28000	582090.00000	326.12000	321.43	4.69
10	370979.16000	582088.94000	325.40000	321.43	3.97
10	370980.00000	582089.00000	328.06000	321.43	6.63
10	370981.09000	582088.94000	327.78000	321.43	6.35
10	370982.09000	582088.81000	326.73000	321.30	5.43
10	370983.00000	582088.88000	328.64000	321.30	7.34
10	370984.19000	582088.69000	327.06000	321.30	5.76
10	370985.13000	582088.63000	327.03000	321.30	5.73
10	370986.59000	582088.31000	322.68000	321.33	1.35
10	370987.50000	582088.31000	324.36000	321.33	3.03
10	370988.41000	582088.25000	324.59000	321.33	3.26
10	370989.09000	582088.50000	328.68000	321.33	7.35
10	370989.97000	582088.44000	329.15000	321.33	7.82
10	370990.31000	582087.75000	326.37000	321.47	4.90
10	370989.31000	582087.81000	327.10000	321.33	5.77
10	370988.59000	582087.75000	325.20000	321.33	3.87
10	370987.38000	582087.94000	326.80000	321.33	5.47
10	370986.63000	582087.88000	324.72000	321.33	3.39
10	370985.56000	582087.94000	324.88000	321.30	3.58
10	370984.34000	582088.19000	328.17000	321.30	6.87
10	370983.34000	582088.31000	329.15000	321.30	7.85

Table 4.1 Laser point attribute table joined with plot data

Appendix 4.1 Processing in Stata to generate statistics at different spatial resolutions in LiDAR data

Stata batch file

```
* Image processing in Stata pjw dec 04
* Version 1.0 purpose to take lidar data into Stata, calculate stats and export
* to image processing software
* set spatial resolution by altering rounding
gen long rx = round(x,2)
gen long ry= round(y,2)
* group x and y (Easting & Northing) then generate a grid value for each group
egen grid = group( rx ry)
*  calculate statistics:  maximum height
egen maxh =max(h), by(grid)
* calculate statistics: percentileheights
egen pc10 =pctile(h) , by(grid) p(10)
* calculate statistics
egen median = pctile(h) , by(grid) p(50)
* collapse and summarise dataset into grid size i.e. 2 m
qui bysort rx ry (maxh) : keep if _n == 1
* sort data by  descending Northing and ascending Easting : Note minus is important
gsort - ry rx
* format values for export to ENVI - necessary to do this as ENVI cannot cope with . or
*missing values
format maxh %9.2f
format pc10 %9.2f
format median %9.2f
* check geographic extent for outliers using a scatterplot- you may have a couple of
* extra grid created on the edge of the dataset that need to be deleted
scatter ry rx, scheme(lean1)
* returns number of columns or samples in image
qui tab rx
ret li
```

```
* returns number of row or lines in image
qui tab ry
ret li

*export to an ASCII format
outfile maxh medianh sdh using "U:\PHD Dataset\STATA
files\data\mixeaxENVI.raw", replace
```

After this process the raw data is rounded to the desired grid spacing with all the calculated statistics held within the statistics package in a row format. Figure 4.2 displays the spatial extent of 1 band of data (i.e. one of the statistics calculated). The next stage grids these data (same resolution as the rounding performed on the raw data) and exports it to ENVI to generate a multi-band image, each band represents a different statistic.

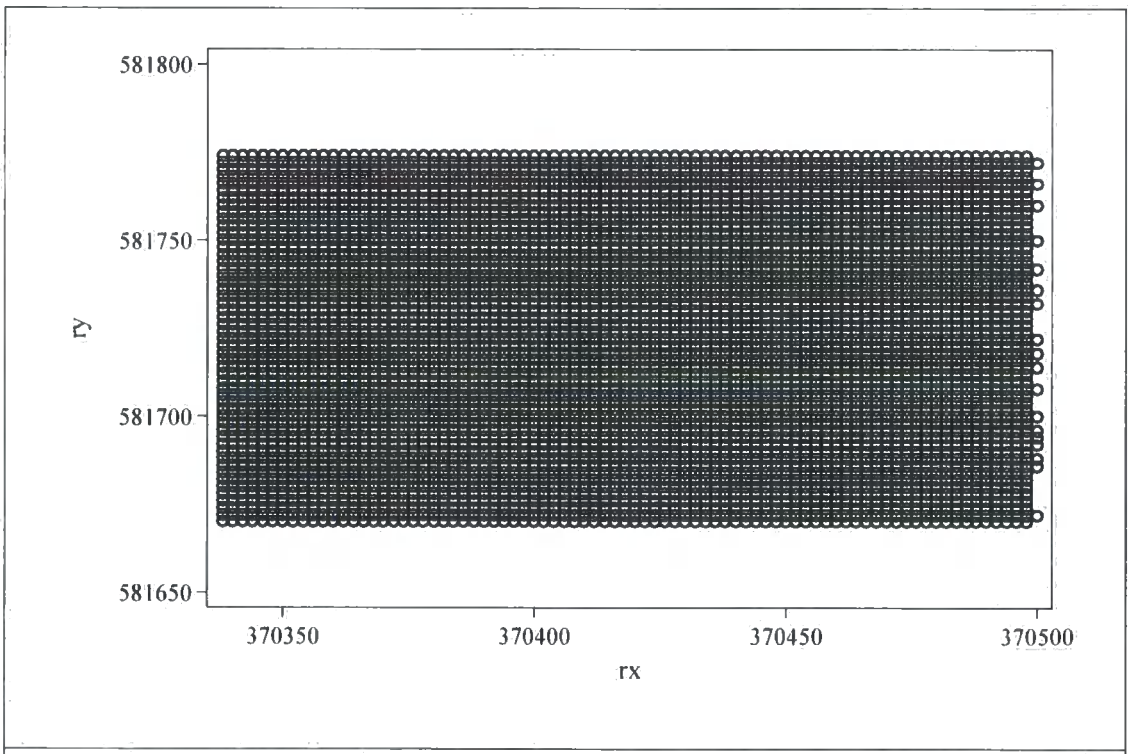

Figure 4.2 LiDAR data resampled and summarised at 2 m grid. Note presence of outlier grid cells.

Appendix 4.2 Image processing in ENVI

1. IKONOS Orthorectification

The RPC (Rational Polynomial Coefficients or Rapid Positioning Coordinates) sensor model is used to orthorectify data from the IKONOS sensors. The RPC ortho-rectification process combines several sets of input data to place each pixel in the correct ground location. The following inputs are required: the image to be rectified, the RPC coefficients, and elevation information. Furthermore, the offset between mean sea level and the gravitational potential surface known as the Geoid is required so the elevation can be correctly interpreted. Finally, if the source image does not have approximate geolocation information available, the rough location of the image on the earth's surface must be computed to provide a location base needed.

1. Select the following option:

" From the main ENVI menu bar Orthorectification >Orthorectify IKONOS

2. In the file selection dialog select the image to be orthorectified. Click Open.

The input image must be linked to the RPC coefficients contained in an ancillary text file. These coefficients are required for the rational function expansion to convert ground coordinates into sensor coordinates. These coefficients are provided in an ancillary text. Once you select a file for input, an RPC coefficient filename consisting of the root name of the source image plus _rpc.txt.

After you select an input file, the Enter Orthorectification Parameters dialog appears (Figure 4.3). Designate the technique used for re-sampling by clicking the button next to the Image re-sampling label and selecting Nearest Neighbour, Bilinear, or Cubic Convolution.

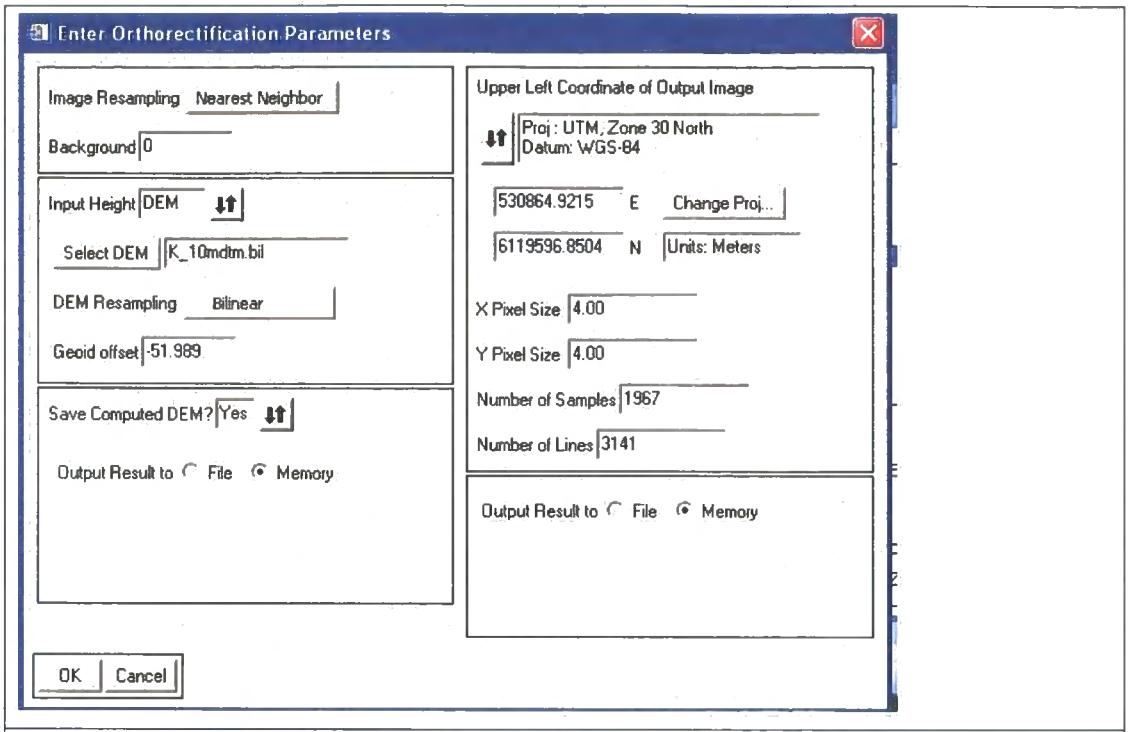

Figure 4.3 Parameters required for Ortho-correction of IKONOS data.

The selected re-sampling technique is used to determine the pixel values in the input image when it is converted from its current orientation into the new orientation. The default is Bilinear. To specify a value for pixels in the output image that are outside the bounds of the source image, enter a value in the Background text box.

3. Specify the location of the DTM - select nearest neighbour re-sampling

The DEM re-sampling technique is used to convert the DEM from the source coordinate system to Geographic, WGS-84, which is required for input into the RPC algorithm. A full projection is performed to convert each DEM coordinate into the correct coordinate system.

Specify the Geoid Offset: according to Ordnance survey this is 51.989 m for the area of interest. The Geoid offset is a constant value that is added to every value in the DEM to account for the difference between a spheroid mean sea level, used in most available DEM data, and the constant geopotential surface known as the GEOID. The RPC coefficients are created based on geoid height, and this information must be used to provide accurate ortho-rectification. Figures 4.4 and 4.5 show one of the IKONOS bands and the 30 m DTM, respectively.

Figure 4.4 IKONOS band prior to correction.

Figure 4.5 30 m DTM (note file name incorrectly named "K_10mdtm.bil").

2. Convert map projection

Convert Map Projection was used to convert your geo-referenced files to another map projection. The conversion is done by warping the file into the new projection.

1. Select Map Convert Map Projection.
2. Select the input geo-referenced file and click OK.
3. The Convert Map Projection Parameters dialog appears with the input projection shown at the top of the dialog. The available output projections, from the map_proj.txt file are displayed in the Select Output Map Projection list

4. In the Select Output Map Projection list, select the output projection by clicking on the desired type and entering the necessary parameters

5. Click OK.

6. The map projection is converted by warping the file using a grid of control points.

7. In the Number of Warp Points X/Y text boxes, define the number of control points to be used in the X and Y directions.

Using many warp points increases the warping time considerably, but can significantly increase the accuracy of the conversion.

6. Click OK.

The Convert Map Projection function uses the standard registration parameters dialog to perform the warping of the image to the new projection When the Registration Parameters dialog appears, select the warp method: Triangulation

8. Select the re-sampling method: Nearest Neighbour

9. Enter the output filename and select output to File or Memory.

10. Click OK to convert your data to the new projection.

Appendix 6.1 result of two-tailed *t* test on mean height of first and last pulse data

```
.ttest meanfp == meanlp, unpaired level(99)


Two-sample t test with equal variances

------------------------------------------------------------------------------
Variable |     Obs        Mean    Std. Err.   Std. Dev.   [99% Conf. Interval]
---------+--------------------------------------------------------------------
  meanfp |      60     9.59473    .9116816    7.061855    7.168053    12.02141
  meanlp |      60    9.654251    .9167055     7.10077    7.214202     12.0943
---------+--------------------------------------------------------------------
combined |     120    9.624491    .6437188    7.051587    7.939379     11.3096
---------+--------------------------------------------------------------------
    diff |           -.0595213     1.29287               -3.444431    3.325389
------------------------------------------------------------------------------
Degrees of freedom: 118

                 Ho: mean(meanfp) - mean(meanlp) = diff = 0

     Ha: diff < 0                 Ha: diff != 0                 Ha: diff > 0
       t =  -0.0460                 t =  -0.0460                 t =  -0.0460
   P < t =   0.4817             P > |t| =   0.9634             P > t =   0.5183
```

Appendix 6.2 Calculation of LiDAR canopy length (Lk_l)

1. Maximum first pulse height - height percentile (5, 10, 20,..,60)
2. Regress field-measured canopy length against LiDAR derived measure. Note lkl = LiDAR derived measure using returns above the 5th height percentile.

Table Summary of regression R^2 and RMS error

Model	R^2	RMSE (m)
lkl 5	0.595	1.266
lkl 10	0.640	1.195
lkl 20	0.653	1.173
lkl 30	0.619	1.228
lkl 40	0.580	1.290
lkl 50	0.542	1.347
lkl 60	0.500	1.407

Appendix 6.3 National network of Permanent Mensuration Sample Plots (PSPs)

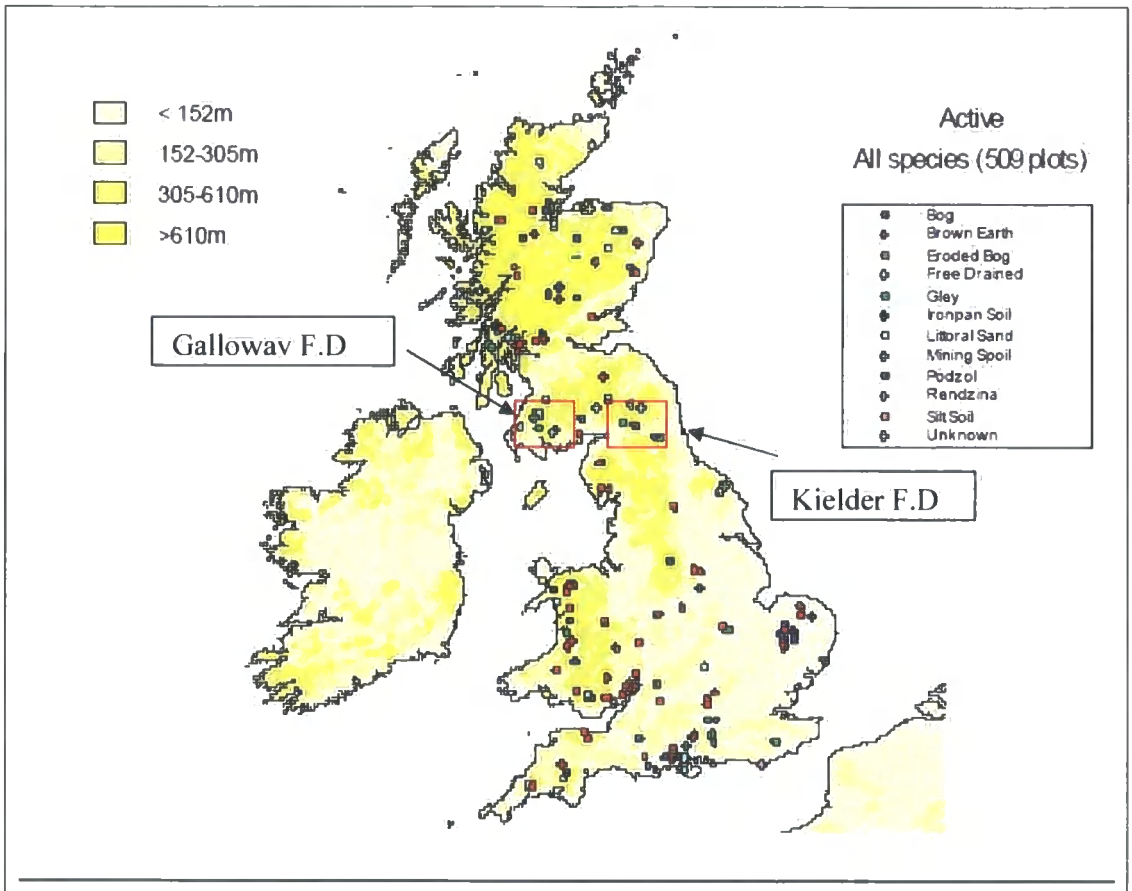

Location of Permanent Mensuration Sample Plots (PSPs).

Appendix 6.4 regression and multiple regression models used to predict volume

(i) Polynomial model

```
 regress totalvol  predhdom_all  predhdom_allsq if plotid <899

      Source |       SS       df       MS              Number of obs =      56
-------------+------------------------------           F(  2,    53) =  376.08
       Model |  3830816.22     2  1915408.11           Prob > F      =  0.0000
    Residual |  269930.367    53  5093.02579           R-squared     =  0.9342
-------------+------------------------------           Adj R-squared =  0.9317
       Total |  4100746.58    55  74559.0288           Root MSE      =  71.365

------------------------------------------------------------------------------
    totalvol |      Coef.   Std. Err.      t    P>|t|     [95% Conf. Interval]
-------------+----------------------------------------------------------------
predhdom_all |   8.576447   8.255854     1.04   0.304    -7.982699    25.13559
predhdom_a~q |   .8559183   .3009729     2.84   0.006     .2522431    1.459593
       _cons |  -52.96225   40.07368    -1.32   0.192    -133.3399    27.41537
------------------------------------------------------------------------------
```

(i) Gompertz model

```
.  nl gom3 totalvol predhdom_all if plotid <900, nolog
(obs = 56)

      Source |       SS       df       MS              Number of obs =      56
-------------+------------------------------           F(  3,    53) =  677.99
       Model |  9741453.3      3   3247151.1           Prob > F      =  0.0000
    Residual |  253836.792    53  4789.37344           R-squared     =  0.9746
-------------+------------------------------           Adj R-squared =  0.9732
       Total |  9995290.1     56  178487.323           Root MSE      =  69.2053
                                                      Res. dev.     =  630.3904
3-parameter Gompertz function, totalvol=b1*exp(-exp(-b2*(predhdom_all-b3)))
------------------------------------------------------------------------------
    totalvol |      Coef.   Std. Err.      t    P>|t|     [95% Conf. Interval]
-------------+----------------------------------------------------------------
          b1 |   1056.378   255.3348     4.14   0.000     544.2413    1568.515
          b2 |   .1202038    .034308     3.50   0.001     .0513908    .1890169
          b3 |   18.25013   2.214326     8.24   0.000     13.80875    22.69151
------------------------------------------------------------------------------
 (SEs, P values, CIs, and correlations are asymptotic approximations)
```

(ii) Logistic model

```
(obs = 56)

      Source |       SS       df       MS              Number of obs =      56
-------------+------------------------------           F(  3,    53) =  686.29
       Model |  9744445.96     3  3248148.65           Prob > F      =  0.0000
    Residual |  250844.139    53  4732.90828           R-squared     =  0.9749
```

```
-------------+------------------------------           Adj R-squared =    0.9735
       Total |   9995290.1    56  178487.323           Root MSE      =   68.79614
                                                      Res. dev.     =   629.7263
3-parameter logistic function, totalvol= b1 / (1 + exp(b2 * predhdom_all + b3))
------------------------------------------------------------------------------
    totalvol |      Coef.   Std. Err.      t    P>|t|     [95% Conf. Interval]
-------------+----------------------------------------------------------------
          b1 |   778.6607   82.57702     9.43   0.000     613.0322    944.2893
          b2 |  -.2809195   .0517156    -5.43   0.000    -.3846477   -.1771912
          b3 |   5.202486   .8079042     6.44   0.000     3.582036    6.822937
------------------------------------------------------------------------------
 (SEs, P values, CIs, and correlations are asymptotic approximations)
```

(iv) Multiple regression using polynomial model

Volume

```
. sw regress totalvol  (predhdom_all  predhdom_allsq)  lkl lkv cvfp kurtlp_1
skewlp_1 pczeroall if plotid <899, pe(0.05)
                      begin with empty model
p = 0.0000 <  0.0500  adding   predhdom_all predhdom_allsq

      Source |       SS       df       MS              Number of obs =      56
-------------+------------------------------           F(  2,    53) =  376.08
       Model |  3830816.22     2  1915408.11           Prob > F      =  0.0000
    Residual |  269930.367    53  5093.02579           R-squared     =  0.9342
-------------+------------------------------           Adj R-squared =  0.9317
       Total |  4100746.58    55  74559.0288           Root MSE      =  71.365

------------------------------------------------------------------------------
    totalvol |      Coef.   Std. Err.      t    P>|t|     [95% Conf. Interval]
-------------+----------------------------------------------------------------
predhdom_all |   8.576447   8.255854     1.04   0.304    -7.982699    25.13559
predhdom_a~q |   .8559183   .3009729     2.84   0.006     .2522431    1.459593
       _cons |  -52.96225   40.07368    -1.32   0.192    -133.3399    27.41537
```

Appendix 7.1 LiDAR near infrared intensity for Clatteringshaws transect

Variable	Description	LiDAR DN values			
		Mean (m)	SD (m)	Min. (m)	Max. (m)
Iall	Intensity all	78	22	35	159
vegp90	Intensity above 90th height percentile	71	13	37	120
vegp75	Intensity above 75th height percentile	74	13	39	113
vegp50	Intensity above 50th height percentile	73	14	36	114
vegp25	Intensity above 25th height percentile	76	14	43	129

Appendix 7.2 Summary of LiDAR distribution measures for sample plots

Pure Sitka spruce

Coefficient of variation

Percentiles		Smallest		
1%	.07	.07		
5%	.08	.08		
10%	.08	.08	Obs	53
25%	.1	.08	Sum of Wgt.	53
50%	.11		Mean	.1279245
		Largest	Std. Dev.	.0555863
75%	.14	.26		
90%	.21	.26	Variance	.0030898
95%	.26	.29	Skewness	1.824438
99%	.32	.32	Kurtosis	5.864233

Mean height

	Percentiles	Smallest		
1%	8	8		
5%	9	9		
10%	10	9	Obs	53
25%	12	9	Sum of Wgt.	53
50%	16		Mean	14.62264
		Largest	Std. Dev.	2.962759
75%	17	18		
90%	18	18	Variance	8.777939
95%	18	19	Skewness	-.6706873
99%	19	19	Kurtosis	2.35069

skewness

	Percentiles	Smallest		
1%	-1.25	-1.25		
5%	-.94	-.98		
10%	-.76	-.94	Obs	53
25%	-.52	-.86	Sum of Wgt.	53
50%	-.24		Mean	-.2728302
		Largest	Std. Dev.	.3711229
75%	-.08	.23		
90%	.16	.37	Variance	.1377322
95%	.37	.53	Skewness	-.1530126
99%	.57	.57	Kurtosis	3.173512

Percent ground returns

	Percentiles	Smallest		
1%	0	0		
5%	1	1		
10%	1	1	Obs	53
25%	2	1	Sum of Wgt.	53
50%	4		Mean	5.566038
		Largest	Std. Dev.	5.119756
75%	6	17		
90%	15	17	Variance	26.2119
95%	17	20	Skewness	1.652421
99%	22	22	Kurtosis	4.974538

Sitka spruce/lodgepole pine mixture

Coefficient of variation

Percentiles		Smallest		
1%	.18	.18		
5%	.18	.2		
10%	.19	.2	Obs	10
25%	.2	.21	Sum of Wgt.	10
50%	.22		Mean	.227
		Largest	Std. Dev.	.03335
75%	.26	.23		
90%	.275	.26	Variance	.0011122
95%	.28	.27	Skewness	.3516239
99%	.28	.28	Kurtosis	1.856782

meanh

Percentiles		Smallest		
1%	10	10		
5%	10	10		
10%	10	10	Obs	10
25%	10	10	Sum of Wgt.	10
50%	11		Mean	10.7
		Largest	Std. Dev.	.6749486
75%	11	11		
90%	11.5	11	Variance	.4555556
95%	12	11	Skewness	.3656751
99%	12	12	Kurtosis	2.294468

skewness

Percentiles		Smallest		
1%	-.74	-.74		
5%	-.74	-.63		
10%	-.685	-.47	Obs	10
25%	-.47	-.41	Sum of Wgt.	10
50%	-.195		Mean	-.211
		Largest	Std. Dev.	.3503157

75%	.16	-.04		
90%	.205	.16	Variance	.1227211
95%	.24	.17	Skewness	-.1156949
99%	.24	.24	Kurtosis	1.621734

Percent ground returns

	Percentiles	Smallest		
1%	25	25		
5%	25	31		
10%	28	31	Obs	10
25%	31	31	Sum of Wgt.	10
50%	35		Mean	34.5
		Largest	Std. Dev.	5.169354
75%	38	37		
90%	41	38	Variance	26.72222
95%	43	39	Skewness	-.1856827
99%	43	43	Kurtosis	2.493009

Pure lodgepole pine

Coefficient of variation

	Percentiles	Smallest		
1%	.16	.16		
5%	.17	.17		
10%	.18	.17	Obs	62
25%	.21	.17	Sum of Wgt.	62
50%	.23		Mean	.2443548
		Largest	Std. Dev.	.0538553
75%	.28	.36		
90%	.3	.38	Variance	.0029004
95%	.36	.38	Skewness	.7646102
99%	.38	.38	Kurtosis	3.205268

Mean height

	Percentiles	Smallest		
1%	7	7		
5%	8	7		
10%	9	8	Obs	62
25%	9	8	Sum of Wgt.	62

50%	10		Mean	10.01613
		Largest	Std. Dev.	1.194138
75%	11	12		
90%	11	12	Variance	1.425965
95%	12	12	Skewness	-.4387975
99%	12	12	Kurtosis	2.800671

skewness

	Percentiles	Smallest		
1%	-1.57	-1.57		
5%	-1.39	-1.46		
10%	-1.2	-1.43	Obs	62
25%	-.95	-1.39	Sum of Wgt.	62
50%	-.365		Mean	-.4456452
		Largest	Std. Dev.	.5663157
75%	.04	.34		
90%	.22	.35	Variance	.3207135
95%	.34	.43	Skewness	-.2563628
99%	.58	.58	Kurtosis	1.926134

Percent ground returns

	Percentiles	Smallest		
1%	22	22		
5%	24	22		
10%	28	23	Obs	62
25%	31	24	Sum of Wgt.	62
50%	36		Mean	36.01613
		Largest	Std. Dev.	7.1092
75%	40	50		
90%	43	50	Variance	50.54072
95%	50	52	Skewness	.3160901
99%	56	56	Kurtosis	3.252191

Appendix 7.3 One-way ANOVA for testing difference between plantation species types for LiDAR and SPOT 5 NIR response and various canopy density measures.

```
ANOVA
Summary of LiDAR intensity
sppgroup         Mean    Std. Dev.       Freq.

Pine     46.419355    6.5375295          62
Sitka    78.039548    9.2578969         177
mix      55.1         4.2018514          10

Total    69.24498    16.294178          249

Analysis of Variance
Source              SS         df      MS            F     Prob > F

Between groups     47993.3363      2   23996.6681    330.70     0.0000
Within groups      17850.7199    246   72.5639022

Total              65844.0562    248   265.500227

Bartlett's test for equal variances:  chi2(2) =  15.3785
Prob>chi2 = 0.000

Comparison of int_p50 by sppgroup
(Bonferroni)
Row Mean-|
Col Mean         Pine      Sitka

Sitka          31.6202
                0.000

mix             8.68065   -22.9395
                0.009       0.000


Summary of spotnir
sppgroup    Mean       Std. Dev.       Freq.

Pine     40.725806      .77182676          62
Sitka    48.107345     2.183305           177
mix      42.8           .42163702          10

Total    46.056225     3.7509208          249

Analysis of Variance
Source           SS           df      MS            F          Prob > F

Between groups   2612.31369     2   1306.15684    366.42      0.0000
Within groups     876.899162  246      3.56463074

Total            3489.21285    248     14.0694067

Bartlett's test for equal variances:  chi2(2) =  83.1777  Prob>chi2 =
0.000

Comparison of spotnir by sppgroup
(Bonferroni)
```

```
Row Mean-|
Col Mean      Pine       Sitka

Sitka        7.38154
             0.000

mix          2.07419    -5.30734
             0.04        0.000
```

Coefficient of Variation LiDAR only

```
. oneway  cv_h sppgroup if sppgroup>" ", tabulate bon

           |          Summary of cv_h
   sppgroup |        Mean   Std. Dev.       Freq.
------------+------------------------------------
       Pine |   .24435484   .05385533          62
      Sitka |   .12875706   .05514065         177
        mix |        .227      .03335          10
------------+------------------------------------
      Total |   .16148594   .07460515         249

                      Analysis of Variance
    Source              SS         df      MS            F      Prob >
F
------------------------------------------------------------------------

Between groups      .658289455       2   .329144728    112.14     .0000
 Within groups      .722060727     246   .002935206
------------------------------------------------------------------------

    Total           1.38035018     248   .005565928

Bartlett's test for equal variances:  chi2(2) =   3.1903  Prob>chi2 =
0.203
```

```
                    Comparison of cv_h by sppgroup
                            (Bonferroni)
Row Mean-|
Col Mean |       Pine      Sitka
---------+----------------------
   Sitka |   -.115598
         |      0.000
         |
     mix |   -.017355    .098243
         |      1.000      0.000
```

Percent ground returns LiDAR only

```
. oneway  pczero sppgroup if sppgroup>" ", tabulate bon

           |          Summary of pczero
   sppgroup |        Mean   Std. Dev.       Freq.
------------+------------------------------------
       Pine |   36.016129   7.1091996          62
      Sitka |   4.9378531   4.3656175         177
        mix |  34.5         5.1693541          10
------------+------------------------------------
      Total |  13.863454   14.954684          249
```

```
                        Analysis of Variance
    Source              SS         df      MS            F     Prob >
F
------------------------------------------------------------------------
Between groups      48785.5572      2   24392.7786    898.59    0.0000
 Within groups      6677.80026    246   27.1455295
------------------------------------------------------------------------
--
    Total           55463.3574    248    223.64257

Bartlett's test for equal variances:  chi2(2) =  23.9602  Prob>chi2 =
0.000

                    Comparison of pczero by sppgroup
                              (Bonferroni)
Row Mean-|
Col Mean |       Pine      Sitka
---------+----------------------
   Sitka |   -31.0783
         |      0.000
         |
     mix |   -1.51613    29.5621
         |      1.000      0.000
```

Skewness LiDAR only

```
. oneway  skew sppgroup if sppgroup>" ", tabulate bon

           |         Summary of skew_veg
   sppgroup |        Mean   Std. Dev.       Freq.
------------+------------------------------------
       Pine |  -.44564516   .56631574          62
      Sitka |   -.2979096   .38674432         177
        mix |       -.211   .35031573          10
------------+------------------------------------
      Total |  -.33120482   .44060643         249

                        Analysis of Variance
    Source              SS         df      MS            F     Prob > F
------------------------------------------------------------------------
Between groups      1.15269784      2   .576348922      3.02    0.0508
 Within groups      46.9925405    246   .191026587
------------------------------------------------------------------------
    Total           48.1452383    248   .194134025

Bartlett's test for equal variances:  chi2(2) =  15.1078  Prob>chi2 =
0.001

                    Comparison of skew_veg by sppgroup
                              (Bonferroni)
Row Mean-|
Col Mean |       Pine      Sitka
---------+----------------------
   Sitka |    .147736
         |      0.069
         |
     mix |    .234645     .08691
         |      0.349      1.000
```

Mean height LiDAR only

```
. oneway  mean_h sppgroup if sppgroup>" ", tabulate bon

           |          Summary of mean_h
   sppgroup |        Mean   Std. Dev.       Freq.
------------+------------------------------------
       Pine |   10.016129   1.1941378          62
      Sitka |   14.627119    2.571025         177
        mix |        10.7   .67494856          10
------------+------------------------------------
      Total |   13.321285   3.0468765         249

                       Analysis of Variance
    Source              SS         df      MS      F     Prob > F
------------------------------------------------------------------------
Between groups      1047.82349      2   523.911744    102.74    0.0000
Within groups       1254.4737     246   5.09948659
------------------------------------------------------------------------
    Total           2302.29719    248   9.28345641

Bartlett's test for equal variances:  chi2(2) =  52.6701  Prob>chi2 =
0.000

                       Comparison of mean_h by sppgroup
                                (Bonferroni)
Row Mean-|
Col Mean |       Pine      Sitka
---------+----------------------
   Sitka |    4.61099
         |      0.000
         |
     mix |    .683871   -3.92712
         |      1.000      0.000
```